4th BBC
2024 Kaunas

4th Baltic Biophysics Conference

Abstract Book

2024 October 3-4th

Faculty of Pharmacy

Lithuanian University of Health Sciences

Sukilėlių av. 13, Kaunas

Lithuania

LITHUANIAN BIOPHYSICAL SOCIETY

Content

Foreword	3
The Team	4
Program	6
Oral Presentations	12
Poster Presentations	41
Index	129
Sponsors	135

Foreword

Dear Baltic Biophysics Conference Participants,

It is my great pleasure and honor to welcome all of you, from abroad and within Lithuania, to the 4th Baltic Biophysics Conference taking place in Kaunas, Lithuania.

The aim of the Conference is to gather researchers in the field of biophysics from the Baltic Sea region and other countries to share their latest achievements, to stimulate scientific interactions and collaborations, and to motivate young bright minds. I believe that this event will trigger new ideas for grant applications to the local and foreign research funding organizations, as well as the research exchanges between laboratories.

The scientific program of the Conference is rich and varied with 1 Keynote Lecture, 14 Invited Lectures, 13 Oral Presentations, 87 Poster Presentations. I would like to express my sincere gratitude to all those who took part in organizing the Conference and, in particular, to the European Biophysical Societies' Association and other Sponsors who helped us to keep down the costs for all participants.

This meeting is jointly organized by the Lithuanian University of Health Sciences, Vilnius University, Vytautas Magnus University, Vilnius Gediminas Technical University, Center for Physical Sciences and Technology, National Cancer Institute, and Kaunas University of Technology.

In conclusion, I would like to extend a warm welcome to you all once again and wish you success in your work during the BBC-2024 Conference.

Kind regards,

Conference Host

Prof. Vytenis Arvydas Skeberdis

The Team

Conference host:

Prof. Vytenis Arvydas Skeberdis, Lithuanian University of Health Sciences, Institute of Cardiology

Scientific organizing committee:

Prof. Saulius Šatkauskas, Vytautas Magnus University, Research Institute of Natural and Technological Sciences,

Prof. Vytenis Arvydas Skeberdis, Lithuanian University of Health Sciences, Institute of Cardiology,

Dr. Paulius Ruzgys, Vytautas Magnus University, Research Institute of Natural and Technological Sciences,

Dr. Vilmantas Pupkis, Vilnius University, Life Sciences Center,

Dr. Greta Butkienė, National Cancer Institute,

Prof. Aidas Alaburda, Vilnius University, Life Sciences Center,

Dr. Gytis Baranauskas, Lithuanian University of Health Sciences, Neuroscience Institute,

Dr. Agnė Kalnaitytė-Vengelienė, Vilnius University, Faculty of Physics,

Dr. Arūnas Stirkė, Center for Physical Sciences and Technology,

Dr. Regina Mačianskienė, Lithuanian University of Health Sciences, Institute of Cardiology,

Prof. Tomas Tamulevičius, Kaunas University of Technology,

Dr. Rimantas Treinys, Lithuanian University of Health Sciences, Institute of Cardiology,

Dr. Gražvydas Lukinavičius, Max Planck Institute for Multidisciplinary Sciences, Department of NanoBiophotonics,

Prof. Daumantas Matulis, Vilnius University, Life Sciences Center,

Prof. Aušra Saudargienė, Lithuanian University of Health Sciences, Neuroscience Institute.

Local organizing committee:

Dr. Ieva Sarapinienė, Lithuanian University of Health Sciences, Institute of Cardiology,

Dr. Lina Kraujalienė, Lithuanian University of Health Sciences, Institute of Cardiology,

Dr. Rokas Mickus, Lithuanian University of Health Sciences, Institute of Cardiology,

Dr. Rimantas Treinys, Lithuanian University of Health Sciences, Institute of Cardiology,

Dr. Vilmantas Pupkis, Vilnius University, Life Sciences Center,

Dr. Greta Butkienė, National Cancer Institute,

Dr. Paulius Ruzgys, Vytautas Magnus University, Research Institute of Natural and Technological Sciences,

Neringa Barauskaitė-Šarkinienė, Vytautas Magnus University, Research Institute of Natural and Technological Sciences,

Dr. Tadas Kraujalis, Lithuanian University of Health Sciences, Institute of Cardiology.

Program

Day 1 – October 3rd (Thursday) 2024			
Time	Presenter	Institution	Title of the Lecture
8.30-9.00 Hall	Registration of the participants		
A-202	***Opening Ceremony*** Prof. Saulius Šatkauskas		
9.00-9.05	Chairman of Lithuanian Biophysical Society **Prof. Saulius Šatkauskas**	Vytautas Magnus University, **Lithuania**	Welcome address
9.05-9.10	Dean of the Faculty of Pharmacy **Prof. Ramunė Morkūnienė**	Lithuanian University of Health Sciences, **Lithuania**	Welcome address
9.10-9.15	Head of the Scientific Committee **Prof. Vytenis Arvydas Skeberdis**	Lithuanian University of Health Sciences, **Lithuania**	Conference agenda
A-202	***Session 1*** Chairmen – Prof. Saulius Šatkauskas and Prof. Vytenis Arvydas Skeberdis		
9.15-10.00	**Prof. Maria Sunnerhagen** *Keynote, K*	Linköping University, **Sweden**	The Marvelously Complex MYC - understanding an IDP in action
10.00-10.30	**Dr. Gražvydas Lukinavičius** *Invited, I01*	Max Planck Institute for Biophysical Chemistry, Göttingen, **Germany**	Labeling biomolecules for live-cell nanoscopy
10.30-11.00	**Prof. Yaw-Kuen Li** *Invited, I02*	National Yang Ming Chiao Tung University, **Taiwan**	Innovative Diagnostics – from one drop to one breath
11.00-11.30 Hall	***Coffee Break***		
A-202	***Session 2*** Chairmen – Prof. Ričardas Rotomskis and Dr. Vilmantas Pupkis		
11.30-12.00	**Prof. Reet Kurg** *Invited, I03*	Institute of Technology, University of Tartu, **Estonia**	Extracellular vesicles as carriers of biological material
12.00-12.15	**Dr. Giedrė Valiulienė** *O01*	Vilnius University, Life Sciences Center, **Lithuania**	The influence of microRNA-146a-5p on the effect of transcranial magnetic stimulation therapy
12.15-12.30	**Dr. Martynas Gavutis** *O02*	Department of Nanoengineering, Center for Physical Sciences and Technology, Vilnius, **Lithuania**	Sparsely tethered biomimetic membrane for analytical assays
12.30-12.45	**Dr. Rima Budvytytė** *O03*	Vilnius University, Life Sciences Center, **Lithuania**	The Interaction of Heat Shock Proteins with Lipid Membranes: Novel Diagnostic Target

12.45-13.40	***Lunch Break***		
13.40-15.00 Hall	***Poster Session & Coffee Break***		
A-202	***Session 3*** Chairmen – Dr. Gytis Baranauskas, Dr. Regina Mačianskienė		
15.00-15.30	**Dr. Samuel Solomon** *Invited, I04*	University College London, **UK**	Layer-specific conjunction of visual and locomotor signals in mouse superior colliculus
15.30-16.00	**Prof. Ziad M. Hafed** *Invited, I05*	Werner Reichardt Centre for Integrative Neuroscience (CIN), and Hertie Institute for Clinical Brain Research, **Germany**	Vision-for-perception versus vision-for-action: dissociable contributions of primate primary visual cortex and superior colliculus visual responses to active orienting
16.00-16.30	**Dr. Gytis Baranauskas** *Invited, I06*	Lithuanian University of Health Sciences, **Lithuania**	How the primary visual cortex processes information - insights gained from optogenetic stimulation
16.30-17.00	**Dr. Adam Williamson** *Invited, I07*	St. Anne's University Hospital, Brno, **Czech Republic**	Clinical Results of Non-invasive Deep Brain Stimulation in Epilepsy and Parkinson's patients using Temporal Interference
18.00-19.00	***Lithuanian Biophysical Society (LBFD) members meeting*** ***Visiting of museum of the History of Lithuanian Medicine and Pharmacy (the number of visitors is limited)***		
19.00-22.00	***Gala Dinner at Volfas Engelman Gallery, Kaunakiemio st. 2, Kaunas***		

Day 2 – October 4th (Friday) 2024			
Time	Presenter	Institution	Title of the Lecture
A-202	***Session 4*** Chairmen – Prof. Daumantas Matulis, Dr. Gražvydas Lukinavičius		
9.00-9.30	**Dr. Ivana Nikić-Spiegel** *Invited, I08*	Werner Reichardt Centre for Integrative Neuroscience, Tübingen, **Germany**	Axonal injury: from advanced imaging to chemical biology-based tools for minimally invasive protein labeling
9.30-10.00	**Dr. Laura Ballerini** *Invited, I09*	SISSA, Trieste, **Italy**	Graphene to manipulate synapses, neurons and neuronal networks at the nanoscale
10.00-10.15	**Prof. Saulius Bagdonas** *O04*	Vilnius University, Faculty of Physics, **Lithuania**	Spectroscopic properties of $TPPS_4$ J-aggregates formed at different pH values
10.15-10.30	**Dr. Robertas Guzulaitis** *O05*	Vilnius University, Life Sciences Center, **Lithuania**	Activation of L2/3 neurons in the primary somatosensory cortex during motor output
10.30-10.45	**Dr. Kęstutis Maciūnas** *O06*	Lithuanian University of Health Sciences, Institute of Cardiology, **Lithuania**	Transmural Influence of Ion Currents on Cardiac Optical Maps During Ischemia: A Multidisciplinary Approach
10.45-11.15 Hall	***Coffee Break***		

A-202	***Session 5*** Chairmen – Dr. Mindaugas Zaremba, Dr. Mindaugas Šnipas		
11.15-11.45	**Dr Mindaugas Zaremba** *Invited, I10*	Vilnius University, Life Sciences Center, **Lithuania**	The missing part: the Archaeoglobus fulgidus Argonaute forms a functional heterodimer with an N-L1-L2 domain protein
11.45-12.15	**Dr. Franz-Josef Meyer-Almes** *Invited, I11*	University of Applied Sciences, Darmstadt, **Germany**	Unprecedented binding sites on HDAC enzymes
12.15-12.30	**Anastasija Kudrevceva** *O07*	Vilnius University, Life Sciences Center, **Lithuania**	Protein-ligand binding affinity prediction using descriptors derived from Voronoi tessellation
12.30-13.10	***Lunch Break***		
13.10-13.45	***Poster Session***		
A-202	***Session 6*** Chairmen – Dr. Vilma Kisnierienė, Prof. Aidas Alaburda		
13.45-14.15	**Dr. Christian Gusbeth** *Invited, I12*	Karlsruhe Institute of Technology (KIT), Institute of Pulsed Power and Microwave Technology (IHM), **Germany**	Biological Signalling Supports Biotechnology: Cell Death Triggers Protein Release from *Chlorella vulgaris*
14.15-14.45	**Dr. Petar Lambrev** *Invited, I13*	Biological Research Centre, Szeged, **Hungary**	Ultrafast energy transfer in photosynthetic supercomplexes probed by two-dimensional electronic spectroscopy
14.45-15.00	**Dr. Vilma Kisnierienė** *O08*	Vilnius University, Life Sciences Center, **Lithuania**	Do chloroplasts necessitate the action potential generation in plants?
15.00-15.15	**Gabrielė Rankelytė** *O09*	Centre for Physical Sciences and Technology, **Lithuania**	Electrostatic Interactions in Photosynthetic Complexes
15.15-15.30	***Coffee Break***		
A-202	***Session 7*** Chairmen – Prof. Vytenis Arvydas Skeberdis, Dr. Rimantas Treinys		
15.30-16.00	**Dr. Hanna Wacklin-Knecht** *Invited, I14*	Scientific Support Division, European Spallation Source ERIC, Lund, **Sweden**	A new view into the mechanism of apoptosis-regulating Bcl-2 proteins in mitochondrial membrane mimics using neutron reflection
16.00-16.15	**Prof. Anna Niedźwiecka** *O10*	Institute of Physics, Polish Academy of Sciences, Warsaw, **Poland**	Intrinsically Disordered Coral Acid-Rich Protein AGARP Regulates Calcium Carbonate Growth via Liquid Phase Separation
16.15-16.30	**Dr. Mindaugas Šnipas** *O11*	Lithuanian University of Health Sciences, Institute of Cardiology, **Lithuania**	Model-based Evaluation of Biophysical Properties of Gap Junction Channels from Electrophysiological Data recorded at Macroscopic and Single-Channel Levels
16.30-16.45	**Dr. Vytautas Raškevičius** *O12*	Lithuanian University of Health Sciences, Institute of Cardiology, **Lithuania**	Investigating Novel Connexin-43 Gap Junction Inhibitors via Computational Analysis
16.45-17.00	**Dr. Eivina Radzevičiūtė-Valčiukė** *O13*	State Research Institute Centre for Innovative Medicine, Vilnius, **Lithuania**	Changes in Immune Cell Subpopulations Following High-Frequency Nanosecond Bipolar and Unipolar Calcium Electrochemotherapy *in vivo*
17.00-17.15	***Closing Ceremony***		

Poster Presentations		
Poster	Presenter	Title
P01	Sonata Adomavičiūtė-Grabusovė	Surface Enhanced Raman Scattering (SERS) and Infrared Absorption (SEIRA) Spectroscopies for *in situ* Imaging of Biomolecules
P02	Dobilas Kirvelis	Neuro-Recursion in the Visual Analyser
P03	Martynas Vencius	Evaluation of load on bone mimicking material around the dental implant using polarized light
P04	Algis Bertulis	Expansion of perceived size of components of visual stimulus
P05	Eglė Mickevičiūtė	Mitigating bipolar cancellation effects in nano-electrochemotherapy: impact of pulse asymmetry and electric field intensity
P06	Barbora Lekešytė	The Synergy of Nisin with Nanosecond and Microsecond Pulse Bursts for Electrochemotherapy
P07	Modestas Mažerimas	Electrochemical and Morphological Insights into Colistin-Induced Reorganization of Tethered Bilayer Lipid Membranes
P08	Laura Baliulytė	A DFT study of $TPPS_4$ monomers, dimers and their absorption spectra
P09	Robertas Petrolis	Evaluation of diagnostical information carried by ECG signals registered by different lead systems: The Multivariate analysis approach
P10	Veronika Malyško-Ptašinskė	Determining the Delay between Opposite Phases of Bipolar Pulses to Optimize Electrochemotherapy
P11	Orestas Makniusevičius	The effect of the anesthetic propofol on connexins of cardiovascular system
P12	Augustinas Želvys	Investigating the Impact of Electroporation Combination with Cannabinoids on CHO-K1 cells
P13	Mindaugas Ilickas, Brigita Abakevičienė	Development and Evaluation of Biocide-Polymer Nanocomposite Coatings for Enhanced Antimicrobial Protection
P14	Raimonda Celiešiūtė-Germanienė	Investigating the Role of Plasma Voltage in Modulating PEF-Induced Effects on *Chlorella vulgaris*
P15	Paulina Malakauskaitė	Effects of Nanosecond Pulses Delivered at Ultra-High Frequency on Mitochondrial Depolarization, ROS, Cell Permeabilization and Cell Viability
P16	Miglė Šarpilo	Mechanism of CRISPR-Cas3 helicase using magnetic tweezers
P17	Marijus Plečkaitis	Nanomaterials for Bimodal Imaging: Unlocking Potential in Biomedical Applications
P18	Parveen Akhtar	Energy transfer between iron-stress-induced protein A and Photosystem I probed by two-dimensional electronic spectroscopy
P19	Gabrielė Vasiliauskaitė	Investigation of Aggregation Ability of Chlorophyllin and Chlorophyllin-Chitosan Complexes
P20	Andrius Pečiulis	Biochip for Controlled Mechanical Stress Investigations in Living Cells
P21	Adei Abouhagger	Integrated Microfluidic Chip for Cultivating and Sensing Microbial Biofilms
P22	Muhammad Usman Khalid	Chemical Synthesis of Niobium Penta-oxide Nanomaterials for the Antimicrobial Applications
P23	Elena Osteikaitė	Non-linear Microscopy for Cervical Cancer Diagnostics
P24	Justinas Venckus	Assessing Cell Viability and Electrotransfer Efficiency in the Concurrent and Separate Delivery of Proteins, Small Fluorescent Molecules, and Nucleic Acids using Varying High-Voltage Pulse Numbers
P25	Silvija Ambrazevičiūtė	Electroporation-Based Sensitization: Optimal Conditions for CHO and 4T1 Cell Lines to Balance Cell Viability and Membrane Permeabilization
P26	Edita Voitechovic	On the Way of Development of Versatile Optical Sensor for the Monitoring of the Biological Molecule Interactions by the Surface Plasmon Resonance Imaging
P27	Aras Rafanavičius	Irreversible Electroporation Across Suspension and Monolayer Cultures: A Comparative Evaluation
P28	Marija Kalnaitytė	Effects of biomolecules on the spectroscopic properties and the photostability of CdTe quantum dots
P29	Lina Kraujalienė	Molecular determinants for the differential anionic permeability of Cx26 and Cx30 channels
P30	Rimantė Bandzevičiūtė	Malignant Liver Tissue Diagnostics by Fiber Based ATR IR Spectroscopy

P31	Rimantė Bandzevičiūtė	Investigation of Myocardial Infarction Patient Derived Extracellular Vesicles by IR Spectroscopy and Gas Chromatography - Mass Spectrometry
P32	Irma Martišienė	Relaxant effect of furan-containing compounds on smooth muscles in rat prostate and aorta
P33	Domantas Peckus	Linear and nonlinear optical properties of gold nanourchins in dependence on their spike size
P34	Luka Skurdelytė	The Study of Curli protein aggregation
P35	Viktorija Karalkevičiūtė	Aggregation and liquid-liquid phase seperation of S100A proteins
P36	Gytis Baranauskas	Optogenetic analysis reveals specific synaptic pathways for ON and OFF responses in the rat visual cortex
P37	Ernestas Urbanskas	Effects of Simultaneous Transfer of Two Plasmids on Gene Electrotransfer Efficiency
P38	Aistė Peštenytė	Structural Study of S100A9 Using DEER Spectroscopy
P39	Rasa Miliukaitė	Effect of Photoactive Magnesium Chlorophyllin on *Scenedesmus* sp. Microalgae at Different Environment Conditions
P40	Vilmantas Pupkis	Inositol hexakisphosphate (IP_6) alters voltage dependence of Ca^{2+} channels in *Nitellopsis obtusa*
P41	Aušrinė Navickaitė	Discrimination of *Nitellopsis obtusa* Responses to Environmental Stressors via Fluorescence Spectroscopy
P42	Emilė Pečiukaitytė	Saturated Phospholipids for Upconverting Nanoparticles and Chlorin e6 Complex Formation
P43	Augustė Kavalevskaja	Mesenchymal Stem Cell-Mediated Nanoparticle Transfer to Cancer Cells
P44	Gerda Anužienė	Identification of Pathogenic Bacteria and Yeast by means of ATR IR Spectroscopy
P45	Monika Pankevičiūtė-Bukauskienė	A Computational Approach for Precision Targeting Cancer Cells Through the Integration of Metabolic Modelling and RNA-seq
P46	Rokas Mickus	The potency of Cx43 gap junction inhibitors is influenced by phosphorylation
P47	Austėja Mikalčiūtė	Modelling the absorption spectra of light-harvesting antenna complexes
P48	Gintarė Jančiukė	Resveratrol exerts distinct effects on intercellular communication through Cx43 and Cx45 gap junctions
P49	Gabrielė Zuokaitė	Molecular modelling and experimental examination of terpenes effects on Cx43 gap junction gating
P50	Ieva Lankutytė	Effects of cardiotropic drugs on vascular stiffness and diastolic pressure ratio
P51	Dominyka Adamonė	Optical and transmural microelectrode investigations of rabbit cardiac electrical activity after electroporation
P52	Julija Arbačiauskaitė	The activity of the rodent primary auditory cortex during the circadian rhythm
P53	Tadas Kraujalis	Impact of N-Terminus Mutations on Voltage Gating in Connexin-36 Channels: A Biophysical and Computational Study
P54	Eglė Vansevičiūtė	Environmental factors affecting the efficiency of nystatin on *Candida* spp. yeasts
P55	Tomas Stanevičius	Study of Xylose Transport in Modified *Ogataea polymorpha* Yeast During Alcoholic Fermentation
P56	Alėja Marija Daugėlaitė	Mesenchymal Stem Cells as Nanocomplex Vehicles to Colon Cancer Cells of Distinct Phenotype
P57	Justina Miknaitė	Effect of Environmental Conditions on β2-Microglobulin Liquid-Liquid Phase Separation
P58	Greta Tamoliūnaitė	Atomic Force Microscopy of $TPPS_4$ Aggregates
P59	Tomas Klinavičius	Colloidal Silver Nanoparticle Size Distribution Determination from UV–Vis Extinction Spectra Using Deep Learning
P60	Virginija Dudutienė, Daumantas Matulis	Design and Synthesis of Novel Covalent CAIX Inhibitors

P61	Lukas Keršys	AI-Driven Analysis of Cell Imaging
P62	Agnė Kalnaitytė-Vengelienė	Spectroscopic studies of effects of CuInZnS/ZnS quantum dots on green microalgae
P63	Jekaterina Skibickaja	Influence of Cell Shape on Lipid Droplet and Plasma Membrane Microviscosity in Mesenchymal Stem Cells
P64	Paulius Ruzgys	Enhanced Gene Delivery by Combining Nanosecond Electric Pulses with Low-Amplitude Continuous Waves
P65	Viktoras Mažeika	Double Stokes polarimetry: a novel method for investigating fibrillar structures with SHG microscopy
P66	Nataša Svirskienė	Effects of Metformin on Spontaneous Ca^{2+} Signals in Cultured Microglia Cells under Normoxic and Hypoxic Conditions
P67	Simona Steponkienė	Targeted Therapy of Cancer by Multifunctional Nanoplatforms and Mesenchymal Stem Cells
P68	Shahd Elkhider	Mechanical Resistance of Spray-Coated Antiviral Coatings Based on fs-Laser Ablated Copper Nanoparticles
P69	Indrė Lapeikaitė	Intercellular electrical communication in macroalgae: investigation of glutamate-induced modulations of action potential propagation and transmission
P70	Rimgailė Tamulytė	Detergent-Like Membrane Solubilization Induced by the Pro-Inflammatory S100A8 Protein
P71	Vilius Poderys	Investigation of Novel Upconverting Nanoparticle – Bovine Serum Albumin Stabilised Gold Nanoclusters – Chlorin e6 Photo Drug Platform for PDT
P72	Vilius Poderys	Theoretical modelling of self-assembling $TPPS_4$ and $TPPS_3$ supramolecular aggregates of core-tail J-type
P73	Augustas Morkvėnas	Morphology-Dependent Effects of $GdPO_4:Eu^{3+}$ nanoparticles on *Daphnia magna*
P74	Džiugas Jurgutis	Monitoring Lipid Droplet Microviscosity After Mesenchymal Stem Cell Differentiation
P75	Goda Mažeikaitė	A spectroscopic study of photosensitizers: riboflavin and magnesium chlorophyllin
P76	Artūras Polita	Revealing Lipid Order Differences Between Cancerous and Non-Cancerous Cells Using Fluorescent Viscosity Probes
P77	Ugnė Borinskytė	Impact of Microsecond and Nanosecond Pulses on the Bystander Effect
P78	Skaistė Talanovaitė	Spectroscopic studies of $TPPS_4$ and $TPPS_3$ Aggregation
P79	Rūta Bagdonaitė	Effect of Alkylphospholipids on the Biophysical Properties of Model Lipid Bilayers
P80	Austėja Bareikytė	Prostate Cancer Imaging with Nonlinear Optical Microscopy
P81	Neringa Barauskaitė-Šarkinienė	Bystander Effect Induced by Combined Calcium Electroporation, Bleomycin Electrotransfer, and Irreversible Electroporation
P82	Ernestas Urniežius	Enhancing Precision in Computational Drug Design: The Role of Intrinsic Versus Observed Binding Parameters
P83	Gintautas Saulis	Comparison of the Thresholds for Electroporation and Excitation for Pulses within Nanosecond–Millisecond Duration Range
P84	Gintautas Saulis	Generation of Hypochlorous Acid by High-Voltage Pulses and its Influence on the Cell Plasma Membrane
P85	Baltramiejus Jakštys	Behaviour and importance of annexin A4 protein for active membrane repair after electroporation
P86	Vilius Marma	The Influence of Circular Arcs on Length Perception
P87	Paulius Andriūnas	Lateral Diffusion in Biocompatible Stainless Steels During Patterned Plasma Nitriding

Oral Presentations

The Marvelously Complex MYC - understanding an IDP in action

Maria Sunnerhagen[1]

[1]Department of Physics, Chemistry and Biology, Campus Valla, Linköping University, Sweden
maria.sunnerhagen@liu.se

The MYC protein is a master transcription factor involved in the regulation of numerous pathways important for normal cellular growth and function. Deregulation of MYC is a well-known risk factor and driver in both neuronal and nonneuronal tumour types, making the MYC oncoprotein a key player in several human cancers. Tight regulation of MYC at multiple levels including transcriptional, translational and/or post-transitional levels, is thereby essential to avoid tumour development and progression. It has been shown that interrupting such regulation leads to tumor shrinkage by apoptosis, but since MYC has extensive IDP properties, specific targeting has been hampered by lack of knowledge on how to pursue such interruption in vivo. In our research, we investigate the biophysical properties of MYC and its interactions using a full range of methods, extending from NMR, crystallography and SAXS/SANS over biophysical methods such as ITC, SPR, nanoDSF and mass spectrometry (BioID, HDX), to cell biology analysis in cellulo and in-vivo. Our long-term aim is to facilitate targeting of MYC in therapeutic contexts.

Labeling biomolecules for live-cell nanoscopy

Gražvydas Lukinavičius[1]

[1]Chromatin Labeling and Imaging research group, Department of NanoBiophotonics, Max Planck Institute for Multidisciplinary Sciences, Am Fassberg 11, 37077 Göttingen, Germany
grazvydas.lukinavicius@mpinat.mpg.de

A large toolbox of fluorescent dyes and proteins enables highlighting cellular structures of interest and following their dynamics in living cells. Small fluorescent probes are especially useful because they're easy to use and don't require changing the cell's genes. These probes are made by combining a desired fluorophore with a targeting moiety – a well characterized high affinity ligand or inhibitor binding to a particular biomolecule. Theoretically, this modular design can provide almost endless colour palette of the probes. In practice, it can be challenging to find the right combination of fluorophore, targeting molecule, and linker molecule to make a probe that works well. The probe's behaviour is influenced by multiple factors: aggregation, metabolism, off-target interactions, efflux and binding to extracellular structures or proteins. I will exemplify this by examining a several series of the probes targeting DNA and cytoskeletal proteins. The optimized probes yield images of outstanding quality in stimulated emission depletion (STED) and single molecule localization (SML) nanoscopy of living and fixed cells.

Invited presentation

Innovative Diagnostics --- from one drop to one breath

Yaw-Kuen Li[1], Ko Shing Chang[1], Jeng-Tzong Sheu,[2] Ping-Hsien,[3]
[1]National Yang-Ming Chiao Tung University, Department of Applied Chemistry, Hsinchu, Taiwan
[2] National Yang-Ming Chiao Tung University, Institute of Biomedical Engineering, Hsinchu, Taiwan
[3] National Taiwan University Hospital, Institute of Pulmonary Medicine, Hsinchu, Taiwan
ykl@nycu.edu.tw

The silicon nanowire field-effect transistor (SiNW-FET) is one of the most sensitive and powerful biosensors. Detection is based on the variation in conductivity caused by a disturbance in charge on the surface of the SiNW-FET, which is only induced by charged analytes including proteins, DNA, antibodies, and viruses. To overcome a SiNW-FET's inherent inability to sense non-charged molecules, such as steroids, is a challenging project. This objective was achieved by engineering Δ^5-3-ketosteroid isomerase with a carbon chain-linked 1,5-EDANS moiety to act as a steroid acceptor. The protein was further immobilized on nanowire surfaces. As a result, the negatively charged 1,5- EDANS moiety, which occupies the steroid-binding site, is ejected and exposed to the nanowire surface in the presence of a steroid. Using the electrical response produced by the 1,5-EDANS moiety, the steroid concentration is calculated. A femtomolar level of sensitivity can be achieved with this novel nano-bio-device.[1]

Breathomics is a non-invasive approach that analyzes volatile organic compounds (VOCs) in exhaled breath for medical diagnostic purposes. As part of our project, we will develop a data base of VOCs for the purpose of predicting disease. By using selected-ion flow-tube mass spectrometry (Sift- MS), breath samples from over 6000 individuals were quantitatively analyzed on more than 300 selected VOCs. The prediction accuracy of the Random Forest model was 91% for the interstitial lung disease (ILD) study. The accuracy of lung cancer prediction with XGBoost modelling is 95%.[2] In conjunction with extensive blood checkup data, our data base can be very useful for developing non-invasive, intelligent diagnoses.

Invited presentation

[1] K. S. Chang, C. C. Chen, J.-T. Sheu, and Y.-K. Li, *Sensors and Actuators, B: Chemical*, **138**, 148-153 (2009)
[2] P. H. Tsou, Z. L. Lin, Pan, *et al Cancers*, **13**, 1-14. (2021).

Extracellular vesicles as carriers of biological material

Reet Kurg[1]

[1]Institute of Technology, University of Tartu, Nooruse 1, 50411 Tartu, Estonia
reet.kurg@ut.ee

Extracellular vesicles (EVs) are a heterogenous group of membrane vesicles released into the extracellular space by all types of cells. EVs contain the content of its origin cells and carry a cargo of soluble and membrane-bound proteins, lipids, metabolites and nucleic acids. They are involved in cell-cell communication through regulation of a range of biological processes. EVs are potential candidates for medical applications as biomarkers in diagnostics and show substantial promise as novel treatment strategies of diseases. EVs possess a number of characteristics that qualify them as promising vehicles for drug delivery. The origin, biogenesis and targeting of EVs will be discussed in the light of EV features that are relevant for targeted drug delivery.

Invited presentation

Layer-specific conjunction of visual and locomotor signals in mouse superior colliculus

Stefano Zucca[1], Auguste Schulz[2], Aman Saleem[1], Samuel Solomon[1]

[1] Institute of Behavioural Neuroscience, University College London, London, United Kingdom
[2] Machine Learning in Science, University of Tübingen & Tübingen AI Center, Tübingen, Germany
s.solomon@ucl.ac.uk

The meaning of sensory signals is often critically ambiguous. For example, a looming visual image may signal the presence of an approaching predator, or the entrance to a place of refuge. Organisms could resolve some of this ambiguity by establishing whether a pattern of visual stimulation matches that expected from their self-movement, or is more likely to arise from object movement. We therefore asked whether self- and object movement produce different patterns of neural activity in superior colliculus (SC), an evolutionarily conserved, multimodal brain area implicated in visually-guided approach and avoidance.

We used high-density electrodes to record neural activity from superficial (SCs) and intermediate (SCim) layers while animals either approached an object, or the same object loomed toward it, in virtual reality. The virtual environment appeared immersive - animals quickly ran towards the object when its virtual movement was matched to their locomotion, and usually stopped moving when the same virtual object moved independently.

We found that neural activity in SCs was dominated by visual response – most neurons had small receptive fields, and were highly active when the edge of the object passed through their receptive field. Neural activity in SCim showed greater influence of self-movement (locomotion) – many neurons showed large visual receptive fields, and activity in most neurons was highly dependent on whether the animal was moving or not. To establish whether convergence of visual and locomotion signals could allow animals to distinguish the cause of visual loom we measured population activity during approach and loom conditions, and applied logistic regression. We found that SC activity, particularly SCim activity, could reliably categorise epochs of time as arising from approach or loom, even when these involved identical sequences of visual images.

We conclude that convergence of visual and locomotion signals in SC, particularly SCim, could allow animals to know whether visual stimulation results from self-movement or may indicate potential threat.

Invited presentation

Vision-for-perception versus vision-for-action: dissociable contributions of primate primary visual cortex and superior colliculus visual responses to active orienting

Ziad M. Hafed[1,2]

[1]Werner Reichardt Centre for Integrative Neuroscience (CIN), University of Tübingen, Otfried-Müller-Str. 25, 72076 Tübingen, Germany
[2]Hertie Institute for Clinical Brain Research, University of Tübingen, Otfried-Müller-Str. 27, 72076 Tübingen, Germany
ziad.m.hafed@cin.uni-tuebingen.de

The primary visual cortex (V1) directly projects to the superior colliculus (SC) and is believed to provide sensory drive for eye movements. Consistent with this, a majority of saccade-related SC neurons also exhibit short-latency, stimulus-driven visual responses, which are additionally feature-tuned. However, direct neurophysiological comparisons of the visual response properties of the two anatomically-connected brain areas are surprisingly lacking, especially with respect to active looking behaviors. I will describe a series of experiments characterizing visual response properties in primate V1 and SC neurons, exploring feature dimensions like visual field location, spatial frequency, orientation, contrast, and luminance polarity. The results suggest a substantial, qualitative reformatting of SC visual responses when compared to V1. For example, SC visual response latencies are actively delayed, independent of individual neuron tuning preferences, as a function of increasing spatial frequency, and this phenomenon is directly correlated with saccadic reaction times. Such "coarse-to-fine" rank ordering of SC visual response latencies as a function of spatial frequency is much weaker in V1, suggesting a dissociation of V1 responses from saccade timing. Consistent with this, when we next explored trial-by-trial correlations of individual neurons' visual response strengths and visual response latencies with saccadic reaction times, we found that most SC neurons exhibited, on a trial-by-trial basis, stronger and earlier visual responses for faster saccadic reaction times. Moreover, these correlations were substantially higher for visual-motor neurons in the intermediate and deep layers than for more superficial visual-only neurons. No such correlations existed systematically in V1. Thus, visual responses in SC and V1 serve fundamentally different roles in active vision: V1 jumpstarts sensing and image analysis, but SC jumpstarts moving. I will finish by demonstrating, using V1 reversible inactivation, that, despite reformatting of signals from V1 to the brainstem, V1 is still a necessary gateway for visually-driven oculomotor responses to occur, even for the most reflexive of eye movement phenomena. This is a fundamental difference from rodent studies demonstrating clear V1-independent processing in afferent visual pathways bypassing the geniculostriate one, and it demonstrates the importance of multi-species comparisons in the study of oculomotor control.

Invited presentation

How the primary visual cortex processes information - insights gained from optogenetic stimulation

Gytis Baranauskas[1]

[1]Laboratory of Neurophysiology, Neuroscience Institute, Lithuanian University of Health Sciences, Kaunas, Lithuania gytis.baranauskas@lsmu.lt

The primary visual cortex or area V1 is the most studied visual area in the brain, and, probably, one of the most studied brain areas in general. There is a good reason for that. In the primary visual cortex, the sensory inputs are well defined, they represent images. Moreover, a good deal is known what image features are mostly represented by V1 neurons. Every V1 neuron responds only to images presented inside the receptive field (RF), a small fraction of the viewing field. Although many stimulus features/parameters may influence responses, the visual response amplitude mainly depends on the stimulus orientation, movement direction and size. In spite of multiple studies addressing the mechanisms of orientation and direction selectivity in the primary visual cortex, one of the main issues, the contribution of two major cell types, the pyramidal neurons and the interneurons, to the selectivity of visual responses in area V1 was unsettled before the era of optogenetics.

It is not surprising that, when an over a decade ago the first optogenetic tools suitable to study interneuron function appeared, almost all optogenetic studies on V1 focussed on the issues of orientation and direction selectivity. Surprisingly, other fundamental features of the area V1 neurons, such as signal-to-noise ratio (SNR) and the RF area were hardly investigated. Therefore, my focus was to study these two parameters of visual neurons since they directly determine visual information content of a neuron: the location of the visual stimulus can be pinpointed more accurately if the RF area is reduced, and a visual stimulus can be detected with fewer errors if SNR is increased.

It turns out that optogenetic stimulation of either pyramidal neurons or interneurons leads to the same result, an increased SNR, and a reduced RF area of both pyramidal cells and interneurons. Thus, both types of stimulation increase information content of area V1 neurons. Stimulation of interneurons produces an overall inhibitory effect; however, this effect is more pronounce on noise than on the visual responses, therefore the SNR is improved. Similarly, the inhibitory effect on RF flanks is more pronounced than in the RF centre leading to the reduced RF area. Stimulation of pyramidal neurons immediately activates inhibitory interneurons, that in turn suppress their activity, leading to an overall inhibitory effect. Moreover, these two effects can be observed on both ON and OFF types of responses, that are triggered by the bright stimulus onset and offset respectively. Interestingly, the effects on ON and OFF responses are independent, i.e., at a single neuron level the effect size on the ON response does not predict the effect size on the OFF response. Nevertheless, on average, the effect size on both types of responses is similar, suggesting the presence of a global control of the balance between ON and OFF responses.

It is concluded that pyramidal neurons are connected with each other by at least two types of negative feedback pathways selective to ON and OFF responses. In addition, there is a global network that balances both the amplitude and the RF area of ON and OFF responses.

Invited presentation

Clinical results of non-invasive deep brain stimulation in epilepsy and Parkinson's patients using temporal interference

Adam Williamson[1]

[1]St. Anne's University Hospital (FNUSA), Pekařská 53, 602 00, Brno, Czech Republic
adam.williamson@fnusa.cz

Temporal Interference Stimulation (TIS) is an innovative non-invasive brain stimulation technique which enables targeted modulation of deep brain structures by applying high-frequency electrical fields. In this study, we present clinical results from two patient cohorts: those with medication-refractory mesiotemporal epilepsy (MTLE) and those with Parkinson's disease (PD).

In the epilepsy cohort, TIS targeted the hippocampus in 13 patients with stereoelectroencephalography (sEEG) depth electrodes. TIS at an envelope frequency of 130 Hz significantly reduced interictal epileptiform discharges (IEDs) and high-frequency oscillations (HFOs), including fast ripples, suggesting its potential as a non-invasive alternative for neuromodulation in epilepsy.

In the Parkinson's cohort, TIS targeted the subthalamic nucleus (STN) in 7 patients. The results demonstrated a significant reduction in pathological beta oscillations, similar to those achieved by conventional deep brain stimulation (DBS), indicating that TIS can effectively modulate motor symptoms in PD patients without the need for invasive surgery.

These findings highlight TIS as a promising tool for non-invasive deep brain stimulation, offering potential therapeutic benefits for patients with epilepsy and Parkinson's disease, particularly for those who are not candidates for traditional surgical interventions. Further research is warranted to explore long-term outcomes and refine stimulation parameters for individualized treatment.

Invited presentation

Axonal injury: from advanced imaging to chemical biology-based tools for minimally invasive protein labeling

Ivana Nikić-Spiegel[1]

[1]Werner Reichardt Centre for Integrative Neuroscience, University of Tübingen, Otfried-Müller-Straße 25, 72076 Tübingen, Germany
ivana.nikic@cin.uni-tuebingen.de

The growing demands of advanced fluorescence and super-resolution microscopy benefit from the development of small and highly photostable organic fluorescent dyes. However, direct attachment of organic dyes to the protein of interest remains challenging. This challenge can be addressed by labelling unnatural amino acids (UAAs) with click chemistry.

Techniques developed to expand the genetic code permit the residue-specific encoding of UAAs armed with "clickable" chemical handles into proteins. Such UAAs can be labeled with tetrazine-functionalized organic dyes with bioorthogonal click chemistry in living cells. The minimal size of the UAA and the possibility to couple the fluorophores directly to the protein of interest with single-residue precision in living cells are the main advantages of this labelling approach.

However, until recently, click chemistry-based protein labelling has only been used in conventional cell lines, and not in complex, non-dividing cells, such as primary neurons. In my presentation, I will discuss our recent work in which we established and applied this type of labelling for advanced microscopy studies of different classes of neuronal proteins, including cytoskeletal elements [1] and ion channels [2].

Invited presentation

[1] Arsić A, Hagemann C, Stajković N, Schubert T, Nikić-Spiegel I. Minimal genetically encoded tags for fluorescent protein labeling in living neurons. Nat Commun. 2022;13(1):314. Published 2022 Jan 14. doi:10.1038/s41467-022-27956-y

[2] Stajković N, Liu Y, Arsić A, et al. Direct fluorescent labeling of NF186 and NaV1.6 in living primary neurons using bioorthogonal click chemistry. J Cell Sci. 2023;136(12):jcs260600. doi:10.1242/jcs.260600

Graphene to manipulate synapses, neurons, and neuronal networks at the nanoscale

Laura Ballerini[1]

[1]International School for Advanced Studies (SISSA), Via Bonomea, 265, 34136 Trieste, Italy
laura.ballerini@sissa.it

In neural interface engineering, the use of carbon-based nanomaterials has opened an additional area of development. This area exploits the (nano)material-properties in the production of bioactive interfaces for long-term implantation. In recent years, we have gained an improved understanding of micro and nano-engineered materials developed to investigate emergent biological adaptive and integrated behaviors. This new class of materials can improve exploring fundamental biological phenomena as well as contribute to biomedical and clinical applications. I will present our results concerning carbon-based nanomaterials, I will describe the effects of such materials on neuron signalling when synaptic function and plasticity are modulated by tight interactions between the biosystem and the nanomaterials, in vitro and in vivo.

Invited presentation

The missing part: the *Archaeoglobus fulgidus* Argonaute forms a functional heterodimer with an N-L1-L2 domain protein

Elena Manakova[1], Edvardas Golovinas[1], Reda Pocevičiūtė[1], Giedrius Sasnauskas[1], Arunas Silanskas[1], Evelina Zagorskaitė[1], Edvinas Jurgelaitis[1], Algirdas Grybauskas[1], Česlovas Venclovas[1], Mindaugas Zaremba[1]

[1]Vilnius University, Department, Life Sciences Center, Institute of Biotechnology, Vilnius, Lithuania
mindaugas.zaremba@bti.vu.lt

Argonaute (Ago) proteins are present in all three domains of life (bacteria, archaea and eukaryotes). They use small (15-30 nucleotides) oligonucleotide guides to bind complementary nucleic acid targets and are responsible for gene expression regulation, mobile genome element silencing, and defence against viruses or plasmids. According to their domain organization, Agos are divided into long and short Agos. Long Agos found in prokaryotes (long-A and long-B pAgos) and eukaryotes (eAgos) comprise four major functional domains (N, PAZ, MID and PIWI) and two structural linker domains L1 and L2. The majority (~60%) of pAgos are short pAgos, containing only the MID and inactive PIWI domains. Here we focus on the prokaryotic Argonaute AfAgo from *Archaeoglobus fulgidus* DSM4304. Although phylogenetically classified as a long-B pAgo, AfAgo contains only MID and catalytically inactive PIWI domains, akin to short pAgos. We show that AfAgo forms a heterodimeric complex with a protein encoded upstream in the same operon, which is a structural equivalent of the N-L1-L2 domains of long pAgos [1]. This complex, structurally equivalent to a long PAZ-less pAgo, outperforms standalone AfAgo in guide RNA-mediated target DNA binding. Our findings provide a missing piece to one of the first and the most studied pAgos.

Funding: this work was supported by the Research Council of Lithuania (LMTLT) [S-MIP-23-131 and S-MIP-20-37 to M.Z.].

Invited presentation

[1] Nucleic Acids Res. 2024 Mar 21;52(5):2530-2545. doi: 10.1093/nar/gkad1241

Unprecedented binding sites on HDAC enzymes

Franz-Josef Meyer-Almes[1]

[1]Department of Chemical Engineering and Biotechnology, University of Applied Sciences Darmstadt, Stephanstr. 7, 64295 Darmstadt, Germany
pfranz-Josef.meyer-almes@h-da.de

Screening of ultra-low-molecular weight ligands successfully identified viable chemical starting points for a variety of drug targets. Here we report electrophilic fragments that allow the mapping of potential binding sites for covalent inhibitors by biochemical screening and mass spectrometry (Fig. 1). Small electrophilic heterocycles and their N-quaternized analogues were first characterized in the glutathione assay to analyze their electrophilic reactivity. Next, the library was used for systematic mapping of potential covalent binding sites available in human histone deacetylase 8 (HDAC8). The covalent labeling of HDAC8 cysteines has been proven by tandem mass spectrometry measurements, and the observations were explained by mutating HDAC8 cysteines. As a result, screening of electrophilic MiniFrags identified three potential binding sites suitable for the development of allosteric covalent HDAC8 inhibitors. One of the hit fragments was merged with a known HDAC8 inhibitor fragment using different linkers, and the linker length was optimized to result in a lead-like covalent inhibitor.

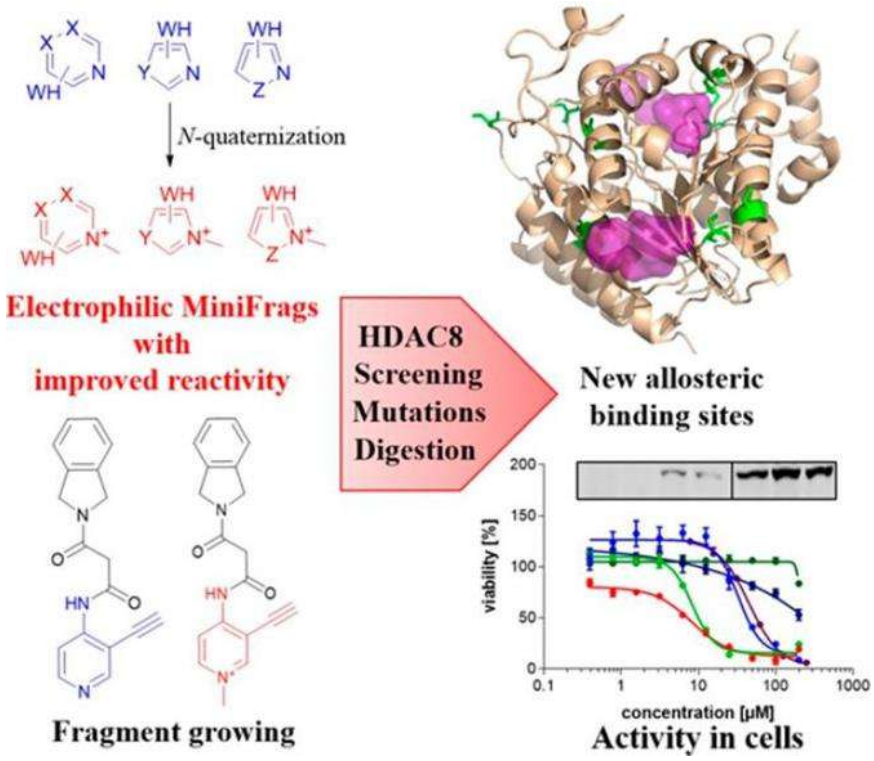

Fig. 1. Scheme of biophysical screening of low-molecular-weight fragments (MiniFrags)

Invited presentation

[1] A.B. Keeley, A. Kopranovic, V. Di Lorenzo et al. Electrophilic MiniFrags Revealed Unprecedented Binding Sites for Covalent HDAC8 Inhibitors. *J. Med. Chem.* **67**, 572-585 (2024).
[2] L. Petri, P. Abranyi-Balogh, I. Timea et al. Assessment of Tractable Cysteines for Covalent Targeting by Screening Covalent Fragments. *Chembiochem*, **22**, 743-753 (2021).

Biological Signalling Supports Biotechnology: Cell Death Triggers Protein Release from *Chlorella vulgaris*

Christian Gusbeth, Alexander Müller, Wolfgang Frey

Karlsruhe Institute of Technology (KIT), Institute of Pulsed Power and Microwave Technology (IHM), Hermann-von-Helmholtz-Platz 1, 76344 Eggenstein-Leopoldshafen, Germany

Multiple studies have demonstrated that following Pulsed Electric Fields (PEF) treatment, an incubation period exceeding 6 h in buffer is necessary to enhance the bio-accessibility of cell components such as proteins and lipids. This enhancement is primarily attributed to enzymatic processes activated during incubation, which facilitate the release of proteins and promote the solvent extraction of lipids from various microalgal species. The induction of this autolytic process can be triggered by various means, including dark anoxia, where microalgae are incubated in darkness for 24 to 48 h, or even by PEF treatment with very low specific energies (< 5 J/g). Notably, in *Chlorella vulgaris*, there's evidence suggesting the presence of a specific cell death inducing factor (CDIF) of protein origin, which triggers cell death in intact cells. The prevailing concept suggests that CDIF plays a pivotal role during the algae incubation period post-PEF treatment, prompting cell death and subsequent autolytic processes, thereby enhancing the extraction process. The search for the identity of the CDIF led to the assumption that radical oxygen species (ROS) may play a decisive role as signalling molecules, which are involved in many cell signalling pathways. To investigate this mechanism, we examined the intra- and intercellular ROS production during the incubation of fresh algal suspensions with algal extract containing CDIF, as well as with extract alone. While algal cell death induced by PEF treatment, even at low specific energies, resulted in a significant increase in intracellular ROS, no alterations in inter- and intracellular ROS were observed during cell incubation with CDIF-containing extract. This discrepancy may be attributed to the extract's antioxidant-rich composition, which not only contains CDIF but also suppresses ROS levels. This observation suggests that ROS depletion disrupts cell signalling pathways, ultimately leading to programmed cell death. To validate this hypothesis, we evaluated the cytotoxicity of antioxidants such as Trolox, glutathione, and ascorbic acid on algal cells at various concentrations. Surprisingly, ascorbic acid increased algal mortality over a 24 h incubation period and promoted the release of proteins, correlating with algal mortality. Based on these insights, we investigated the potential of enhancing the extraction process by combining PEF treatment with a subsequent incubation step in the presence of ascorbic acid. Our investigation unveiled a significant increase in protein yield compared to applying PEF treatment alone. This finding bears significance as the synergistic application of cell disruption and ascorbic acid not only enhances the yield of extracted cell components from algae but also shields them from oxidative degradation. This would allow for the development of new downstream processes that align with environmentally conscious practices, marking a significant step towards a more sustainable and efficient approach in biotechnological applications.

Invited presentation

Inter-subunit energy transfer in photosynthetic supercomplexes observed by two-dimensional electronic spectroscopy

Petar H. Lambrev[1], Parveen Akhtar[1,2], Sumit Singhal[1], Howe-Siang Tan[3]

[1]HUN-REN Biological Research Centre, Szeged, Hungary
[2]ELI-ALPS, Szeged, Hungary
[3]School of Chemistry, Chemical Engineering and Biotechnology, Nanyang Technological University, Singapore
lambrev.petar@brc.hu

Photosynthesis is a fundamental biological process sustaining virtually all life on Earth. All oxygenic photosynthetic organisms, from the most ancient cyanobacteria to higher plants, share common basic mechanisms and biochemical components. This includes the reaction centres of the photosystems - I and II - that work in tandem to extract electrons and protons to produce ATP and NADPH that is then used for the fixation of carbon dioxide. Despite the evolutionary conservative nature of the photosynthetic machinery, photosynthetic organisms have evolved remarkably diverse light-harvesting antenna systems adapted and tailored to the specific living conditions in each possible habitat. The light-harvesting complexes increase the absorption cross-section of the photosystems and actively and dynamically regulate the excitation flow to the reaction centres balancing efficient energy capture and photoprotection. In recent years, the structures of many different antenna-reaction centre supercomplexes have been determined potentially revealing different strategies and mechanisms ensuring efficient light harvesting. Ultrafast time-resolved spectroscopy and more specifically two-dimensional electronic spectroscopy (2DES) is a powerful tool to probe the excitation energy transfer from the antenna to the reaction centre [1]. Here we have employed 2DES to investigate the dynamics of excitation energy transfer in several types of multisubunit antenna and antenna-reaction centre supercomplexes isolated from plants and algae. A comparison between supercomplexes from plants and the diatom *Thalassiosira pseudonana* revealed markedly different antenna organizations and energy transfer dynamics [2,3]. Rapid energy transfer on timescales of a few picoseconds was measured between the fucoxanthin-chlorophyll protein (FCP) complexes and both photosystems II and I, suggesting a previously underappreciated functional aspect of the FCPs antenna system. Despite structural and dynamic differences, a universal cross-species strategy for light harvesting is proposed as a blueprint for artificial energy-converting systems.

Invited presentation

[1] P. H. Lambrev, P. Akhtar, H.-S. Tan, *BBA-Bioenergetics* **1861**, 148050 (2020).
[2] H. L. Nguyen, T. N. Do et al., *Sci. Adv.*, **10**, eadh0911 (2024).
[3] P. Akhtar, Y. Feng et al., *J. Phys. Chem. Lett.*, **15**, 5838-584 (2024).

A new view into the mechanism of apoptosis-regulating Bcl-2 proteins in mitochondrial membrane mimics using neutron reflection

Hanna Wacklin-Knecht[1,2], Sophie Ayscough[2,1], Luke Clifton[3], Jörgen Åden[1,2], Ameeq Ul Mushtaq[4], Tobias Sparrman[4], Gerhard Gröbner[4]

[1]European Spallatoin Source ERIC, Scientific Support Division, P.O.Box 176, SE- 22100 Lund, Sweden
[2]Lund University, Department of Chemistry, Division of Physical Chemistry, P.O.Box 124, SE- 22100 Lund, Sweden
[3]ISIS Pulsed Neutron and Muon Source, Rutherford Appleton Laboratory, Didcot, Oxfordshire OX11 OQX, UK
[4]Department of Chemistry, University of Umeå, SE-90187 Umeå, Sweden
hanna.wacklin-knecht@ess.eu

Mitochondrial apotosis, or programmed cell death, is an essential process that is tightly regulated by the Bcl-2 protein family. In response to apoptotic signals, pro-apoptotic Bax is recruited to the mitochondrial outer membrane (MOM) where it triggers cell death by perforating the mitochondrial outer membrane, unless it is inhibited by the Bcl-2 protein residing in the MOM. Although intensively studied, the detailed mechanism by which these proteins interact with each other and the lipids in the MOM to create apoptotic pores has remained elusive. We have developed a methodology to probe their detailed mechanism at the membrane interface using specular neutron reflection (NR) in combination with NMR and FTIR methods to probe the structural basis and kinetics of the interactions. NR of full-length Bcl-2 reconstituted into supported lipid bilayers (SLB) and solid-state NMR showed conclusively that Bcl-2 is fully embedded in the lipid bilayer [1]. Bax initially adsorbs on the lipid bilayer surface, where it creates pores by extracting lipids and forms Bax/lipid clusters that are deposited on the membrane surface, as shown in Fig. 1 [2]. Time-resolved NR and FTIR spectroscopy also revealed two kinetically distinct phases in the pore formation process, which were dependent on the levels of cardiolipin present. Lipid removal by Bax is minimal in the absence of cardiolipin, confirming its role as a key activator. Bcl-2 reconstituted into lipid bilayers does not prevent Bax binding but inhibits it by preventing lipid removal and pore formation in a concentration dependent manner [3]. Our findings provide a new view and a robust structural basis for understanding the initial steps of programmed cellular death and its regulation.

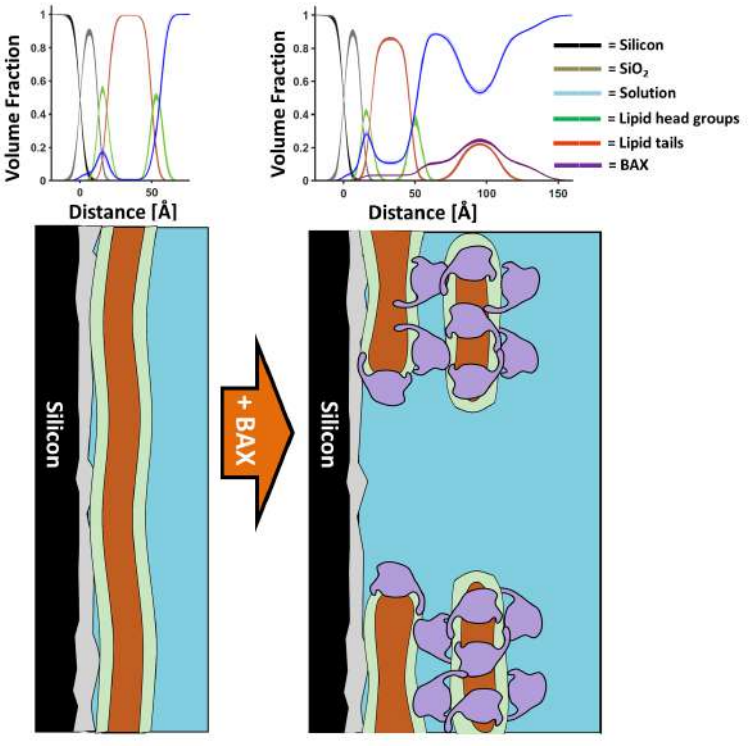

Fig. 1. A model for Bax pore formation. Component volume fraction profiles from before (A) and after (B) the interaction of Bax with mitochondrial model membranes (90 mol % POPC –10 mol % TOCL). s (C and D) show how this component distribution in the Z direction can be understood in terms of the distribution of Bax across the membrane-water interface (D)

[1] A. U. Mushtaq, J. Aden, L. A. Clifton, H. Wacklin-Knecht, M. Campana, A.P.G Dingeldein, C. Persson, T. Sparrman, G. Grobner. *Commun. Biol.* ***4***, 507 (2021).
[2] L.A. Clifton, H.P. Wacklin-Knecht, J.Ådén, A.U. Mushtaq, T. Sparrman, G. Gröbner. Science Advances. 9, eadg7940 (2023).

Invited presentation

The influence of microRNA-146a-5p on the effect of transcranial magnetic stimulation therapy

Giedrė Valiulienė[1], Aistė Zentelytė[1], Vladas Valiulis[1,2], Kastytis Dapšys[2], Arūnas Germanavičius[2], Rūta Navakauskienė[1]

[1] Vilnius University, Life Sciences Center, Institute of Biochemistry, Sauletekio av. 7, LT-10257 Vilnius, Lithuania.
[2] Vilnius, Lithuania; Republican Vilnius Psychiatric Hospital, Parko str. 21, LT-11205 Vilnius, Lithuania.
giedre.valiuliene@bchi.vu.lt

Treatment-resistant depression (TRD) is a complex issue. While repetitive transcranial magnetic stimulation (rTMS) is frequently employed, its effectiveness varies, underscoring the need for a better understanding of both depression and rTMS mechanisms. In our previous study [1], we observed significantly higher levels of pro-inflammatory interleukins-6 and -8 in TRD patients compared to drug responders, which correlated with more severe symptoms. TRD patients also exhibited higher levels of interleukin-18 and lower levels of the anti-neuroinflammatory miR-146a-5p compared to healthy controls. Expression levels of miR-16-5p, miR-93-5p, and particularly miR-146a-5p correlated with clinical changes following rTMS treatment. Our findings suggest that TRD patients are in a heightened inflammatory state, with miR-146a-5p showing potential as a predictor of rTMS success.

We expanded our study to investigate the molecular effects of rTMS in relation to miR-146a-5p inhibition and upregulation using the SH-SY5Y neural cell model. To modulate miR-146a-5p function, we used mirVana miRNA mimics and inhibitors. RNA-seq analysis revealed that in neuro-differentiated SH-SY5Y cells, inhibition of miR-146a-5p activates the expression of genes associated with neuroactive ligand-receptor interactions, while mimicking miR-146a-5p represses this expression. However, the effects of the miR-146a-5p mimic on SH-SY5Y cells were reversed upon stimulation with different rTMS protocols (both iTBS and cTBS). Additionally, iTBS stimulation in miR-146a-5p mimic-treated SH-SY5Y cells significantly repressed the expression of PDGF and NOTCH pathway genes, potentially contributing to the therapeutic effects of rTMS. Furthermore, the Agilent Seahorse Cell Mito Stress Test kit was used to assess the impact of miR-146a-5p and rTMS stimulation on mitochondrial respiration in SH-SY5Y cells. The results indicated that iTBS and cTBS stimulation caused significant differences in Basal respiration, Maximal respiration, and Spare capacity only in miR-146a-5p mimic-treated cells, but not in those treated with the inhibitor.

These findings provide new insights into the molecular mechanisms underlying rTMS treatment in TRD and suggest that miR-146a-5p modulation may play a crucial role in regulating the therapeutic efficacy of rTMS.

[1] G. Valiuliene, V. Valiulis, A. Zentelyte, et a., *Biomed Pharmacother*, **166**, 115313 (2023).

Sparsely tethered biomimetic membrane for analytical assays

Martynas Gavutis[1]

[1] Department of Nanoengineering, Center for Physical Sciences and Technology, Vilnius, Lithuania
martynas.gavutis@ftmc.lt

We describe an adjustable sparse tethering system for model lipid membrane phases.

We show that hydrophobic tethers dispersed in a stable matrix of protein-repellent molecules can be either randomly distributed over a supporting surface or phase segregated into nanoclusters of at least 40 molecules [1-2]. We determined the role of the tethering assemblies during the tethered bilayer lipid membrane (tBLM) formation from the initial intermolecular interactions in the vesicle–surface contact zone, to the resulting equilibrium tBLM by employing the MD simulation and the QCM-D real time experimental techniques. We found that either homogeneously mixed or nanocluster- forming tethers equally well promote spontaneous formation of the tBLM on SAMs. The key factors driving the vesicle fusion on this type of molecular surfaces were the tether insertion into vesicles attaching to the surface, along with their deformation [3]. Further on, we determined the interfacial tBLM structure by employing polarized neutron reflectometry (NR) technique. In addition to SAM and lipid layers we were able to parametrize the solution interlayer thickness and confirm the very low density of tethers. Finally, we reconstituted the deuterated outer membrane protein F (OmpF) into tBLMs and demonstrated the potential of our SAM platform to study more complex membrane systems.

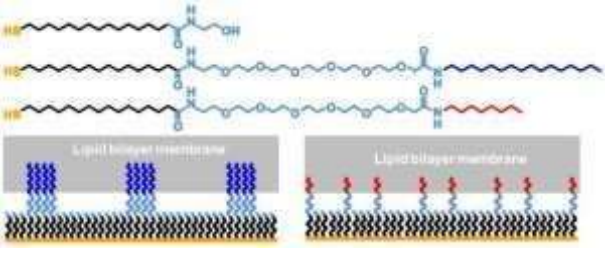

Fig. 1. Chemical structures of SAM forming compounds (top) and schematic of tethered bilayer lipid membranes (bottom).

[1] H-H Lee et al., J. Phys. Chem. B 122, 8201 (2018)
[2] E. Schulze and M. Stein, J. Phys. Chem. B 122, 7699 (2018)
[3] M. Gavutis et al., Nanoscale 15, 9759 (2023)

The Interaction of Heat Shock Proteins with Lipid Membranes: Novel Diagnostic Target

Rima Budvytyte[1], Aiste Gulla[2], Julija Razumiene[1]

[1]Institute of Biochemistry, Department of Bioelectrochemistry and Biospectroscopy, Life Sciences Center, Sauletekio av. 7, LT-10257, Vilnius
[2] Vilnius University Hospital, Santaros Clinics, Lithuania
rima.budvytyte@gmc.vu.lt

Many members of the underlying heat shock proteins (HSP) are expressed at low levels under physiological conditions and act as chaperones, while others emerge only during stressful conditions to assure cell protection by reassembling protein homeostasis and interfering with apoptotic pathways [1]. As an intracellular polypeptide HSP70 and HSP90 can be exposed on the plasma membrane and/or released into the circulation. However, the role of HSP70 and HSP90 in various nondisease and disease conditions remains unknown.

Our research experiments were designed and performed with heat shock proteins (HSP90 and HSP70) that play key role in the cell membrane damage mechanisms identified in Acute Pancreatitis (AP) and cancer and etc., cases [2], which later can be used as biomarkers for AP and cancer detections.

For the study of biomolecular interactions with membranes, we have developed tethered bilayer lipid membranes (tBLMs) as a long-term stable and versatile experimental model for protein reconstitution and for lipid-protein interaction studies [3]. In this work, different isoforms of HSP's were used to investigate their interaction with tBLM (Fig.1) [4]. These HSP's proteins exhibited the membrane damaging properties as probed by the electrochemical impedance spectroscopy (EIS). Membrane composition was found to be one of the important factors affecting the interaction of the HSP proteins to phospholipid membranes.

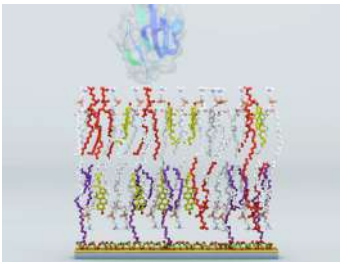

Fig. 1. Representative image of tethered lipid bilayer membranes (tBLM) interaction with HSP70.

1. I. Horváth, G. Multhoff, A. Sonnleitner, L. Vígh. *(BBA) -Biomembranes,* **1778**, 1653-1664 (2008).
2. Z. Balogi, G., Multhoff, J.T. Kirkegaard, E. Lloyd- Evans, T. Yamashima, M. Jäättelä, et al., *Progress in Lipid Research*, **74,** 18-30 (2019).
5. R. Budvytyte, F. Ambrulevičius, E. Jankaityte, G. Valincius. *Bioelectrochemistry,* **145,** 108091 (2022).
4. R.Budvytyte, A. Milasiute, D. Vitkus, K. Strupas, A. Gulla, I. Sakinyte, J. Razumiene. *Biomedicines*, **9**, 755 (2021).

Spectroscopic properties of $TPPS_4$ J-aggregates formed at different pH values

Saulius Bagdonas[1], Agnė Kalnaitytė-Vengelienė[1], Parveen Akhtar[2], Petar Lambrev[2], Virginijus Barzda[1,3,4] and Ricardas Rotomskis[1,5]

[1]Vilnius University, Faculty of Physics, Laser Research Center, Saulėtekio av. 9, III bld., Vilnius, Lithuania
[2]Eötvös Loránd Research Network, Biological Research Centre, Institute of Plant Biology, Temesvári körút 62, Szeged 6726, Hungary
[3]University of Toronto Mississauga, Department of Chemical and Physical Sciences, 3359 Mississauga Rd, Mississauga L5L 1C6, Canada
[4]University of Toronto, Department of Physics, 60 St. George St. Toronto, Toronto M5S 1A7, Canada
[5]National Cancer Institute, Biomedical Physics Laboratory, P. Baublio str. 3b, LT-08406 Vilnius, Lithuania
saulius.bagdonas@ff.vu.lt

Self-assembly of functional molecular materials into well-defined nanostructures depending on various noncovalent interactions has attracted increasing research interest for both material synthesis as well as for device integration [1]. Due to its highly conjugated structure, 5,10,15,20-tetrakis(4-sulfonatophenyl)porphyrin ($TPPS_4$) has the advantages of chemical stability and ease of structural manipulation, making it an attractive building block for self-assembly into nano- and microscale structures. The tendency of porphyrins to form molecular aggregates finds application in the production of photosensitive films or even in the creation of organic photovoltaic cells and highly functional optoelectronic devices. Indeed, it has been observed that the diprotonated form of $TPPS_4$ efficiently self-associates into large, ordered aggregates in aqueous media depending on the concentration of the compound, the ionic strength and pH value, as well as the initially chosen sequence of events that trigger the aggregation process [2]. Although the spectroscopic features and exciton interactions in $TPPS_4$ aggregates are known, it is still unclear which types of aggregates form under specific conditions and what role the different ionic forms of $TPPS_4$ play in initiating of this process.

In this work, the samples were prepared from red powder of $TPPS_4$ disodium salt by dissolving it in distilled water. Different $TPPS_4$ concentrations (from 10^{-4} M to 10^{-6} M) with pH 1 as well as three $TPPS_4$ concentrations ($5x10^{-5}$ M, $2x10^{-5}$ M and 10^{-5} M) with different pH values (from 0.5 to 4) were prepared by adding appropriate volumes of 1 M HCl to the $TPPS_4$ stock solution. Steady-state absorption, fluorescence and CD spectra were recorded to monitor time-induced spectral changes, while time-resolved measurements were performed to evaluate the spectral dependence of fluorescence intensity relaxation in a heterogeneous molecular system.

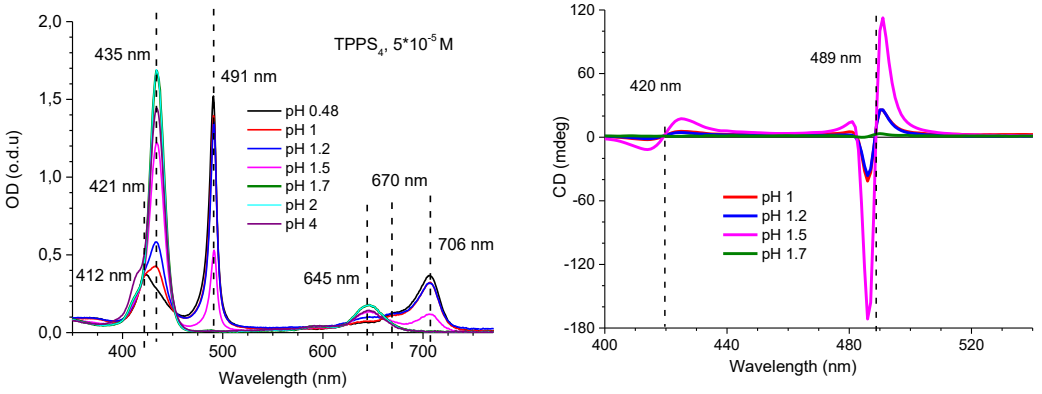

Fig. 1. Absorption spectra of $TPPS_4$ recorded at different pH values (left) and the corresponding CD spectra (right)

Analysis of spectroscopic data showed that small changes in the acidic pH range from 2 to 1 can significantly affect the formation of chiral J-aggregates in the samples (Fig. 1). In particular, $TPPS_4$ samples with the most intense absorption band at 491 nm did not show the highest intensity of the corresponding CD band, the presence of which indicates the formation of chiral compounds. Likewise, the samples possessing the highest CD signal were prepared in solutions with higher pH values than those that lead to the most rapid formation of J-aggregates. Spectroscopically determined properties of chiral J-aggregates of $TPPS_4$ will be presented and the main internal and external factors influencing their formation will be discussed.

[1] R. Y. Chakrabarty, P. S. Mukherjee, P. J. Stang, *Chem. Rev.*111, 6810-6918 (2011).
[2] R. Zagami, M. A. Castriciano, A. Romeo, and L. M. Scolaro, *J Porphyr Phthalocya.* 27, 463-470 (2023).

Activation of L2/3 neurons in the primary somatosensory cortex during motor output

Guzulaitis Robertas[1,2], Palmer Lucy M[1]

[1] Florey Institute of Neuroscience and Mental Health, University of Melbourne, Australia
[2] The Life Sciences Center, Vilnius University, Vilnius, Lithuania
robertas.guzulaitis@gmc.vu.lt

Rodents rely heavily on somatosensation to explore their surrounding environment. The primary somatosensory cortex (S1) plays a pivotal role in the encoding and perception of tactile stimuli. Although S1 neurons also receive non-tactile inputs, it remains unclear whether S1 neurons similarly encode non-tactile sensory-based behaviour.

Whole-cell patch clamp recordings were employed to investigate the voltage response of layer 2/3 (L2/3) pyramidal neurons in S1 during the execution of either a tactile-based or an auditory-based association task in mice. A robust and sustained voltage response was evoked in L2/3 pyramidal neurons during correct responses in both tasks, indicating that the response was not dependent on the delivery of the tactile stimuli. Furthermore, L2/3 pyramidal neurons were active during spontaneous motor bouts, with voltage responses starting prior to the onset of motor output. Moreover, comparable motor-related activation was also observed in L2/3 neurons in the primary motor cortex (M1). The activation of M1 neurons preceded that of S1 neurons, indicating that the latter may be driven by the former i.e. S1 driven by M1. However, optogenetic suppression of M1 did not affect the motor-correlated activity observed in the L2/3 neurons of S1. Therefore, it can be concluded that L2/3 pyramidal neurons in S1 are active during motor output, with the primary source of activation being brain areas other than M1.

Transmural Influence of Ion Currents on Cardiac Optical Maps During Ischemia: A Multidisciplinary Approach

Kęstutis Maciūnas[1,2], Vaidotas Marozas[2], Regina Mačianskienė[1], Steven E. Williams[3], Rimantas Treinys[1] and Jonas Jurevičius[1]

[1]Lithuanian University of Health Sciences, Institute of Cardiology, Kaunas, Lithuania
[2]Kaunas University of Technology, Kaunas, Lithuania
[3]University of Edinburgh, Centre for Cardiovascular Science, Edinburgh, United Kingdom
kestutis.maciunas@lsmu.lt

Introduction: Cardiac alternans and ion current dysregulation are linked to various heart diseases, including arrhythmias. While optical mapping is a promising method to explore these phenomena, the detailed impact of specific ion currents on transmural optical signals remains underexplored. Understanding these effects is essential for advancing cardiac imaging techniques and uncovering arrhythmogenic mechanisms, especially under ischemic conditions.

Purpose: This study aims to investigate how specific ion currents transmurally affect cardiac optical maps during ischemia. A multidisciplinary approach integrating mathematical modeling, optical mapping, and multilayer microelectrode recordings was employed.

Methods: Electrical propagation was simulated using the Mahajan-Shiferaw ventricular cell model, while voltage-sensitive dye signals were generated through Monte Carlo photon transport simulations. Ex-vivo experiments were conducted using a Langendorff-perfused rabbit heart, stained with near-infrared dye di-4-ANBDQBS. Simultaneous electrical and optical action potential recordings were made using microelectrodes and optical mapping, with light excitation from LEDs and emission captured by an EMCCD camera. We analyzed the spatiotemporal patterns of action potentials under both ischemic and control conditions.

Results: The ventricular tissue model was calibrated with experimental microelectrode data using global optimization techniques. Optical parameters specific to the tissue and dyes were incorporated to enhance model accuracy. Simulations revealed that reducing peak conductances of sodium, potassium, and calcium ions channels progressively altered optical maps, with substantial changes observed at higher levels of ion conduction reduction. Simulating alternans by modifying SERCA pump dynamics demonstrated a marked sensitivity of optical signals to ischemic alterations. These results highlighted the capacity of optical mapping to detect ischemic changes in action potentials from deeper myocardial layers.

Conclusions: This study illustrates the utility of optical mapping for detecting ischemia-induced changes in transmural action potentials through near-infrared voltage-sensitive dyes. These findings provide insights into the transmural effects of arrhythmogenic mechanisms and may inform the development of therapeutic strategies to address ischemic arrhythmias.

Acknowledgement: This work was supported by the Kęstutis Maciūnas postdoctoral project (P-PD-23-155), funded by the Lithuanian Science Council.

Protein-ligand binding affinity prediction using descriptors derived from Voronoi tessellation

Anastasija Kudrevceva, Justas Dapkūnas

Institute of Biotechnology, Life Sciences Center, Vilnius University, Lithuania
anastasija.kudrevceva@gmc.stud.vu.lt

The estimation of protein and small drug-like ligand binding affinity is one of the important tasks in modern drug development. To this end, a variety of computational predictors were developed during the last decades. However, they possess various drawbacks, such as insufficient prediction accuracy, long computation time or dependence on data similarity to the training set. Therefore, designing an efficient computational method to predict the binding affinity for diverse protein-ligand complexes remains an unsolved challenge [1].

Here we present the development of computational models for the prediction of protein-ligand binding affinity based on Voronoi tessellation of the 3D structure of molecular complex [2]. Voronoi tessellation is a computational geometry approach which allows to compute molecular descriptors independently of subjectively chosen parameters, such as interatomic distance thresholds. Voronoi tessellation-based methods were successfully applied to analyze various biomolecular interactions, but this approach has been only rarely used for protein-ligand interactions. Attempting to exploit its advantages, we developed machine learning models for prediction of protein-ligand binding affinity using descriptors derived from Voronoi tessellation of protein-ligand complexes (interatomic contact areas, annotated according to atom properties, and molecular volume change upon complex formation), supplemented by the number of protein-ligand hydrogen bonds. Models were trained utilizing experimentally derived structures and binding affinity data from the high-quality subset of the PDBbind database [3] using different machine learning algorithms (Random Forest, Gradient Boosting Machine and Partial Least Squares).

We investigated the performance of our models using 4 independent datasets of protein-ligand complexes with known binding affinity: 1176 structures from the high-quality subset of PDBbind [3], a dataset of diverse structures published after 2019 [1], CASF-2016 benchmark [4], and 12 protein targets dataset [1,5]. On these datasets, the correlation between experimental and predicted binding affinity ranges from 0.41 to 0.75. In all cases non-linear methods tended to provide more accurate predictions. Our models demonstrated better binding affinity prediction compared to the classical methods, although they were outperformed by some of the recent deep learning-based scoring functions. Furthermore, we demonstrated that the accuracy of prediction depends on the similarity of the target protein to the training set proteins even for such simplistic models.

[1] G. Durant, F. Boyles, K. Birchall et al., *bioRxiv*, doi:10.1101/2023.10.30.564251 (2023).
[2] K. Olechnovič, Č. Venclovas, *J Comput Chem*, **35**, 672–681 (2014).
[3] Z. Liu, Y. Li, L. Han et al., *Bioinformatics*, **31**, 405-12 (2015).
[4] M. Su, Q. Yang, Y. Du et al., *J Chem Inf Model*, **59**, 895–913 (2019).
[5] A. Tosstorff, M. G. Rudolph, J. C. Cole et al., *J Comput Aided Mol Des*, **36**, 753-765 (2022).

Do chloroplasts necessitate the action potential generation in plants?

Vilma Kisnierienė, Ilvika Maleckaitė, Indrė Lapeikaitė, Vilmantas Pupkis

Institute of Biosciences, Life Sciences Center, Vilnius University, Sauletekio ave. 7- V125, LT-10257, Vilnius, Lithuania
vilma.kisnieriene@gf.vu.lt

For many decades the investigations of plant electrical signals both under natural conditions and upon exposure to various environmental factors have been performed using green internodal cells of Charophytes, whose main physiological functions are photosynthesis and light perception. It should be noted that the thallus of Charophytes consists of an axial stem of giant multinucleate cells joined end to end by multicellular nodal complexes with leaf-like green branchlets. These giant algae are anchored in the soil by root-like colorless rhizoids and protonemata cells [1]. Green colour of chloroplasts in the internodal cells depends on chlorophyll *a* and *b* ratio also carotenoids. As soon as dark growing chloroplast free protonemata cells penetrate the substrate and reach the light a complex series of signaling events are initiated that lead to the regeneration of the green colour. Similarly to terrestrial plants Charophyta rhizoids not only anchor the thallus, but also absorb nutrients and are essential for gravity perception. Gravity and light as physical cues regulate apical growth and various tropisms. Minerals have to be transported from rhizoids to growing parts of the thallus and various signals need to pass from cell to cell. As unique physiological function Characeae possess very fast cytoplasmic streaming which is observed not only in green but in chloroplast free cells also. It was confirmed that cytoplasmic streaming is arrested by action potential (AP) generation but to date electrical signalling in the nonphotosynthesising cells of macroalgae was not described.

As a foundation of plant electrophysiology, APs are readily measured and well characterized in *Characeaen* algae internodes [2]. In presented project we focus on chlorophyll free cells of *Nitellopsis obtusa* and parameters of their electrophysiological responses are compared with those of green cells grown in light. Real-time electrophysiological responses provide information about electrical signalling in plants under various conditions. The two-electrode voltage/current clamp measurements in single internodal *Nitellopsis obtusa* cells enable the identification of the dynamics of membrane ion transport systems at the rest and during excitation *in vivo*. In this work the ability of rhizoids to generate action potential was confirmed and the difference between membrane potentials and the other electrophysiological properties from chloroplast-containing light-growing cells was found. Although the resting potential and the conductance of membrane before excitation are the same in both cell types, differences were observed in AP parameters. The action potential peak of chlorophyll free cells is negative while in photosynthesising cells the overshoots are recorded. Also repolarization rate is twice as fast in the colourless cells compared to green internodal cells. Reversal potentials of total, Ca^{2+} and Cl^- currents during excitation in chlorophyll free cells are observed at a more negative membrane potential than that of green internodal cells. We conclude that electrophysiological parameters are different in soil growing and photosynthesis performing cells of *Nitellopsis obtusa* and electrical signalling can be involved in gravity and phothosynthesis regulation. Ongoing electrophysiological studies with a combination of other biophysical methods on both types of the *Characeaen* cells are required to shed light on electrical signalling function at cellular level *in vivo*.

[1] M. Beilby, *Front. Plant Sci.* 7:1052*,* 1-20 *(* 2016).
[2] V. Kisnieriene, K. Trębacz, V. Pupkis, et al., *Ann. of Bot*. 130(4), 457-475 (2022).

Electrostatic Interactions in Photosynthetic Complexes

Gabrielė Rankelytė[1,2], Jevgenij Chmeliov[1,2], Andrius Gelzinis[1,2] , Leonas Valkunas[1,2]

[1]Institute of Chemical Physics, Faculty of Physics, Vilnius University, Saulėtekio Ave. 9, III bld., Vilnius, Lithuania
[2]Department of Molecular Compound Physics, Centre for Physical Sciences and Technology, Savanorių Ave. 231, Vilnius, Lithuania
gabriele.rankelyte@ftmc.lt

Photosynthesis is one of the most important processes on Earth. The most efficient organisms that carry out photosynthesis are land plants or higher plants. In the thylakoid membrane of chloroplasts there are two systems that carry out photosynthesis – Photosystem I (PSI) and Photosystem II (PSII), both with their own light harvesting complexes – LHCI and LHCII. PSI is the most efficient light-to-energy conversion apparatus with quantum yield almost equal to 1 [1]. One of the conditions needed for high efficiency is very fast energy transfer between the molecules in light harvesting complex (LHCI). Light-harvesting complex of PSI absorbs and emits light at the longest wavelengths compared to other pigment-protein complexes. In plants, light harvesting antenna of PSI is composed of four species of LHCI complexes. They all have very similar structure; however, their spectral properties are different.

The excitation dynamics in LHCI is highly affected by the charge-transfer (CT) states that occur between two or more pigments. Some sites in which CT states occur in LHCI are known; however, they do not completely explain the spectral properties of this antenna, such as the red-shifted peak in fluorescence spectrum. The energy of the excited states of pigments (including the CT states) are highly affected by the surrounding environment, consisting of other pigments (chlorophylls and carotenoids) and the protein chain. Therefore, it is necessary to account for the environment to model light-harvesting complexes properly.

LHCI structure was obtained as the 1st–4th chains of PSI complex structure [2] (see Fig. 1), freely available at Protein Data Bank (PDB ID: 5L8R). We performed quantum chemical calculations to obtain energies of chlorophyll dimer CT states *in vacuo* using "VU HPC" Saulėtekis supercomputer. For all four protein chains, we estimated the most probable protonation pattern in neutral solution. We then included the environment (chlorophylls, carotenoids and the protein chain) in our calculations by obtaining atomic partial charges of both environmental blocks and dimers of interest and evaluating the electrostatic interaction between these charges using CDC (charge-density coupling) method [3].

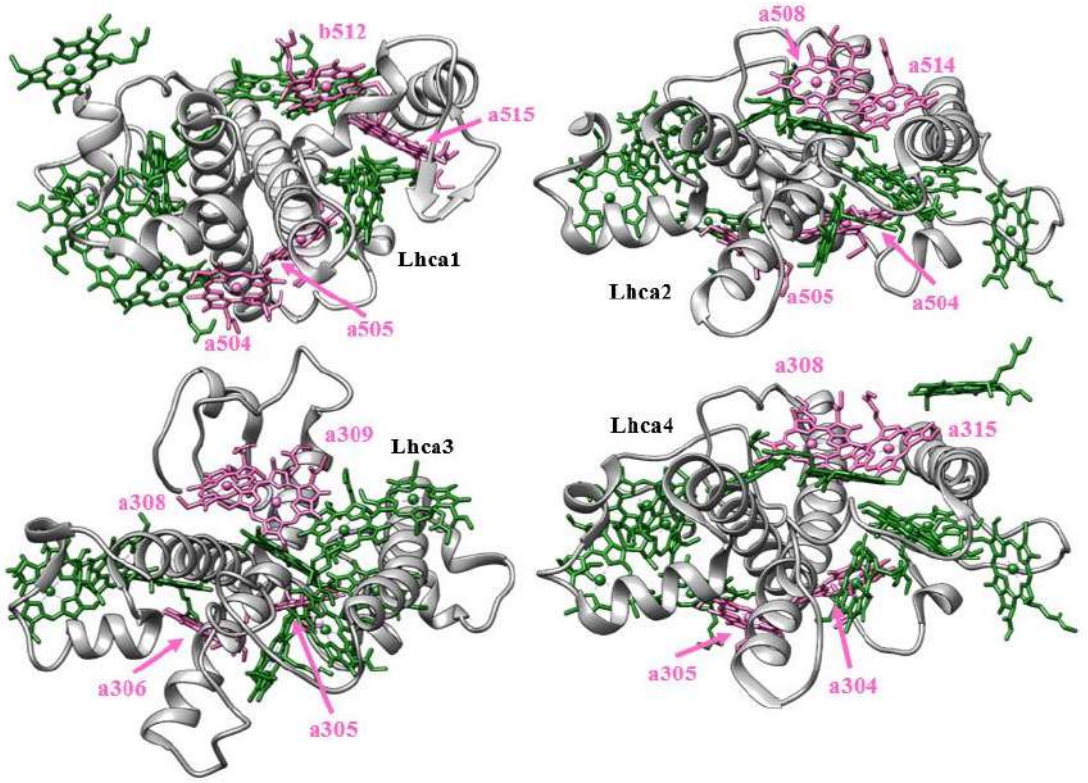

Fig. 1. Lhca1-4 light-harvesting subcomplexes of Photosystem I. Protein chain is depicted in grey, chlorophylls – in green. Some chlorophyll dimers, that were analysed in this work, are highlighted in pink. Carotenoid molecules are not in the picture.

[1] R. Croce, H. van Amerongen, *Photosynth. Res*. **116**, 153-166 (2013).
[2] Y. Mazor, A. Borovikova, I. Caspy, N. Nelson, *Nat. Plants*, **3**, 17014-17014 (2017).
[3] T. Renger, F. Müh, *Phys. Chem. Chem. Phys*. **15**, 3348-3371 (2013).

Intrinsically Disordered Coral Acid-Rich Protein AGARP Regulates Calcium Carbonate Growth via Liquid Phase Separation

Anna Niedźwiecka[1], Barbara P. Klepka[1], Agnieszka Michaś[1], Tomasz Wojciechowski[2]

[1]Laboratory of Biological Physics, Institute of Physics, Polish Academy of Sciences, Aleja Lotnikow 32/46, PL-02668 Warsaw, Poland
[2]International Research Centre MagTop, Institute of Physics, Polish Academy of Sciences, Aleja Lotnikow 32/46, PL-02668 Warsaw, Poland
annan@ifpan.edu.pl

Biomineralization through the non-classical crystallization pathway [1] is hypothesized to involve a transient liquid phase of calcium carbonate that forms in the presence of biopolymers [2,3]. In the process of coral biocalcification, these biopolymers likely include coral acid-rich proteins (CARPs), which are secreted into the extracellular skeletal organic matrix. However, direct evidence for the presence of this liquid phase associated with proteins has not yet been observed and they role has not been elucidated.

In this work, we have cloned and obtained for the first time the intrinsically disordered aspartic and glutamic acid-rich protein (AGARP). This is the first CARP cloned from *Acropora millepora*, a well-known scleractinian coral from the Great Barrier Reef that serves as a model species for biomineralization and ecological research, and the fifth recombinant CARP obtained to date overall [4]. We investigate the biophysical and biochemical properties of AGARP and show that AGARP can play a significant role in the early stages of calcium carbonate nucleation and crystal growth.

Additionally, we demonstrate that liquid-liquid phase separation can play a crucial role in calcium extracellular transport and in the regulation of calcium carbonate solid phases formation within a viscous, crowded environment. Our work offers a novel perspective on biomineralization processes, highlighting the importance of liquid-liquid phase separation in these biophysical mechanisms.

The work was supported by Polish National Science Centre grant no. 2016/22/E/NZ1/00656 to AN. The studies were performed in the NanoFun laboratories co-financed by ERDF within the Innovation Economy Operational Programme POIG.02.02.00-00-025/09.

[1] M. Jehannin, A. Rao, H. Cölfen, *J. Am. Chem. Soc.* 141, 10120–10136 (2019).
[2] Y. Xu, K. C. H. Tijssen, P. H. H. Bomans, A. Akiva, H. Friedrich, A. P. M. Kentgens, N. A. J. M. Sommerdijk, *Nat. Commun.* 9, 2582 (2018).
[3] J. T. Avaro, S. L. P. Wolf, K. Hauser, D. Gebauer, *Angewandte Chemie International Edition* 59, 6155–6159 (2020).
[4] T. Mass, J. L. Drake, L. Haramaty, J. D. Kim, E. Zelzion, D. Bhattacharya, P. G. Falkowski, *Curr Biol* 23, 1126–1131 (2013).

Model-based Evaluation of Biophysical Properties of Gap Junction Channels from Electrophysiological Data recorded at Macroscopic and Single-Channel Levels

Mindaugas Šnipas[1,2], Tadas Kraujalis[1,3], Lina Kraujalienė[1], Lukas Gudaitis[1,4], Orestas Makniusevičius[1], Vytautas K. Verselis[5]

[1]Lithuanian University of Health Sciences, Institute of Cardiology, Laboratory of Intercellular Communication, Sukilėlių pr. 15, Kaunas, Lithuania
[2]Kaunas University of Technology, Faculty of Mathematics and Natural Sciences, Department of Mathematical Modelling, Studentų g. 50, Kaunas, Lithuania
[3]Kaunas University of Technology, Faculty of Informatics, Department of Applied Informatics, Studentų g. 50, Kaunas, Lithuania
[4]KU Leuven, Department of Cardiovascular Sciences, Laboratory of Experimental Cardiology, UZ Herestraat 49, Leuven, Belgium
[5]Albert Einstein College of Medicine, Dominick P. Purpura Department of Neurosciences, 1410 Pelham Parkway South 710 Bronx, New York City, USA
mindaugas.snipas@ktu.lt

Electrophysiological recording via the patch clamp technique allows for the assessment of the biophysical properties of various types of ion channels. However, electrophysiological recordings of gap junction (GJ) channels poses challenges due to their unique intercellular configuration and natural clustering into plaques, making it difficult to obtain reliable data at a single-channel level. Additionally, until recently, no mathematical models adequately explained both the steady-state and kinetic properties of GJ channel gating, which is crucial for model-based evaluation of single-channel level characteristics. Consequently, the methods for accurately correlating data recorded at macroscopic and single-channel levels have been lacking in studies of gap junctional electrophysiology.

To address these issues, we combined our previously published four-state model (4SM) of GJ channel gating with probabilistic methods, such as maximum likelihood estimation (MLE)-based analysis of single-channel level currents and stationary noise analysis of macroscopic level electrophysiological recordings.

First, we address evaluation of biophysical single-channel-level properties of GJ channels, such as open-state probability and unitary conductance, using data from macroscopic-level recordings. Second, we consider MLE-based methodologies to extract information about gating parameters of GJ channels from electrophysiological recordings with observable unitary events. The validity of the proposed methodologies is first illustrated through stochastic simulations and further extended to real electrophysiological data. Overall, our findings show that these techniques can provide valuable insights into biophysical properties of GJ channels.

Investigating Novel Connexin-43 Gap Junction Inhibitors via Computational Analysis

Vytautas Raškevičius, Gabrielė Zuokaitė, Rokas Mickus, V. Arvydas Skeberdis

Lithuanian University of Health Sciences, Institute of Cardiology, Sukilėlių pr. 15, Kaunas, Lithuania
Vytautas.Raskevicius@lsmu.lt

Cardiac arrhythmias depend on intercellular communication through gap junctions (GJ) composed of Connexin-43 (Cx43). The search for novel specific and potent agents capable of modulating the GJ activity often employs molecular docking techniques, which estimate the binding affinities of various ligands to the target proteins. However, the predictions generated by this method frequently contrast with their biological potencies.

In this study, we combined the Quantitative Structure-Activity Relationship (QSAR) modelling and molecular docking for the identification of new potent inhibitors of Cx43 GJs with enhanced accuracy. Our QSAR models are based on the structural analysis of 16 known Cx43 GJ inhibitors with experimentally determined concentrations required for 50% inhibition of Cx43 GJ conductance (eIC$_{50}$). This analytical approach allows to correlate the chemical structures of compounds with their eIC$_{50}$ies and further apply it in search of new inhibitors predicting their potencies (pIC$_{50}$) and choosing the most potent ones for estimation of their eIC$_{50}$ies by dual whole-cell patch-clamp techniques.

The pIC$_{50}$ies of Cx43 GJ inhibitors, derived from both 2D-QSAR and 3D-QSAR (compounds exhibiting high structural flexibility omitted) models, demonstrated strong correlation with their respective eIC$_{50}$ies (correlation coefficient (R) was 0.83 and 0.98, respectively), in contrast to pIC$_{50}$ies obtained from molecular docking (R = 0.77).

Further, using our established QSAR models, we chose d-limonene, a monocyclic monoterpene, and farnesene, an acyclic sesquiterpene, as promising putative inhibitors of Cx43. An experimental examination was performed in Novikoff rat hepatoma cell pairs expressing endogenous Cx43. The eIC$_{50}$ies estimated for these compounds (30 μM and 1.3 μM, respectively) well harmonized with their pIC$_{50}$ies obtained by 2D-QSAR model (14 μM and 0.6 μM, respectively), whereas the pIC$_{50}$ies derived from molecular docking were less accurate (66 μM and 16 μM, respectively). It is important to note that 3D-QSAR modelling (pIC$_{50}$ies were 42 μM and 50 μM, respectively) was less reliable for farnesene due to the substantial number of rotatable bonds in its structure.

Overall, our results indicate that QSAR modelling has the potential to facilitate the discovery of selective and potent GJ inhibitors, paving the way for innovative therapeutic strategies for communication-dependent diseases.

Changes in Immune Cell Subpopulations Following High-Frequency Nanosecond Bipolar and Unipolar Calcium Electrochemotherapy *in vivo*

Eivina Radzevičiūtė-Valčiukė[1,2], Augustinas Želvys[1,2], Eglė Mickevičiūtė[1,2], Jovita Gečaitė[1], Paulina Malakauskaitė[1,2], Barbora Lekešytė[1,2], Veronika Malyško-Ptašinskė[2], Auksė Zinkevičienė[1], Vytautas Kašėta[1], Julita Kulbacka[1,3], Joanna Rossowska[4] and Vitalij Novickij[1,2]

[1]State Research Institute Centre for Innovative Medicine, Vilnius, Lithuania.
[2]Vilnius Gediminas Technical University, Faculty of Electronics, Vilnius, Lithuania
[3]Wroclaw Medical University, Wroclaw, Poland
[4]Hirszfeld Institute of Immunology and Experimental Therapy, Wroclaw, Poland
eivina.radzeviciute@imcentras.lt

Calcium electroporation, or calcium electrochemotherapy (CaECT) is a novel and effective cancer treatment which relies on the cytotoxic effects of increased calcium ion delivered via electroporation-induced membrane pores [1]. Recent studies have demonstrated that using sub-microsecond pulses compressed into high-frequency (MHz) bursts significantly enhances the effectiveness of the CaECT methodology compared to standard ns protocols, due to residual transmembrane potential. However, this improvement applies to monophasic procedures, whereas bipolar nanosecond pulses trigger a bipolar cancellation (BPC) phenomenon. BPC effects are mostly reported for IRE, with few studies on bipolar ECT [2]. Nonetheless, bipolar nsPEF can improve electric field homogeneity due to its higher frequency components, induce less muscle excitation and pain, and reduce the effects of electrolysis and oxidation. This study investigates the effects of unipolar and bipolar sub-microsecond pulses (7 kV/cm, 300 ns, 250 pulses, 1 MHz) within the framework of calcium electrochemotherapy (CaECT) and compares them to ESOPE (1.5 kV/cm, 100 µs, 8 pulses, 1 Hz). The primary focus was on characterizing BPC in vivo and determining the immune response elicited by these treatments.

Mammary carcinoma tumors were induced by subcutaneously injecting Balb/C mice with 4T1-Luc cells. Upon reaching the desired tumor volume (~50 mm³), CaECT at a concentration of 250 mM was administered using different electric field protocols. Subsequently, tumor response was assessed through volumetric measurements and bioluminescence imaging. At the end of the experiment, spleens, lymph nodes, and blood samples from the mice were collected and analyzed using multi-color flow cytometry.

Our study demonstrated that both microsecond and sub-microsecond range uni- and bipolar pulses can be effectively utilized in calcium-based electrochemotherapy (ECT), resulting in partial or complete response of 4T1 tumors. The induction of a systemic immune response after CaECT was indicated by an increased percentage of splenic central memory T cells, a decrease in $CD4^+$ regulatory T cells in both the spleen and tumor-draining lymph nodes, and a reduction in myeloid-derived suppressor cells (MDSCs) in the lymph nodes. Interestingly, the bipolar CaECT protocol employed for murine breast cancer treatment did not exhibit significant effects related to BPC phenomena, which was predict ed by the in vitro viability and permeabilization data supporting the research. However, the potential of CaECT to modulate the immune system indicates its promise as a therapeutic approach for managing metastases and for developing innovative, effective cancer treatment strategies capable of inducing long-term anti-tumor immunity.

Acknowledgment: The research was supported by the Research Council of Lithuania (Grant Nr. S-MIP-23-124).

[1] S. K. Frandsen, M. Vissing, and J. Gehl, "A comprehensive review of calcium electroporation —A novel cancer treatment modality," *Cancers (Basel).*, vol. 12, no. 2, pp. 1–21, 2020, doi: 10.3390/cancers12020290.

[2] A. G. Pakhomov, S. Grigoryev, I. Semenov, M. Casciola, C. Jiang, and S. Xiao, "The second phase of bipolar, nanosecond-range electric pulses determines the electroporation efficiency," *Bioelectrochemistry*, vol. 122, p. 123, Aug. 2018, doi: 10.1016/J.BIOELECHEM.2018.03.014.

Poster Presentations

Surface Enhanced Raman Scattering (SERS) and Infrared Absorption (SEIRA) Spectroscopies for *in situ* Imaging of Biomolecules

Sonata Adomavičiūtė-Grabusovė[1], Marius Balodis[1], Viacheslav Artyushenko[2], Valdas Šablinskas[1]

[1]Institute of Chemical Physics, Vilnius University, Sauletekio av. 3, LT-10257 Vilnius, Lithuania
[2]Artphotonics GmbH, Rudower Chaussee 46, 12489 Berlin, Germany
sonata.adomaviciute@ff.vu.lt

Vibrational spectroscopy serves as a versatile analytical tool with significant importance in biological analysis. Its rapid execution, high sensitivity, and non-destructive nature make it particularly valuable for sensitive biological samples. Applications of vibrational spectroscopy include virus identification, cancer tissue recognition, and bioimaging [1]. Specifically relevant to biological applications is a well-known enhancement method for conventional spectroscopy, which intensifies spectral signals and enhances selectivity for certain biomolecules [2]. This phenomenon is widely recognized as surface-enhanced Raman scattering (SERS) or surface-enhanced infrared absorption (SEIRA) spectroscopy. Nevertheless, when applying these techniques, it becomes critical to adapt them for broader real-life usage. In this research, both types of surface-enhanced vibrational spectroscopy will be utilized to improve the signal obtained from molecules of biological interest. This includes expanding the applicability of SEIRA and SERS techniques for direct and remote sensing applications, using optical fiber performance for *in situ* research.

Since the primary challenge in fiber-based Raman sensors lies in the Raman background of the optical fiber material, we designed a two-fiber system to function as a reliable SERS probe with minimal or no Raman interference. Specifically, we employed two fused-silica optical fibers: one with a 100 µm diameter for Raman scattering excitation and another with a 600 µm diameter for signal collection (Fig. 1(A)). We tested the capabilities of this probe by recording SERS spectra from a 1 mM adenine solution in an aqueous medium. The most intense SERS spectral bands of adenine were observed at 738 cm^{-1} (corresponding to the ring breathing mode) and at 1347 cm^{-1} (associated with ring vibration). Our dual-fiber SERS probe system demonstrated promising results, achieving the strongest SERS signal for adenine when the angle between the fibers was 140º–160º (Fig. 1(C)).

For the fiber-based SEIRA study, we employed polycrystalline (PIR) silver halide fibers specifically designed for the infrared range. The employed ATR Loop Probe consisted of two PIR fibers (900/1000 µm core/clad diameter) and $AgCl_{0.25}Br_{0.75}/AgCl_{0.5}Br_{0.5}$ core/clad composition. The detachable loop tips were made of 700 µm diameter uncladded PIR fiber with an $AgCl_{0.25}Br_{0.75}$ core composition, serving as the ATR sensitive element (Fig. 1(B)). After depositing polyvinylpyrrolidone (Ag-PVP) nanoparticles onto the fiber loop tips, we achieved a 90-fold enhancement in the naphthalene molecule signal. This enhancement enabled the detection of naphthalene, a toxic organic compound, in water the characteristic naphthalene band at 783 cm^{-1} (corresponding to the out-of-plane C–H deformation) (Fig. 1(D)). Our study involved a series of experiments, including reproducibility and signal stability studies, as well as investigations into the synthesis and deposition methods of the silver nanoparticles on the fiber loop.

Ultimately, our research shows promise for expanding the applicability of SERS and SEIRA methods in remote fiber-based sensing and the analysis of biologically relevant molecules. These studies lay the foundation for future research aimed at refining and expanding the capabilities of SERS and SEIRA spectroscopy for biological fluid analysis.

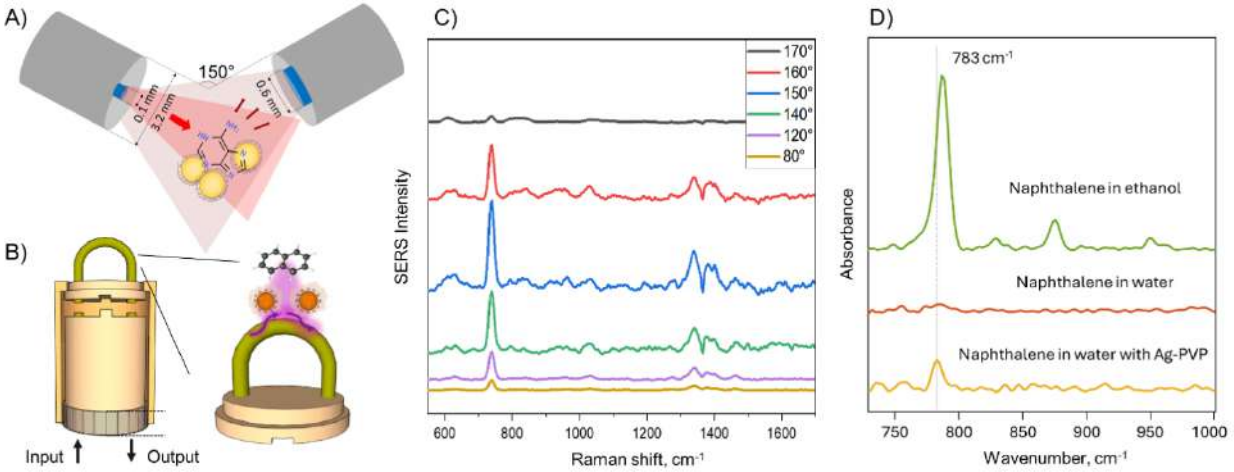

Fig. 1. Fiber-based schemes of SERS (A) and SEIRA (B), along with the SERS spectra of adenine using different angles between the excitation and collection fibers (C), and the IR absorption and SEIRA spectra of naphthalene in water (D).

[1] Wang, H.; Lee, D.; Wei, L. Toward the Next Frontiers of Vibrational Bioimaging. Chemical & Biomedical Imaging 2023, 1 (1), 3–17.
[2] Wang, H. L.; You, E. M.; Panneerselvam, R.; Ding, S. Y.; Tian, Z. Q. Advances of Surface-Enhanced Raman and IR Spectroscopies: From Nano/Microstructures to Macro-Optical Design. Light Sci Appl. 2021, 10 (1), 161.

Neuro-RECURSION in the VISUAL ANALYSER (The Visual Dreams as the Functioning's Recursive Neuro-Computer in the Neocortex of Visual Analyser)

Dobilas Kirvelis[1]

[1]Lithuanian Scientific Society, J. Basanavičiaus g. 6, Vilnius, Lithuania
dobilas@kirvelis.lt

In the last decade, a radically different scientific concept of developing Life on Earth - as Bio-RECURSION - has emerged [1-4]. From the point of view of this concept, Life is the formation of Closed-Loop Coding- Decoding (CL-CD) chem-matter (bio-chem) procedure that appeared ~8.3 billion years ago, after the discovery and installation of Recursive Informatics technologies (Fig. 1). Recursive mathematics was understood and formed only ~90 years ago, which in 1950-60 initiated modern Computers and Computing. This shows that the **essence of life is Bio-Informational** DNA-Comp and Neuro-Comp Recursion ***Soft*** technologies while Biochem's only ***Hard***. This presentation is the theoretical interpretation of the results of the psychophysiological experimental research on the identification of images of the vision analyser, (carried out in 1980-2013), from the point of view of functional organization and activity analysis of the **Neuro-Recursive computer** positions. The visual dreams, visual mental thinking and hallucinations are seen as recursive phenomena of the manifestation of informational neuro-recursive events. A duration of 8-10 milliseconds for one hypothesis is considered to be the duration of the one iteration, and the latent period of 16 milliseconds is the time required to test the primary recurencial hypothesis. **The Bio-Information** (*Organic - Organizing forces*) as the essence of Life was already seen exactly 220 years ago (1804) atVilnius University by ***Jędrzej Śniadecki,*** (*Teoria jestestw organicznych,* t.1, 1804).

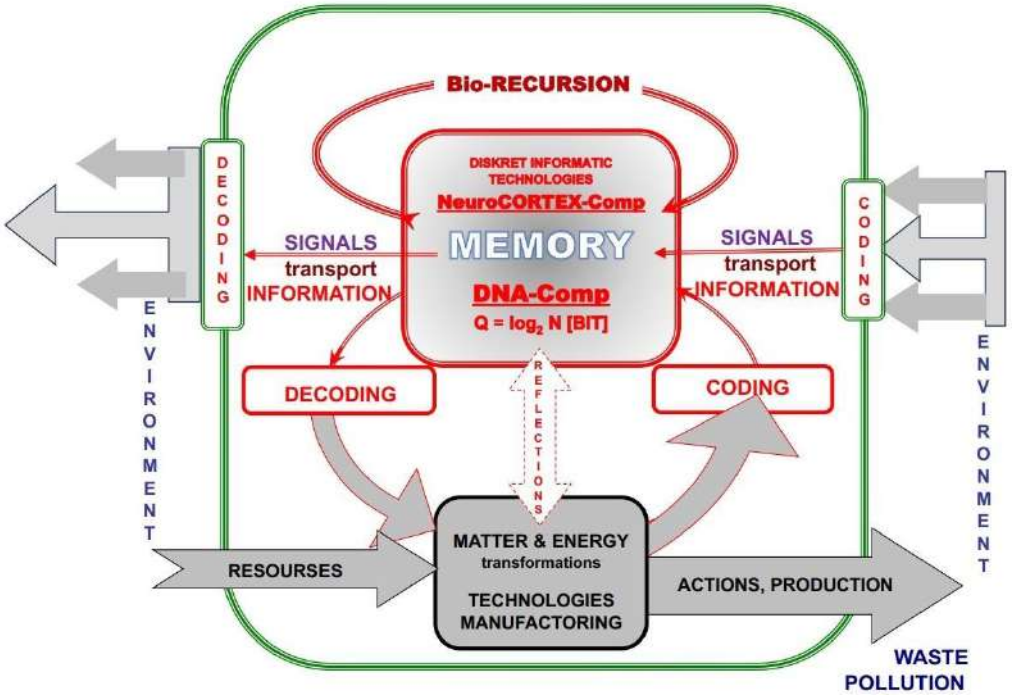

Fig. 1. Functional structure of the Living and Recursion-Organised Systems.
Red arrows - **Signal-Information** paths, thick dark arrows – **Matter-Energy** events

[1] Kirvelis D. Kodavimas-Dekodavimas uždaros kilpos principu gyvosiose sistemose. HP Mokslo Darbų apžvalga, VU, Biologija (01 B), 48 pg. (2009).
[2] O'Neil S. T. Bio/Recursion: Exploring CS and Bioinformatics. 160 (2018).
[3] Kirvelis D., Beitas K. Informational Closed-Loop Coding-Decoding Control Concept as the Base of the Living or Organized Systems Theory. American Institute of Physics 1051, 293-306 (2007).
[4] Hui Y. Recursivity and Contingency, (London, Rowman & Littlefield International Ltd.) 336 (2019).

Evaluation of load on bone mimicking material around the dental implant using polarized light

Martynas Vencius[1] , Pijus Beleckas[1] , Julius Vengelis[2] , Gintaras Janužis[3]

[1]Faculty of Odontology, Medical Academy, Lithuanian University of Health Sciences, Kaunas, Lithuania
[2]Laser Research Center, Faculty of Physics, Vilnius University, Vilnius, Lithuania
[3]Department of Maxillofacial Surgery, Faculty of Odontology, Medical Academy, Lithuanian University of Health Sciences, Kaunas, Lithuania
martynas.vencius@outlook.com

There are many methods for testing dental implant osseointegration which is a big topic these days [1]. One of the most common dental implant testing methods usually investigates the static load received by the implant itself [2]. We decided to try a new and innovative method using polarized light for testing material around dental implants and how this dental implant affects this surrounding material when a static load is received. Since there is no methodology in literature we needed to find the most transparent and homogenic material for testing which would give least intensity and polarized light centre changes in the camera images. This would mean that our material is stable and it would give least noise while using it with dental implants.

This study aim was to evaluate polarized light fraction in camera images and to find the most homogenic bone mimicking material which could be used for testing with dental implants.

We used 3 different testing subjects. First subject material was UV curable acrylic resin “UV Creation” , second was epoxy resin “Epoxy Super Ultra - 2cm” and third was the same epoxy resin “Epoxy Super Ultra - 2cm”, but with different casting technique, this means that second workpiece was casted vertically in to the casting form and third workpiece was casted horizontally in to the casting form. The 3 identical workpeaces of 1x1x3cm dimensions were made with each material and techniques. After that the workpeace were placed in the specially made press and the polarized light is directed into a specific spot. Using a CCD (SP602U) camera and BeamStar 1.52 software the rotation of polarized light is measured. Then the workpieces were loaded with 50 N force and the polarized light changes were detected. We calculated polarized light intensity changes without 50 N load and with 50 N load, also polarized light centre change was calculated, so we could determine in which subject polarized light fraction is the highest.

First UV curable acrylic resin material “UV Creation” had mean intensity changes of 16,44 and polarized light centre changes of 40,95. Second material epoxy resin “Epoxy Super Ultra - 2cm (casted vertically)” had mean intensity changes of 2,12 and polarized light centre changes of 10,81. Third material epoxy resin “Epoxy Super Ultra - 2cm (casted horizontally)” had mean intensity changes of 0,46 and polarized light centre changes of 1,38.

After comparing 3 different workpieces and analyzing polarized light camera shots we can say that the most transparent and homogenic material for testing is third epoxy resin “Epoxy Super Ultra - 2cm (casted horizontally)”. This means that molecule arrangement in this material affected by load changes the least. Third epoxy resin “Epoxy Super Ultra - 2cm (casted horizontally)” was closer to second epoxy resin “Epoxy Super Ultra - 2cm (casted vertically)” , but as we mentioned before it was the same material just different casting techniques, so we can say that casting technique also affects molecular arrangement in epoxy resins. Also, there is a need for tests with dental implants so we could determine dental implant impact on different kind of materials.

[1] Kittur N, Oak R, Dekate D, Jadhav S, Dhatrak P. Dental implant stability and its measurements to improve osseointegration at the bone-implant interface: A review. Materials Today: Proceedings. 2021 Jan 1;43:1064–70.

[2] 14:00-17:00. ISO 14801:2016. ISO. [žiūrėta 2023 m. lapkričio 20 d.]. Adresas: https://www.iso.org/standard/61997.html

Expansion of perceived size of components of visual stimulus

Bertulis Algis[1], Bielevicius Arunas[1], Surkys Tadas[1]

Institute of Biological Systems and Genetics Research, Lithuanian University of Health Sciences, Kaunas, Lithuania
bertulisalgis@gmail.com

Introduction. The present study focuses on the expansion effect of the relative size of isolated stimulus parts like angles, broken lines, and short stripes. Subjects (M, N, O, L, Ë, A, B, R, P, H, K, and Г) matched the test distance to the referential stimuli length by adjusting the position of the terminal spot. The testing distance was limited to the terminal spot and the vertex or sideline of a referential figure. The starting referential stimulus was the contour pentagon (facsimile in Fig. 1). Lines and their combinations were removed from the pentagon to show separate parts. The background's luminance and the stimuli lines were 0.01 cd/m^2 and 23 cd/m^2, respectively.

Results. A. All modified stimuli caused the effect of length expansion, which did not significantly differ in strength from the entire pentagon (13.8 arc min; Fig 1 medial section). The illusion grew slightly from 13.8 to 15.7 arc min P = 0.397 (Welch's t-test) in the stimulus without a lower horizontal line and from 13.8 to 15.2 arc min P = 0.561 in that without the bottom two lines.

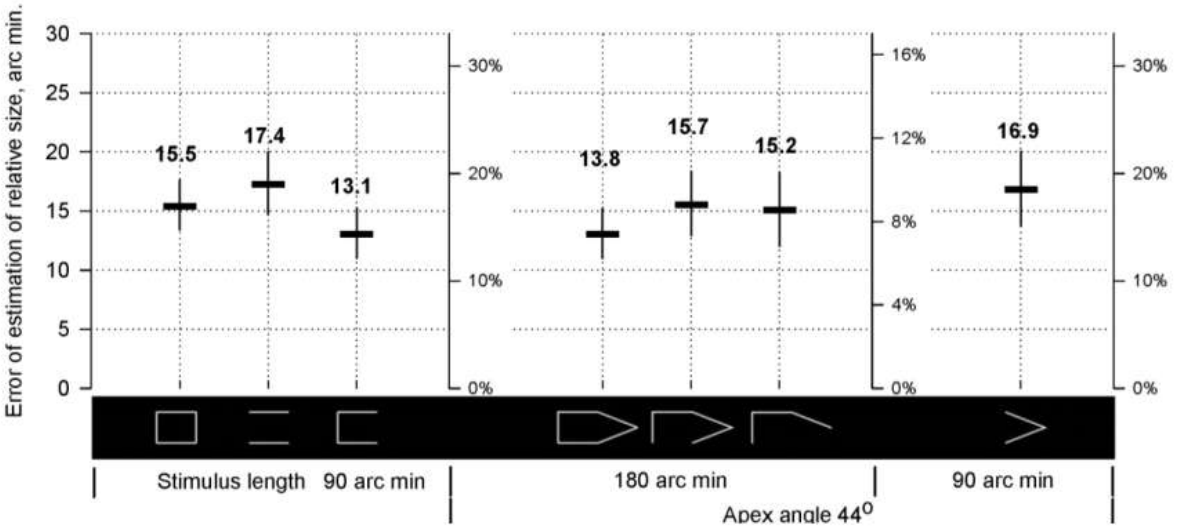

Fig.1 Expansion of length of stimulus components in comparison with the entire contour.

B. An angle, a pair of wings (Fig. 1 right section) was twice shorter than the pentagon, but the illusion, on the contrary, increased from 13.8 to 16.9 arc min P = 0.176. **C**. When the open rectangle was presented (left section in Fig.1), the illusion strength did not change: 13.8 → 13.1 arc min P = 0.716, regardless of the stimulus change in spatial structure. **D.** When the vertical segment was removed from the open rectangle, and two parallel horizontal lines remained, the illusion increased: 13.1 → 17.4 arc min P = 0.015. **E.** If two vertical segments were added to the two horizontal lines to make the stimulus a rectangle, the strength of the illusion slightly decreased: 17.4 → 15.5 arc min P = 0.278.

Conclusions. Components of a visual stimulus presented as isolated should be considered full-fledged objects in the size comparison procedure. The individual shape of an object determines the strength of the size expansion. A sum of the expansions of the size of stimulus parts significantly differs from the expansion of the whole. The present experimental data favor the functional relationships of the contour segments forming the shape, not the integration of reactions to each segment during the relative size estimation.

Mitigating bipolar cancellation effects in nano-electrochemotherapy: impact of pulse asymmetry and electric field intensity

Eglė Mickevičiūtė[1,2], Vitalij Novickij[1,2]

[1] State Research Institute Centre for Innovative Medicine, Department of Immunology and Bioelectrochemistry, Vilnius, Lithuania
[2] Vilnius Gediminas Technical University, Faculty of Electronics, Vilnius, Lithuania
vitalij.novickij@vilniustech.lt

The phenomenon known as bipolar cancellation is observed when negative phase of the bipolar pulse diminishes the effect of the positive phase of the pulse. Our study aimed to investigate how to mitigate bipolar cancellation effects on cellular response under varying electric field intensities and asymmetric pulses (5-15 kV/cm,↑200ns+↓200ns, ↑200ns+↓400ns, and ↑200ns +↓600ns bipolar 1 MHz repetition frequency pulse bursts, n = 100). Initially, it was demonstrated that the cancellation effect is extremely strong when the pulses are closely spaced (1 MHz frequency), resulting in a lack of cell membrane permeabilization and the consequent failure of electrochemotherapy in vitro and in vivo (B16-F10 cell line, C57BL/6 mice, n = 24). Subsequently, in this study we show that the asymmetry of the pulse improves permeabilization and the bipolar cancellation effect is diminished. The most effective reduction in bipolar cancellation, leading to reversible electroporation, was achieved with 12.5 kV/cm x ↑200+↓400ns, 1 MHz. The results of this study contribute to the development of new approaches in pulse modulation for a more effective and safe electrochemotherapy procedure.

[1] Pakhomov, A.G.; Semenov, I.; Xiao, S.; Pakhomova, O.N.; Gregory, B.; Schoenbach, K.H.; Ullery, J.C.; Beier, H.T.; Rajulapati, S.R.; Ibey, B.L. Cancellation of Cellular Responses to Nanoelectroporation by Reversing the Stimulus Polarity. Cell. Mol. Life Sci. 2014, 71, 4431–4441.
[2] Wasson, E.M.; Alinezhadbalalami, N.; Brock, R.M.; Allen, I.C.; Verbridge, S.S.; Davalos, R.V. Understanding the Role of Calcium-Mediated Cell Death in High-Frequency Irreversible Electroporation. Bioelectrochemistry 2020, 131, 107369.

The Synergy of Nisin with Nanosecond and Microsecond Pulse Bursts for Electrochemotherapy

Barbora Lekešytė[1,2], Vitalij Novickij[1,2]

[1] *State Research Institute Centre for Innovative Medicine, Department of Immunology and Bioelectrochemistry, Vilnius, Lithuania*
[2] *Vilnius Gediminas Technical University, Faculty of Electronics, Vilnius, Lithuania*
Presenting author: barbora.lekesyte@imcebtras.lt

Electrochemotherapy (ECT) involves applying a pulsed electric field (PEF) to enhance the transmembrane delivery of chemotherapy drugs. Drug delivery is facilitated via hydrophilic pores, which are formed due to electroporation. Therefore, control of the pore density, stability, and size are crucial parameters to ensure effective drug delivery. At the same time, nisin is a naturally occurring peptide with antibacterial properties, which can potentially improve ECT. Its unique structure promotes protein aggregation at pore edges, potentially impacting pore healing processes. Additionally, nisin has been shown to enhance the efficacy of chemotherapy on various cancer cell lines, suggesting it may have synergistic anticancer effects. The potential of nisin to improve drug delivery by alteration of pore induction or resealing and the potential additive anticancer effects offer hope for its therapeutic applications together with ECT. Currently, the effects of nisin are not yet characterized in the context of ECT.

Therefore, the main goal of this work is to gather experimental evidence demonstrating the capability of nisin to affect pores induced in the membranes of cancer cells via electroporation. Here, we combine electrochemotherapy using microsecond: 0.6–1.5 kV/cm × 100 µs × 8 (1 Hz) and nanosecond: 6 kV/cm × 300 ns × 100 (1, 10, 100 kHz and 1 MHz) electric field pulses. We show that nisin significantly affects electroporation. The synergistic effects (improved permeabilization and molecular electrotransfer) are especially profound with increased pulse burst frequency. Additionally, nisin decreases the permeabilization thresholds, affects pore resealing, and exerts anticancer effects similar to conventional ECT. Importantly, the nisin was shown to be non-toxic for the cells by itself, providing reassurance about potential applicability in the context of electrochemotherapy.

Acknowledgments: The research was supported by the Research Council of Lithuania, Grant Nr. S-MIP-24-74.

Keywords: nanosecond pulses, nisin, pores, drug delivery, permeabilization, resealing, electrochemotherapy

Electrochemical and Morphological Insights into Colistin-Induced Reorganization of Tethered Bilayer Lipid Membranes

Modestas Mažerimas[1], Rima Budvytyte[1,2]

[1] Life Sciences Center, University of Vilnius, Vilnius, Lithuania
[2]Institute of Biochemistry, Department of Bioelectrochemistry and Biospectroscopy, Life Sciences Center, Sauletekio av. 7, LT-10257, Vilnius
modestasma13@gmail.lt

As antimicrobial resistance becomes an increasingly urgent threat and the discovery of new antibiotics approaches a bottleneck, alternative solutions, such as antimicrobial peptides (AMPs), are gaining importance [1]. AMPs are typically small, cationic molecules whose primary mode of action involves incorporation into bacterial membranes, followed by disruption of bilayer integrity through various mechanisms [2]. Surface-sensitive techniques like electrochemical impedance spectroscopy (EIS) and atomic force microscopy (AFM) can be employed to detect changes caused by peptide incorporation, revealing alterations in both electrochemical and morphological properties of the bilayer.

Given the complexity of bacterial membranes, *in vitro* model membrane mimetics provide versatile platforms for studying membrane interactions [3].

In these studies, tethered bilayer lipid membranes (tBLMs) (Fig. 1) are supported by self-assembled monolayer (SAM). SAM consist of tether molecules (Fig. 1 C) that attach to the gold surface (Fig. 1 A) and anchor the fused lipid bilayer (Fig. 1 D), while spacer molecules (Fig. 1 B) regulate the density of tether molecules [4]. Such structure plays a major role enabling electrochemical analytical techniques like EIS [5].

Our experimental results demonstrate that tBLMs exposed to the antimicrobial peptide colistin exhibited reduced conductance of the lipid bilayer. The extent of colistin-induced effects varied with factors such as peptide concentration, ion concentration in the solution, and the structural composition of the bilayer lipids. Initially, these conductance changes were attributed to increased membrane stiffness and lipid ordering. However, AFM experiments revealed the formation of additional phospholipid bilayer structures, suggesting a new hypothesis: that colistin induces reorganization of the bilayer into a non-lamellar state.

In summary, our findings indicate that tBLMs, in combination with EIS and AFM, offer a robust platform for screening and characterizing the activity of AMPs against bacterial membranes.

Figure 1. Schematic depiction of tethered bilayer lipid membrane, where: (a) gold-plated glass plate; (b) spacer molecules; (c) lipid bilayer tethering anchoring molecules; (d) phospholipid bilayer [4].

1. Luo Y, Song Y. Mechanism of Antimicrobial Peptides: Antimicrobial, Anti-Inflammatory and Antibiofilm Activities. Int J Mol Sci. 2021 Oct 22;22(21):11401.

2. Boparai JK, Sharma PK. Mini Review on Antimicrobial Peptides, Sources, Mechanism and Recent Applications. Protein Pept Lett. 2019 Dec 10;27(1):4–16.

3. Arya SS, Morsy NK, Islayem DK, Alkhatib SA, Pitsalidis C, Pappa AM. Bacterial Membrane Mimetics: From Biosensing to Disease Prevention and Treatment. Biosensors. 2023 Jan 26;13(2):189.

4. Budvytyte R, Ambrulevičius F, Jankaityte E, Valincius G. Electrochemical assessment of dielectric damage to phospholipid bilayers by amyloid β-Oligomers. Bioelectrochemistry. 2022 Jun;145:108091.

5. Andersson J, Köper I. Tethered and Polymer Supported Bilayer Lipid Membranes: Structure and Function. Membranes. 2016 May 30;6(2):30.

A DFT study of $TPPS_4$ monomers, dimers and their absorption spectra

Laura Baliulyte[1], Darius Abramavicius[1]

[1]Vilnius University, Institute of Chemical Physics, Sauletekio 3, LT-10257, Vilnius, Lithuania
laura.baliulyte@ff.vu.lt

Recently there has been growing interest in 5,10,15,20-tetrakis(4-sulfonatophenyl) porphyrin ($TPPS_4$) for applications in photodynamic therapy (PDT). $TPPS_4$ molecules have been extensively investigated because they efficiently self-associate from monomers to large H- (face-to-face) or J- (side-by-side) aggregates in aqueous solution depending on the pH value and compound concentration. The prevalent form of $TPPS_4$ depends on the pH of the solvent: $H_2TPPS_4^{4-}$ dominates in alkaline (pH ≈ 12) and neutral solutions (pH ≈ 7), $H_4TPPS_4^{2-}$ dominates in a pH range of ≈ 4–3, $H_6TPPS_4^{0}$ is prevalent at a pH of ≈ 1, and $H_8TPPS_4^{2+}$ appears to dominate at even lower pH. It is still not understood what type of aggregates are formed in specific conditions. In the present work we show that monomeric forms dominate at pH = 12.1, pH = 7.1, pH = 4.1, pH = 3.0, and pH = −1.0, in contrast, J-dimers become a dominant form at pH = 1.0. These results coincide with the literature reporting that $TPPS_4$ (in a form where a half of the peripheral SO_3^- groups is replaced by SO_3H) tends to form J-aggregates in acidified aqueous media. This is because of the electrostatic repulsion being weakened between $TPPS_4$ molecules in the acidic solution (pH < 2) [1]. These quantum chemistry (it was used density functional theory (DFT) CAM-B3LYP/6-31G(d,p) and polarizable continuum model (PCM) method) studies suggest an aggregate seeds structure at the molecular level. A number of structural transformations of $TPPS_4$ have been determined when changing the acidity from pH = 12.1 to pH =−1.0. It reveal that 5 different forms of $TPPS_4$ monomers and 10 dimers were found as possible candidates for $TPPS_4$ aggregate precursors. Calculated absorption spectra coincide with experimentally measured spectra [2]. According to our calculations, the aggregation is related to zwitterion formation, and the growth proceeds starting from Z2 (SO_3H groups are adjacent) monomers. The absorption spectra of Z2 monomer and $J_3^{(0)}$ dimer (and also structure of $J_3^{(0)}$ dimer) are shown in Fig.1.

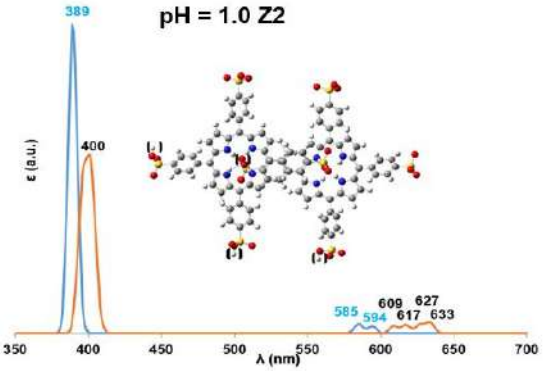

Fig.1. The calculated absorption spectra of $H_6TPPS_4^{0}$ (Z2) monomer (blue lines) and the corresponding $J_3^{(0)}$ dimer (orange lines) and structure of $J_3^{(0)}$ dimer

Acknowledgements: Computations were performed on resources at the supercomputer “VU HPC” of Vilnius University in the Faculty of Physics location.

[1] Y. Xiu, X. Zhang, Y. Feng, R. Wei, S. Wang, Y. Xia, M. Cao, and S. Wang, “Peptide-mediatedporphyrin based hierarchical complexes for light-to-chemical conversion” , Nanoscale 12(28),15201–15208 (2020).
[2] L. Baliulyte, D. Abramavicius, S. Bagdonas, A. Kalnaityte, V. Poderys, R. Rotomskis, and V.Barzda, “Comparative quantum chemical and spectral characterization of meso-tetra (4-sulfonatophenyl) porphine forms as seeds for J-and H-aggregates”, AIP Advances, 13(10) (2023).

Evaluation of diagnostical information carried by ECG signals registered by different lead systems: The Multivariate analysis approach

Robertas Petrolis[1,2], Arturas Grigaliunas[1], Algimantas Krisciukaitis[1,2], Renata Paukstaitiene[1]

[1]Department of Physics, Mathematics and Biophysics, Lithuanian University of Health Sciences, Eiveniu st. 4, Kaunas, Lithuania

[2]Neuroscience Institute, Lithuanian University of Health Sciences, Laboratory of Biophysics and Bioinformatics, Eiveniu st. 4, Kaunas, Lithuania

robertas.petrolis@lsmu.lt

Electrocardiogram (ECG) signal reflects electrical processes taking part in the human body. Various lead combinations and registering systems are designed in aim to reflect as much as possible of valuable diagnostical information at the same time minimizing representation of concurrent electrical processes in the human body. On the other hand, designers of the lead systems aim to minimize the number of leads used making the registering of the signals less obtrusive for the patient. Assessment of suitability of the registered signals and their diagnostic value remains challenging because of broad variety of the diagnostic applications where ECG signals are used. Anyway, the general purpose of ECG registering systems is to reflect three-dimensional changes of the electrical field in the body during excitation of heart muscle, so, spatial positioning of the leads is optimized for few particular diagnostic cases (e.g. 12-lead ECG). Classical approach of orthogonal Franc leads system could be considered as „Golden Standard" in ECG registering comprehensively reflecting all electrical activity of the heart. Multivariate analysis method Principal Component Analysis (PCA) [1] gives an optimal representation of variance in multidimensional data. Multilead ECG signal could be considered as multidimensional data, therefore the PCA will give optimal representation of variance in it, what actually is the valuable diagnostic information. In ideal case, if all registering systems are concerned as equally good, this optimal representation of variance in ECG signal should be the same, regardless to the particular lead system used. Various transforms are proposed to obtain it: for example, 12-lead signal from special 4-lead registered signals, or Frank orthogonal leads from 12-leads by using deep neural network [2,3]. Here we propose the method to assess the diagnostical value of ECG signal, registered by some "new lead system" (Neural Network based 3-lead reconstruction from 12-lead ECG), comparing PCA representation of its result to the one obtained from some „Golden Standard" system like 12-lead or Orthogonal Frank leads.

We analysed 12-lead and orthogonal Frank lead ECG recordings from healthy and myocardial infarction patients from open-access PhysioNet PTB Diagnostic ECG Database [4]. The recordings in this Database are unique because the same multilead signal was register synchronically in 12-lead and Orthogonal Frank lead systems. We compared the optimal representation of electrical activity registered by both "standard" systems and "new lead system" – Neural Network transformed signal. The complexity of the signal (amount of carried information) could be reflected by minimal amount principal components needed for optimal its' representation. We found that third principal component becomes important only in myocardial infarction cases (Fig.1, Table 1). The differences in coefficients of third principal component revealed limitations of Neural Network based signal transform. The presented case is an example how any newly designed ECG registering system could be evaluated in regard to the information carried by the registered signals.

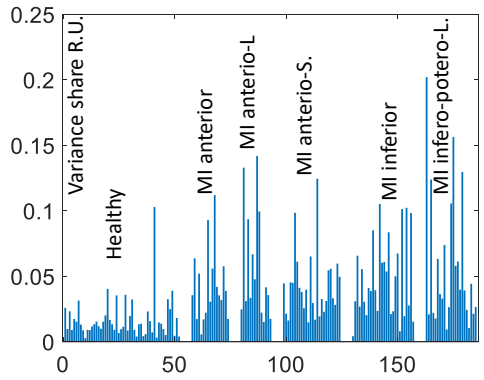

Fig.1. Relative signal variance shares of the third principal component in signals from healthy and MI patients

Table.1. Differences in relative signal variance shares of the third principal component in signals from healthy and MI patients.

	3 rd. Principle Component variance	
	Median value	Min - Max
Healthy	13,3613 x 10^{-3}	2,7698 x 10^{-3} - 102,9076 x 10^{-3}
MI anterior[a]	35,5682 x 10^{-3}	5,6021 x 10^{-3} - 111,9721 x 10^{-3}
MI anterio-lateral[b]	38,6318 x 10^{-3}	15,0957 x 10^{-3} - 141,7964 x 10^{-3}
MI anterio-septal[c]	38,8362 x 10^{-3}	14,7949 x 10^{-3} - 124,4988 x 10^{-3}
MI inferior[d]	40,2521 x 10^{-3}	4,2664 x 10^{-3} - 105,2145 x 10^{-3}
MI infero-potero-lateral[e]	39,1799 x 10^{-3}	9,4489 x 10^{-3} - 202,0234 x 10^{-3}
Independent-Samples Kruskal-Wallis Test p value <0,001. Pairwise comparisons of Healthy to [a,b,c,d,e] < 0,001		

[1] Castells, F., Laguna, P., Sörnmo, L. et al. Principal Component Analysis in ECG Signal Processing. EURASIP J. Adv. Signal Process. 2007, 074580 (2007).

[2] Dawson D, Yang H, Malshe M, Bukkapatnam ST, Benjamin B, Komanduri R. Linear affine transformations between 3-lead (Frank XYZ leads) vectorcardiogram and 12-lead electrocardiogram signals. *J Electrocardiol*. 2009 Nov-Dec;42(6):622-30.

[3] Smith GH, Van den Heever DJ, Swart W. The Reconstruction of a 12-Lead Electrocardiogram from a Reduced Lead Set Using a Focus Time-Delay Neural Network. Acta Cardiol Sin. 2021 Jan;37(1):47-57.

[4] Kreiseler, D.; Bousseljot, R. Automatisierte EKG-Auswertung mit Hilfe der EKG-Signaldatenbank CARDIODAT der PTB. Biomedizinische Technik, Band 40, Ergänzungsband 1 (1995) S 319

Determining the Delay for Opposite Phases of Bipolar Pulses to Optimize Electrochemotherapy

Veronika Malyško-Ptašinskė[1], Aušra Nemeikaitė-Čėnienė[2], Eivina Radzevičiūtė-Valčiukė[1,2], Eglė Mickevičiūtė[2], Paulina Malakauskaitė[2], Barbora Lekešytė[2] and Vitalij Novickij[1,2]

[1] Faculty of Electronics, Vilnius Gediminas Technical University, Vilnius, Lithuania
[2] Department of Immunology and Bioelectrochemistry, State Research Institute Centre of Innovative Medicine, Vilnius, Lithuania
veronika.malysko-ptasinske@vilniustech.lt

Electroporation techniques using nanosecond bipolar pulses often face a challenge known as the bipolar cancellation effect (BPC). This occurs when the second pulse partially or completely negates the impact of the first, leading to reduced permeabilization of the cell membrane and lowering the overall effectiveness of the electroporation-based treatments, including electrochemotherapy (ECT) [1]. To mitigate this issue, introducing a temporal gap between the positive and negative phases of the bipolar pulses during electroporation has been proposed [2-3], although the exact thresholds remain obscure. In our study, we explore the effects of different interphase delay durations (ranging from 0 ms to 95 ms) on symmetric bipolar nanosecond electrochemotherapy (with 300- and 500 ns pulses) using cisplatin, and apply 10 Hz, 100 Hz, and 1 kHz protocols in vitro. The mouse hepatoma MH-22a cell line as a model. We assess how cell membrane permeabilization and viability vary under different bipolar pulsed electric field conditions. Additionally, our research highlights the applicability of symmetrical bipolar pulses for ECT and examines how their efficiency depends on interphase delay. We also compare the results with those obtained from monopolar pulses with the same parameters.

Our results show that with a 0 ms interphase delay, the permeabilization rate of MH-22a cells decreased by approximately 30%, confirming the presence of the cancellation effect across all tested burst frequencies. However, we identified a critical delay threshold between the positive and negative pulse phases that significantly reduces bipolar cancellation, allowing treatment efficacy comparable to monophasic pulses with the same parameters. The results indicate that with certain interphase delay value bipolar pulses induced a molecular uptake similar to that of unipolar pulses.

[1] Pakhomov, Andrei G., Iurii Semenov, Shu Xiao, Olga N. Pakhomova, Betsy Gregory, Karl H. Schoenbach, Jody C. Ullery, Hope T. Beier, Sambasiva R. Rajulapati, and Bennett L. Ibey. "Cancellation of cellular responses to nanoelectroporation by reversing the stimulus polarity." Cellular and molecular life sciences 71. 4431-4441. (2014).

[2] Łapińska, Zofia, Vitalij Novickij, Nina Rembiałkowska, Anna Szewczyk, Magdalena Dubińska-Magiera, Julita Kulbacka, and Jolanta Saczko. "The influence of asymmetrical bipolar pulses and interphase intervals on the bipolar cancellation phenomenon in the ovarian cancer cell line." Bioelectrochemistry 153. 108483(2023).

[2] Valdez, Chris M., Ronald Barnes Jr, Caleb C. Roth, Erick Moen, and Bennett Ibey. "The interphase interval within a bipolar nanosecond electric pulse modulates bipolar cancellation." Bioelectromagnetics 39, no. 6. 441-450. (2018).

THE EFFECT OF THE ANESTHETIC PROPOFOL ON CONNEXINS OF CARDIOVASCULAR SYSTEM

Orestas Makniusevičius[1], Tadas Kraujalis[1,2], Mindaugas Šnipas[1,3], Lukas Gudaitis[1], Lina Kraujalienė[1]

[1]Lithuanian University of Health Sciences, Medical Academy, Institute of Cardiology, Kaunas, Lithuania
[2]Kaunas University of Technology, Department of Applied Informatics, Kaunas, Lithuania
[3]Kaunas University of Technology, Department of Mathematical Modelling, Kaunas, Lithuania
orestas.makniusevicius@lsmu.lt

Propofol is a widely used general anesthetic, which causes a rapid induction of anesthesia and rapid recovery after it. The most prominent side effect of propofol is the decrease of systemic vascular resistance that leads to hypotension [1]. Moreover, in some cases, propofol has been shown to inhibit cardiac conduction and cause bradycardia that can result in cardiac arrest. The propofol effect on the induction of bradycardia has been known for more than 30 years, but its pathophysiological mechanism is still not fully understood. One of the putative mechanisms for the conduction block could be the ability of propofol to change the activity of human atrial muscarinic cholinergic receptors [2]. It is also known that propofol may directly inhibit the sinoatrial (SA) node cells. Furthermore, according to certain research, the effect of propofol on the conduction system varies depending on the concentration of the drug. On the other hand, propofol was shown to have a protective effect against ventricular arrhythmias during myocardial ischemia [3]. Thus, the influence of propofol on the heart rhythm remains controversial.

The side effect of propofol may manifest itself through its action on different targets. Indeed, several studies have shown that propofol may regulate cell coupling through gap junction (GJ) channels formed of Cx43. However, it is unclear how propofol affects all cardiac connexins, not just connexin-43 (Cx43). As known Cx43, Cx45, Cx37 and Cx40 form gap junction channels in cardiac and vascular system. These connexins are required for coordination of vascular responses and play a key role in ensuring propagation of action potential in cardiac tissue.

The aim of this study was to get a better understanding the capacity of propofol to affect cardiovascular connexins. First, we compared the effect of propofol concentrations on GJs formed by Cx40, Cx43, Cx45 and Cx37 which were expressed exogenously in human cervix epithelial adenocarcinoma cells (HeLa). The junctional conductance was measured using double whole-cell patch clamp method. Our data show that Cx40 and Cx43 channels exhibit similar sensitivity to propofol, while Cx45 channels are only sensitive to much higher propofol concentrations than Cx40 and Cx43 channels. Of all the connexins under research, the most surprising finding showed that Cx37, the vascular system connexin and an important player in coronary heart disease, is also the most susceptible to propofol, meaning it is more sensitive to lower concentrations of the drug.

It was suggested that propofol may affect Cx43 GJ channels through activation of protein kinase C (PKC), which in turn phosphorylates Cx43 and reduces coupling through GJs [4]. In our study, the kinase inhibitor GF109203X was used to assess this putative pathway of propofol action on GJs. It is established that low concentrations of GF109203X specifically inhibit PKC while higher concentrations inhibit both PKC and protein kinase A (PKA). Our data showed that low (40 nM) concentration of GF109203X significantly reduced inhibition of Cx43 channels by propofol, indicating that propofol regulates Cx43 channels in PKC-dependent manner, which is in good agreement with already published studies. In contrast, both concentrations of GF109203X had no effect on inhibition of Cx40 channels by propofol, indicating that neither PKC nor PKA is involved in regulation of these channels by the anesthetic. This preliminary data suggest that propofol may have a prominent, connexin specific effect on GJs.

[1] Royse, C. F., Liew, D. F. L., Wright, C. E., Royse, A. G., & Angus, J. A. (2008). Persistent Depression of Contractility and Vasodilation with Propofol but Not with Sevoflurane or Desflurane in Rabbits. *Anesthesiology*, *108*(1), 87–93. https://doi.org/10.1097/01.anes.0000296077.32685.26

[2] Aguero Peña, R. E., Pascuzzo-Lima, C., Granado Duque, A. E., & Bonfante-Cabarcas, R. A. (2008). Depresión de la función miocárdica inducida por propofol: Posible participación del receptor colinérgico muscarínico auricular. *Revista Española de Anestesiología y Reanimación*, *55*(2), 81–85. https://doi.org/10.1016/S0034-9356(08)70514-0

[3] Hirata, N., Kanaya, N., Kamada, N., Kimura, S., & Namiki, A. (2009). Differential Effects of Propofol and Sevoflurane on Ischemia-induced Ventricular Arrhythmias and Phosphorylated Connexin 43 Protein in Rats. *Anesthesiology*, *110*(1), 50–57. https://doi.org/10.1097/ALN.0b013e318190b537

[4]Wickley, P. J., Ding, X., Murray, P. A., & Damron, D. S. (2006). Propofol-induced Activation of Protein Kinase C Isoforms in Adult Rat Ventricular Myocytes. *Anesthesiology*, *104*(5), 970–977. https://doi.org/10.1097/00000542-200605000-00013

Investigating the Impact of Electroporation Combination with Cannabinoids on CHO-K1 cells

Augustinas Želvys[1,2], Povilas Kavaliauskas[3,4], Ramunė Grigalevičiūtė[3,5], Vitalij Novickij[1,2]

[1]State Research Institute Centre for Innovative Medicine, Department of Immunology and Bioelectrochemistry, Santariškių g. 5, Vilnius, Lithuania
[2]Faculty of Electronics, Vilnius Gediminas Technical University, Saulėtekio al. 11, Vilnius, Lithuania
[3]Biological Research Center, Lithuanian University of Health Sciences, Tilzes str. 18/7, Kaunas, LT-47181, Lithuania
[4]Joan and Sanford I. Weill Department of Medicine, Weill Cornell University, 1300 York Avenue, NY 1109. New York, United States
[5]Department of Animal Nutrition, Lithuanian University of Health Sciences, Tilzes str. 18 Kaunas, LT-47181, Lithuania
augustinas.zelvys@imcentras.lt

The relentless pursuit of new anticancer drugs remains a critical focus in medical research due to the ongoing challenges in effectively treating various forms of cancer. In recent times, research has highlighted that cannabinoids, especially the non-psychoactive types, have significant medical and pharmacological activities, potentially qualifying them as antitumor candidates. Combination antitumor agents with reversible electroporation is known as electrochemotherapy (ECT), when pulsed electric field (PEF)-mediated drug delivery boosts the efficacy of chemotherapeutic drugs, leading to a more effective tumor eradication compared to standard chemotherapy. In this study we explore the effects of electroporation combined with cannabinoids – Cannabidiol (CBD), Cannabinol (CBN) and Cannabigerol (CBG) – on the viability and reactive oxygen species (ROS) generation in Chinese Hamster Ovary (CHO-K1) cells. Cannabinoids, as potential anticancer agents, were introduced to CHO-K1 cells using both microsecond (μsPEF) and nanosecond (nsPEF) electroporation to enhance cellular uptake and efficacy. Our findings indicate that this combination significantly impacts cell viability and induces higher ROS generation compared to electroporation without drugs. The results highlight the promise of using electroporation to potentiate the therapeutic effects of cannabinoids, paving the way for novel cancer treatment strategies.

Development and Evaluation of Biocide-Polymer Nanocomposite Coatings for Enhanced Antimicrobial Protection

Mindaugas Ilickas[1], Asta Guobienė[1], Brigita Abakevičienė[1,2]

[1]Institute of Materials Science, Kaunas University of Technology, Kaunas, Lithuania
[2]Department of Physics, Kaunas University of Technology, Kaunas, Lithuania
mindaugas.ilickas@ktu.edu

The development and application of protective biocide-based coatings are crucial for safeguarding public health and preventing the transmission of diseases caused by microorganisms [1]. A pertinent example is the COVID-19 pandemic, which is caused by the SARS-CoV-2 virus. The relationship between hygiene and disease underscores the importance of surface modification and advancements in antimicrobial coatings [1]. The challenges posed by Gram-positive and Gram-negative bacteria, as well as antibiotic-resistant bacteria and viruses, are driving the search for and development of novel disinfectants and biocidal agents [2]. Additionally, bacteriophage φ6 serves as a valuable substitute for testing enveloped viruses [3], such as SARS-CoV-2, as it does not require a high-security BSL laboratory for conducting antiviral assays.

In this work, chemically synthesized biocidal agents – specifically, solutions of ampicillin sodium salt (A), benzalkonium chloride (BAC), hexadecyltrimethylammonium bromide (CTAB), 2-mercaptopyridine N-oxide sodium salt (NaPT), and triclosan (T) – were incorporated into a polyvinyl butyral (PVB) polymer matrix to produce a biocide-polymer nanocomposite. Coatings of varying thicknesses were applied using a commercial slot-die coater (Ossila Ltd, UK). Subsequent physical and antimicrobial evaluations were performed on the resultant coatings.

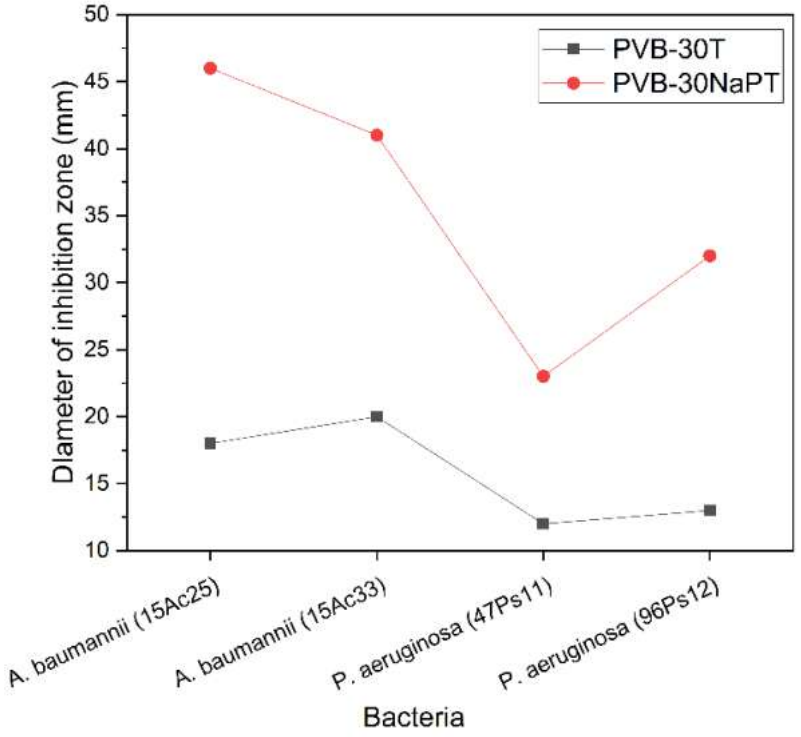

Fig. 1. Results from the Kirby-Bauer disk diffusion assay

The Kirby-Bauer disk diffusion susceptibility assay revealed that the PVB-30T sample exhibited the smallest zone of inhibition, measuring 12 mm, against the *P. aeruginosa* strain 47Ps11. In contrast, the PVB-30NaPT sample displayed the largest zone of inhibition, measuring 44 mm, against the *A. baumannii* strain 15Ac25. The zone of inhibition observed against the Gram-positive bacterium *A. baumannii* is approximately 1.5 times greater than that observed against the Gram-negative bacterium *P. aeruginosa*, indicating superior efficacy of the tested substances against Gram-positive bacteria. Furthermore, the zone of inhibition for the PVB-30NaPT sample is 2.0 to 2.5 times larger compared to that of the PVB-30T sample. These findings underscore the significance of developing durable antimicrobial coatings to mitigate the spread of infectious diseases.

[1] K.C. de Castro, J.M. Costa. Journal of Polymer Research, **28** (2021).
[2] S. Bhatt, R. Pathak, V.D. Punetha, M. Punetha. J Mater Sci, **58**, 7839-7867 (2023).
[3] Á. Serrano-Aroca. Int J Mol Sci, **23** (2022).

Investigating the Role of Plasma Voltage in Modulating PEF-Induced Effects on *Chlorella vulgaris*

Raimonda Celiešiūtė-Germanienė [1], Kamilė Jonynaitė[1], Rolandas Uscila[2], Skirmantas Keršulis[1], Žydrūnas Kavaliauskas[2], Liutauras Marcinauskas[2], Arūnas Stirkė[1], Voitech Stankevič[1]

[1]State Research Institute, Center for Physical Sciences and Technology, Department of Functional Materials and Electronics, Sauletekio ave. 3, Vilnius, Lithuania
[2]Lithuanian Energy Institute, Plasma Processing Laboratory, Breslaujos str. 3, Kaunas, Lithuania
raimonda.celiesiute@ftmc.lt

The combination of gliding arc discharge (GAD) plasma and pulsed electric fields (PEF) is of scientific interest for enhancing the effectiveness of PEF-induced outcomes as both plasma and pulsed electric fields are emerging technologies that have individually shown potential in microalgae treatment [1-4].

The underlying mechanism is believed to involve plasma-generated radicals that promote lipid oxidation, which disrupts membrane integrity and boosts the overall efficacy of the combined treatment compared to using plasma or PEF independently. Moreover, this combined approach has been shown to synergistically elevate intracellular reactive oxygen species (ROS) production, influencing cytotoxicity and cell death pathways. Nevertheless, the specific effects of this combined effect on microalgae remain poorly understood.

To address this gap, the present study was conducted to examine synergistic effect of GAD plasma and PEF on fresh water microalgae *Chlorella vulgaris*. For this purpose, the GAD reactor was powered by an AC supply, which included a 270 kHz AC generator connected to a high-voltage transformer with a 1:33 ratio. Concentrated algal biomass was subjected to plasma treatment under the following conditions: a compressed air flow rate of 22.8 l/min, an electrode-to-suspension distance of 30 mm, and a treatment duration of 300 seconds. The discharge voltage of the GAD plasma was regulated by adjusting the output voltage of the AC generator (V_{out}) within the range of 50-250 V. Following plasma treatment, the algal suspension was exposed to PEF, utilizing parameters such as a pulse duration of 7 μs, 1-10 exponential pulses at a frequency of 1 Hz, and an electric field strength of 24-25 kV/cm. Changes in both suspension properties and cellular characteristics of untreated and treated algal samples were assessed.

The results indicate that the effects induced by the combined treatment are dependent on the plasma voltage. Applying a lower plasma voltage (V_{out} = 130 V) in combination with a single PEF pulse led to an increase in algal cell permeability, similar to that observed with PEF treatment alone. At 24 hours post-treatment, the release of nucleic acids and proteins was comparable to levels seen in the ultrasound-treated control. These findings were accompanied by altered cell morphology, indicating that programmed cell death may have been initiated. Conversely, raising the AC generator output voltage above 170 V produced a varied response in the algae to the combined treatment. Although cell permeability increased in the majority of the algal population, DNA leakage decreased as plasma voltage increased. This reduction was particularly evident at plasma voltages of 210-250 V in conjunction with PEF, where DNA release remained comparable to untreated cells even after 24 hours. A similar pattern was observed for protein release, with a marked decline following exposure to high-voltage plasma and PEF. Additionally, microscopic analysis revealed that the algae, although metabolically inactive, maintained a structural integrity resembling that of intact cells. In conclusion, varying plasma output voltages lead to different changes in algal cells after combined plasma and PEF treatment, influencing the efficiency of PEF for protein extraction and altering the cell death mechanisms in *C. vulgaris*.

Acknowledgement: This work was supported by the Research Council of Lithuania under Grant P-MIP-22-257.

[1] L. Buchmann, I.Brändle, I. Haberkorn et al., *Bioresour. Technol.* **291**, 121870 (2019).
[2] M. Beyrer, M.C. Pina-Perez, D. Martinet et al., *Food Control.* **118**, 107378 (2020).
[3] D. Krust, C. Gusbeth, A.S.K. Müller et al., *Bioelectrochemistry*. **143,** 107991 (2022).
[4] M.M. El-Sheekh, M.A. Abd Al-Halim, S.A. Mohammed., *Algal Res*. **70**, 102983 (2023).

Effects of Nanosecond Pulses Delivered at Ultra-High Frequency on Mitochondrial Depolarization, ROS, Cell Permeabilization and Cell Viability

Paulina Malakauskaitė[1,2], Vytautas Kašėta[3], Vitalij Novickij[1,2]

[1] State Research Institute Centre for Innovative Medicine, Department of Immunology and Bioelectrochemistry, Vilnius, Lithuania
[2] Vilnius Gediminas Technical University, Faculty of Electronics, Vilnius, Lithuania
[3] State Research Institute Centre for Innovative Medicine, Department of Stem Cell Biology, Vilnius, Lithuania
paulina.malakauskaite@imcentras.lt

It is theoretically predicted that ultrashort nanosecond pulses could be utilized to permeabilize intracellular membranes, including mitochondria [1]. Such a phenomenon would have high applicability in cancer treatment context and could be employed for shifting toward immunogenic cell death as well as induction of immune response [2]. However, currently there is a lack of experimental evidence on the interaction of pulsed electric fields with mitochondria and their function.

In this study, for the first time, we characterize the effects of ultra-high repetition frequency (1–5 MHz) nanosecond pulses (6–18 kV/cm, 100 and 300 ns) in the context of mitochondrial depolarization (Tetramethylrhodamine, methyl ester (TMRM)), ROS generation (MitoSOX), cell plasma membrane permeabilization (YO-PRO-1) and cell viability. As a reference, standard microsecond range parametric protocols were used (100 µs × 8 pulses).

Our pilot data indicate that depending on the pulse repetition frequency, the efficiency of electroporation can be modulated, i.e., the higher is the frequency, the higher is the permeabilization. Also, the oxidation level has a dose-dependent scaling with pulse burst amplitude, while 100 ns pulses induce significantly lower oxidation than 300 ns pulses. In the context of TMRM fluorescence, our data indicate that treatment of cells with pulsed electric fields induces mitochondrial depolarization, however, the selectivity of the phenomenon is questionable and requires further research. Importantly, the results of our study show that boosting the pulse repetition frequency towards 5 MHz significantly improves the effects of 100 ns pulses, i.e., the protocols cause effective electroporation even in fields, which are considered sub-threshold for this pulse duration range. Therefore, derivation of new and more effective protocols for electroporation-based procedures can be performed without the increase of the energy input.

[1] Kotnik T, Pucihar G, Rebersek M, Miklavcic D, Mir LM. *Biochim Biophys Acta*. **1614**(2):193-200 (2003).
[2] Liu Z, Zou Y, Sun Y, Chen X, Chen X, Ren Z. *Anal Cell Pathol (Amst)*. **2021:9913716**. (2021).

Mechanism of CRISPR-Cas3 helicase using magnetic tweezers

Miglė Šarpilo[1], Algirdas Toleikis[1]

[1] Vilnius University, Life Science Center, 7 Saulėtekio Ave, Vilnius, Lithuania
migle.sarpilo@gmc.stud.vu.lt

CRISPR-Cas provides RNA-guided adaptive immunity against invading genetic elements. CRISPR systems consist of multiple Cas proteins, which are responsible for CRISPR-dependent cell immunity mechanisms. The effector complex in CRISPR I-E consists of Cascade and Cas3. Cascade is responsible for foreign DNA targeting. Meanwhile, Cas3, which possesses helicase and nuclease activities, is a key protein of the system, necessary for crRNA-guided interference against virus proliferation.

Although single-component Class 2 CRISPR systems, such as type II Cas9 are widely used for genome-editing, the research on multi-component Class 1 proteins, including Cas3, of the same system has been less developed. Components of the I-E CRISPR system have already been used as a genome-editing tool to generate big deletions. However, the detailed mechanism by which Cas3 achieves its function is not well understood. This study aims to elucidate the mechanism of Cas3 DNA unwinding and shredding. We are using single-molecule force microscopy, namely, **magnetic tweezers (MT)** (Fig. 1) and RepX helicase as a model to optimise MT methodology to probe the mechanical aspects of Cas3 unwinding activity ir the nearest future. Greater knowledge of the Cas3 mechanism of action would improve the application of Cas3 as a tool for genome editing.

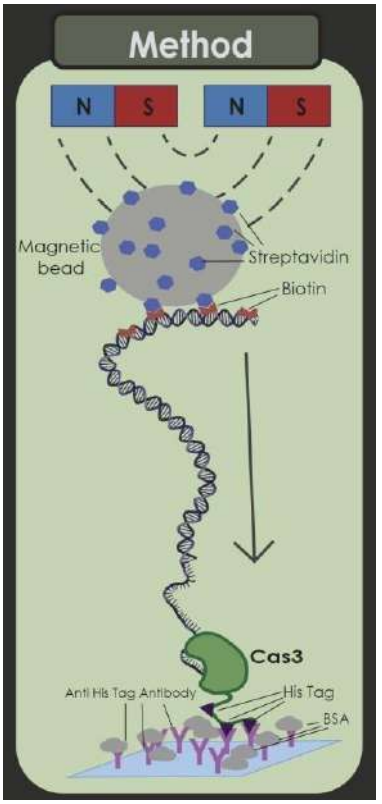

Fig. 1 Magnetic tweezers as a tool for protein research

Nanomaterials for Bimodal Imaging: Unlocking Potential in Biomedical Applications

Marijus Pleckaitis[1,2], Greta Butkiene[1], Vilius Poderys[1], Jonas Venius[1,3], Marius Burkanas[3], Giedre Grinciene[4], Souad Ammar-Merah[5], Arunas Jagminas[4], Virginijus Barzda[6,7], Ricardas Rotomskis[1], Vitalijus Karabanovas[1,8]

[1]Biomedical Physics Laboratory, National Cancer Institute, P. Baublio str. 3b, Vilnius, LT-08406, Lithuania
[2]Life Sciences Center, Vilnius University, Sauletekio av. 7, Vilnius, LT-10257, Lithuania
[3]Medical Physics Department, National Cancer Institute, Santariskiu str. 1, Vilnius, LT-08660, Lithuania
[4]State Research Institute Center for Physical Sciences and Technology, Sauletekio Ave. 3, Vilnius, LT-10257, Lithuania
[5]Université Paris Cité, CNRS, ITODYS, UMR 7086, 15 Rue Jean Antoine Ba, F-75251 Paris, France
[6]Department of Chemical and Physical Sciences, University of Toronto Mississauga, 3359 Mississauga Rd, Mississauga, L5L 1C6, Canada
[7]Department of Physics, University of Toronto, 60 St. George St. Toronto, Toronto, M5S 1A7, Canada
[8]Department of Chemistry and Bioengineering, Vilnius Gediminas Technical University, Sauletekio av. 11, Vilnius, LT-10223, Lithuania
marijus.pleckaitis@nvi.lt

Despite ever-improving technologies and medical advancements, the individual diagnostic methods currently used in clinics to detect various diseases, such as early-stage cancer, remain insufficient. Therefore, new approaches and novel strategies are needed. Nanomedicine offers the potential to integrate and combine various imaging modalities using nanomaterials. Nanomaterials designed for bimodal imaging combine two complementary imaging techniques to achieve superior diagnostic accuracy and unlock potential in biomedical applications.

In this study, we explored different combinations of imaging modalities in various nanomaterials: photoluminescence [1] or upconversion emission [2] combined with magnetic resonance imaging, fluorescence with non-linear optical imaging [3], and photoluminescence with SPECT/CT imaging [4]. Numerous nanomaterials, including protein-stabilized gold nanoclusters, upconverting nanoparticles, iron oxide magnetic nanoparticles, $TPPS_4$ molecular aggregates and technetium-99m, were utilized to realize these imaging modalities. Moreover, we investigated the potential biomedical applications of the nanomaterials we studied and demonstrated that they exhibit unique properties, are colloidally stable, and are biocompatible with tested cell lines, making them promising candidates for theranostic applications. For instance, magnetic iron oxide nanoparticles decorated with photoluminescent gold nanoclusters can be effectively combined to produce a bimodal imaging nanoplatform with both magnetic and optical properties, suitable for magnetic resonance imaging and optical biopsy [1]. Additionally, when exposed to visible light, these nanoparticles are capable of generating singlet oxygen and other reactive oxygen species, which are essential for photodynamic therapy in cancer treatment.

The creation of dual-mode imaging nanomaterials offers a fresh approach to overcoming current challenges in the detection and management of various illnesses. These materials have the potential to improve patient outcomes and reduce the risk of unwanted side effects by combining therapeutic and imaging capabilities.

[1] Pleckaitis, M. *et al.* Magnetic Nanoparticles Decorated with Gold Nanoclusters–Applications in Cancer Theranostics. *Advanced Materials Interfaces* **10**, 2300462 (2023).
[2] Parvizian, M. *et al.* Up-converting β-$NaY_{0.8}[Yb_{0.18}Er_{0.02}]F_4$ nanoparticles coated by superparamagnetic γ-Fe_2O_3 nanosatellites: Elaboration, characterization and in vitro cytotoxicity. *RSC Advances* (2024) (Just accepted).
[3] Pleckaitis, M. *et al.* Structure and principles of self-assembly of giant "sea urchin" type sulfonatophenyl porphine aggregates. *Nano Res.* **15**, 5527–5537 (2022).
[4] Jarockyte, G. *et al.* Biodistribution of Multimodal Gold Nanoclusters Designed for Photoluminescence-SPECT/CT Imaging and Diagnostic. *Nanomaterials* **12**, 3259 (2022).

Energy transfer between iron-stress-induced protein A and Photosystem I probed by two-dimensional electronic spectroscopy

Parveen Akhtar[1], Howe-Siang Tan[2], Petar H. Lambrev[1]

[1]HUN-REN Biological Research Centre, Szeged, Hungary
[2]School of Chemistry, Chemical Engineering and Biotechnology, Nanyang Technological University, Singapore
akhtar.parveen@brc.hu

Cyanobacteria - the oldest group of oxygenic photosynthetic organisms – are ecologically significant primary producers and have potential biotechnological applications. The photosynthetic apparatus of cyanobacteria, similar to algae and higher plants, consists of thylakoid membranes hosting the membrane protein complexes of the photoinduced electron-transport chain, including the photosystems I and II (PSI and PSII) binding chlorophyll *a* and carotenoids as pigment cofactors. In many environments, including oceans and freshwater systems, cyanobacteria face iron scarcity. As iron is a critical nutrient for photosynthesis, cyanobacteria have evolved various mechanisms to adapt to low iron conditions, ensuring their survival and continued photosynthetic activity. One of these adaptations involves the production of the pigment-protein complex called IsiA (Iron-Stress Induced A protein). IsiA forms ring-like structures around PSI and is thought to serve as a chlorophyll storage or an auxiliary light-harvesting antenna of PSI, expanding its ability to absorb light when the production of PSI core complexes is restricted due to the lack of iron. Thus, IsiA is the only membrane-bound peripheral light-harvesting complex in cyanobacteria.

Recent studies have elucidated the structure of the PSI-IsiA complex in the model cyanobacterium Synechocystis sp. PCC 6803. Spectroscopic studies have demonstrated efficient energy transfer from IsiA to PSI. Ultrafast time-resolved spectroscopy, particularly two-dimensional electronic spectroscopy (2DES), is a powerful technique for probing the excitation energy transfer from the antenna to the reaction centre[1]. 2DES is a spectroscopic technique capable of mapping the transfer of excitation energy in complex systems containing multiple pigments having different excitation energies, and hence absorbing at different wavelengths. We have employed 2DES to study the dynamics of excitation energy transfer in various types of multisubunit antenna and antenna-reaction centre supercomplexes isolated from plants[2], algae[3] and cyanobacteria[4,5.] In this work, we have investigated the light-harvesting function of IsiA in isolated IsiA-PSI supercomplexes by 2DES[5]. By analyzing the excitation dynamics of isolated IsiA, isolated PSI and the IsiA-PSI supercomplex, we have been able to identify different components of energy transfer from IsiA to the PSI core complex with lifetimes from about 2 to 20 picoseconds. This lifetime heterogeneity suggests that there are multiple routes of energy transfer or that the results reflect structurally different IsiA-PSI supercomplexes.

To complement the experimental data, we performed theoretical computations applying Förster resonance energy transfer theory to the available structural data of IsiA-PSI. The calculations suggest that the energy transfer from IsiA to PSI should occur over a single major timescale. Therefore, we ascribe the experimentally observed lifetime heterogeneity to structural variations in IsiA-PSI. In summary, despite the complexity of energy transfer dynamics, the data reveal that IsiA is a remarkably efficient antenna of PSI essentially doubling its effective absorption cross-section. Understanding the structural basis of efficient light-harvesting will prove important for the design of bioinspired solar technologies.

[1] P. H. Lambrev, P. Akhtar, H.-S. Tan, *BBA-Bioenergetics* **1861**, 148050 (2020).
[2] H. L. Nguyen, T. N. Do et al., *Sci. Adv.*, **10**, eadh0911 (2024).
[3] P. Akhtar, Y. Feng et al., *J. Phys. Chem. Lett.*, **15**, 5838-584 (2024).
[4] P. Akhtar, I. Caspy et al., *J. Am. Chem. Soc.*, **143**, 14601-14612 (2021).
[5] P. Akhtar, S. Jana, P. H. Lambrev, H.-S. Tan, *Front. Plant. Sci.*, **15** (2024).

Investigation of Aggregation Ability of Chlorophyllin and Chlorophyllin-Chitosan Complexes

Gabrielė Vasiliauskaitė[1], Irina Buchovec[1]

[1]Vilnius university, Institute of Photonics and Nanotechnology, Light Research Group, Saulėtekis av. 3, Vilnius, Lithuania
gabriele.vasiliauskaite@ff.vu.lt

Food deficiency is a global issue, with up to 40 % of crops lost due to plant pathogens. This problem is associated with the increasing resistance of microorganisms to antibiotics and antimicrobial technologies, such as pesticides. One of the most promising technologies is antimicrobial photodynamic inactivation (API), which relies on a photosensitizer (PS), light and molecular oxygen [1]. A PS absorbs light, and when excited, it reacts with molecular oxygen in the environment to generate reactive oxygen species (ROS) [2]. ROS induce oxidative stress and inactivate microorganisms. The natural PS chlorophyllin (Chl) is an anionic compound, which limits its ability to bind to microbial membranes, leading to reduced efficiency in microorganism inactivation. Conversely, the anionic Chl can form a complex with the natural cationic polymer chitosan (CHS), resulting in the Chl-CHS complex. This complex can bind to microbial membranes and penetrate them more easily [3]. However, Chl is prone to aggregation, which can influence API efficiency. The aim of this study is to evaluate the aggregation potential of magnesium Chl (MgChl), copper Chl (CuChl) and their complexes with CHS (MgChl – CHS and CuChl – CHS).

In the first stage of work, three stock solutions were prepared: 0.01% MgChl and 0.01% CuChl in deionised water (diH_2O) and 1% CHS in a mixture of diH_2O and HCl. These stock solutions were used to obtain 0.01% Chl – 1% CHS complexes. All stock solutions were then diluted in 0.9 % NaCl or phosphate – buffered solution (PBS) to obtain working concentrations: 0.001% Chls (Fig. 1 A: table 1) and 0.001% Chl – 0.1% CHS complexes (Fig. 1 A: table 2). The pH of all working solutions was adjusted using 0.1 M NaOH and 0.1 M HCl (Fig. 1 A: table 3 and 4). For further studies the degree of aggregation of the Chls and Chl – CHS complexes with different pH values (Fig.1 A: table 2, 3 and 4) was evaluated before and after mixing solutions with aggregate detergent Triton X-100 using spectroscopic method (Fig. 1 B).

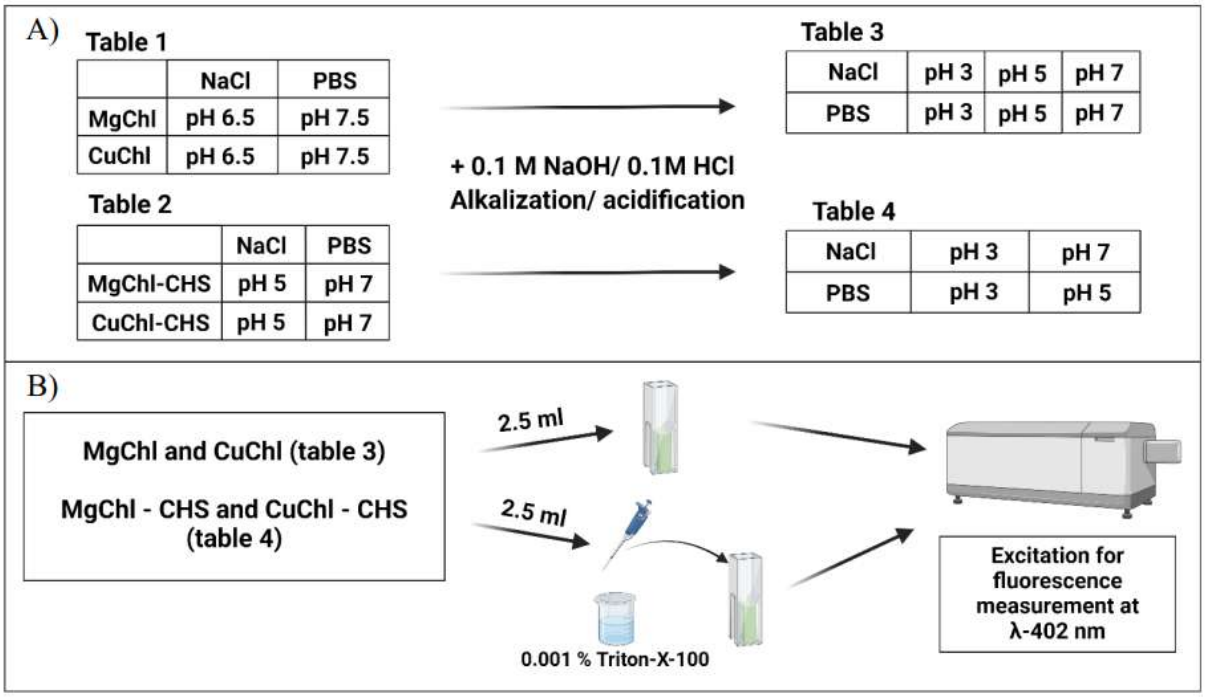

Fig. 1. Experiments scheme: A) pH adjustments (alkalization/acidification); B) aggregation measurement.

This study showed that the CuChl – CHS complex is more aggregated than CuChl alone in both solutions, regardless of pH. Aggregation of CuChl and the CuChl – CHS complex was highest in NaCl solution at pH 3 and 5. MgChl showed the most aggregation in NaCl solution at pH 3, while MgChl – CHS complex aggregation was greatest in both NaCl and PBS solutions at pH 5.

In future work, the effect of the aggregation of the MgChl-CHS and CuChl-CHS complexes, as well as separate MgChl and CuChl, on the photophysical and antimicrobial properties of these materials will be investigated.

[1] Hamblin, M.R. (2016). Current Opinion in Microbiology, 33, 67–73.
[2] A. Rapacka-Zdoncyk, et al. (2021). Frontiers in Medicine, 2296-858X.
[3] I. Buchovec, et al. (2016). Photochemical and Photobiological Sciences, 15, 506.

Biochip for Controlled Mechanical Stress Investigations in Living Cells

Andrius Pečiulis[1], Airina Mazėtytė-Godienė[1], Tomas Rakickas[1], Tadas Jelinskas[1], dr. Martynas Gavutis[1]

[1]Department of Nanoengineering, Center for Physical Sciences and Technology, LT-02300 Vilnius, Lithuania
andrius.peciulis@ftmc.lt

Mechanobiology is a new interdisciplinary field that studies the mechanisms by which cells sense and respond to mechanical signals from the environment. The mechanical forces and stresses play a crucial role in processes such as morphogenesis, cell migration, polarization, and proliferation [1]. Understanding the molecular, cellular, and tissue-level changes induced by these forces could offer new insights into tissue physiology and disease progression, potentially leading to innovative approaches in regenerative medicine [2]. For further development of this field a cell growth platform is needed, that would provide the control over the cell environment. Such a platform could be achieved by employing hydrogels as cell growth substrate [3].

Our main goal is to create a hydrogel-based platform for myoblast growth and differentiation. For this purpose, we chose to fabricate a biochip with hydrogel of a tunable stiffness and create different patterns of fibronectin on top of this substrate. The hydrogel chosen for this task was polyacrylamide, which is commonly used for mimicking extracellular matrix environment, with well-defined properties, low cost, plethora of preparation protocols and prospects for easy functionalization [4]. This approach allowed us to control the area of myoblast cell attachment and differentiation into muscle fibers. We further stimulated these fibers with the electric current and successfully registered cellular contractions.

Within the framework of this project functionalized polyacrylamide chips were fabricated, with polyacrylamide hydrogel containing carboxyl groups via introduction of methacrylic acid. This allowed us to employ NHS/EDC reaction to allow for covalent binding of fibronectin to the hydrogel surface. During cell seeding experiments, mouse myoblasts (cell line: C2C12) were seeded on the patterned polyacrylamide chips and left to grow and differentiate, resulting in formation of muscle fibers on the fibronectin patterned areas. The cell growth and differentiation were tracked on a weekly basis, by brightfield microscopy. Wide field fluorescent microscopy was utilized to visualize the fibronectin patterns.

Furthermore, the Quantitative Imaging AFM was used to measure stiffness (Youngs modulus) of differently prepared polyacrylamide substrates. We selected 50kPa polyacrylamide substrate based on the literature data on the tissue mechanics. A custom-made electric stimulation system in tandem with an inverted bright field microscope was employed to observe and register myoblast contractions. Additionally, we tested various methods for polyacrylamide patterning, that could allow for a more intricate control over cells in future research.

The main advantages of our system are the control of the cell growth area and the substrate stiffness. Although such a type of platform requires further investigation and refinement, it holds promise for drug screening and disease modelling.

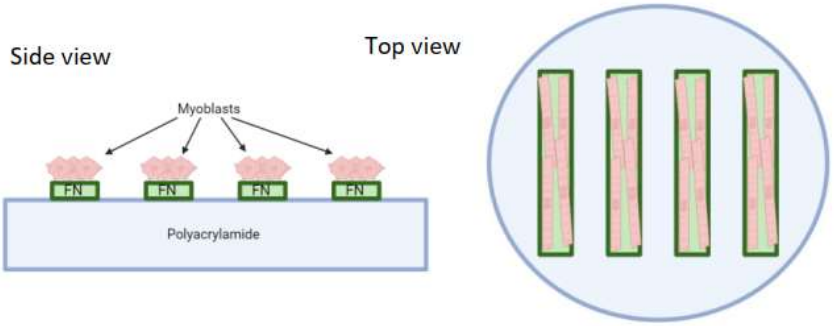

Figure 1. A schematic overview of polyacrylamide biochip, for myoblast growth. FN – fibronectin.

[1] U. Blache *et al.*, "Engineered hydrogels for mechanobiology," *Nature Reviews Methods Primers*, vol. 2, no. 1, p. 98, 2022, doi: 10.1038/s43586-022-00179-7.

[2] S. Min *et al.*, "Versatile human cardiac tissues engineered with perfusable heart extracellular microenvironment for biomedical applications," *Nat Commun*, vol. 15, no. 1, Dec. 2024, doi: 10.1038/s41467-024-46928-y.

[3] Cėpla, V., Rakickas, T., Stankevičienė, G., Mazėtytė-Godienė, A., Baradokė, A., Ruželė, Ž., & Valiokas, R. nas. (2020). Photografting and Patterning of Poly(ethylene glycol) Methacrylate Hydrogel on Glass for Biochip Applications. ACS Applied Materials and Interfaces, 12(29), 32233–32246. https://doi.org/10.1021/acsami.0c04085

[4] A. Gandin *et al.*, "Simple yet effective methods to probe hydrogel stiffness for mechanobiology," *Sci Rep*, vol. 11, no. 1, Dec. 2021, doi: 10.1038/s41598-021-01036-5.

Integrated Microfluidic Chip for Cultivating and Sensing Microbial Biofilms

Adei Abouhagger[1], Eivydas Andriukonis[1], Kamile Kasperavičiute[1], Arunas Stirke[1] and Wanessa Melo[1*]

[1]State Research Institute Centre for Physical Sciences and Technology—FTMC, Department of Functional Materials andElectronic, Vilnius, Lithuania
adei.abouhagger@ftmc.lt

Biofilm-associated infections present major challenges in wound care, often resulting in chronic infections and resistance to treatments [1]. To tackle these issues, we designed an advanced microfluidic 'Lab-on-a-chip' platform that replicates the dynamic microenvironment where biofilms thrive, enabling real-time analysis of biofilm growth, structural maturation, and response to therapies. This cutting-edge approach not only enhances infection control strategies but also accelerates the development of more effective treatments for biofilm-related infections [2]. The platform incorporates five independent channels, complete with inlets, outlets, growth chambers, and sensing chambers that can be integrated with electrodes for real-time biophysical measurements. Constructed with cyclo-olefin copolymer (COC) slides and Off- stoichiometry thiol-ene (OSTE) polymer microchannels, this PDMS-free design offers a versatile and dynamic environment for studying the physical properties of biofilms.

The microfluidic chip fabrication process: it includes multiple steps that are designed to ensure precise functionality and reliability (see **Figure 1**). Moreover, the microchip was integrated with electrodes to perform electrochemical measurements.

Microbial biofilm growth: a cell suspension of *E. coli* in phosphate-buffered saline (PBS) with a concentration of 10^7 cells/mL was introduced into the growth chamber of the microfluidic chip and incubated at 37°C for 1.5 hours to allow forcell adhesion. Next, brain heart infusion (BHI) was set to a flow rate of 10 µL/min for 24 hours at 37°C. Subsequently, PBS was used to wash off the residual growth medium. Biofilm was fixed with 4% formaldehyde. Finally, the samples were stained with 0.5 µg/mL 4′,6-diamidino-2-phenylindole (DAPI) for 15 minutes in the dark, and visualized using confocal laser scanningmicroscopy.

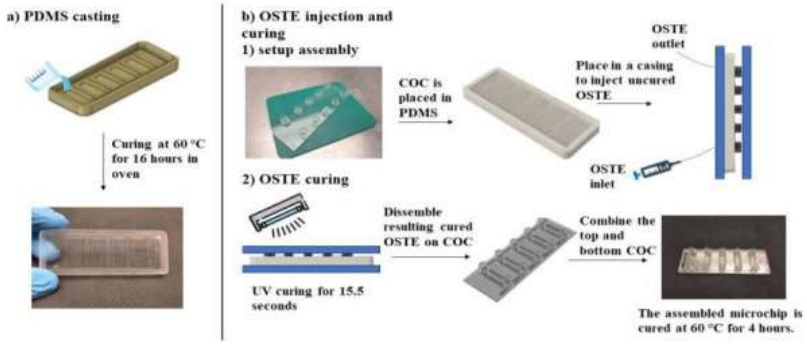

Fig. 1. Microfluidic chip fabrication procedure. Partly made with Fusion 360. a) the PDMS pouring and curing process. b) OSTE injection and curing procedure.

A homemade microfluidic chip was successfully fabricated using a series of steps and various methodologies, including computer-aided design (CAD), photolithography, etching, and bonding processes. The *E. coli* biofilm was successfully grown and Confocal microscopy showed a uniform and even biofilm layer (**Figure 2A**). Our microchip represents a significant advancement in biofilm research and miniaturized biochemical analysis systems. This novel device promises an advanced future applications in laboratory and clinical settings (3D model of the device in **Figure 2B**).

Fig. 2 A) Uniform biofilm growth across growth channel **B)** schematic representation of the Microfluidic chip

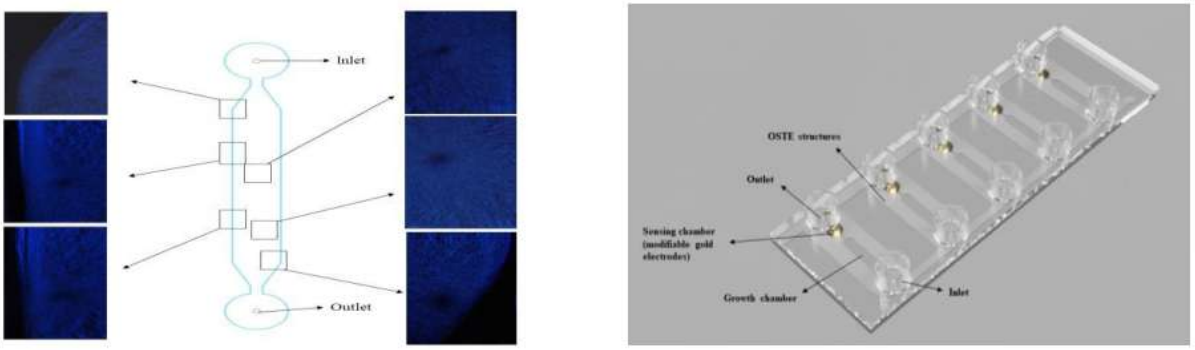

[1] A. G. Abdelhamid and A. E. Yousef, 'Combating Bacterial Biofilms: Current and Emerging Antibiofilm Strategies for Treating Persistent Infections', *Antibiotics*, vol. 12, no. 6, p. 1005, Jun. 2023, doi: 10.3390/antibiotics12061005.
[2] J. Alcàcer-Almansa, B. V. Arévalo-Jaimes, N. Blanco-Cabra, and E. Torrents, 'Methods for studying biofilms: Microfluidics and translation in theclinical context', in *Methods in Microbiology*, vol. 53, Elsevier, 2023, pp. 195–233. doi: 10.1016/bs.mim.2023.04.002.

Chemical Synthesis of Niobium Penta-oxide Nanomaterials for the Antimicrobial Applications

*Muhammad Usman Khalid[1], Monika Kirsnytė-Šniokė[1], Arunas Stirke[1] Wanessa Melo[1]

[1]State Research Institute Center for Physical Sciences and Technology-FTMC, Department of Functional Materials and Electronics, Vilnius, Lithuania

*Muhammad.usmanbajwa@ftmc.lt

Niobium pentoxide (Nb_2O_5) is a transition metal oxide with a wide range of properties that make it a potentially valuable and highly adaptable material in many different sectors [1,2] This study investigates the chemical synthesis of niobium pentoxide (Nb_2O_5) nanoparticles using hydrofluoric acid (HF) as a catalyst to facilitate the dissolution and reprecipitation of niobium precursors. By controlling the molar ratio of HF, temperature, and reaction time, highly crystalline Nb_2O_5 nanoparticles were successfully synthesized. The synthesized nanoparticles were characterized using scanning electron microscopy (SEM), (**Figure A**) and transmission electron microscopy (TEM) (**Figure B**) to determine their structural and morphological properties. Notably, the use of hydrofluoric acid led to the formation of well-defined orthorhombic crystalline phases with enhanced surface area, which are critical for catalytic and biomedical applications. In addition, this study will explore the application of these Nb_2O_5 nanoparticles in inhibiting biofilm formation of *Escherichia coli* and *Pseudomonas aeruginosa*. Antibiofilm preliminary results showed a potential that Nb_2O_5 effectively reduces biofilm metabolic activity (~65% and 95%, respectively, (**Figure C**). These results show the possibility to use the Niobium nanoparticles to overcome the biofilms of its microorganisms, so that more experiments will be performed.

Figure (A) SEM image of Nb_2O_5 nanoparticles, (B) TEM image of Nb_2O_5 nanoparticles**,** (C) Effect of Nb_2O_5 nanoparticle on metabolic activity of gram-negative biofilms.

[1] F. Holtzberg, A. Reisman, M. Berry and M. Berkenblit, J. Am.Chem. Soc., 1957, 79, 2039–2043.
[2] G. Brauer, Z. Anorg. Allg. Chem., 1941, 248, 1–31.

Non-linear Microscopy for Cervical Cancer Diagnostics

Elena Osteikaitė[1], Viktoras Mažeika[3], Mykolas Mačiulis[1], Martynas Riauka[1], Edvardas Žurauskas[4], Rūta Čiurlienė[5] and Virginijus Barzda[1,2]

[1]Laser Research Center, Vilnius University, Saulėtekio Ave 9 corp. III, Vilnius, Lithuania
[2]Chemical and Physical Sciences, Department of Physics, University of Toronto, Mississauga, Ontario, Canada
[3]Institute of Biosciences, Life Sciences Center, Vilnius University, Saulėtekio Ave 7, Vilnius, Lithuania
[4]Department of Pathology, Forensic Medicine and Pharmacology, Faculty of Medicine, Vilnius University, Vilnius, Lithuania
[5]Oncogynecology Department, National Cancer Institute, Santariškių St. 1, Vilnius, Lithuania
elena.osteikaite@ff.vu.lt

The search for new approaches in cancer diagnostics and prognostics remains a relevant and important subject in the field of histopathology. Polarimetric non-linear microscopy offers new information for oncology investigations [1, 2]. A second harmonic generation (SHG) is observed when extracellular matrix collagen is illuminated with a pulsed laser light. The SHG signal provides insight into the orientation and the ultrastructure of the collagen fibres. A third harmonic generation (THG) can be simultaneously detected with the SHG, and highlights the cell's nuclei. In this work, five samples with cervical cancer diagnosis have been investigated by using non-linear microscopy and the Double Stokes-Mueller Polarimetry (DSMP) method. A statistical analysis of polarimetric images was performed, that further deepened the understanding of collagen changes in the cancerous tissues.

In this investigation, polarized laser pulses have been used to excite the sample tissue. The collagen produces a SHG signal, which has been analysed with polarization state analyser. By using the DSMP method, a variety of polarimetric ultrastructure parameters are obtained, such as *C*-ratio that reveals the orientation of collagen molecules out of the image plane [1], and *R*-ratio that depends on the structural organization of fibers in the focal volume [2]. During the polarimetric image analysis, maps of polarimetric parameters are generated, furthermore, the polarimetric SHG signal from the areas at the vicinity of the tumour margin and further away, in the normal tissue region, have been recorded. The polarimetric parameter maps can be colocalized and compared with the THG maps that show the cell nuclei (Fig. 1).

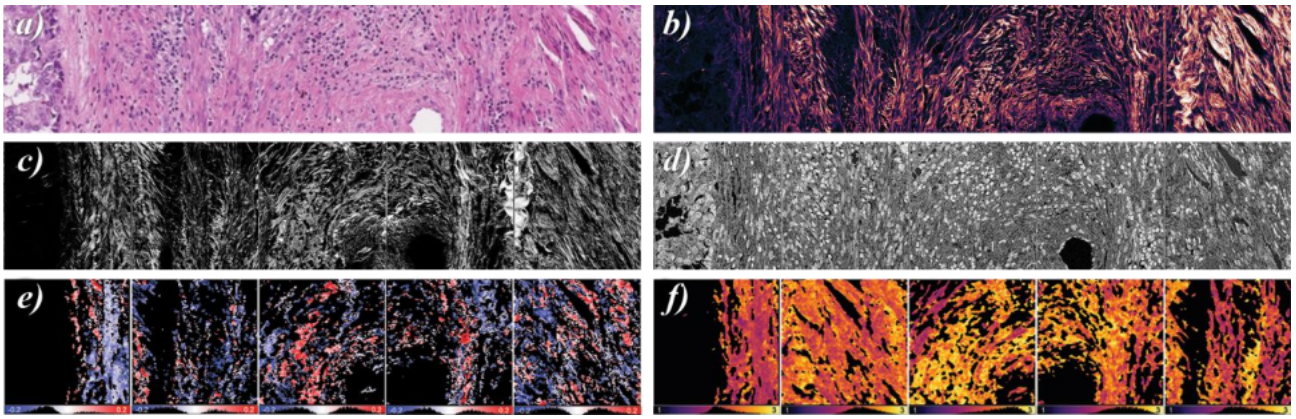

Fig. 1. Non-linear microscopy results of the human cervix endometrioid adenocarcinoma. **a)** Bright view microscopy image, **b)** fluorescence microscopy images, **c)** SHG and **d)** THG images (presented in logarithmic scale), **e)** *C* and **f)** *R*-ratio distribution maps (DSMP measurements).

The changes in collagen structure and the distribution of cancerous cells can be correlated, and the influence of cancer cells on the extracellular matrix can be studied. The comparison of collagen and cell nuclei is examined by using Kruskal-Wallis test followed by the Principal Component Analysis (PCA). These tests allow to recognise the parameters of most importance – they show a significant difference between the cancer and normal structure of extracellular matrix collagen.

By combining the optical non-linear effects, laser microscopy and statistical tests, we observe the variations of collagen structures that can be used for cancer diagnostics, prognostics and treatment planning.

[1] K. Mirsanaye, Digital Histopathology with Second Harmonic Generation Microscopy, PhD thesis, University of Toronto, 2022
[2] A.Golaraei, Polarimetric second-harmonic generation microscopy of the hierarchical structure of collagen in stage i-iii non-small cell lung carcinoma, Biomedical Optics Express, 2020.

Assessing Cell Viability and Electrotransfer Efficiency in the Concurrent and Separate Delivery of Proteins, Small Fluorescent Molecules, and Nucleic Acids using Varying High-Voltage Pulse Numbers

Justinas Venckus, Ernestas Urbanskas, Salvijus Vykertas, Baltramiejus Jakštys, Paulius Ruzgys, Saulius Šatkauskas

Faculty of Natural Sciences, Vytautas Magnus University, Universiteto g. 10-507, Akademija, Kauno raj. LT-53361, Kaunas, Lithuania
justinas.venckus@vdu.lt

Introducing proteins into living cells via electroporation (EP) could be used for CRISPR-Cas9 gene editing, cell therapy, and intracellular sensing [1], but theoretical model for their delivery *in vitro* is yet to be established [2]. To gain more insight into how protein behaves during EP, its potential synergies and interferences with other migrating molecules, such as small fluorophores and nucleic acids, could be observed: its co-delivery with small fluorophores, like propidium iodide (PI), may allow to monitor membrane integrity in real time, whilst concurrent electrotransfer with nucleic acids may be applied for more complex experimental designs, involving Cas9 with guide RNA. Due to proteins' size and charge, their migration through small electropores may be impeded [3,4]. Adjusting pulse numbers might improve their uptake by providing more time for their entry, however it should be optimized in terms of cell viability and its ability to maintain the cargoes for longer periods. The aim of this study is to determine how the efficiency of concurrent and separate delivery of proteins, PI, and pDNA into mammalian cells and their viability depends on different high-voltage (HV) pulse numbers.

Chinese Hamster Ovary (CHO) cells were suspended in low-conductivity EP medium (0.2 S/m, 270 mOsm, pH 7.2) with bovine serum albumin (BSA) Alexa Fluor 488 and PI or far-red (633 nm excitation, 675/25 nm emission) fluorescent protein mCardinal-encoding plasmid (pRFP), and then received 1, 9, or 17 HV pulses (1 Hz, 1000 V/cm, 60 µs). Controls were not exposed to HV pulse. BSA^+ (488 nm and 530/30 nm, respecitvely) and PI^+ (488 nm and 585/40 nm, respectively) cell percentages were measured 30 min post-EP using BD Accuri™ C6 flow cytometer. BSA and pRFP uptake was assessed via flow cytometry and ZEISS Axio Observer 7 microscope followed by cell viability determined by MTT-PMS test 24 h post-EP. Data (mean ± SD) were analyzed with a one-way Bonferroni test ($p<0.05$, n=3).

In accordance with the results (Fig. 1 A-D), BSA and PI uptake showed a dose-response to the number of HV pulses, however at 9-17 HV pulses PI^+ cell percentage decreased ($p<0.05$), indicating that while more HV pulses increase membrane permeability, the BSA limits the PI entry. Comparably, with higher HV pulses BSA and pRFP uptake also increased with more pulses 24 h after procedure ($p<0.05$), however pRFP uptake was smaller in the BSA-supplemented samples suggesting that cells may prioritize survival over producing new proteins (RFP) during electrotransfection. Based on MTT-PMS assay, cell viability decreased with the increasing number of pulses, with the lowest viability (27.28%) observed when both BSA and pRFP were introduced together at 17 HV pulses ($p<0.05$). This implies a larger disruption of membrane integrity and increased stress when managing multiple macromolecules at once.

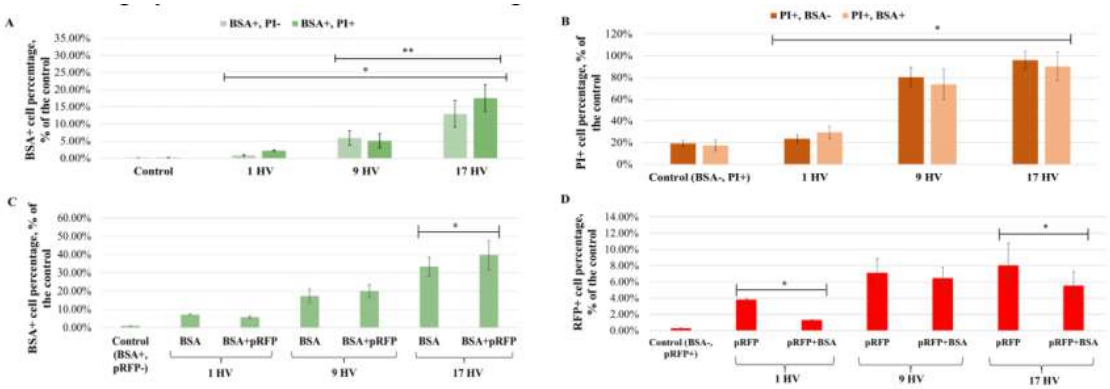

Fig. 1. The percentage of cells positive for BSA, PI, and RFP, as measured by flow cytometry, in relation to different HV pulse numbers (1, 9, and 17 pulses at 1 Hz, 1000 V/cm, 60 µs): A) BSA^+ cell percentage with and without PI 30 min post-EP; B) PI^+ cell percentage with and without BSA 30 min post-EP; C) BSA^+ cell percentage with and without RFP plasmid 24 h post-EP; D) RFP^+ cell percentage with and without BSA 24 h post-EP. Statistical significance was determined by a one-way Bonferroni test, with * and ** denoting $p<0.05$ and $p<0.01$, respectively, compared to control groups and ensuing experiments. Error bars show the standard deviation of the mean (n=3).

Conclusions: these foundings point to an intricate interplay among BSA, PI, and pRFP as each cargo may influence the delivery of the others whilst affecting membrane integrity and cell viability.

[1] N. Pathak, C. A. Patino, N. Ramani, P. Mukherjee, D. Samanta, S. B. Ebrahimi et al., *Nano Lett*. **23**, 3653-3660 (2023).
[2] A. Muralidharan and P. E. Boukany, *Trends Biotechnol*. **42**, 780-798 (2024).
[3] Y. Cao, H. Chen, R. Qiu, M. Hanna, E. Ma, M. Hjort et al., *Sci. Adv.* **4**, eaat8131 (2018).
[4] M. P. Stewart, R. Langer, and K. F. Jensen, *Chem. Rev*. **118**, 7409-7531 (2018).

Electroporation-Based Sensitization: Optimal Conditions for CHO and 4T1 Cell Lines to Balance Cell Viability and Membrane Permeabilization

Silvija Ambrazevičiūtė[1], Neringa Barauskaitė[1], Paulius Ruzgys[1], Saulius Šatkauskas[1]

[1]Biophysical Research Group, Faculty of Natural Sciences, Vytautas Magnus University, Universiteto g. 10, Akademija, Kauno raj., Lithuania
silvija.ambrazeviciute@vdu.lt

The process of increasing plasma membrane permeability by applying high-intensity electric fields is called electroporation. Depending on the amplitude and number of electric pulses applied, electroporation can be either reversible, with subsequent recovery of membrane permeability, or irreversible. Reversible electroporation is widely used to introduce drugs into cells and is known as electrochemotherapy [1].

Despite growing awareness, screening, and intensive research into new therapeutic strategies, cancer remains one of the leading causes of death globally, with the number of diagnosed cases increasing each year [2]. Many cancer cases require extensive drug treatment known as chemotherapy. While chemotherapy is effective, it is associated with significant side effects, including toxicity to the entire body, not just the tumour. Electrochemotherapy provides a solution by allowing for a reduction in the dose of cytotoxic drugs while enhancing their effectiveness. It also enables the precise delivery of the drug directly to the tumour cells. Despite these improvements, there remains a risk that more resistant tumour cells may survive and proliferate. Recent studies are focused not only on optimizing the electrochemotherapy protocol but also on improving the efficiency of drugs and other modulatory molecules delivery to the tumour cells.

Electroporation-based cell sensitization involves inducing delayed cell hypersensitivity to electric pulses by extending the duration of the electroporation treatment while maintaining the same cumulative energy input [3]. This property significantly increases cell permeability, thereby promoting more efficient transport of molecules into the cell.

Current research focused on determining the protocol for electroporation-based sensitization of Chinese hamster ovary (CHO) and murine mammary cancer (4T1) cells and evaluating its effectiveness. Electroporation experiments were conducted using a self-made electroporation medium (0.1 S/m, 270 mOsmol) and stainless-steel electrodes with a 2 mm wide gap. The electroporation parameters included one or eight high-voltage (HV) pulses with a duration of 100 µs, repeated at a 1 Hz frequency, with an additional HV pulse delivered after 0, 1, 5, 10, and 15 minutes. Pulse intensity was set at 1.4 kV/cm. Cell viability was assessed by performing a clonogenic assay, which evaluated the cells' ability to form colonies 6 days after the electroporation. The control group, which was not exposed to electric fields, was used to establish a baseline, with the number of colonies formed by control cells representing 100% viability. Electropermeabilization efficiency was measured by adding propidium iodide (PI) and determining the count of permeabilized cells using a flow cytometer. The PI was excited at a wavelength of 488 nm, and the emission was collected at 574 nm.

Obtained results indicated that the CHO cell line was more sensitive to repetitive electric pulses. CHO cells maintained over 90% viability after treatment with a single HV pulse and with an additional pulse after 5 minutes, as well as after treatment with a single set of eight HV pulses and an additional pulse after 1 minute. Least percentage of viable cells were obtained after treatment with a set of eight HV pulses followed by an additional pulse after 15 minutes. While performing experiments with 4T1 cell line an interesting observation was made. Cells treated with only one HV pulse exhibited increased activity, forming twice as many colonies as the control. Viability remained above 90% for most electroporation conditions, except for treatments involving a single set of eight HV pulses and an additional pulse after 10 minutes. The lowest viability for 4T1 cells was recorded after treatment with a set of eight HV pulses followed by an additional pulse after 10 minutes.

Following these results, PI uptake was evaluated, as it directly correlates with membrane permeabilization during electroporation-based sensitization. Based on the viability results of the CHO cell line, the optimal electroporation parameters were identified by selecting conditions that maintained cell viability above 90%. The best operating conditions for CHO cells were one HV pulse followed by an additional pulse after five minutes. Under these conditions, PI uptake was 89.3% ± 3.8% of all the affected cells. In contrast, for the 4T1 cell line, the optimal electroporation conditions involved a set of eight HV pulses followed by an additional HV pulse after one minute. These parameters achieved 99.2% ± 0.5% PI uptake of all the affected cells.

To summarize, cell viability and permeabilization experiments revealed that CHO and 4T1 cell lines require different electroporation conditions to achieve optimal cell sensitization and higher uptake of exogenous molecules without significantly affecting cell viability. Furthermore, 4T1 cells were more resistant to electric pulses, indicating that they can endure harsher conditions while maintaining viability and the ability to form new colonies.

[1] U. Probst, I. Fuhrmann, L. Beyer, and P. Wiggermann, "Electrochemotherapy as a new modality in interventional oncology: A review," Jan. 01, 2018, *SAGE Publications Inc.* doi: 10.1177/1533033818785329.

[2] Z. Łapińska, U. Szwedowicz, A. Choromańska, and J. Saczko, "Electroporation and Electrochemotherapy in Gynecological and Breast Cancer Treatment," Apr. 01, 2022, *MDPI*. doi: 10.3390/molecules27082476.

[3] J. Dermol, O. N. Pakhomova, A. G. Pakhomov, and D. Miklavčič, "Cell electrosensitization exists only in certain electroporation buffers," *PLoS One*, vol. 11, no. 7, Jul. 2016, doi: 10.1371/journal.pone.0159434.

On the Way of Development of Versatile Optical Sensor for the Monitoring of the Biological Molecule Interactions by the Surface Plasmon Resonance Imaging

Edita Voitechovic[1], Tomas Rakickas[1], Ignas Bitinaitis[1], Victor Reshetnyak[2,3], Anatoly Suprun[2], Liudmyla Shmeleva[2], Alexandr Belosludtsev[1]

[1] Center for Physical Sciences and Technology, Savanoriu ave. 231, LT-02300 Vilnius, Lithuania
[2] Taras Shevchenko National University of Kyiv, Volodymyrska Street 64/13, 01601 Kyiv, Ukraine
[3] School of Physics and Astronomy, University of Leeds, Leeds LS2 9JT, United Kingdom
edita.voitechovic@ftmc.lt

Surface plasmon resonance (SPR) technique for the monitoring of the biomolecule interactions have been established in the end of 20 century. Since then it has become a gold standard for, e.g., new drug testing. The significant improvement of SPR method was made by the incorporation of the camera into SPR setup. That let acquire, beside label free and real time analysis, the image of the analysed surface. Nowadays, there are a number of possible configurations of the SPR imaging (SPRI) setups [1]. Our investigations are based on prism-coupled phase interrogation SPRI using a null-ellipsometer, whose main advantages are (1) the measurements of the angles instead of light flux, which partly allows to avoid problems of the stability of the light source or non-linearity of the detectors; (2) the possibility of precise quantitative analysis of the adhered molecules on the chip surface, instead of recording relative units (RUI) or shades of grey. The raw output of the measurements is the changes of the Δ and Ψ angles, which were obtained from the determination of the angles of ellipsometer components: polarizer (P), compensator (C) and analyser (A) after the elliptically polarized light interaction with the surface of the sample at a certain angle of incidence (AOI).

Our work is devoted to the improvement of the classical approach of the null-ellipsometry for the investigations of the organic molecule interactions for several tasks: (1) for the monitoring of diverse sizes of the bio-molecules at the same time on the same sensor surface; (2) for the monitoring of the thickness and the anisotropy of organic lipid layers at the same time. These tasks can be achieved using the advance optical sensor instead of a classical – gold-covered glass slide. Applying theoretical modelling of the possible optical sensors, the advanced sensor chips were suggested, formed and tested. The sensor chip for the first task was made on the BK7 glass slide combining the deposition of niobium oxide and silicon oxide. The sensor chip allowed the measurements of the organic layer thickness with the linear sensitivity of 2.55° of Δ per 1 nm of organic layer at AOI of 61° up to 50 nm of total organic layer thickness. The sensor chip for the second task was a coupled plasmon-waveguide resonator [2] made on the BK7 glass slide combining the deposition of silver, niobium oxide and silicon oxide. That allowed the observation of the two peaks of p- and s-polarizations, which can be used for acquisition of the desired information. Further investigations with the lipid membranes will demonstrate the influence of both peaks for the characterization of the homogeneity and anisotropy of the lipid membranes and the interactions with the proteins.

Acknowledgments.

This project has received funding from the Research Council of Lithuania (LMTLT), agreement No S-LU-24-3. From Ukrainian party the project has received funding from the Ministry of Education and Science of Ukraine (MES), agreement No M/60-2024.

[1] Z. Huo, et al., *Talanta*, 2023, **255**, 124213.
[2] I. D. Alves and S. Lecomte, *Acc. Chem. Res*., 2019, **52**, 1059-1067.

Irreversible Electroporation Across Suspension and Monolayer Cultures: A Comparative Evaluation

Aras Rafanavičius[1], Ingrida Šatkauskienė[2`], Saulius Šatkauskas[1,2]

[1]Vytautas Magnus University, Department of Biochemistry, Universiteto st. 10, Akademija, Lithuania
[2] Vytautas Magnus University, Research Institute of Natural and Technological Sciences, Cell Tissue Biotechnology Research Group, Universiteto st. 10, Akademija, Lithuania
aras.rafanavicius@vdu.lt

Irreversible electroporation (IRE), also known as pulsed field ablation (PFA), is a technique that uses short, strong electrical pulses to create transient pores in the cell plasma membrane, resulting in cell death due to membrane damage and sudden loss of homeostasis. This process has been employed for malignant tissue ablation since 2005 and has more recently attracted attention for treating cardiac arrhythmias, especially atrial fibrillation. This condition affects at least 60 million patients worldwide [1]. IRE has been explored due to its non-thermal course of action and tissue specificity compared to conventional thermal ablation methods [2]. Numerous studies over the years have evaluated the efficacy of PFA in both in vitro and in vivo settings. Nevertheless, the studies differ in electrode configurations, medium compositions and electrical parameters, rendering direct comparisons challenging. Additionally, much of the data from clinical trials remain undisclosed, leaving the optimal conditions for safe and effective ablation still undetermined [3]. Thus, this study aims to identify the parameters that would maximize mortality while minimizing energy use.

In the study, Chinese hamster ovary cell suspensions were subjected to electroporation using parallel stainless-steel electrodes. The viability of suspended cells was assessed using a clonogenic assay and a membrane integrity assay via flow cytometry, with propidium iodide (PI) staining. Reversible and irreversible electroporation zones in cell monolayers, plated 24 h prior and exposed to the same EP conditions, were identified using fluorescence microscopy. For imaging, cells were stained with PI either before EP or 30 min after, followed by analysis of composite images to evaluate the total affected areas. In addition, temperature changes during the treatment were registered in the area between electrodes. Results from the monolayer electroporation were compared with a finite element model of the electrical field distribution in the system.

A number of electroporation parameters were analyzed, including pulse duration, amplitude, frequency and number, while maintaining a consistent single pulse energy. The efficiency of IRE was found to depend on the electric field strength when the total electric energy was held constant. In cell suspensions, increasing the number of pulses led to higher ablation efficiency, with the observed effect plateauing at 10 pulses. In monolayer cultures, the areas of both IRE and RE expanded consistently across the entire range of pulses tested, up to 50 pulses, with the effects of additional pulsation beyond this point remaining uncharted. Notably, exposure to electric fields under the conditions examined did not result in a significant temperature rise, suggesting that cell death occurred primarily through non-thermal mechanisms.

[1] X. Dong, B.Wang, F. Hou, et al., *EP Europace*, **25(3)**, 793-803 (2023).
[2] D. Schaack, B, Schmidt, S. Tohoku et al., *Arrhythmia Electrophysiol. Rev.*, **12** (2023).
[3] M. Casciola, T. K. Feaster, M. J. Caiola, et al., *Front. Physiol.*, **13** (2023).

Effects of biomolecules on the spectroscopic properties and the photostability of CdTe quantum dots

Marija Kalnaitytė, Agnė Kalnaitytė-Vengelienė, Saulius Bagdonas

Vilnius University, Faculty of Physics, Laser Research Center, Saulėtekio av. 9, III bld., Vilnius, Lithuania
marija.kalnaityte@ff.stud.vu.lt

Water soluble quantum dots (QDs) are characterized by a broad absorption band, narrow emission and a high photoluminescence quantum yield. Moreover, their spectroscopic properties respond predictably to environmental changes, allowing QDs to be used as probes or indicators [1]. In the biomedical field, QDs with a core-shell structure, whose optical properties are less sensitive to the environmental influences, are increasingly being used. However, by studying changes in the spectroscopic properties of core-type QDs, it is possible to track the interaction of biomolecules with the QD surface, which affects the photostability, toxicity and biocompatibility of QDs. Mg-chlorophyllin (Chl) is a photoactive biomolecule that is often used in studies of drugs with antimicrobial properties. When illuminated, Mg-Chl has a dual effect on the microenvironment, acting as a photosensitizer and antioxidant.

In this work, we investigated the changes in optical density (OD) and fluorescence (FL) of water soluble CdTe-MSA QDs ($2.5*10^{-6}$ g/ml), as well as their photostability in distilled water (DW) and in the presence of Mg-Chl ($1.5*10^{-5}$ M) or/and bovine serum albumin (BSA) ($1.5*10^{-5}$ M). Spectroscopic measurements of 1 ml samples were carried out in narrowed quartz cuvettes (4 mm x10 mm). Between measurements, the samples were stored in centrifuge tubes (1.5 ml) at room temperature in the dark. In photostability experiments, an area of about 1 cm^2 of samples in quartz cuvettes was irradiated with a violet LED (404 ± 9 nm (FWHM), 30 mW/cm^2). The total dose (18 J/cm^2) was collected in intervals of 1.8 J/cm^2 (from 0 J/cm^2 to 5.4 J/cm^2), 3.6 J/cm^2 (up to 12.6 J/cm^2) and 5.4 J/cm^2. The samples were mixed before each measurement.

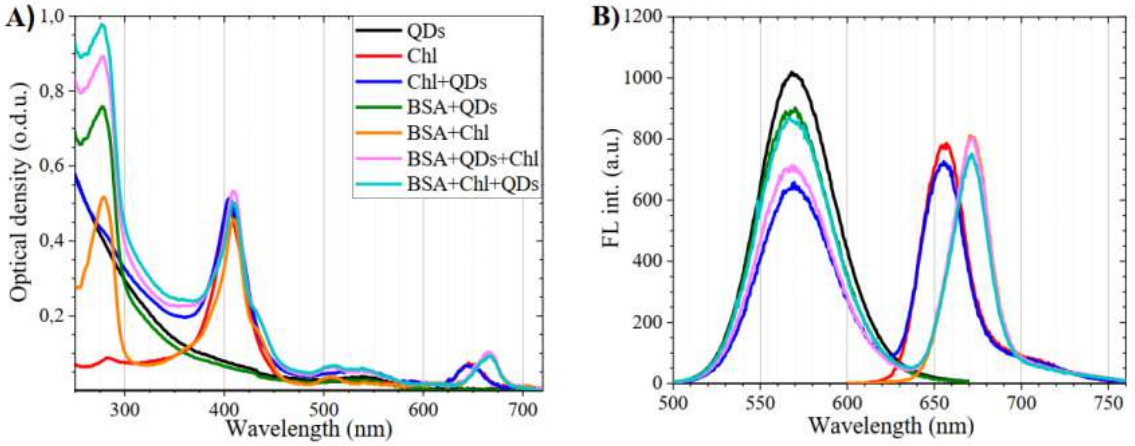

Fig.1 Initial spectra of optical density (A) and FL intensity (B) of CdTe-MSA QDs, Mg-Chl and their mixture (λ_{ex} =405 nm, excitation and emission slits 3 and 2.5) in DW and in the presence of BSA.

The initial OD of QDs did not change significantly in samples with BSA or Chl compared to DW (Fig. 1A). However, the FL intensity of QDs in DW was the highest and decreased by about 11% and by 37% in the samples with BSA and Chl (Fig.1B). Furthermore, optical changes of the mixture samples revealed the importance of the order of addition of QDs and Chl to the BSA solution. The FL spectra showed that in the case of the BSA+QDs+Chl sequence, the intensity of the spectral QDs band at 570 nm decreased 31% compared to that in DW, and by 15% the case of the BSA+Chl+QDs sequence. This importance of the order of addition was especially revealed in FL changes immediately after irradiation with a violet LED and after a day.

[1] J.Yao, M. Yang, Y. Duan, *Highly fluorescent CdTe nanocrystals: Synthesis, characterization, property, mechanism, and application as a sensor for biomolecule analysis*, J. Mater. Res., Vol. 29, No. 5, (2014)

Molecular determinants for the differential anionic permeability of Cx26 and Cx30 channels

Lina Kraujalienė[1], Tadas Kraujalis[1,2], Mindaugas Šnipas[1,3], Vytas K. Verselis[4]

[1]Lithuanian University of Health Sciences, Institute of Cardiology, Sukileliu av. 15, Kaunas, Lithuania
[2]Kaunas University of Technology, Department of Applied Informatics, Studentu st. 50, Kaunas, Lithuania
[3]Kaunas University of Technology, Department of Mathematical Modelling, Studentu st. 50, Kaunas, Lithuania
[4]Albert Einstein College of Medicine, Dominick P. Purpura Department of Neuroscience, 1300 Morris Park Avenue, Bronx, NY10461
lina.kraujaliene@lsmu.lt

Two closely-related connexins (Cx), Cx26 and Cx30, are expressed in the cochlea, where they contribute to Ca^{2+} signaling by forming gap junction channels between cells [1]. Cxs can also function as hemichannels in cell membrane connecting intracellular and extracellular compartments. It is suggested that hemichannels of Cx26 play an important role in cochlea by conducting different signaling molecules including ATP [1, 2]. Mutations in Cx26 and Cx30 lead to hearing loss or defective audition. While these two Cxs share similar amino acid sequence and overall structure, their function and properties differ. Gap junction channels formed by these Cxs have been shown to have different permeability profiles, with Cx30 showing a strongly reduced preference for anionic tracers [3].

The pore-forming segment of the first extracellular loop identified by computational studies of the Cx26 crystal structure to form a parahelix and a narrowed region of the pore, differs at a single residue at position 49. Cx26 contains an Ala and Cx30 a charged Glu at this position, which is shown to be pore-lining. To assess whether the Ala/Glu difference affects permeability, we modelled and quantified Lucifer Yellow transfer between HeLa cell pairs expressing wild type (WT) Cx26 and Cx30 and variants with reciprocally substituted Glu and Ala at position 49. Cx26(A49E) and Cx30(E49A) substitutions essentially reversed the Lucifer yellow permeability profile when accounting for junctional conductance. Moreover, using a calcein efflux assay in a single cells, we observed a similar reduced anionic preference in undocked Cx30 hemichannels and a reversal with reciprocal Ala/Glu substitutions. Thus, our data indicate that Cx26 and Cx30 gap junction channels and undocked hemichannels retain similar permeability characteristics and that a single residue differences in the first extracellular loop can largely account for theirs differential permeabilities to anionic tracers. The higher permeability to anionic permeants of Cx26 compared with Cx30 suggests that these Cxs may serve distinct signaling functions in the cochlea, perhaps reflected in the vastly higher prevalence of Cx26 mutations in human deafness.

[1] F. Anselmi, V. H. Hernandez, G. Crispino et al., *PNAS* **105**, 18770-18775 (2008).
[2] J. Chen, P. Chen, B. He et al., *Frontiers in Cellular Neuroscience* **15**, 1-12 (2022).
[3] D. Manthey, K. Banach, T. Desplantez et al., *J. Membrane Biol.* **181**, 137-148 (2001).

Malignant Liver Tissue Diagnostics by Fiber Based ATR IR Spectroscopy

Rimantė Bandzevičiūtė[1], Christian Teske[2], Justinas Čeponkus[1], Valdas Šablinskas[1], Gerald Steiner[3]

[1]Institute of Chemical Physics, Faculty of Physics, Vilnius University, Saulėtekio Av. 3, LT-10257 Vilnius, Lithuania
[2]Department of Visceral, Thoracic and Vascular Surgery, University Hospital Carl Gustav Carus Dresden, Dresden University of Technology, Fetscherstr. 74, 01037 Dresden, Germany
[3]Clinical Sensoring and Monitoring, Faculty of Medicine Carl Gustav Carus, Dresden University of Technology, Fetscherstr. 13, 01307 Dresden, Germany
rimante.bandzeviciute@ff.vu.lt

Various types of primary and secondary malignancies can grow in liver tissue. Primary liver cancer is the sixth most frequently diagnosed malignancy worldwide with higher incidence and mortality rates in men [1]. Treatment of liver malignancies includes various methods such as surgical resection, chemotherapy and radiotherapy; however, surgical treatment is the only curative approach for most types of liver tumors. Complete removal of the cancer ensuring negative tumor margins improves the outcome of a patient, therefore, an accurate assessment of the tissue during the surgery is an important factor for the success of the treatment. In this regard, fast, reliable and minimally invasive methods for intraoperative tumor margin assessment are needed for liver surgery.

In this study, a fiber based spectroscopy system consisting of silver halide ATR (attenuated total reflection) fiber probe coupled with a portable compact FT IR (Fourier transform infrared) spectrometer was applied for normal and tumorous liver tissue investigation. The system is light and compact; thus it can be easily fitted on a mobile table for the intraoperative tissue analysis in the operating room. Tissue samples were collected from liver surgical resections due to primary (hepatocellular carcinoma (HCC) and cholangiocarcinoma (CCC)) or secondary (metastasis from colorectal cancer, gallbladder carcinoma, pancreatic ductal adenocarcinoma, adenoma of esophagogastric junction and adrenal gland carcinoma) liver tumors. Samples were investigated immediately after the surgery; in total 46 patients were included in the study.

Mean spectra of liver normal tissue and primary tumors (HCC and CCC) are presented in fig. 1. Spectra of normal and tumorous HCC tissue show higher levels of glycogen in comparison with tumorous CCC tissue. This is illustrated by spectral bands located at 1027 cm^{-1} which are assigned to ν(C-O), ν(C-C), δ(C-O-H) vibrations and 1155 cm^{-1} assigned to ν(C-O) vibrations. Presence of glycogen in liver tissue can be explained by its function of glycogen storage in hepatocytes which work as a reservoir of glucose required for other tissues in the body. While HCC tumors show presence of glycogen, reduced absorbance values of glycogen spectral bands of CCC tissue spectra can be explained by nature of the tumor – CCC tumors forms out of cholangiocytes which do not accumulate glycogen. Besides the decreased absorbance values of the glycogen spectral bands, increased absorbance values of spectral bands corresponding to collagen located at 1034, 1207, 1240, 1283 and 1317 cm^{-1} are observed. Increased collagen levels are related to growth of the desmoplastic stroma of the tumor which is rich in connective tissue containing collagen. This desmoplastic reaction is a common feature of CCC tumors [2]. In case of HCC tumors, differences between normal and tumorous tissue spectra are not that obvious as for the CCC tumors; however, application of statistical analysis shows good results for the classification between normal and tumorous tissues: sensitivity and specificity of the method is 72-74 % and 80-82%, respectively.

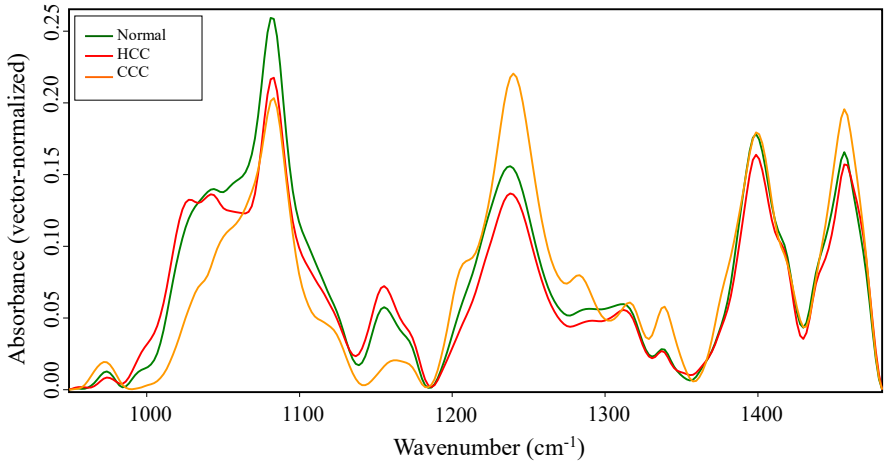

Fig. 1. Mean ATR IR spectra of liver normal and primary tumor (hepatocellular carcinoma (HCC) and cholangiocarcinoma (CCC)) tissue.

[1] H. Sung, J. Ferlay, R. L. Siegel et al., CA. Cancer J. Clin., 71(3), 209-249 (2021)
[2] B. Blechacz. Cholangiocarcinoma: Current Knowledge and New Developments, Gut Liver, 11 (1), 13–26 (2017).

Investigation of Myocardial Infarction Patient Derived Extracellular Vesicles by IR Spectroscopy and Gas Chromatography - Mass Spectrometry

Rimantė Bandzevičiūtė[1], Emilis Gabrielis Byčius[2], Vytautas Žėkas[2], Inga Bikulčienė[2], Tautvydas Taraškevičius[1], Dovilė Karčiauskaitė[2], Justinas Čeponkus[1]

[1]Institute of Chemical Physics, Faculty of Physics, Vilnius University, Saulėtekio Av. 3, LT-10257 Vilnius, Lithuania
[2] Department of Physiology, Biochemistry, Microbiology and Laboratory Medicine, Institute of Biomedical Sciences, Faculty of Medicine, Vilnius University, M. K. Čiurlionio st. 21, LT-03101, Vilnius, Lithuania
rimante.bandzeviciute@ff.vu.lt

During pathological processes, various changes occur in the human body including changes in tissue microenvironment, metabolic and signalling pathways of cells, and bodily fluids. In the case of heart failure, biomarkers such as natriuretic peptides, or cardiac troponins could be used for stratification, prediction of outcomes and biomarker-guided therapy. However, a substantial proportion of patients with heart failure may present with normal levels of these markers and thereby risk stratification of poor outcomes including death could fail [1]. There is a strong need to improve the discriminative value of traditional markers. One such marker could be extracellular vesicles (EVs). EVs are defined as heterogeneous cell-derived membranous particles that originate from the cellular endosomal system or direct budding from the plasma membrane [2]. EVs are actively released by all cell types into the peripheral blood, intercellular fluid, pericardial fluid, lymph and urine [3]. As important mediators of intercellular communication, EVs may link concomitant conditions with target organ damage and thereby play a pivotal role in the development of various heart failure phenotypes [4]. Unfortunately, EV markers specific to any of the heart failure phenotypes remain to be identified and characterized.

In this study, infrared (IR) spectroscopy and gas chromatography - mass spectrometry (GC/MS) were applied for the investigation of EVs samples prepared from the human blood of 27 healthy individuals and 12 patients three months after the myocardial infarction. IR spectroscopy is a sensitive method for the qualitative and quantitative chemical analysis, thus chemical changes in the EVs are expected to be observable in the IR spectra. By applying GC/MS, EVs fatty acid (FA) composition was analysed. The mean IR spectra of EVs in Phosphate Buffered Saline (PBS) solution isolated from the blood of healthy individuals and patients with myocardial infarction are presented in Fig. 1 A. The dominance of proteins indicated by prominent spectral bands assigned to Amide I and Amide II groups and located at 1644 and 1543 cm^{-1}, respectively, and phosphate groups indicated by spectral bands located in spectral range between 1200 and 700 cm^{-1}, is observed in both spectra. More relevant albeit not that obvious at first glance differences between spectra of EVs of healthy and diseased individuals are observed in spectral range between 1480 and 1425 cm^{-1} (enlarged area of all individual spectra is presented in fig. 1 B). This spectral region is mostly related to $\delta(CH_2)$ and $\delta(CH_3)$ vibrations of proteins and suggests that changes in protein content can be observed in EVs due to myocardial infarction. After the application of statistical spectral analysis, spectra of EVs samples of healthy individuals and patients with myocardial infarction can be classified into two separate groups with accuracy of 89 % and 100 % for healthy and diseased individuals, respectively. The levels of saturated FAs (i.e., C14:0, C16:0) and monounsaturated FAs (i.e., C18:1ω9, C20:1ω9) showed statistically significant differences between the study groups. C14:0, C18:1ω9 and C20:1ω9 were observed higher in EVs samples of myocardial infarction patients (p=0.04, p=0.02, p=0.03). While the level of C16:0 was found to be lower in diseased individuals (p=0.04).

To conclude, changes in protein content and FA composition can be observed by applying methods of IR spectroscopy and GC/MS. These changes allow successful classification between healthy individuals and patients with myocardial infarction.

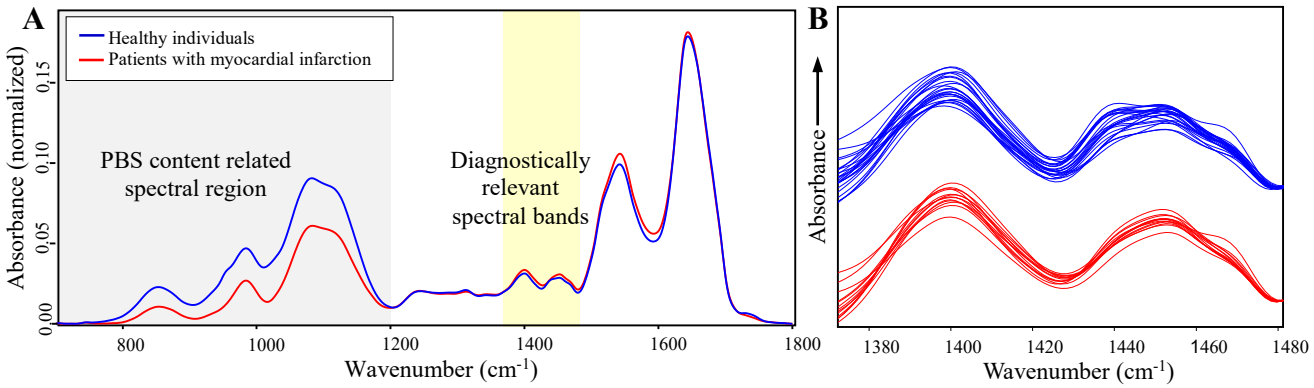

Fig. 1. Mean ATR IR spectra of EVs derived from healthy individuals and patients with myocardial infarction (A) and individual ATR IR spectra of healthy and diseased individuals (B).

[1] F.H. Verbrugge, K. Omote, Y.N.V. Reddy et al., Eur.Heart J. 43 (20), 1941–195 (2022).
[2] I.C. Kim, B.S. Yoo, Diagnostics (Basel) 12 (6), 1366 (2022).
[3] Shah, T. Patel, J.E. Freedman, NEJM 379 (10), 958–966 (2018).
[4] A.E. Berezin, A.A. Berezin. J. Mol. Sci. 23 (3), 1774 (2022)

Relaxant effect of furan-containing compounds on smooth muscles in rat prostate and aorta

Irma Martišienė, Vilma Zigmantaitė, Fausta Borusevičiūtė, Jonas Jurevičius

Laboratory of Membrane Biophysics, Institute of Cardiology, Lithuanian University of Health Sciences, Sukilėlių Ave. 15, LT50162 Kaunas, Lithuania
irma.martisiene@lsmuni.lt

A variety of compounds containing a furan ring are used in both synthetic and herbal medicine. Many are known to be toxic, but some, such as the antihypertensive drug prazosin, are used in medical practice. Recently, an essential oil extracted from the flowering plant *Elsholtzia ciliata* has been shown to not only have antiproliferative and antiarrhythmic effects but also exhibit hypotensive properties [1,2]. Chromatographic analysis of this essential oil showed that the predominant components are dehydroelsholtzia ketone and elsholtzia ketone. Both of these compounds have a furan ring in their molecular structure. Dynamic changes in vascular diameter are primarily influenced by the contractile activation and inactivation processes of contractile proteins within vascular smooth muscle cells. Therefore, this study was designed to examine the effect of *E. ciliata* essential oil (EO) and other furan ring-containing compounds, such as 2-acetylfuran (2AF) and 5-methylfurfural (5MFF), on smooth muscle contraction [3].

Male Wistar rats weighing 500–700 g were used. The study was conducted following the guidelines outlined in the EU Directive 2010/63/EU for protecting animals used for scientific purposes and was approved by the Lithuanian Commission on the Ethics of the Use of Experimental Animals at the State Food and Veterinary Services under Permission No. G2-199. Tension measurements were performed on isolated prostate strips (1.5–2 mm in width, 2–3 mm in length) of the ventral lobe and intact aortic rings (~ 2 mm in length). Preparations were mounted in a constant perfusion system chamber, stretched to a resting tension of 1–1.5 g, and equilibrated for 60 minutes. Preparations were exposed twice to 100 mM KCl containing Tyrode‘s solution to obtain a maximal contractile response. Before beginning measurements of exposure to tested compounds, the preparations were washed with normal Tyrode solution until the basal tone level was restored. First, prostate strips and aortic rings were pre-contracted with 0.3 μM or 1 μM phenylephrine, respectively. After reaching a steady-state level, the tested compound was cumulatively added in concentrations ranging from 0.01 μL/mL to 3 μL/mL. The change in tension was evaluated to phenylephrine-induced contraction. The concentration-response curves for α_1-adrenergic agonist phenylephrine in the prostate were generated through the cumulative introduction of phenylephrine, with concentrations ranging from 0.03 μM to 30 μM. To investigate the effects of tested compounds on α_1-adrenergic receptors, the prostate strips were initially pretreated for 15 min with one of the compounds, i.e., EO, 2AF, or 5MFF, and then phenylephrine was added in an analogical cumulative pattern. Data were fitted to the Hill equation.

The results showed that EO, 2AF, and 5 MFF caused a concentration-dependent reduction in the phenylephrine-induced contraction of the prostate and aorta. The inhibitory effect of EO was significantly more pronounced in the prostate compared to the aorta. The half-maximal inhibitory concentration (IC_{50}) of EO for the prostate was 0.24 ± 0.03 μL/mL (n = 10) and for the aorta was 0.72 ± 0.11 μL/mL (n = 4, $p < 0.05$ vs. prostate). 2AF and 5MFF caused half of the maximal relaxation of the precontracted prostate at a higher concentration compared to EO. However, the effect of 2AF and 5MFF on aorta contraction was similar to that of EO, i.e., all the compounds induced half of the maximal relaxation of the precontracted aorta at similar concentrations. The results showed that smooth muscles in the prostate were more sensitive to the effects of 5MFF than in the aorta, while the effects of 2AF were not significantly different in both tissues. An assessment of the dose response of phenylephrine under control conditions and in the presence of EO, 2AF, or 5MFF showed that tested compounds altered the responsiveness of smooth muscle cells in the prostate to phenylephrine. Under control conditions, the half-maximal effective concentration (EC50) of phenylephrine was 0.18 ± 0.03 μM (n = 5). In the presence of EO, 2AF, or 5MFF, EC50 of phenylephrine values were 0.81 ± 0.3 μM (n = 5), 0.89 ± 0.11 μM (n = 5), and 0.69 ± 0.23 μM (n = 4), respectively, $p < 0.05$ vs. control. Analysis of the affinity of EO for α_1-adrenergic receptors in the prostate suggested that EO at a certain range of concentrations has a competitive antagonistic effect on α_1-adrenergic receptors.

In conclusion, our study demonstrates that EO, 2AF, and 5MFF have a relaxing effect on smooth muscles in the prostate and aorta which may be related to the inhibition of α_1-adrenoreceptors.

[1] R. Macianskiene, L. Pudziuvelyte, J. Bernatoniene et. al., *Biomolecules* **10**, 948 (2020).
[2] V. Zigmantaitė, E. Jonušaitė, R. Grigalevičiūtė et. al., *Pharmaceuticals (Basel).* **15(8),** 982 (2022).
[3] I. Martišienė, V. Zigmantaitė, L. Pudžiuvelytė et. al., *Pharmaceuticals (Basel).* **16(10)**, 1464 (2023).

Linear and nonlinear optical properties of gold nanourchins in dependence on their spike size

Domantas Peckus[1], Fatima Albatoul Kasabji[2], Maziar Moussavi[1], Joel Henzie[3], Loic Vidal[2], Asta Tamulevičienė[1], Arnaud Spangenberg[2], Tomas Tamulevičius[1], Karine Mougin[2], Sigitas Tamulevičius[1]

[1]Institute of Materials Science, Kaunas University of Technology, K. Baršausko St. 59, LT-51423 Kaunas, Lithuania
[2]Institut de Science des Matériaux de Mulhouse IS2M UMR 7361, 15 rue Jean Starcky, F 68100 Mulhouse, France
[3]International Center for Materials Nanoarchitectonics (WPI-MANA), National Institute for Materials Science (NIMS), Tsukuba, 305-0044, Japan
domantas.peckus@ktu.lt

Plasmonic metallic nanoparticles have shown great promise due to their variety of applications such as photocatalysis, biosensors, SERS etc. [1]. So far, the best analysed plasmonic properties are demonstrated by gold and silver nanoparticles of shapes like spheres, nanorods, nanocubes, and bipyramids. Due to recent advances in chemical synthesis methods, gold nanoparticles of new shapes, such as nanourchins, nanostars, and nanoflowers, have been synthesised that in general have the core of the sphere with some outgrowths such as spikes or petals (Fig. 1). To our knowledge, these outgrowths dramatically change the plasmonic properties of Au nanospheres (Au NPs), but the physical background is not fully understood [2]. A better understanding of the influence of spikes and core size influence on plasmonic properties of Au nanourchins (Au NUs) nanostars, and nanoflowers could lead to new applications where the highly efficient surface of nanoparticles is expected. Currently, it is known that Au NUs outperforms Au NPs in the field of medicine such as cancer therapy, biomarkers, optical imaging, diagnostics, etc. [3].

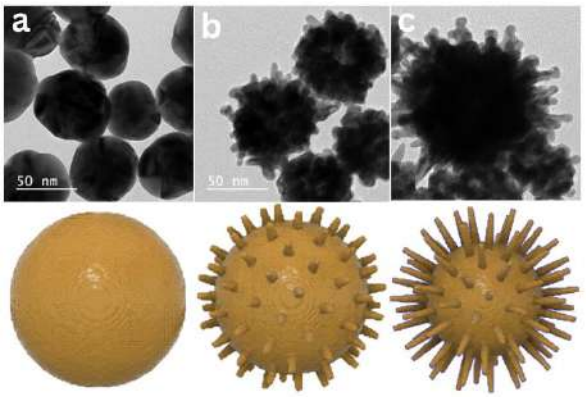

Fig. 1. TEM image and model of Au NPs (**a**); Au NUs short spikes (**b**) and Au NUs long spikes (**c**).

In our work, we analysed nanoparticles of Au NUs. The main objective of the research was to systematically study how the size of spikes of nanourchins changes their plasmonic properties. For this, we used Au NUs with different lengths of spikes and one specific case where spikes are 0 size (spheres) (Fig. 1). We analysed how the size of the spikes influences the steady-state absorption spectra and the transient absorption spectra (TAS) dynamics.

The results show that Au NUs with very short spikes (< 7 nm) have steady-state and dynamical optical properties quite similar to Au NPs, while long spikes (> 12 nm) changed the optical and plasmonic properties significantly. Au NUs with short spikes has an absorption band at 500 – 700 nm that is quite similar to spheres while Au NUs with long spikes have a second very broad absorption peak at 500 – 1000 nm. FDTD simulations helped us to explain these differences.

The Au nanospheres and Au NUs with various spike sizes were excited at 350, 500, 600, 700, 750 and 800 nm during TAS measurements. The TAS spectra of Au nanospheres and Au NUs with short spikes did not show any significant dependence on the excitation wavelength, while Au NUs with long spikes showed similar TAS spectra to Au NPs and Au NUs short spikes under excitation at 350, 500, 600 nm but TAS spectra become significantly different under excitation at 700, 750 and 800 nm. We can explain this effect using the FDTD simulation results: under excitation at 350, 500 and 600 nm we excite Au NPs, while under excitation at 700, 750 and 800 nm we excite the system Au NPs+spikes. That becomes very clear for Au NUs with long spikes. In the future, these findings can be used as a guidance for synthesis of right-sized Au NUs cores and spikes for various applications. It can also help to pick the best excitation wavelength for desired applications that could lead to the preparation of very flexible plasmonic materials in the future.

The studies were carried out within the NANOTRAACES project carried out under the M-ERA.NET 2 scheme, MERANET-22-2, and co-funded by Research Council of Lithuania.

[1] G.V. Hartland, *Chem. Rev.* **111**, 3858-3887 (2011).
[2] D. Issaad, H Moustaoui, A. Medjahed et al., *J. Phys. Chem. C* **121**, 18254-18262 (2017).
[3] D. M. Samhadaneh, S. Chu, D. Maysinger et al., *Nanomedicine (Lond.)* **15**, 829–832 (2020).

The Study of Curli Protein Aggregation

Luka Skurdelytė, Darius Šulskis, Vytautas Smirnovas

Amyloid research sector, Institute of Biotechnology, Life Sciences Center, Saulėtekio al. 7, Vilnius, Lithuania
luka.skurdelytė@gmc.stud.vu.lt

As the morbidity of neurodegenerative diseases increases, more evidence is being found that the gut microbiota is involved in the progression of these diseases [1]. Amyloid proteins are involved in the progression of these diseases by activating the body's immune system [2], and one of such amyloids is the Curli protein, which is expressed by *E.coli* bacteria in the gut. Curli fibrils are a part of the biofilms that are formed in the event of stress and can activate immune response, which is transmitted through the brain-gut axis leading to the onset of neurodegenerative diseases. Curli consists of CsgA and CsgB subunits, CsgA is the aggregating subunit, and CsgB initiates aggregationand fibril formation on the cell surface [3]. Little is known about the aggregation of Curli proteins compared to other amyloid proteins. Therefore, certain mechanisms of aggregation and its inhibitionare not yet fully elucidated.

The goals of this research was to apply the methodology of Curli protein production, characterize CsgA fibril aggregation, and determine if bacterial periplasmic chaperone DegP can inhibit it. We used classical cloning and protein purification techniques to prepare CsgA, CsgB and DegP proteins; followed the kinetics of CsgA aggregation using amyloid-specific fluorescent Thioflavin T (ThT) dye and determined the morphology of CsgA fibrils by cryogenic electron microscopy (Cryo-EM).

During this study, plasmids containing *csgB* and *csgC* were constructed and CsgA protein purification was optimized. CsgA aggregated according to nucleation-dependent kinetics, and aggregation was dependent on protein concentration. Utilizing Cryo-EM, we determined that CsgA can form fibrils with distinct morphologies. Finally, CsgA aggregates and bacterial chaperone DegP inhibited CsgA aggregation. Therefore, other periplasmic chaperones and their interactions with CsgAwill be investigated in future studies.

[1] Zhu S, Jiang Y, Xu K, Cui M, Ye W, Zhao G, et al. The progress of gut microbiome research related to brain disorders. Journal of Neuroinflammation. 2020 Jan 17;17(1):25.
[2] Shabbir U, Arshad MS, Sameen A, Oh DH. Crosstalk between Gut and Brain in Alzheimer's Disease: The Role of Gut Microbiota ModulationStrategies. Nutrients. 2021 Feb;13(2):690.
[3] Barnhart MM, Chapman MR. Curli Biogenesis and Function. Annu Rev Microbiol. 2006 Oct 1;60(1):131–47.

Aggregation and liquid-liquid phase seperation of S100A proteins

Viktorija Karalkevičiūtė[1], Ieva Baronaitė[1], Mantas Žiaunys[1], Darius Šulskis[1], Vytautas Smirnovas[1]

[1]Sector of Amyloid Research, Institute of Biotechnology, Life Sciences Centre, Vilnius University

viktorija.karalkevičiūtė@gmc.stud.vu.lt

S100 is a family of calcium-binding proteins, consisting of isoforms with structural similarity but functional diversity[1]. S100 proteins regulate various proteins involved in cellular functions like calcium homeostasis, cell growth, differentiation, cytoskeleton dynamics, and energy metabolism[1]. Several members are known to be important in neurodegeneration by signaling neuroinflammation and forming amyloid fibrils. One of them is S100A9, which is well-studied, but the roles of S100A1 and S100A8 remain relatively unexplored.

S100A1 is mostly found in the brain, skeletal and cardiac muscles, while S100A8 is primarily present in astrocytes[2,3]. Both proteins share the same interaction pathways with tau, RAGE, and RyR proteins, which are involved in Alzheimer‘s disease cascade[4]. It is known that S100A8 can form a heterodimer with S100A9 called calcprotectin[1], but interaction with S100A1 is still not investigated. Both S100A1 and S100A8 are expressed in the cerebral cortex as per the Human Protein Atlas (https://www.proteinatlas.org/)[5] and share structural similarities[1]. Thus, one of our goals was to elucidate their potential complex formation.

Additionally, we explored the possibility of S100A proteins (S100A1, S100A8, S100A9) undergoing liquid-liquid phase separation (LLPS). LLPS is an emerging area of research exploring the relationship between phase transitions and neurological disease. During LLPS, proteins form membraneless organelles, which enable them to perform their functions or faciliate aggregation. However, currently, there are no available LLPS studies of S100A proteins.

We monitored the aggregation of S100A proteins using Thioflavin T (ThT) fluorescence, and the resulting aggregates were analyzed via Atomic Force Microscopy (AFM). Liquid-liquid phase separation (LLPS) was tracked by measuring ThT fluorescence and turbidity. The droplets were visualized usinf fluorescence microscopy.

Our research demonstrated that S100A1 and S100A8 form fibrilar aggregates in the presence of each other, a process chaperoned by calcium ions. Furthermore, the S100A1 did not undergo LLPS, but S100A8 and S100A9 formed aggregates and droplets amidst crowding reagents. Future studies will explore the relationship between LLPS behaviour of S100A and other proteins associated with neurogenerative disorders.

(1) Donato, R.; Cannon, B. R.; Sorci, G.; Riuzzi, F.; Hsu, K.; Weber, D. J.; Geczy, C. L. Functions of S100 Proteins. *Curr. Mol. Med.* **2013**, *13* (1), 24–57.

(2) Wright, N. T.; Cannon, B. R.; Zimmer, D. B.; Weber, D. J. S100A1: Structure, Function, and Therapeutic Potential. *Curr. Chem. Biol.* **2009**, *3* (2), 138–145. https://doi.org/10.2174/187231309788166460.

(3) Cristóvão, J. S.; Gomes, C. M. S100 Proteins in Alzheimer’s Disease. *Front. Neurosci.* **2019**, *13*.

(4) Bertheloot, D.; Latz, E. HMGB1, IL-1α, IL-33 and S100 Proteins: Dual-Function Alarmins. *Cell. Mol. Immunol.* **2017**, *14* (1), 43–64. https://doi.org/10.1038/cmi.2016.34.

(5) Uhlen, M.; Oksvold, P.; Fagerberg, L.; Lundberg, E.; Jonasson, K.; Forsberg, M.; Zwahlen, M.; Kampf, C.; Wester, K.; Hober, S.; Wernerus, H.; Björling, L.; Ponten, F. Towards a Knowledge-Based Human Protein Atlas. *Nat. Biotechnol.* **2010**, *28* (12), 1248–1250. https://doi.org/10.1038/nbt1210-1248.

Optogenetic analysis reveals specific synaptic pathways for ON and OFF responses in the ratvisual cortex

Gytis Baranauskas[1], Jonathan Kozal[2]

[1]Laboratory of Neurophysiology, Neuroscience Institute, Lithuanian University of Health Sciences, Kaunas, Lithuania
[2]Faculty of Medicine, Lithuanian University of Health Sciences, Kaunas, Lithuaniagytis.baranauskas@lsmu.lt

Background: ON and OFF responses are generated in the visual pathway of all mammals following an increase and a decrease in stimulus brightness respectively. This generation of these two fundamental types of visual responses occurs in the retina and their specificity at synaptic level is at least partially preserved in the superior colliculus and the lateral geniculate nucleus, an intermediate visual pathway stations from the retina to the cortex. It was believed that in the cortex this segregation of ON and OFF pathways is mostly lost. However, recent findings suggest that this is not the case. Our experiments further support the hypothesis that ON and OFF pathway specificity is preserved up to the primary cortex, at least in rodents since pyramidal neurons can control each type of response independently. Moreover, there is a mechanism that maintains a balance between these two types of responses since the average effect of optogenetic stimulation of pyramidal neurons on ON and OFF responses is similar.

Methods: Wistar rats were anesthetized by peritoneal injections of urethane (1.5 – 2.0 g/kg), then they were placed in a stereotaxic frame. The recordings were done 4-6 weeks following an injection of a virus containing channelrhodopsin (ChR2) under a short CamKII promoter in the primary visual cortex area V1. ChR2 reacts to blue 465nm light by the opening of ion channels resulting in depolarization and activation of the neuron. A tetrode with an attached optical fiber for a 465nm blue LED stimulation was placed in the virus injected area within the deep cortical layers of the primary cortex (area V1). Bright spots were presented on a dark grey background for visual stimulation. Initially, a single neuron RF area was determined during visual stimulation and then the RF area was evaluated again during optic fiber mediated 465nm LED stimulation of pyramidal neurons (CamKII positive cells). Further analysis of recorded data performed by employing Igor pro, Matlab, KlustKwik software packages.

Results: During optogenetic stimulation of pyramidal neurons the RF area of OFF responses was reduced to a median value of 70% of control ($p < 0.001$, $n = 24$, Wilcoxon signed-rank test, WSR test) while the RF area of ON responses to a median value of 79% of control ($p < 0.027$, $n = 24$, WSR test). Although there was no significant difference in the extent of area reduction ($p > 0.3$, $n = 24$, Kruskal-Wallis test), there was no correlation between the effect size on the ON and the OFF response RF area for single neurons (Spearman's $\rho = 0.03$, $p > 0.5$). Similarly, the OFF response amplitude was reduced to median value of 84% ($p < 0.013$, $n = 24$, WSR test) while the ON response amplitude to 82% ($p < 0.001$, $n = 22$, WSR test). Again. although there was no significant difference in the extent of reduction in the ON and OFF response amplitudes ($p > 0.7$, $n = 24$ and 22, Kruskal-Wallis test), there was no correlation between the effect size onthe ON and the OFF response amplitude for single neurons (Spearman's $\rho = 0.25$, $p > 0.2$).

Conclusions: In the primary visual cortex optogenetic activation of pyramidal neurons reduced the RF area and the response amplitude of ON and OFF responses to similar extent. However, there was no correlation of these effects on the ON and the OFF responses at single neuron level. In other words, at single neuron level the OFF-response control by the pyramidal neurons was independent of the ON response control indicating the presence of synaptic pathways originating in the pyramidal neurons that are specific for ON and OFF responses, confirming ON and OFF pathway segregation in the primary visual cortex. Moreover, the similarity of changes induced upon ON and OFF responses by optogenetic stimulation indicates the presence of a global mechanism that keeps balance between the amplitudes of OFF and ON responses as well as between their areas.

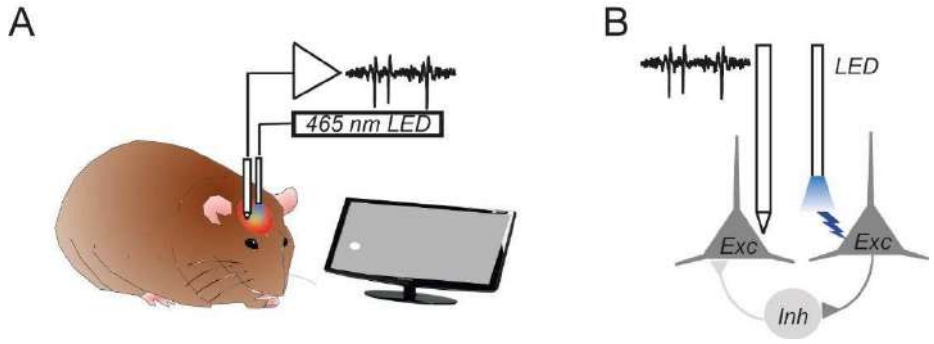

Fig. 1. The schematics of experiments

Effects of Simultaneous Transfer of Two Plasmids on Gene Electrotransfer Efficiency

Ernestas Urbanskas[1], Baltramiejus Jakštys[1], Paulius Ruzgys[1], Salvijus Vykertas[1], Justinas Venckus[1], Saulius Šatkauskas[1]

[1]Vytautas Magnus University, Faculty of Natural Sciences, Universiteto g. 10, Akademija, 53361 Kauno r. sav. Lithuania
ernestas.urbanskas@vdu.lt

Introduction

Gene electrotransfer (GET) is a commonly used technique for delivering plasmid DNA (pDNA) into the cells by applying electric pulses that permeabilize the cell membrane [1]. GET has proven to be highly effective in facilitating the transfer of naked plasmid DNA (pDNA) [2].

Gene transfer of small plasmid DNA (pDNA) is generally straightforward [3]. However, implementing gene therapy often necessitates the transfer of larger genes, which can pose additional challenges [4]. For transfection of large genes, viral vectors are often not ideal due to their limited capacity for carrying large DNA sequences. Additionally, they present significant safety concerns, particularly for clinical applications [3]. In contrast, electrogene transfer is a safer alternative that is not constrained by plasmid size, making it a more versatile option for gene transfection. However, in vitro, electrotransfection efficiency significantly decreases as the size of the plasmid increases [5].

The primary objective of this research was to evaluate the effectiveness of gene electrotransfer (GET) by simultaneously transferring plasmid DNA (pDNA) of different sizes.

Methods

Experiments were conducted utilizing the Chinese hamster ovary (CHO-K1) cell line, employing 3,6 joules of energy pulses changing pulse strength and duration to assess the GET, by using two sizes of pDNA. The efficiency of transfecting the Green Fluorescent Protein (pEGFP-N1, 4.7 kb) and Red Fluorescent Protein (mCardinal, 6.2 kb) plasmids was examined by quantifying the count of transfected cells through the employment of a flow cytometer (AccuriTM C6, USA) 24 hours after the application of high voltage (HV) pulses. Additionally, the viability of the cells after GET was determined using the MTS assay.

Results

The transfection efficiency of pEGFP-N1 is approximately 2-3 times higher than that of mCardinal when used separately, with pEGFP-N1 achieving up to 60% efficiency compared to around 20% for mCardinal. Cell viability remains relatively consistent regardless of the plasmid DNA used. Simultaneous transfer of both plasmid DNAs does not significantly impact the transfection efficiency of pEGFP-N1. However, it results in a significant increase in the transfection efficiency of mCardinal. Cell viability significantly decreases with the simultaneous transfer of both plasmid DNAs, likely due to the higher total concentration of plasmid DNA. Fluorescent intensity increases for both plasmids after simultaneous transfer, across most of the parameters tested.

Conclusions

In summary, the transfection efficiency of the smaller plasmid pEGFP-N1 is significantly higher than that of the larger plasmid mCardinal. The size of the plasmid DNA does not notably affect cell viability following gene electrotransfer. Co-transfection with both plasmids does not significantly alter the transfection efficiency of pEGFP-N1. However, simultaneous transfer of both plasmid DNAs, particularly with longer pulses, enhances the transfection efficiency of mCardinal and results in a greater overall amount of plasmid DNA being transferred.

[1] M. P. Rols, "Electropermeabilization, a physical method for the delivery of therapeutic molecules into cells," *Biochim Biophys Acta Biomembr*, vol. 1758, no. 3, pp. 423–428, Mar. 2006, doi: 10.1016/j.bbamem.2006.01.005.

[2] C. Rosazza, S. H. Meglic, A. Zumbusch, M.-P. Rols, and D. Miklavcic, "SCIENCE BENTHAM Send Orders for Reprints to reprints@benthamscience.ae Gene Electrotransfer: A Mechanistic Perspective," *Curr Gene Ther*, vol. 16, pp. 98–129, 2016, doi: 10.2174/1566523216666160331130040.

[3] L. L. Lesueur, L. M. Mir, and F. M. André, "Overcoming the Specific Toxicity of Large Plasmids Electrotransfer in Primary Cells In Vitro," *Mol Ther Nucleic Acids*, vol. 5, p. e291, Jan. 2016, doi: 10.1038/mtna.2016.4.

[4] S. P. Quenneville *et al.*, "Nucleofection of muscle-derived stem cells and myoblasts with φC31 integrase: Stable expression of a full-length-dystrophin fusion gene by human myoblasts," *Molecular Therapy*, vol. 10, no. 4, pp. 679–687, Oct. 2004, doi: 10.1016/j.ymthe.2004.05.034.

[5] S. Ribeiro *et al.*, "Plasmid DNA Size Does Affect Nonviral Gene Delivery Efficiency in Stem Cells," *https://home.liebertpub.com/cell*, vol. 14, no. 2, pp. 130–137, Apr. 2012, doi: 10.1089/CELL.2011.0093.

Structural Study of S100A9 Using DEER Spectroscopy

Aistė Peštenytė[1], Gediminas Usevičius[1], Darius Šulskis[2], Ieva Baronaitė[2], Vytautas Smirnovas[2], Jūras Banys[1], Mantas Šimėnas[1]

[1]Faculty of Physics, Vilnius University, Saulėtekio al. 3, LT-10257, Vilnius, Lithuania
[2] Sector of Amyloid Research, Institute of Biotechnology, Life Sciences Centre, Vilnius University, LT-10257 Vilnius, Lithuania
aiste.pestenyte@ff.stud.vu.lt

Double electron-electron resonance (DEER) spectroscopy is a powerful tool in structural biology, used to probe biomolecules such as proteins, RNA, and DNA by measuring nanoscale distances between unpaired electron spins [1]. This pulsed electron paramagnetic resonance (EPR) technique employs microwave pulses at different frequencies to detect one electron spin while exciting the other (Fig. 1) [2]. By tracking the changes in dipole interactions between these electron spins throughout the experiment, DEER provides detailed insights into molecular structure. It addresses challenges encountered with systems lacking unpaired electrons, such as many biomolecules, by employing spin labels through site-directed spin-labeling (SDSL) [2]. Unlike other methods, DEER is not limited to crystallized samples or constraints on molecular weight. The integration of SDSL with DEER offers a robust approach for structural analysis, revealing local structural changes, molecular interactions, and conformational dynamics, thus advancing understanding of biomolecular architecture and function [1].

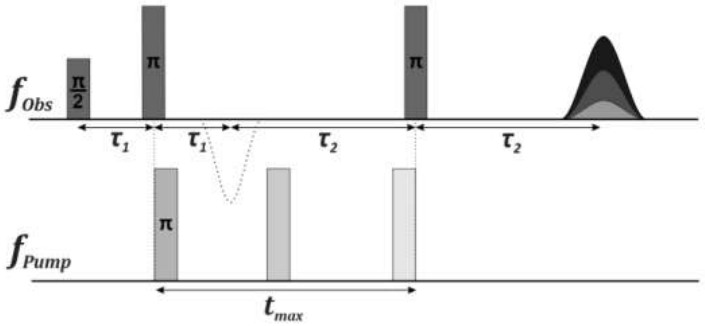

Fig. 1. Microwave pulse sequence of the DEER experiment.

To evaluate the practical applications and limitations of DEER spectroscopy, we investigated the calcium-binding protein S100A9, which is implicated in Alzheimer's and Parkinson's diseases. In this study, we measured the distance distribution (Fig. 2) between two cysteine residues using a nitroxide radical as a spin label.

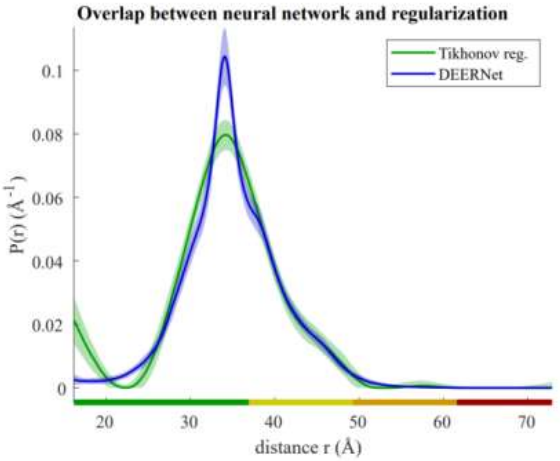

Fig. 2. Distance distribution between two electron spins in the S100A9 protein.

[1] Indra D. *et al., Use of electron paramagnetic resonance to solve biochemical problems,* Biochemistry 2013, 52, 35, 5967–5984
[2] Jeschke G. *DEER distance measurements on proteins.* Annual review of physical chemistry. 2012 May 5;63:419-46.

Effect of Photoactive Magnesium Chlorophyllin on *Scenedesmus sp.* Microalgae at Different Environment Conditions

Rasa Miliukaitė[1,2], Danielė Gedminaitė[1], Agnė Kalnaitytė-Vengelienė[1]

[1]Biophotonics group of Laser Research Center, Faculty of Physics, Vilnius University, Saulėtekio av. 9, bld. 3, Vilnius, Lithuania

[2]Life Sciences Center, Vilnius University, Saulėtekio av. 7, Vilnius, Lithuania

rasa.miliukaite@ff.stud.vu.lt, agne.kalnaityte@ff.vu.lt

Magnesium chlorophyllin (Mg-Chl) is synthetically outsourced molecule from naturally abundant chlorophyll with similar molecular structure and spectroscopic properties. Because of its porphyrin structure, chlorophyllin is photoactive molecule and is researched for its' dual – photooxidative and antioxidative – properties. Chlorophyllin is already reported to act as a photodynamic therapy agent against harmful bacteria [1] and a potential safety measure to avoid human and animal cell oxidative stress [2, 3]. Although derived from natural chlorophyll, chlorophyllin effect on plant and algae cells is not yet thoroughly studied.

Microalgae are sensitive to changes in environmental conditions and are one of the first organisms from biosphere to respond to these changes. Also, additional environmental stressors, such as nanoparticles (NP) could lead to varying physiological responses at different growth conditions. It is already known that NPs can cause oxidative stress for algae cells [4], although research for solutions how to prevent or reduce negative NP effect is limited.

In this study Mg-Chl effect was studied on autofluorescence (AF) and photosynthesis of *Scenedesmus sp.* (Sc. sp.) microalgae using non-invasive and relatively fast spectroscopy and microscopy methods. Microalgae were grown in modified Wilkins-Chalgren growth media (MWC) and different illumination conditions – under 12/12-hour day/night light (combined white LED, 6W) cycle with 34 µmol photon/m^{2}s illumination and under partial shade. Fluorescence (FL) was measured using steady state fluorometers LS 55 (Perkin Elmer) for measurements in 10x4 mm cuvettes and an optical fibre system with AvaSpec-3648 spectrometer (Avantes) for measurements from the bottom of Petri plates. For time resolved fluorometry and photosynthetic parameters calculations Pulse-Amplitude-Modulated (Junior-PAM) fluorometer (Heinz Walz GmbH) was used. To study photoinduced Mg-Chl effect, violet light (VL) irradiation (404±9 nm, 54 J/cm^2 dose) was used to excite Mg-Chl and potentially cause oxidative stress for algae cells.

Differing growth conditions revealed that algae grown under 34 µmol photon/m^{2}s illumination expressed lower electron transfer rate (ETR) and higher quantum yield of non-photochemical fluorescence quenching (Y(NPQ)) than algae that were grown under partial shade. Furthermore, under 34 µmol photon/m^{2}s illumination grown and additionally illuminated with VL algae' ETR and Y(NPQ) were temporarily reduced (after a day ETR and Y(NPQ) already recovered to initial values). Moreover, it was registered that VL induced photobleaching of FL intensity of Mg-Chl (50 µM) and a 1.6-time decrease of algae AF (Fig. 1. A). VL and Mg-Chl cumulative effect was also evaluated for AF and photosynthetic parameters of algae. Fluorescence measurements immediately after irradiation revealed a sudden two-fold algae AF decrease from the initial value but decrease of ETR induced by light exposed Mg-Chl (Fig. 1. B) was smaller than those induced only by VL. After 24 hours measured AF spectra and photosynthesis parameters showed no significant Mg-Chl effect on *Sc. sp.* algae. Therefore, chlorophyllin did not cause any additional oxidative stress for algae beyond that caused by irradiation. These findings build a foundation for Mg-Chl research as an antioxidant agent for algae cell treatment after NP impact.

This research is partially funded by Research Council of Lithuania, agreement No. P-ST-23- 111.

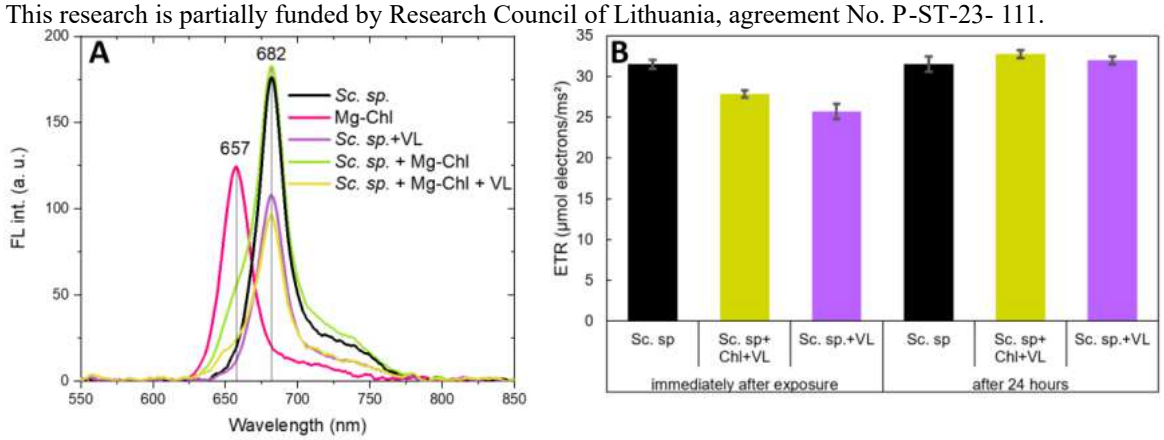

Fig. 1. Magnesium chlorophyllin Mg-Chl, violet light (VL) and their cumulative effect on *Scenedesmus sp.* algae grown under 34 µmol photon/m^{2}s illumination. **A** – fluorescence spectra λ_{ex}=405 nm; **B** – relative electron transfer rate (ETR), averaged from fluorescence kinetics in actinic light (error bars represent 95% confidence interval).

[1] I. Buchovec, E. Vyčaitė et al., *Int. J. Mol. Sci*. **24**, 722, (2023).
[2] U. J. Yang, T. S. Park, S. M. Shim, *J. Toxicol. Environ. Health. A.* **76**(23), 1307-1315, (2013).
[3] J. P. Kamat, K. K. Boloor, T. P. A. Devasagayam, *Biochim. Biophys. Acta, Mol. Cell Biol. Lipids*, **1487**(2-3), 113-127, (2000).
[4] K. Yao, X. Lv et al., *Environ, Sci. Technol*. **52**(24), 14445-14451, (2018).

Inositol hexakisphosphate (IP_6) alters voltage dependence of Ca^{2+} channels in *Nitellopsis obtusa*

Vilmantas Pupkis[1], Indrė Lapeikaitė[1], Vilma Kisnierienė[1]

[1]Department of Neurobiology and Biophysics, Life Science Center, Vilnius University, Sauletekio av. 7, LT-10257, Vilnius, Lithuania
vilmantas.pupkis@gmc.vu.lt

Upon exposure to non-damaging external stimuli, plants generate action potentials – electrical signals that propagate with an intrinsic velocity and constant signal shape enabling information transfer to the distal parts of the plant body. A propagated action potential alters various physiological processes, resulting in suppressed photosynthetic activity, enhanced cellular respiration, initiated stress hormone synthesis, and changes in gene expression. In photosynthetic organisms, the initial plasma membrane depolarisation during action potential generation is caused by Ca^{2+} influx into the cytoplasm. In Characean algae, the molecular identity of these Ca^{2+} channels is unknown. Moreover, their theoretical regulation via second messengers requires additional experimental justification [1]. We tested a proposed second messenger inositol hexakisphosphate (IP_6), which in theory can activate Ca^{2+} channels [2].

The intracellular two-electrode technique in current clamp and voltage clamp modes was used on the internodal cells of Characean macroalgae *Nitellopsis obtusa*. Membrane potential, conductance, and parameters of electrically-elicited action potentials as well as excitation transients were registered. A segment of a cell was externally exposed to 75 µM or 150 µM of IP_6 for 30 min. In addition, cytoplasmic streaming (cyclosis) velocity and its alterations were observed since it can be used as a proxy for the dynamics of intracellular Ca^{2+} concentration. In these experiments, *N. obtusa* cells were exposed to a 150 µM IP_6 solution for 30 min.

Experiments revealed that 75 IP_6 hyperpolarises the action potential excitation threshold, putatively activating Ca^{2+} channels at more negative membrane potential values (Fig. 1). These results were confirmed by the shifted Ca^{2+} current I/V curves in the negative direction during voltage clamp experiments. It also should be noted that the exposure to IP_6 did not affect the maximal membrane conductance during excitation. IP_6 also did not alter the cyclosis velocity, either during rest, or after cell electrical excitation.

These results indicate that IP_6 does not activate *N. obtusa* Ca^{2+} channels by increasing their open probability, but shifts its voltage dependence to more negative membrane potential values, thus lowering the excitation threshold and making the cell more excitable.

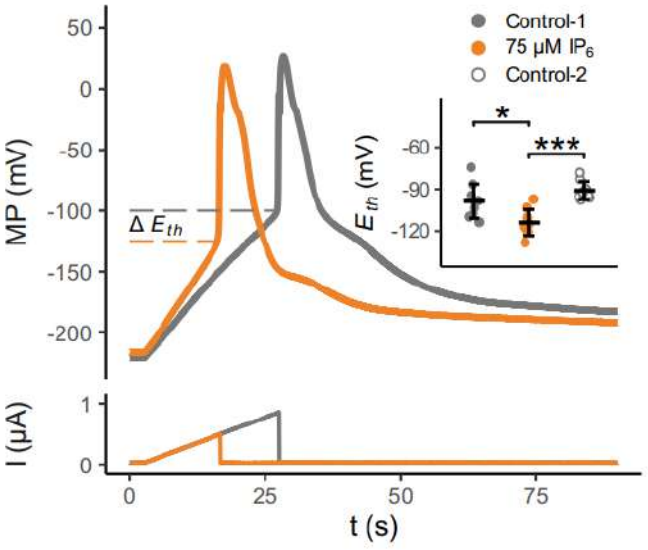

Fig. 1. Typical electrically-elicited action potentials of *Nitellopsis obtusa* internodal cells under control conditions and after exposure to inositol hexakisphosphate (IP_6). Note the hyperpolarised excitation threshold E_{th}, which is highlighted in the inset. n=9.

[1] Kisnieriene, V., Lapeikaite, I., Pupkis, V., Beilby, M. *Front Plant Sci*, **10**, 82 (2019).
[2] Krinke, O., Novotná, Z., Valentová, O., Martinec, J. *J Exp Bot*, **58**(3), 361-376 (2007).

Discrimination of *Nitellopsis obtusa* Responses to Environmental Stressors via Fluorescence Spectroscopy

Aušrinė Navickaitė[1], Vilmantas Pupkis[1], Agnė Kalnaitytė-Vengelienė[2], Indrė Lapeikaitė[1], Vilma Kisnierienė[1], Saulius Bagdonas[2]

[1]Vilnius University, Department of Neurobiology and Biophysics, Saulėtekio av. 7, LT-10257, Vilnius, Lithuania
[2]Vilnius University, Laser Research Center, Saulėtekio av. 9, LT-10222, Vilnius, Lithuania
ausrine.navickaite@gmc.stud.vu.lt

In the natural environment, plants and algae are exposed to a wide range of adverse conditions. Photosynthesis is particularly sensitive to sudden changes in ambient factors and can be monitored via non-invasive optical methods. The use of fluorescence-based techniques in plant research is widespread; alterations in fluorescence (FL) signal reflect changes in photosynthesis [1]. However, the response of plants to different environmental stressors often results in indistinguishable changes in the recorded autofluorescence (aFL) spectra. To improve the diagnostic potential of FL measurements in practical applications, it is essential to determine and select appropriate FL parameters.

Herbicides such as diuron (DCMU) inhibit photosynthetic electron transport through well-established mechanisms of action [2], making them a valuable tool for validating FL-based techniques, aimed at detecting impaired photosynthetic performance. The effect of 100 µM DCMU was studied at the single cell level under selected illumination conditions: darkness, maintenance light (9.5 ± 0.2 µmol m^{-2} s^{-1}), darkness and subsequent illumination with intense white LED light (829 µmol m^{-2} s^{-1}) for 15 min and 30 min. aFL spectra were recorded at 1 mm intervals along internodal cells of the macroalga *Nitellopsis obtusa* using an optical fiber system coupled to a controlled stepper motor. A low intensity (0.13 mW) LED light source emitting at 405 nm was used for excitation.

The aFL spectra of *N. obtusa* internodal cells had a main peak at 680 nm and a shoulder in the far-red region at about 740 nm (Fig. 1a). FL intensities measured at these wavelengths varied along the cell and correlated with changes in the FL intensity ratio between 680 nm and 750 nm (F680/F750). DCMU increased the peak intensity value at 680 nm (F680) and decreased the F680/F750 ratio. Investigation of the relationship between selected FL parameters showed a clear separation of algal cells treated with DCMU (Fig. 1b), but the general trend of light-induced changes in FL parameters persisted.

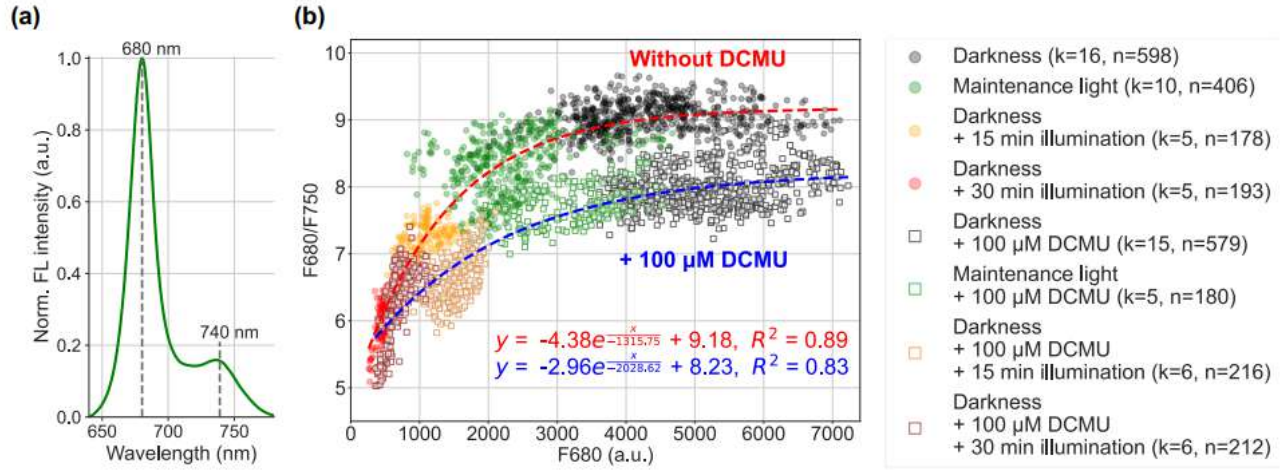

Fig. 1. *N. obtusa* autofluorescence (aFL) spectrum (a) and the relationship between fluorescence parameters: F680 and the F680/F750 ratio, with and without DCMU treatment (b). Dashed lines in (b) show exponential approximations; k – number of cells, n – number of registered spectra, R^2 – determination coefficient

The present study shows that changes in *N. obtusa* autofluorescence parameters: F680 and the F680/F750 ratio, can be used for effective detection of stress-inducing factors affecting photosynthetic activity. The ability to distinguish the effect of the herbicide DCMU not only on dark-adapted cells, but also in the case of light-adapted cells and even after certain doses of excess illumination suggests that the proposed analysis of FL parameters may be useful for integration into remote sensing devices identifying external stressors of *N. obtusa* or other algal species in the field.

[1] Baker N. R. Chlorophyll fluorescence: a probe of photosynthesis in vivo. *Annu Rev Plant Biol*. 2008;59:89-113.
[2] Kirilovsky D., Rutherford A. W., Etienne A. L. Influence of DCMU and ferricyanide on photodamage in photosystem II. *Biochemistry*. 1994;33(10):3087-3095.

Saturated Phospholipids for Upconverting Nanoparticles and Chlorin e6 Complex Formation

Emilė Pečiukaitytė [1,2], Simona Steponkienė [1], Eglė Ežerskytė [1,3], Vaidas Klimkevičius [1,3], Vitalijus Karabanovas [1,4], Ričardas Rotomskis [1,5]

[1] Biomedical Physics Laboratory of National Cancer Institute, Baublio 3B, LT-08406, Vilnius, Lithuania
[2] Life Sciences Center, Vilnius University, Saulėtekio av. 7, LT-10257, Vilnius, Lithuania
[3] Institute of Chemistry, Faculty of Chemistry and Geosciences, Vilnius University, Naugarduko 24, LT-03225, Vilnius, Lithuania
[4] Department of Chemistry and Bioengineering, Vilnius Gediminas Technical University, Saulėtekio av. 11, LT-10223, Vilnius, Lithuania
[5] Biophotonics Group of Laser Research Centre, Vilnius University, Saulėtekio av. 9, c.3, LT-10222, Vilnius, Lithuania

emile.peciukaityte@nvi.lt

Cancer remains one of the leading causes of death worldwide, with more than 1.2 million cancer-related deaths projected to occur within the European Union by 2024 [1]. The application of nanotechnology and nanoparticles in the biomedical field offers opportunities to develop biocompatible theranostic nanoplatforms with customizable features. "Theranostics" refers to the integration of therapeutic and diagnostic functions within a single system, which can reduce treatment delays, eliminate multiple steps in the medical process, enhance patient care, and provide early diagnosis [2].

This study focuses on developing a theranostic nanoplatform composed of phospholipid/polyethylene glycol (PL-PEG)-coated upconverting nanoparticles (UCNPs) carrying Chlorin e6 (Ce6) within the PL-PEG coating, where Ce6 acts as a photosensitizer. UCNPs can be used for cancer diagnosis due to their excellent emission properties, while Ce6 facilitates the generation of singlet oxygen for photodynamic therapy via energy transfer from UCNP to Ce6. However, the formation of UCNP-Ce6 complexes can be challenging due to instability, Ce6 attachment process or lack of energy transfer between UCNP and Ce6.

The aim of this study was to spectroscopically evaluate and compare different methods for complex formation to achieve an efficient nanoplatform with an optimized coating process. A mixture of saturated phosphatidylcholine (HSPC) and phosphatidylethanolamine conjugated with polyethylene glycol (DSPE-PEG) phospholipids were used as the coating layer for $NaGdF_4:Yb^{3+},Er^{3+}@NaGdF_4:Yb^{3+},Nd^{3+}$ UCNPs, as well as for the formation of liposomes. Ce6 was incorporated either through passive diffusion in an aqueous environment or during the film formation process.

The obtained results indicate that the absorption and fluorescence peaks of Ce6 vary depending on the method used for UCNPs-Ce6 complex formation, suggesting different attachment sites for Ce6 within the PL-PEG layer. Furthermore, when Ce6 was loaded into liposomes using the same methods (passive diffusion or during film formation), the results showed a high degree of similarity - the incorporation pattern of Ce6 within the PL-PEG layer differed depending on the method used. Since the functional efficiency of the UCNPs-Ce6 complex is related to the distance between Ce6 and the UCNPs, these findings emphasize the importance of optimizing the complex formation process to achieve maximum effectiveness. The different attachment sites indicate varying depths of Ce6 incorporation within the PL-PEG layer. We believe the nanoplatform developed in this study represents a promising approach for effective cancer treatment and targeted drug delivery. The overall characteristics of the nanoplatform can be modulated by adjusting the phospholipid coating, allowing for precise control over the positioning of Ce6. This study contributes to the understanding of photosensitizers and enhances our overall knowledge of nanoplatforms for cancer therapy.

Acknowledgements
This project has received funding from the Research Council of Lithuania (LMTLT), agreement No. P-ST-24-258.

[1] Santucci, C., Mignozzi, S., Malvezzi, M., Boffetta, P., Collatuzzo, G., Levi, F., La Vecchia, C., & Negri, E. (2024). European cancer mortality predictions for the year 2024 with focus on colorectal cancer. In Annals of Oncology (Vol. 35, Issue 3, pp. 308–316). Elsevier BV. https://doi.org/10.1016/j.annonc.2023.12.003

[2] Skripka, A., Dapkute, D., Valanciunaite, J., Karabanovas, V., & Rotomskis, R. (2018). Impact of Quantum Dot Surface on Complex Formation with Chlorin e6 and Photodynamic Therapy. In Nanomaterials (Vol. 9, Issue 1, p. 9). MDPI AG. https://doi.org/10.3390/nano9010009

Mesenchymal Stem Cell-Mediated Nanoparticle Transfer to Cancer Cells

Augustė Kavalevskaja[1,2], Greta Butkienė[1], Marijus Plečkaitis[1], Alėja Marija Daugėlaitė[1], Ričardas Rotomskis[1]

[1] Biomedical Physics Laboratory, National Cancer Institute, P. Baublio str. 3b, Vilnius, LT-08406, Lithuania
[2] Life Sciences Center, Vilnius University, Saulėtekio Ave 7, Vilnius, LT-10257, Lithuania
auguste.kavalevskaja@gmc.stud.vu.lt

Despite advancements in medical technology, cancer treatment continues to face significant challenges due to late diagnosis, chemotherapeutic resistance, and the immune system's inability to combat mutated cells [1]. Scientists are exploring potentially more effective methods for treating cancer using extremely small nanoparticles (1-100 nm), which could help overcome these challenges [2]. However, nanoparticles don't come without their own limitations. For example, accumulation of nanoparticles in tumours is restricted and requires additional improvements. Improved accumulation could be achieved by using mesenchymal stem cell-mediated delivery of nanoparticles.

The aim of this study was to evaluate the transfer of nanoparticles from mesenchymal stem cells (MSCs) to MDA-MB-231 human breast cancer cells. MSCs isolated from human skin during blepharoplasty procedures were utilized in the experiment. Photoluminescent Qdot™ 625 ITK™ carboxyl quantum dots (Thermo Fisher Scientific, USA) were selected for this study. The MSCs were incubated with the quantum dots for 4 hours, then washed and incubated with MDA-MB-231 cancer cells for 24 hours. The accumulation and distribution of quantum dots were analyzed using a Nikon Eclipse TE2000-S, C1 Plus laser scanning confocal microscope (Nikon, Japan) with a 60× SA 1.4 immersion objective. A diode laser (404 nm), an argon-ion laser (488 nm) and a helium-neon laser (543 nm) were used for the excitation of the samples.

Confocal microscopy analysis revealed that mesenchymal stem cells accumulated Qdot™ 625 ITK™ carboxyl quantum dots, which were biocompatible and showed no toxicity to the cells. Additionally, the MSCs demonstrated the ability to transfer quantum dots to MDA-MB-231 cancer cells, likely through structures resembling tunnelling nanotubes. The study investigated whether MSCs release quantum dots into the medium and if the MDA-MB-231 cancer cells uptake them. The results were positive, indicating that exocytosis and subsequent uptake of the quantum dots occurred, offering a potential method for nanoparticle delivery in cancer treatment. However, further research is needed to optimize nanoparticle transfer and accumulation while seeking to improve therapeutic outcomes.

[1] Siegel, R.L., Miller, K.D., Wagle, N.S., Jemal, A., 2023. Cancer statistics, 2023. CA: A Cancer Journal for Clinicians 73, 17–48.
[2] Vassal, M., Rebelo, S., Pereira, M., 2021. Metal Oxide Nanoparticles: Evidence of Adverse Effects on the Male Reproductive System. International Journal of Molecular Sciences 22, 8061.

Identification of Pathogenic Bacteria and Yeast by means of ATR IR Spectroscopy

Gerda Anužienė[1], Irmantas Arūnas Čiužas[2], Tautvydas Taraškevičius[1], Eglė Lastauskienė[2], Justinas Čeponkus[1]

[1]Institute of Chemical Physics, Faculty of Physics, Vilnius University, Saulėtekio Av. 3, LT-10257 Vilnius, Lithuania
[2]Institute of Biosciences, Life Sciences Center, Vilnius University, Saulėtekio Av. 7, LT-10257 Vilnius, Lithuania
gerda.anuziene@ff.vu.lt

Pathogenic bacteria and yeast cause infectious diseases and complication of these diseases can endanger patients' life. For a long time, it was believed that fungi do not affect infections which are caused by bacteria, but with the development of diagnostic equipment and more research, it has been observed that interaction between bacteria and fungi may worsen patient's condition. In mixed infections, only one domain of pathogenic microorganism (eukaryote or procaryote) can be killed while allowing another to spread even faster. Because different treatment strategies are applied for treating patients, it is crucial to identify the type of pathogenic microorganisms correctly to prescribe medication. Nowadays, methods which are for discrimination of pathogenic microorganisms requires sample preparation and takes a long time till results are presented. ATR IR spectroscopy can be suitable for pathogenic microorganism identification because it often does not require sample preparation, and the collection of the ATR IR absorbance spectrum takes several minutes, thus, the identification of pathogenic microorganisms can be accomplished faster [1-3].

In this work, the method of an attenuated total reflection of infrared radiation (ATR IR) spectroscopy was applied for the analysis. A total of 177 ATR IR absorption spectra were collected which includes two types of yeast (*Candida guilliermondii, Candida parapsilosis*), three types of bacteria (*Staphylococcus aureus, Streptococcus pyogenes, Escherichia coli*) and mixtures between pathogenic yeast and bacteria.

The main difference between ATR IR absorbance spectra of bacteria and yeast were observed in the 1360 cm^{-1} – 1280 cm^{-1} and 1183 cm^{-1} – 930 cm^{-1} spectral regions which are associated with carbohydrates found in bacterial and yeast cell walls. Further analysis also showed that 1360 cm^{-1} – 1280 cm^{-1} spectral region (Fig. 1 (a)) is suitable for the identification of ATR IR absorbance spectra of mixtures of *C. guilliermondi-S. aureus*, *C. parapsilosis-E. coli* and *C. parapsilosis- S. pyogenes* at the ratios [1:1], [1:2], [1:3], [2:1], [3:1], [2:3], [3:2]. As the ratio of the mixture changes, the position of the polysaccharides δ(CH), Amide III spectral bands changes. To evaluate ATR IR spectroscopy applicability for clinical diagnostics K-means statistical analysis was performed. In Fig. 1. (b) most of ATR IR absorbance spectra of pure bacteria are located in the part of the diagram marked with red ellipse, while most the pure yeast spectra are located in the part of the diagram marked with blue ellipse. The spectra of the mixtures are located between the mentioned parts of the diagram, depending on the dominant microorganism in the sample

The results show potential of ATR IR spectroscopy application for the identification of pure pathogenic microorganisms' samples and their mixtures. Using this method pathogenic yeast and bacteria can be identified with 100 % accuracy. Application of K-means statistical analysis also showed that using ATR IR spectroscopy mixtures samples can be successfully separated. In order to apply the method in clinical diagnostics, further detailed studies with larger spectral databases are required.

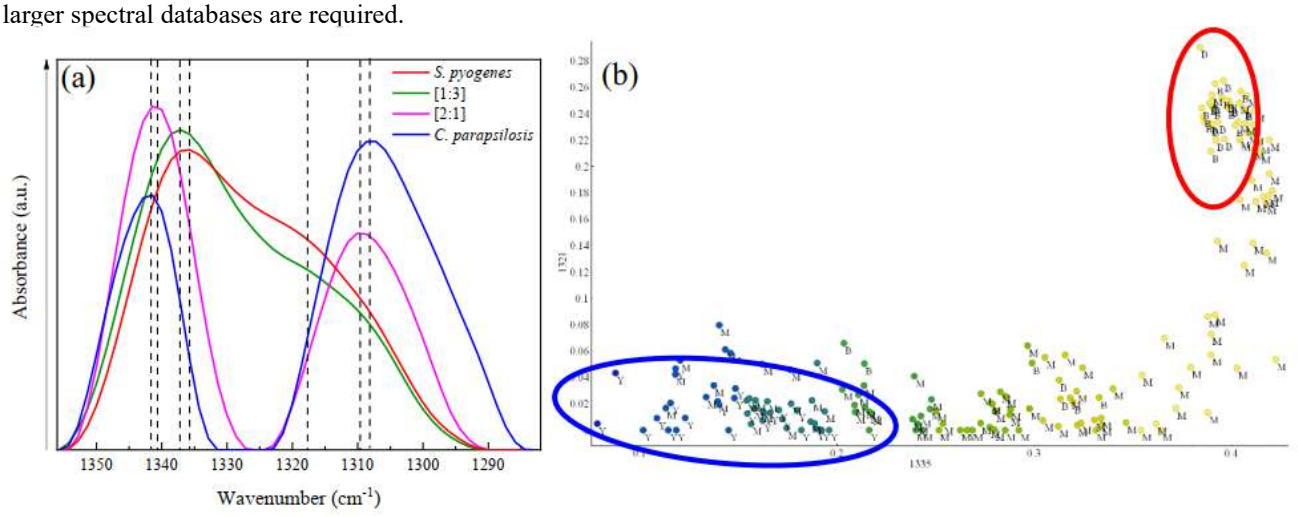

Fig. 1. (a) ATR IR absorption spectra of pure yeast, pure bacteria, and mixtures, (b) K-means plot of ATR IR absorption spectra of bacteria, yeast, and their mixtures.

[1] M. Pigłowski, Int. J. Environ. Res. Public Health **16**, 477 (2019)
[2] M. Harz, P. Rösch, J. Popp, Cytometry **75A**, 104-113 (2009)
[3] B. Buszewski, A. Rogowska, P. Pomastowski, M. Złoch, V. Railean-Plugaru, J. AOAC Int **100**, 1607-1623 (2017)

A Computational Approach for Precision Targeting Cancer Cells Through the Integration of Metabolic Modelling and RNA-seq

Monika Pankevičiūtė-Bukauskienė[1], Sergio Bordel Velasco[1]

[1]Lithuanian University of Health Sciences, Institute of Cardiology, Laboratory of Cell Culture, Sukilėlių pr. 15, LT-50162, Kaunas, Lithuania
monika.pankeviciute-bukauskiene@lsmu.lt

While the number of anti-neoplastic agents targeting specific metabolic pathways remains limited, this area has long been a focus of cancer research and is gaining momentum as modern technologies accelerate drug discovery and development. The overarching goal of therapy is to maximize benefit with minimal harm, meaning treatment strategies must be precise enough to target the root cause of the disease without disrupting normal bodily functions. Cancer arises from a combination of mutations that accelerate cell proliferation. One of the key features of cancer cells is metabolic reprogramming, which enables them to generate building blocks and energy required for rapid division. These mutations can either increase or decrease the production of key metabolites, presenting opportunities for targeted therapies. However, targeting these pathways must be done carefully, as interfering with important metabolic reactions may affect healthy cells. A promising drug target is an enzyme involved in a reaction that normal cells can bypass through alternative pathways, but that cancer cells rely on exclusively.

A Genome Scale Metabolic Model (GSMM) is a comprehensive representation of all metabolic reactions within an organism, presented as a stoichiometric matrix. This matrix lists the coefficients of each metabolite in every reaction. This allows us to evaluate the cell's metabolic capability. While some metabolic fluxes can be measured (e.g. by using ^{13}C labelled substrates), this can be time-consuming. High-throughput techniques like RNA sequencing (RNA-seq) offer a more efficient approach. We aimed to develop a computational method that integrates GSMMs with RNA-seq data to identify personalized therapeutic windows. Unlike the PRIME method, which sets upper limits on reaction rates based on gene expression microarray data, our approach constrains every gene-related reaction using gene expression levels measured as RPMK (reads per million per kilobase). To automate this process, we developed the Python library pyTARG [1], which applies RNA-seq data to human GSMMs. This tool estimates metabolic flux distributions and identifies potential drug targets that could disrupt the production of biomass building blocks in cancer, while having less impact on healthy cells. We tested this approach using RNA-seq data from the Human Protein Atlas and our own sequencing data from MCF-7, MCF-10, and primary breast tumour cells (BCC). Our results align with the Warburg effect, showing higher metabolic fluxes for glucose uptake, glycolysis, and lactic acid production in cancer cells compared to healthy cells. Malignant cells also exhibited a downregulation of the respiratory chain, consistent with known cancer biology. Additionally, the model confirmed increased activity of the oncogene MYC, loss of tumor suppressor TP53, and a lower reaction rate of ATP synthase in cancer cells. The model predicted higher cholesterol biosynthesis in cancer cells, identifying it as a potential therapeutic target. Lower serine uptake was also predicted in breast cancer cells (MCF-7 and BCC), suggesting serine biosynthesis could be explored as a drug target [2]. Furthermore, reduced CO_2 conversion to bicarbonate was predicted due to the downregulation of carbonic anhydrases CA6 and CA2. Carbonic anhydrases, crucial for regulating tumor cell pH, are potential drug targets, though only CA IX and CA XII have been explored so far, leaving other isoforms as future research opportunities.

In conclusion, our computational approach integrating GSMMs with RNA-seq data has shown promising potential for identifying personalized therapeutic windows in cancer treatment. This method not only provides insights into cancer cell metabolism but also offers a platform for precision-targeted therapy, which could minimize harm to healthy cells and improve treatment outcomes.

---

[1] Bordel S. Constraint based modeling of metabolism allows finding metabolic cancer hallmarks and identifying personalized therapeutic windows. *Oncotarget* 2018; 9:19716–29.

[2] Pankevičiūtė-Bukauskienė M, Mikalayeva V, Žvikas V, Skeberdis VA, Bordel S. Multi-Omics Analysis Revealed Increased De Novo Synthesis of Serine and Lower Activity of the Methionine Cycle in Breast Cancer Cell Lines. *Molecules* 2023; 28.

THE POTENCY OF CX43 GAP JUNCTION INHIBITORS IS INFLUENCED BY PHOSPHORYLATION

R.Mickus, V.Raškevičius, V.Mikalayeva, I.Sarapinienė, V.A.Skeberdis.

Institute of Cardiology, Lithuanian University of Health Sciences, 50162 Kaunas, Lithuania
rokas.mickus@lsmu.lt

Connexin 43 (Cx43) is a key mediator of gap junction intercellular communication (GJIC) in most tissues. In our recent research, we identified several new GJ inhibitors derived from nutmeg essential oil. In the current study, using dual whole-cell patch-clamp techniques we found that one of them, the acyclic monoterpene α-pinene, at concentrations close to IC_{50} (27 μM) produced highly variable effects, ranging from no inhibition to complete blockade of Cx43 GJ conductance. Given that the activity of certain protein kinases fluctuates throughout the cell cycle, we hypothesized that such variability could depend on Cx43 phosphorylation status in randomly selected cell pairs. Indeed, the non-selective protein kinase inhibitor staurosporine fully reversed the inhibitory effect of α-pinene (50 μM) and produced the limited (2.5-fold) shift of α-pinene dose-response curve. This suggested that phosphorylation may act as an allosteric effector of positive cooperativity. To further investigate whether α-pinene potency is linked to phosphorylation of Cx43 carboxyl-terminal, we used a truncated Cx43 variant (Cx43K258Kstop-msfGFP) with minimal number of phosphorylatable residues. These GJ channels remained sensitive to α-pinene but its effect became completely insensitive to staurosporine. Further, we found that the effect of staurosporine could be mimicked by selective inhibitors of the Ca^{2+}/calmodulin-dependent kinase II pathway, atypical PKC (which is insensitive to both Ca^{2+} and DAG), and CDK. Compounds whose activity is influenced by receptor phosphorylation may hold promise for developing targeted therapies for diseases associated with high kinase activity, such as cardiac arrhythmias, epilepsy, stroke, essential tremor, inflammation, and cancer.

Modelling the absorption spectra of light-harvesting antenna complexes

Austėja Mikalčiūtė[1], Darius Abramavičius[1]

[1]Institute of Chemical Physics, Faculty of Physics, Vilnius University, Saulėtekio al. 9, Vilnius, Lithuania
austeja.mikalciute@ff.stud.vu.lt

The process of photosynthesis was discovered back in the 17th century, but its molecular mechanisms still pose some questions to the scientific community. One of the most fundamental parts of photosynthesis is the collection of light through multi-pigment light-harvesting antenna complexes. As photosynthesis is a vastly prevalent process – it has adapted to occur both in water and on land, and it can be found in many bacteria, algae, and plant species, therefore, there is a diversity of photosynthetic pigments and light-harvesting complexes. In this work we have tried to model pigment-pigment interaction, absorption spectra, and relaxation rates of three different light-harvesting complexes (Fenna-Matthews-Olson (FMO), light-harvesting 2 (LH2), fucoxanthin-chlorophyll binding protein (FCP)) using their protein structures, while modelling not only the first excited state, but also including the first excited state interactions with the ground state of the pigments. FCP, FMO and LH2 structures from Protein Data Base were used. Ground state (S_0), first vertically excited (S_{01}) and equilibrated (S_{11}) excited states of chlorophyll *a*, c_1, c_2 and bacteriochlorophyll *a* were calculated with GAUSSIAN software [1] using the TD-DFT methodology with a CAM-B3LYP 6-31G(d) basis set. Then from the quantum mechanical calculation results, partial atomic charges were calculated using CHELPG methodology with Multiwfn software [2]. Partial atomic charges of the protein backbone with PARSE and AMBER force fields were obtained via PDB2PQR [3]. From these results via an in-house developed code, pigment-pigment excited state interactions, excitation frequencies, relaxation to ground state rates, and absorption spectra were calculated. Spectra of pigments in *vacuo*, in a protein environment with different force fields, and in a protein environment with the addition of ions in case of adiabatic and non-adiabatic (including ground state of pigments) couplings were compared. The general trend tends to be that due to coupling to the ground state, pigment absorption spectra tend to shift to higher energies, some peak positions and shapes of the spectra change, and some details of the spectra's fine structure can be seen.

Fig. 1. Hamiltonian (in cm^{-1}) of FMO complex.

[1] M. J. Frisch et al., GAUSSIAN 16, Gaussian Inc. Wallingford CT, 2016.
[2] T. Lu and F. Chen, *J. Comput. Chem.*, **33**, 580-592 (2012),.
[3] T. J. Dolinsky, J. E. Nielsen, J. A. McCammon, N. A. Baker, *Nucleic Acids Res.,* **32**, W665-W667 (2004).

Resveratrol exerts distinct effects on intercellular communication through Cx43 and Cx45 gap junctions

Gintarė Jančiukė, Rokas Mickus, Vytenis Arvydas Skeberdis, Ieva Sarapinienė

Lithuanian University of Health Sciences, Institute of Cardiology, Sukilėlių ave. 15, Kaunas, Lithuania
gintare.janciuke@lsmu.lt

Resveratrol is a polyphenol found in variety of plants and well known for its biological properties, including antioxidant, antitumor, cardioprotective, and neuroprotective effects. Additionally, the effects of resveratrol are associated with changes in the expression of connexins (Cx) and gap junction intercellular communication (GJIC) in normal and cancer cells.

Our aim was to elucidate the effect of resveratrol on gap junction conductance (g_j), connexin expression, and viability of HeLa WT cells (lacking Cx) and HeLa cells expressing exogenous Cx43 or Cx45.

We found that viability was reduced in all cases after exposure to 100 μM resveratrol for 48 h. However, HeLa Cx43 cells were more sensitive to resveratrol treatment compared to HeLa WT and HeLa Cx45.

To assess the effect of resveratrol on GJIC, we performed dual whole-cell patch-clamp experiments. Resveratrol inhibited g_j of Cx43 GJs but stimulated g_j of Cx45 GJs. Western blot analysis revealed time- and concentration-dependent changes in Cx43 and Cx45 expression levels. After 24 h of treatment with 10 and 100 μM resveratrol, Cx43 expression was upregulated, whereas after 48 hours, it was downregulated. In contrast, exposure to the highest concentration of resveratrol (100 μM) increased Cx45 levels after both 24 and 48 hours of treatment. Further we examined whether the changes in total Cx43 and Cx45 expression were followed by alterations in Cx45 and Cx43 GJ basal conductance between untreated and resveratrol-preincubated cells (24 h). Cx43 GJ g_j was inhibited by 1 and 10 μM resveratrol, while no effect was observed with 100 μM. In contrast, Cx45 GJ g_j was suppressed by 100 μM resveratrol, presumably due to redistribution of Cx45 to the cytoplasm.

It is well known that synthesis, assembly and function of the GJs is modulated through phosphorylation of Cx at different sites. Therefore, we evaluated changes in Cx43 phosphorylation at pS368, pS373, pS282 and pS279 after 15 min and 24 h of resveratrol treatment. It is known that the phosphorylation of pS282 and pS279 is associated with inhibition of Cx43 GJ conductance, while phosphorylation of pS373 is associated with increased plaque size [1-2]. Indeed, we found that Cx43 GJ g_j decreased while pS282 and pS279 levels increased after both, 15 min and 24 h of resveratrol treatment. Also, concomitantly with elevation of pS373 levels, we observed an increase in Cx43 GJ plaque size after 24 hours of treatment with 100 μM resveratrol.

Our findings suggest that the action of resveratrol on HeLa cell viability and GJIC is connexin type-dependent.

[1] T. Aasen, S. Johnstone, L. Vidal-Brime et al., *Int. J. Mol. Sci.*, ***19***, 1296 (2018).
[2] L. J. Solan, P. D. Lampe, FEBS Letters, **588**, 1423-1429 (2014)

Molecular modelling and experimental examination of terpenes effects on Cx43 gap junction gating

Gabrielė Zuokaitė, Vytautas Raškevičius, Vytenis Arvydas Skeberdis

Lithuanian University of Health Sciences, Institute of Cardiology, Laboratory of Cell Culture, Kaunas, Lithuania
gabriele.zuokaite@vdu.lt

Intercellular communication via gap junctions (GJ), composed of Connexin protein (Cx), is crucial for various physiological processes. Disruptions in Cx43 GJ signaling have been implicated in a range of diseases, including cardiovascular disorders. Terpenes, a class of natural compounds known for their diverse biological activities [1], have emerged as potential modulators of Cx43 function [2].

This study aimed to investigate the effects of selected linear terpenes on Cx43 GJ conductance in Novikoff rat hepatoma cells. Myrcene (a monoterpene), Farnesene (a sesquiterpene), and Squalene (a triterpene) were chosen for their structural diversity and potential pharmacological relevance.

Quantitative structure-activity relationship (QSAR) modeling and molecular docking simulations were employed to predict the inhibitory potencies (pIC$_{50}$ values) and docking sites of these terpenes on the Cx43 protein. QSAR-predicted IC$_{50}$ values were 16, 0.63, and 4 µM for Myrcene, Farnesene, and Squalene, respectively. These data well harmonized with their experimental potencies (eIC$_{50}$) obtained by direct measurement of Cx43 GJ conductance using dual whole-cell patch-clamp techniques: 18, 1.5, and 168 µM for Myrcene, Farnesene, and Squalene, respectively. Respective Hill's coefficients for these compounds (4.1, 2.1, and 2.2, respectively), suggest that they may interact with more than one binding site on Cx43. Interestingly, two docking clusters of Myrcene corresponded to its twofold higher Hill's coefficient than that of Farnesene and Squalene, suggesting that its potency may depend on Cx43 phosphorylation [3].

We conclude that QSAR in combination with molecular docking may significantly facilitate the search of novel potent and specific GJ inhibitors by selecting the putative molecules for electrophysiological confirmation.

[1] Edris A. E. (2007). Pharmaceutical and therapeutic potentials of essential oils and their individual volatile constituents: a review. Phytotherapy research : PTR, 21(4), 308–323. https://doi.org/10.1002/ptr.2072

[2] Mickus, R., Jančiukė, G., Raškevičius, V., Mikalayeva, V., Matulytė, I., Marksa, M., Maciūnas, K., Bernatonienė, J., & Skeberdis, V. A. (2021). The effect of nutmeg essential oil constituents on Novikoff hepatoma cell viability and communication through Cx43 gap junctions. Biomedicine & pharmacotherapy = Biomedecine & pharmacotherapie, 135, 111229. https://doi.org/10.1016/j.biopha.2021.111229

[3] Mickus, R., Raškevičius, V., Sarapinienė, I., Mikalayeva, V., Prekeris, R., Skeberdis, V.A. (2024). Phosphorylation-dependent allosteric regulation of Cx43 gap junction inhibitor potency. Biomedicine & Pharmacotherapy. 174. https://doi.org/10.1016/j.biopha.2024.116550

Effects of cardiotropic drugs on vascular stiffness and diastolic pressure ratio

Ieva Lankutytė[1], Dominyka Adamonė[1], Vilma Zigmantaitė[1], Antanas Navalinskas[1], Jonas Jurevičius [1], Regina Mačianskienė[1]

[1] Lithuanian University of Health Sciences, Institute of Cardiology, Laboratory of Membrane Biophysics, Sukilėlių pr. 15, Kaunas, Lithuania
ieva.lankutyte@lsmu.lt

Research on the relation between diastolic blood pressure (DBP) and pulse wave velocity (PWV) is essential, especially for comprehending cardiovascular risk and the outcomes of various pharmacological interventions. PWV is a widely recognized measure of arterial stiffness, while DBP mainly depends on the artery state. The effect of cardiovascular drugs (CVDs) on these parameters remains inadequately defined, particularly regarding their influence on the DBP to PWV ratio (DBP/PWV). This specific interaction has garnered increasing attention within the field of cardiovascular research. In clinical settings, the DBP/PWV ratio is sometimes used to evaluate the impact of drugs (e.g., antihypertensives, statins, and antidiabetic agents) on arterial stiffness relative to blood pressure control. Each drug acts differently on blood vessels, heart rate, and vascular tone, thus influencing DBP and PWV.

The specific investigation of the DBP/PWV ratio in animal models, including pigs, is somewhat limited. In addition, while some essential oils, such as *E. ciliata* (ECEO), have been reported to have antiarrhythmic [1] and hypotensive or vasodilatory effects [2], till now there has been no research linking the essential oils' action to the modulation of arterial stiffness and DBP/PWV ratio.

In this study, using anesthetized in vivo pigs we aimed to assess the effects of ECEO, compare its effectiveness with various CVDs on the DBP/PWV ratio, and reveal their mechanisms of action. We measured systolic and diastolic blood pressure (SBD and DBP, respectively) and heart rate via invasive catheterization of the carotid artery. The blood pressure waveform and femoral artery pulse were recorded for 30 min and were used to calculate PWV. We assessed the effects of various drugs on heart rate and blood pressure, and calculated pulse wave speed and its relationship to DBP.

Our results demonstrate that in the pig model, essential oils like ECEO have been reported to modulate heart rate and reduce blood pressure [2] and may influence DBP through the relaxation of blood vessels. The drug tends to reduce PWV from 10.5 to a minimal value of 4.1 m/s, and after 30 min reached a new level at 8.9 m/s. If ECEO reduces arterial stiffness and DBP, it might theoretically modulate the DBP/PWV ratio, but this remains unclear and is purely speculative without clinical evidence. Herbal essential oils have not been used or studied for measuring or modulating the DBP/PWV ratio in any significant way in scientific research. They are primarily used for their general health benefits. In this study, for the first time, we addressed arterial stiffness or cardiovascular markers like PWV using ECEO. Furthermore, the modulating effect of other CVDs, such as salbutamol and dobutamine (beta-adrenergic agonists), glycerol trinitrate (nitric oxide donor), diltiazem (calcium channel blocker), and lidocaine (sodium channel blocker), was assessed and compared. We demonstrate that lidocaine, diltiazem, and glycerol trinitrate, like with the ECEO, modified DBP/PWV linear ratio to 5-8 (mmHg / m/s) (Fig. 1). In contrast, using beta-adrenergic agonists (e.g., salbutamol and dobutamine), the calculated slope of DBP/PWV ratio was of bigger value. This might indicate that beta-adrenergic agonists alter blood pressure through mechanisms beyond vascular stiffness alone.

While our data demonstrate that CVDs can influence DBP and PWV, the precise mechanisms by which these drugs differentially affect DBP versus PWV are still unclear. More research is needed to understand drug class-specific effects on the DBP/PWV ratio, dose-dependent effects, their impact on the ratio over time, and/or interaction between drugs since many patients are treated with multiple CVDs simultaneously. In addition, direct measurements of how different CVDs influence DBP and PWV in pig models under various physiological and pathological conditions (e.g., induced hypertension or heart failure) are needed. These models could provide insights into the dynamic changes in arterial stiffness and blood pressure regulation.

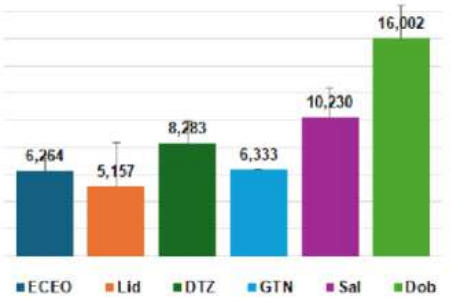

Fig. 1. Effect of different cardiovascular drugs on ratio DBP vs. PWV. DBP – diastolic blood pressure, PWV - pulse wave velocity (arterial stiffness), ECEO – *Elsholtzia ciliata* essential oil, Lid – lidocaine, DTZ – diltiazem, GTN - glycerol trinitrate, Sal – salbutamol, and Dob – dobutamine.

[1] Mačianskienė R et al. Biomolecules, 10, 948 (2020).
[2] Zigmantaitė V et al. Pharmaceuticals, 15, 982 (2022).

Optical and transmural microelectrode investigations of rabbit cardiac electrical activity after electroporation

Dominyka Adamonė[1], Mantė Almanaitytė[1], Ieva Lankutytė[1], Vilma Zigmantaitė[1], Antanas Navalinskas [1], Mindaugas Visockis[2], Justinas Barakauskas[2], Ernestas Urbanskas[2], Saulius Šatkauskas[2], Jonas Jurevičius [1], Regina Mačianskienė[1]

[1] Lithuanian University of Health Sciences, Institute of Cardiology, Laboratory of Membrane Biophysics, Sukilėlių pr. 15, Kaunas, Lithuania
[2]Vytautas Magnus University, Faculty of Natural Sciences, Department of Biochemistry, Universiteto g. 10, Akademija, Kaunas, Lithuania
dominyka.adamone@lsmu.lt

Pulsed-field ablation (PFA) uses electrical pulses to induce non-thermal, irreversible electroporation (EP), which kills cardiac cells in particular tissue locations while limiting injury to adjacent structures. Although safer than thermal ablation, PFA has several drawbacks that limit its widespread clinical use. We wanted to find PFA settings that could impact the depth and size of the ablation zone, and we investigated how PFA affected the functional-electrical activity of the left ventricular tissue in rabbit hearts.

In the study, we induced EP injury in the left ventricle by using special electrodes and used voltage-sensitive NIR fluorescent dye (di-4- ANBDQBS) to measure optical action potentials (APs) and the microelectrode technique to record electrical APs in a single cells transmurally to test the depth of EP injury in Langendorff-perfused rabbit hearts after EP (Fig. 1). We also assessed the effect of EP on the electrical activity in the ventricular wall of cut-open hearts; a cut was performed nearly through the center of the EP zone after EP procedure. An EP system with specialized electrodes (with a 3-mm gap) was used to test the dynamics of EP and detect the area and depth of tissue ablation. We tested various pulse durations (25-100 μs) and voltages (100-800 V) of applied pulses, delivering a series of 20 pulses in 900-ms intervals. Additionally, we used two extra stimulating pulses between every EP pulse to record APs within a 300-ms period, enabling us to monitor changes in APs throughout the entire EP protocol.

Our findings showed that electrical pulses slow down the velocity of AP propagation and can cause partial or complete conduction blocks. The depth of the zones affected by EP, with complete inhibition of electrical activity, can extend up to 3 mm based on the EP parameters. In the areas near the EP, the resting potential, velocity of upstroke, and duration of APs were reduced. Overall, our study demonstrates that our developed system can fully assess changes in the functional activity of electrical signals in EP and the areas close to EP zones.

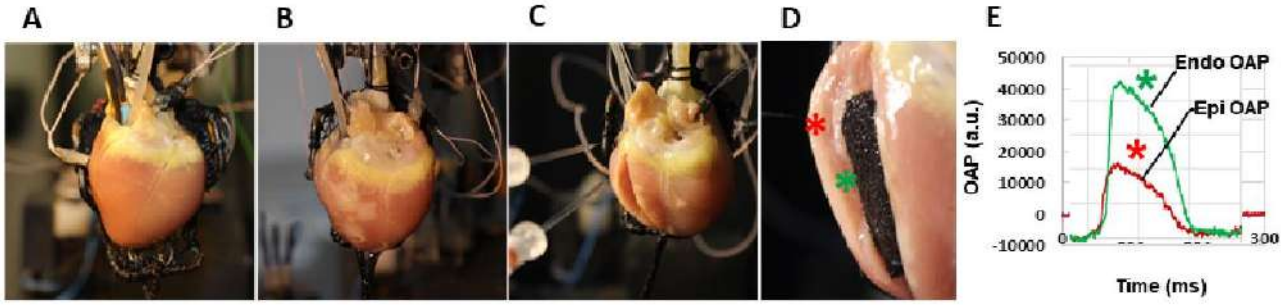

Fig. 1. Electroporation of the left ventricular myocardium of the rabbit heart. (A) Control, (B) rabbit heart after electroporation (EP) and (C) after cutting the EP zone; (D) location of action potentials recording sites: from the epicardium (* - EP affected zone) and from endocardium (* - EP not affected zone), (E) acquired optical action potential (AP) changes depending on the depth of the myocardium at the marked location.

The activity of the rodent primary auditory cortex during the circadian rhythm

Julija Arbačiauskaitė[1], Robertas Guzulaitis[1]

[1]Vilnius University, Department of Neurobiology and Biophysics, 7 Saulėtekio Ave, LT- 10257, Vilnius, Lithuania
julija.arbaciauskaite@gmc.stud.vu.lt

It is widely accepted that bodily processes are regulated by circadian rhythms over a 24-hour period [1]. The circadian rhythm sets not only the sleep-wake cycle but also influences arousal, vigilance, and attention throughout the day. These internal states have been shown to have a direct impact on the brain, where low-frequency oscillations are prevalent during resting, while high-frequency oscillations occur during motor activity or increased arousal [2]. Although diurnal oscillations in the brain are well-established, it is not clear how they affect the auditory system. There is evidence that the hearing system expresses core clock genes, which oscillate in synchrony with the suprachiasmatic nucleus (SCN), the master pacemaker entraining circadian rhythms [3]. Also, hearing sensitivity does change over the day, as demonstrated by acoustic startle response and recovery to noise exposure, but further research involving the functional changes in the auditory system remains sparse [4]. Experiments are often conducted without considering the time of day, which can have a significant impact on the results obtained. Therefore, it is necessary to investigate how brain activity changes under the same recording conditions but at different times of the day.

The aim of this study was to investigate the changes in the auditory system activity over a 24-hour period. To this end, we performed chronic electrocorticogram (ECoG) recordings from freely behaving mice while concurrently monitoring their motor activity. The motor activity of the recorded mice exhibited a well-characterised circadian rhythm, with mice being active at night and resting throughout the day. In line with the circadian motor activity, the brain oscillations also demonstrated circadian changes, with high-frequencies being more prominent at night and low-frequencies being more prominent during the day. Next, we assessed the responsiveness of the auditory system through measuring event-related potentials (ERPs) and auditory steady-state responses (ASSRs). A notable change in auditory ERPs was observed over the course of the 24-hour period, with larger ERPs present during the day. In contrast, the ASSRs remained stable throughout the recordings. This study demonstrates that the auditory system undergoes substantial changes during the day, highlighting the importance of accounting for the time of experiments.

[1] R. W. Logan and C. A. McClung, 'Rhythms of life: circadian disruption and brain disorders across the lifespan', *Nat Rev Neurosci*, vol. 20, no. 1, pp. 49–65, Jan. 2019, doi: 10.1038/s41583-018-0088-y.

[2] D. A. McCormick, M. McGinley, and D. Salkoff, 'Brain State Dependent Activity in the Cortex and Thalamus', *Curr Opin Neurobiol*, vol. 31, pp. 133–140, Apr. 2015, doi: 10.1016/j.conb.2014.10.003.

[3] 'TrkB-Mediated Protection against Circadian Sensitivity to Noise Trauma in the Murine Cochlea', *Current Biology*, vol. 24, no. 6, pp. 658–663, Mar. 2014, doi: 10.1016/j.cub.2014.01.047.

[4] H.-V. V. Ngo, H. Oster, C. Andreou, and J. Obleser, 'Circadian rhythms in auditory hallucinations and psychosis', *Acta Physiologica*, vol. 237, no. 4, p. e13944, 2023, doi: 10.1111/apha.13944.

Impact of N-Terminus Mutations on Voltage Gating in Connexin-36 Channels: A Biophysical and Computational Study

Tadas Kraujalis[1,2], Lukas Gudaitis[1], Mindaugas Šnipas[1,3], Lina Kraujalienė[1]

[1]Lithuanian University of Health Sciences, Institute of Cardiology, Sukilėlių pr. 15, Kaunas, Lithuania
[2]Kaunas University of Technology, Department of Applied Informatics, Studentų g. 50, Kaunas, Lithuania
[3]Kaunas University of Technology, Department of Mathematical Modelling, Studentų g. 50, Kaunas, Lithuania
tadas.kraujalis@lsmu.lt

Gap junction (GJ) channels, formed by the transmembrane protein connexin-36 (Cx36), facilitate electrical coupling between neurons, retinal and pancreas beta cells. Compared to other connexin (Cx) proteins, Cx36 channels display unique biophysical and biochemical characteristics, including very low unitary conductance, low sensitivity to transjunctional voltage (V_j), and high sensitivity to intracellular free magnesium ion concentration ([Mg^{2+}]). Research has shown that the N-terminus domain of connexin channels plays a key role in determining the V_j gating properties of both Cx hemichannels and GJ channels. In this study, we combined electrophysiological recordings, mathematical/computational modeling, and molecular dynamics simulations to assess the role of specific amino acid residues in the N-terminus on the V_j gating properties of Cx36 channels. Our electrophysiological results revealed that single amino acid substitutions—changing negatively charged glutamic acid at positions 3 and 8 to neutral glutamine (E3Q and E8Q), or neutral alanine and histidine at positions 13 and 18 to positively charged lysine (A13K and H18K)—significantly altered the gating behavior of Cx36 channels. To adequately explain the obtained electrophysiological data, we developed a mathematical model by combining our previously published models of GJ channel V_j gating [1] and Mg^{2+} regulation of Cx36 channels [2]. Model fitting data indicated that these changes could not be attributed solely to differences in [Mg^{2+}] sensitivity but involved significant modifications to V_j gating properties. Data obtained from molecular dynamics simulations support this hypothesis and may provide mechanistic explanations for the observed changes in gating properties. Mainly, it demonstrated that single residue substitutions at the N-terminus can alter the electrostatic profile of the channel pore and disrupt critical interactions near gating-associated sites. Data obtained from recordings of heterotypic configurations of variant Cx36 channels, as well as from model fitting experiments, allowed us to infer the V_j gating polarity of Cx36 channels—a property not previously reported in other electrophysiological studies. More precisely, our results suggest that Cx36 hemichannels gate in response to relatively positive V_js, but this gating polarity was reversed by single-residue substitution at the 3rd position of the NT-domain.

[1] M. Snipas, T. Kraujalis, K. Maciunas, L. Kraujaliene, L. Gudaitis, and V.K. Verselis, 4-state model for simulating kinetic and steady-state voltage-dependent gating of gap junctions. Biophysical journal (2020).
[2] M. Snipas, T. Kraujalis, K. Maciunas, L. Kraujaliene, L. Gudaitis, and V.K. Verselis, Four-State Model for Simulating Kinetic and Steady-State Voltage-Dependent Gating of Gap Junctions. Biophysical journal 119 (2020) 1640-1655.

Environmental factors affecting the efficiency of nystatin on *Candida* spp. yeasts

Eglė Vanseviciūtė[1], Rimantas Daugelavičius[1,2]

Department of Biochemistry[1] and Research Institute of Natural and Technological Sciences[2] of Vytautas Magnus University, Universiteto str. 10, Akademija, Kaunas region, Lithuania
egle.vanseviciute@vdu.lt

Candida albicans and *Candida glabrata* are successful commensals of humans, but also are among the most important opportunistic pathogens that cause thousands of superficial or disseminated and fatal infections in hospitalized and immunocompromised individuals every year. There are only four known classes of antifungals, to which these yeasts can acquire resistance, making the treatment of these infections much harder [1]. It is necessary to find new antifungal compounds or ways to strengthen the effect of those already known.

Polyene drug nystatin creates pores in the cell wall, increasing the plasma membrane permeability and osmotic disbalance [2]. This study aimed to evaluate the effect of this antifungal drug on *C. albicans* and *C. glabrata* yeasts in different environments, such as buffer solutions and growth media of various pH levels. The results showed that cells with the deletions of the efflux pumps of ABC superfamily *CDR1* and/or *CDR2*, did not affect the cells' sensitivity to nystatin. This indicates that one of the most popular ways to strengthen the effects of antifungals - by inhibiting efflux pumps - would not improve the efficiency of this antifungal compound. The efficiency analysis was continued by investigating the influence of environmental factors. Effects of nystatin on *Candida* yeasts were followed using real-time methods such as the analysis of lipophilic anion PCB^- binding to the cells. After evaluation of the nystatin effects in citrate-phosphate buffer of different pH, it was discovered that both *C. albicans* and *C. glabrata* cells bound the highest amount of PCB^- ions when the buffer pH is 3. Some differences between the tested yeasts were noted: at pH 6 and pH 8 exposed to nystatin *C. glabrata* cells bound less PCB^- compared to *C. albicans*, but at pH 3 *C. glabrata* cells bound more PCB^- compared to *C. albicans* ones. In addition, the effects of nystatin on both yeast species were stronger in the growth media of pH 3 compared to pH 6. It was also determined whether the medium temperature has an impact on the binding of PCB^-. The results of experiments showed that at 30˚C, nystatin induces more efficient PCB^- binding than at 37˚C.

Environmental factors, such as the pH level of the medium or temperature, can affect the efficiency of antifungal drugs. Our findings suggest that the efficiency of nystatin can be strengthened in an acidic environment, but further research on this problem is still needed.

[1] M. C. Arendrup, T. F. Patterson. *The Journal of Infectious Diseases.* 216, 445-451 (2017).
[2] A. N. Esfahani, Z. Golestannejad et al. *Medicine and Pharmacy Reports.* 92, 368-373 (2019).

Study of Xylose Transport in Modified *Ogataea Polymorpha* Yeast During Alcoholic Fermentation

Tomas Stanevičius[1], Tomas Nenartavičius[1], Andryi Sibirny[3] and Rimantas Daugelavičius[1,2]

[1]Department of Biochemistry and [2]Research Institute of Natural and Technological Sciences, Vytautas Magnus University, Universiteto g., 10, Akademija, 53361 Kaunas region, Lithuania
[3]Department of Molecular Genetics and Biotechnology, Institute of Cell Biology, NAS of Ukraine, Drahomanov Street 14/16, Lviv 79005, Ukraine
tomas.stanevicius1@vdu.lt

The growing concerns about the depletion of fossil fuels and their environmental impact are the driving forces to find alternative energy sources. Bioethanol produced from renewable materials offers a promising alternative fuel, as its combustion releases fewer nitrogen oxides and solid particles into the environment. In particular, second-generation bioethanol, made from lignocellulosic biomass, derived from agricultural and forestry waste, makes it a more sustainable option since it utilizes non-food raw materials [1].

Xylose, the second most abundant monosaccharide after glucose and the most prevalent pentose sugar, is a key component of hemicelluloses. More than half of the world's agricultural plant biomass consists of lignocellulosic crop residues [2]. By utilizing xylose, the bioethanol yield from raw materials can be increased, and maximizing xylose uptake by yeast cells is crucial for improving its use in lignocellulosic bioethanol production.

Ogataea polymorpha, a thermotolerant methylotrophic yeast, is capable of fermenting xylose at elevated temperatures. However, transporting xylose into yeast cells in the presence of both glucose and xylose remains a challenge for efficient lignocellulosic ethanol production. In xylose-utilizing wild-type yeast cultures, xylose consumption begins only after glucose is depleted, leading to longer fermentation periods and incomplete sugar conversion from lignocellulose hydrolysates [3]. This issue arises because transporters responsible for xylose uptake have a stronger affinity for glucose than for xylose. Moreover, some potential xylose transporters are removed from the yeast plasma membrane when glucose levels are low, making it essential to modify these transporters to enhance their stability [4]. For this reason, transporters found in *Saccharomyces cerevisiae* Gal2 and Hxt7 or *O. polymorpha* Hxt1 are seen as potential xylose carriers, and mutagenesis could improve xylose uptake and its utilization in alcoholic fermentation. This research project aims to investigate the importance of the *O. polymorpha* Hxt1 transporter and heterologous modifications of the *S. cerevisiae* Gal2 or Hxt7 transporters in *O. polymorpha* yeast, particularly for high-temperature alcoholic fermentation. Registration of the activity of energy metabolism (respiration, glycolysis, ATP synthesis) allows to determine the rate of glucose and xylose uptake into the cells.

In our experiments, respiration and glycolysis of *O. polymorpha* cells were evaluated in different environmental conditions, such as reduced or increased sugar concentrations, different temperatures, in salt buffers and/or the growth media. Results of the experiments showed that at 40-50 °C consumption of the dissolved oxygen was more intensive and the acidification of the media was higher. It was also detected that a high concentration of one sugar (glucose or xylose) inhibited the entry of the other sugar into *O. polymorpha* cells.

This work was supported by a Grant of the Research Council of Lithuania S-LU-24-2.

[1] Li, B., Xie, C.-Y., Yang, B.-X., Gou, M., Xia, Z.-Y., Sun, Z.-Y., & Tang, Y.-Q. (2020). The response mechanisms of industrial Saccharomyces cerevisiae to acetic acid and formic acid during mixed glucose and xylose fermentation. *Process Biochemistry*, *91*, 319-329. https://doi.org/https://doi.org/10.1016/j.procbio.2020.01.002

[2] Sibirny, A. A. (2023). Metabolic engineering of non-conventional yeasts for construction of the advanced producers of biofuels and high-value chemicals.
BBA Advanc3es, *3*, 100071. https://doi.org/https://doi.org/10.1016/j.bbadva.2022.100071

[3] Vasylyshyn, R., Kurylenko, O., Ruchala, J., Shevchuk, N., Kuliesiene, N., Khroustalyova, G., . . . Sibirny, A. (2020). Engineering of sugar transporters for improvement of xylose utilization during high-temperature alcoholic fermentation in Ogataea polymorpha yeast. *Microbial Cell Factories*, *19*(1), 96. https://doi.org/10.1186/s12934-020-01354-9

[4] Sharma, N. K., Behera, S., Arora, R., Kumar, S., & Sani, R. K. (2018). Xylose transport in yeast for lignocellulosic ethanol production: Current status. *Journal of Bioscience and Bioengineering*, *125*(3), 259-267. https://doi.org/https://doi.org/10.1016/j.jbiosc.2017.10.006

Mesenchymal Stem Cells as Nanocomplex Vehicles to Colon Cancer Cells of Distinct Phenotype

Aleja Marija Daugelaite[1,2], Simona Steponkiene[1], Greta Butkiene[1], Ilona Uzieliene[3], Agata Mlynska[4,6], Egle Ezerskyte[2], Vaidas Klimkevicius[2], Ricardas Rotomskis[1,5], Vitalijus Karabanovas[1,6]

[1]Biomedical Physics Laboratory of National Cancer Institute, P. Baublio St. 3b, Vilnius, Lithuania
[2]Institute of Chemistry, Faculty of Chemistry and Geosciences, Vilnius University, Naugarduko St. 24, Vilnius, Lithuania
[3]Department of Regenerative Medicine, Researcher at State Research Institute Centre for Innovative Medicine, Santariskiu St. 5, Vilnius, Lithuania
[4]Laboratory of Immunology, National Cancer Institute, Vilnius, Lithuania, P. Baublio St. 3b, Vilnius, Lithuania
[5]Biophotonics group, Laser research center, Physics faculty, Vilnius University, Sauletekio Ave. 9, Vilnius, Lithuania
[6]Department of Chemistry and Bioengineering, Vilnius Gediminas Technical University, Sauletekio Ave. 11, Vilnius, Lithuania
aleja.daugelaite@nvi.lt

The heterogeneous nature of colon cancer often poses a significant challenge in identifying the most appropriate treatment option. Colorectal cancer remains the second leading cause of cancer-related deaths worldwide, underscoring the need for innovative and selective treatment approaches [1]. One promising area is nanotechnology, which aims to enhance the diagnosis and treatment of cancer. However, despite the synthesis of various high-quality nanoparticles, their selective delivery remains a major obstacle. Studies have shown that intravenously injected nanoparticles have low specificity, with only a small fraction reaching cancer cells. Their entry into the tumor is hindered by the dense extracellular matrix and the impact of macrophages [2]. A potential solution could be a combination of mesenchymal stem cells (MSCs) and nanoparticles. MSCs are multipotent stem cells with tumor-tropic properties, making them a promising vehicle for anticancer agents, such as therapeutic nanoparticles, chemotherapy drugs, or therapeutic genes, in targeted cancer therapy [3]. MSCs migrate towards cancer due to chemokine gradient and the SDF-1/CXCR4 axis is the key regulator of MSCs migration [4]. However, there are still some gaps in understanding MSCs migration. Currently, there are no studies comparing the migration of MSCs toward different phenotypes of colon cancer cells, leaving it unclear whether MSCs could be a universal carrier or their migratory potential is limited to a specific cancer cell type. Moreover, while MSCs can be isolated from various sources, such as bone marrow, adipose tissue, dental pulp, there is much less information about MSCs derived from skin or menstrual blood, which is the focus of our research.

Our aim was to assess the ability of skin and menstrual blood mesenchymal stem cells to deliver upconverting nanoparticles and chlorin e_6 complex to different phenotypes of colon cancer cells.

In our studies, we demonstrated that upconverting nanocomplex accumulates in skin and menstrual blood MSCs and exhibits no dark toxicity after 24 hours of incubation. Using the Transwell migration assay, we showed that nanocomplexes-loaded MSCs can migrate toward cancer cells, but their migratory potential varies depending on the colon cancer cell phenotype. Additionally, our results revealed that distinct colon cancer cells express different levels of cytokines involved in MSC migration. Furthermore, it was found that skin and menstrual blood MSCs differ in their tumor tropic efficiency. Finally, we demonstrated that MSCs retained nanocomplex inside even after 48 hours of migration experiment.

Overall, our results suggest that MSCs could be used as carriers of upconverting nanocomplex targeting specific phenotypes of colon cancer cells. These findings open new avenues for the development of targeted cancer treatment strategies.

Acknowledgment
This work is part of a project that was supported by the funds of Lithuania (Grant No. S-MIP-22-31).

[1] Y. Xi, P. Xu. Global colorectal cancer burden in 2020 and projections to 2040. *Translational Oncology,* 14(10):101174 (2021).
[2] Q. Dai, S. Wilhelm, D. Ding, A. M. Syed, S. Sindhwani, Y. Zhang, Y. Y. Chen, P. MacMillan, W. C. W. Chan. Quantifying the Ligand-Coated Nanoparticle Delivery to Cancer Cells in Solid Tumors. *ACS Nano*, 12(8):8423–35 (2018).
[3] T. Zhang, R. Lin, H. Wu, X. Jiang, J. Gao. Mesenchymal stem cells: A living carrier for active tumor-targeted delivery. *Advanced Drug Delivery Reviews*, 185, 114300 (2022).
[4] L. Ling, J. Hou, D. Liu, D. Tang, Y. Zhang; Q. Zeng, H. Pan, L. Fan. Important Role of the SDF-1/CXCR4 Axis in the Homing of Systemically Transplanted Human Amnion-Derived Mesenchymal Stem Cells (HAD-MSCs) to Ovaries in Rats with Chemotherapy-Induced Premature Ovarian Insufficiency (POI). *Stem Cell Res Ther*, 13 (1), 79 (2022).

Effect of Environmental Conditions on β2-Microglobulin Liquid-Liquid Phase Separation

Justina Miknaitė, Mantas Žiaunys

Vilnius University Life Sciences Centre, Institute of Biotechnology, Saulėtekio al. 7, Vilnius, Lithuania
j.miknaite@gmail.com

β2-microglobulin is an important component of the major histocompatibility complex class I (MHC-I) molecule, which is found on almost all nucleated cells. Its main role in the immune system is the presentation of peptide antigens to T cells. In addition to its physiological functions, β2M is clinically important because it can cause diseases called amyloidoses. The protein is eliminated by the kidneys and, in the event of kidney dysfunction, the accumulation of the protein in the human body promotes the formation of amyloid fibrils and can lead to dialysis-related amyloidosis.

A rapidly growing area of research is liquid-liquid phase separation (LLPS), the process by which proteins and other biomolecules separate from the bulk solution to form dense, membraneless condensates. Although dozens of proteins have been identified to form condensates, there is currently no information on whether β2M can undergo LLPS.

In the course of this work, the purification process of the protein was optimised. It was found that the highest yield of the protein is obtained by denaturation with guanidine hydrochloride and purification of the protein by ion-exchange chromatography with a Q-Sepharose sorbent. An investigation of the effect of environmental conditions (protein concentration, ionic strength of the solution, denaturant concentration and pH) on β2M LLPS showed that pH is the most important factor in this process. In the pH range of 4 to 5, β2M was able to form protein condensates and aggregates. This finding opens new avenues for understanding the behavior of β2M under different physiological and pathological conditions, potentially linking its phase separation properties to its role in disease mechanisms.

Atomic Force Microscopy of $TPPS_4$ Aggregates

Greta Tamoliūnaitė[1], Teresė Kreišmontaitė[1], Vilius Poderys[1], Ričardas Rotomskis[1,2]

[1]Biomedical Physics Laboratory of National Cancer Institute, Baublio 3B, LT-08406, Vilnius, Lithuania
[2]Biophotonics Group of Laser Research Centre, Vilnius University, Sauletekio 9, c.3, LT-10222, Vilnius, Lithuania
greta.tamoliunaite@gmc.stud.vu.lt

Porphyrins are widely spread biomolecules that can be found in a plethora of biological processes. Usually existing as porphyrin derivatives, these compounds exhibit certain properties that make them desirable to many fields. Such as their ability to self-assemble into complex aggregate structures, depending on the environmental conditions and their concentration. Porphyrin derivatives can be implement in cancer medicine and generating new type of photovoltaic systems where the aggregation could hinder their applicability.

It is well known that our porphyrin derivative of interest - 5,10,15,20-Tetrakis(4-sulfonatophenyl)porphyrin ($TPPS_4$) - forms complex J-type aggregates, when pH of its environment is acidic, influencing the changes in the protonation of the molecule and enabling zwitterions to link electrostatically. At pH=7, when $TPPS_4$ molecules have a neutral core and negative SO_3- groups, at high concentrations, Q absorption bands exhibit a significant Red-shift, showing a never before seen aggregation process. When all SO_3- groups are protonated at pH=-1, $TPPS_4$ concentration-dependant absorption spectrum exhibits changes attributed to J-type aggregation when such process is unlikely due to deficiency of zwitterion (Fig. 1). In turn, affirmed by our prior research, these different aggregate structures can be visualized with atomic force microscopy (AFM).

At pH=7, $TPPS_4$ molecules have a neutral core and negative SO_3- groups so J-type aggregation cannot occur, but at high concentrations, spectral changes indicate spatially different aggregation happening. AFM view, when $TPPS_4$ concentration is low, shows formation of a somewhat uniform layer on the surface of mica. With increasing concentration, $TPPS_4$ loses a uniform layer, forming more complex structures, that do not match J-type aggregates, indicating a different aggregation process. At acidic environment, $TPPS_4$ core protonates enabling electrostatic intermolecular interactions and J-type aggregation begins. With AFM we can depict changes of J-type aggregates on the surface of mica when the concentration increases, rendering more complex aggregate structures in the process. Once environment reaches pH=-1, all SO_3- groups of $TPPS_4$ molecule are protonated indicating no electrostatic interactions to form J-type aggregates, but absorption spectra continues to show the characteristic J-bands (490 nm and 709 nm). In AFM figures we can see aggregate formation that differs from the ones seen at pH=7 and pH=4, but can also share certain similarities, indicating a somewhat similar aggregation to J-type aggregates.

Aggregate structure visualization with AFM allows us to verify the changes seen in absorption spectra in regards to assembly of $TPPS_4$ into different aggregates. AFM and absorption spectroscopy shows that even at pH=7 and pH=-1 $TPPS_4$ aggregation occurs, spectrally and spatially differing from J-type aggregates. Depiction of aggregation in pH=7, pH=4 and pH=-1 provide more information of the process, a more in depth look to aggregate structures and their spacial characteristics.

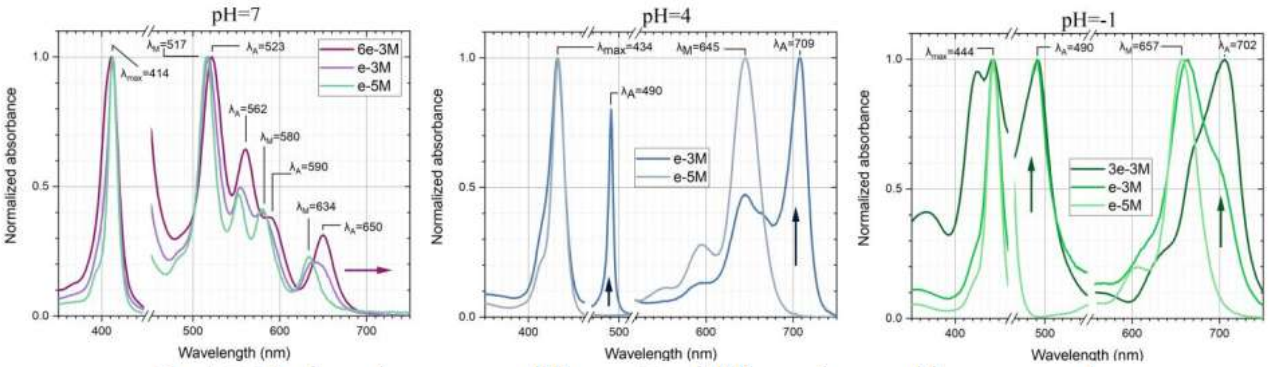

Fig. 1 $TPPS_4$ absorption spectra at different pH and different photosensitizer concentrations.

Colloidal Silver Nanoparticle Size Distribution Determination from UV–Vis Extinction Spectra Using Deep Learning

Tomas Klinavičius[1], Nadzeya Khinevich[1], Asta Tamulevičienė[1,2], Loic Vidal[3], Sigitas Tamulevičius[1,2], Tomas Tamulevičius[1,2]

[1]Institute of Materials Science of Kaunas University of Technology, K. Baršausko St. 59, LT-51423, Kaunas, Lithuania
[2]Department of Physics, Kaunas University of Technology, Studentų St. 50, LT-51368, Kaunas, Lithuania
[3]Institut de Science des Matériaux de Mulhouse IS2M UMR 7361, 15 rue Jean Starcky, F 68100 Mulhouse, France
tomas.klinavicius@ktu.edu

Rapid characterization of colloidal metal nanoparticles (NPs) is gaining significant attention in both academic research and industrial applications. Direct imaging methods, such as electron microscopy, while reliable, tend to be costly and time-consuming. In contrast, indirect optical techniques like UV-Vis spectroscopy, supplemented with spectral analysis based on Mie theory, are quick, widely available and cost-effective. In this study, we introduce a tandem deep neural network (DNN) designed to predict the size distribution and concentration of spherical silver (Ag) colloidal nanoparticles produced through the seeded growth method. During tests using experimentally obtained extinction spectra, the tandem DNN demonstrated accurate prediction of NP size distribution characteristics for particles with radii up to 150 nm, achieving a root mean square percentage error of mean size as low as 1.2% [1].

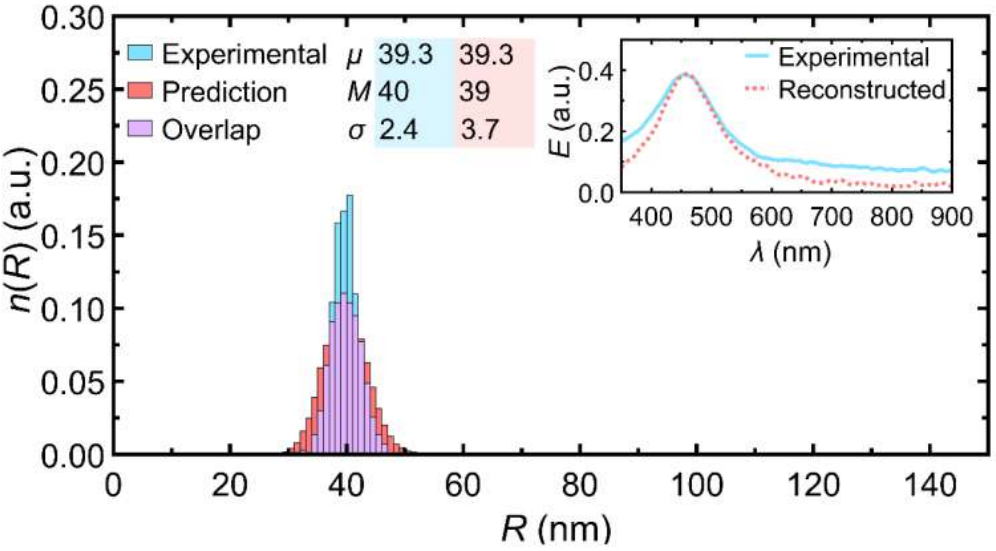

Fig. 1. Results of nanoparticle size distribution prediction from extinction spectrum of silver colloid

[1] T. Klinavičius, N. Khinevich, A. Tamulevičienė et al., *J. Phys. Chem. C.* **128**, 9662–9675 (2024).

Design and Synthesis of Novel Covalent CAIX Inhibitors

Virginija Dudutienė, Aivaras Vaškevičius, Denis Baronas, Asta Zubrienė, Daumantas Matulis

Vilnius University, Life Sciences Center, Institute of Biotechnology, Department of Biothermodynamics and Drug Design, 7 Saulėtekio Ave, LT- 10257, Vilnius, Lithuania
virginija.dudutiene@bti.vu.lt

Drug research focuses mainly on small molecules that can inhibit the biological activity of a protein of interest. The interaction between the small molecule and the protein of interest can be divided into two general categories: non-covalent and covalent interactions.

One of the protein of interest of our research group is carbonic anhydrases (CAs). Carbonic anhydrases are a family of zinc metalloenzymes that catalyze the reversible hydration of CO_2, maintaining various important physiological functions in human body. Overexpression of CA isozymes causes numerous diseases, including cancer which is related to CAIX isozyme [1]. To tackle problems related to overexpression of CAs, numerous inhibitors were designed and synthesized. Majority of CA inhibitors fall within the frame of non-covalent reversible binding mode, and covalent irreversible inhibitors are more of an exception than a relevant strategy. Regarding CAIX, as far as we know, no research on covalent inhibition has been published to date.

For successful employment of the targeted covalent inhibition strategy we need a high affinity element for our protein of interest. Our research group has successfully designed compounds that inhibit CAIX with high affinity and selectivity, and these compounds can be considered good ligands for the targeted covalent inhibition strategy. One of such compounds- 3-(cyclooctylamino)-2,5,6-trifluoro-4-[(2-hydroxyethyl)sulfonyl]benzenesulfonamide (VD11-4-2), exhibited a subnanomolar affinity for CAIX (K_d = 0.05 nM) [2]. In search of high-affinity and high-selectivity inhibitors of CAIX, a series of covalent fluorinated benzenesulfonamide-based derivatives, including VD11-4-2 analogs, were synthesized (Figure 1). Also, a new strategy for the obtainment of vinyl sulfone group-based warhead was developed and successfully applied for synthesis of novel covalent inhibitors.

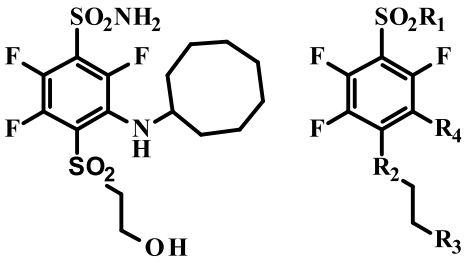

VD11-4-2

Fig. 1. Compound VD11-4-2 and schematic representation of derivatives.

[1] M. Y. Mboge, B. P. Mahon, R. McKennaet et al. Metabolites, 8, 19, 1-31 (2018).
[2] V. Dudutienė, J. Matulienė, A. Smirnov et al. J. Med. Chem. 57, 9435-9446 (2014).

AI-Driven Analysis of Cell Imaging

Lukas Keršys[1], Tadas Kraujalis[1,2], Dalia Čalnerytė[1], Andrius Kriščiūnas[1]

[1] Kaunas University of Technology, Faculty of Informatics, Studentų g. 50-407, Kaunas, Lithuania
[2]Lithuanian University of Health Sciences, Institute of Cardiology, Sukilėlių pr. 15, Kaunas, Lithuania
l.kersys@ktu.edu

Traditional methods for cell analysis often involve manual inspection of extensive datasets of microscopic images and therefore are time-consuming, prone to human error, and limited in scalability. Artificial intelligence (AI)-based cell recognition allows researchers to analyze large datasets of microscopic images more efficiently and with greater precision. This study investigates the use of the AI-based Detectron2 model [1] for cell recognition, with additional custom data extraction pipeline - focusing on extracting various morphological (e.g., size, shape) and imaging parameters (e.g., fluorescence intensity, background brightness). These parameters can be used in evaluating protein expression efficiency, assessing specific biophysical properties, or incorporating them into other computational models. To improve accuracy and exclude dead cells from the analysis, only live cell segmentation was performed.

In this study, the cell segmentation model Detectron2 was trained on annotated samples of live HeLa cells images. Through iterative training and validation, the model achieved over 80% accuracy in identifying live cells. A custom data extraction pipeline was created to parse and calculate additional data using Detectron2 segmentation data. Cell area is counted by the number of pixels within boundary of every detected cell, then converted to μm^2. For fluorescence intensity, the brightness of each pixel within the cell area was measured, enabling a precise evaluation of cellular fluorescence. The automatic protein expression marking was performed by filtering out the values of the difference between the segmentation brightness and average background brightness with a certain threshold.

We applied this model to assess the biophysical properties of connexin26 (Cx26) and its point-mutated variant. Cx26 forms hexameric hemichannels in the plasma membrane, playing a key role in cell communication by allowing the transfer of ions and small molecules between the cell's interior and exterior. HeLa cells were transfected with either wild-type (WT) Cx26 or the variant, both tagged with fluorescent protein at the C-terminus to facilitate identification. To investigate the dependence between fluorescence intensity (FI) and the current through hemichannels, we performed electrophysiology experiments, recording initial current (I_{init}) of the hemichannels and calculating the FI of the corresponding cells using our developed AI architecture. We found a strong correlation between FI and I_{init} in cells transfected with the Cx26 variant, whereas the correlation in cells transfected with WT Cx26 was weaker.

Further, we assessed protein expression in HeLa cells transfected with either WT Cx26 or the variant. By analyzing the fluorescence intensity of each cell, we observed that the average FI in WT Cx26 and its variant was comparable, indicating similar protein expression in both cell types. Finally, we evaluated the uptake of the DAPI fluorescence dye in cells transfected with either protein by calculating whole-cell FI. Our findings indicate that the variant with the introduced negatively charged residue in the extracellular loop of Cx26 significantly increases dye uptake.

In the future, we plan to integrate the AI architecture developed in this study with our recently published mathematical model for fluorescent dye flux through hemichannels [2], enabling more accurate evaluations of dye uptake.

[1] Wu Y., Kirillov A., Massa F., Yen W., Lo R.G. (2019). Detectron2, Available online: https://github.com/facebookresearch/detectron2
[2] Kraujaliene, L., Kraujalis, T., Snipas, M., & Verselis, V. K. (2024). An Ala/Glu difference in E1 of Cx26 and Cx30 contributes to their differential anionic permeabilities. Journal of General Physiology, accepted for publication. https://doi.org/10.1085/jgp.202413600

Spectroscopic studies of effects of CuInZnS/ZnS quantum dots on green microalgae

Rasa Miliukaitė[1], Andrej Dementjev[2], Saulius Bagdonas[1], Agnė Kalnaitytė-Vengelienė[1]

[1] Laser Research Center, Faculty of Physics, Vilnius University, Saulėtekio av. 9, bld. 3, LT-10222, Vilnius, Lithuania
[2] Department of Molecular Compound Physics, Center for Physical Sciences and Technology, Saulėtekio av. 3, LT-10257, Vilnius, Lithuania.
agne.kalnaityte@ff.vu.lt

Evaluation of the cytotoxicity of quantum dots (QDs) is an environmental challenge that is one of the pressing issues of the modern economy and the established green course. QDs can enter aquatic ecosystems through industrial waste and pose a potential risk to water quality. Microalgae living in natural water bodies are sensitive to changes in environmental conditions and are at the beginning of the food chain, so negative impacts on them can be transferred to other organisms, even humans. Artificial environmental stressors such as nanoparticles (NPs) can induce a variety of physiological responses that can be used for early detection of adverse effects of pollutant exposure. Furthermore, there is still a lack of knowledge about how QDs affect microalgae and how these physiological responses to NPs are related to each other.

Yellow CuInZnS core quantum dots with a ZnS shell and a thiol coating with a terminal carboxyl group (Nanooptical materials, USA, 560 ± 10 nm, in borate buffer pH 8.3) were used for experiments. The final concentration in the samples for the interaction of quantum dots with algae was chosen to be 4 µM. An isolated culture of *Desmodemus communis* (obtained from the Collection of pure cultures of algae and cyanobacteria of the Nature Research Centre (Vilnius, Lithuania)) was grown under continuous illumination with a white light source (LED 8000K, 34 µM photons/(m^2·s) at room temperature (20 ±1°C) in modified Wilkins-Chalgren (MWC). Triplets of 400 µl quantum dot and algae samples were prepared in MWC medium.in 96-well plate. To calculate the kinetics of autofluorescence (AF) of algae and the parameters of photosynthesis, the methods of pulsed amplitude-modulated fluorometry (PAM) and steady state fluorometry were used. Coherent anti-Stokes Raman scattering (CARS) spectroscopy was used to determine carotenoid distribution throughout algae cells.

Although during the first day after exposure of green microalgae *Desmodesmus communis* to 4 µM CuInZnS/ZnS QDs, the AF intensity did not differ significantly from the control samples, a change was observed in the FL excitation spectrum - the ratio of peak intensities at 435 and 480 nm (Fig. 1A) changed to the opposite. After 48 hours, the FL intensity began to decrease upon excitation at all selected wavelengths, and after 96 h, the AF intensity excited at 480 nm was even 9 times lower than that of algae not exposed to QDs. The photochemical quantum yield PSII (Y(II)) decreased after 24 h of QDs exposure, as did the quantum yield of non-photochemical fluorescence quenching (Y(NPQ)), which describes how much of the absorbed light energy is dissipated as heat. At the same time, the quantum yield Y(NO), which describes the unregulated energy losses both along the thermal and fluorescence pathways, increased. Thus, it was found that CuInZnS/ZnS QDs in *D. communis* algae disrupt the photoadaptation process: the increase in the intensity of the algae AF caused by actinic light does not decrease, and the values of the NPQ and qP coefficients decrease.

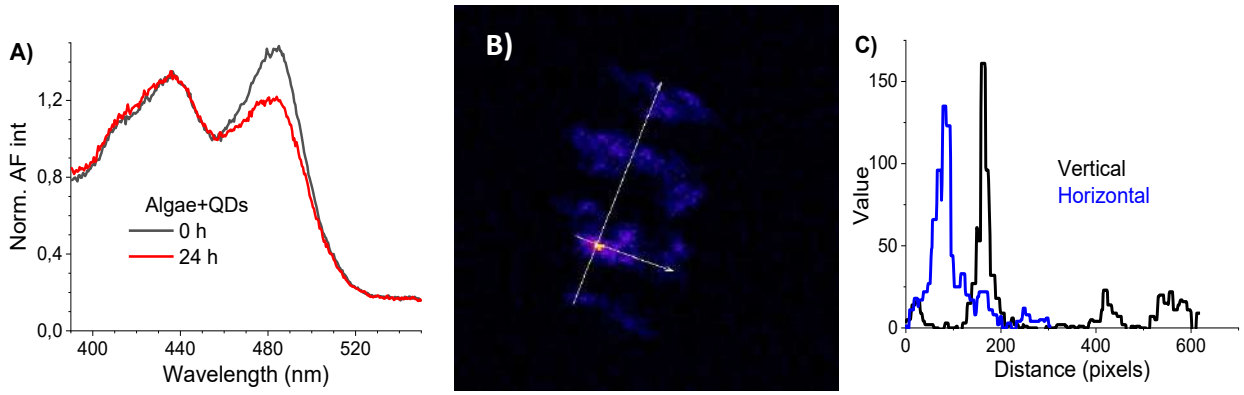

Fig. 1. The fluorescence excitation spectrum of algae immediately after exposure to QDs and after 24 h was recorded at 683 nm and normalized at 456 nm (A). CARS image of algae after 24 h with QDs (B). Signal intensity is normalized to 0 (black)-160 (white); the actual size of the region is 35x35 µm. Distribution of relative intensities of CARS signal along lines through algae (C).

CARS uses near infra-red excitation wavelengths, allowing microscopy to depths of several hundred microns in intact tissues and minimizing photodamage to living and delicate samples [1]. Thus, green microalgae treated with CuInZnS/ZnS quantum dots (Fig. 1B and C) were observed using this method. In images of algae with QDs obtained after 24 h, areas with high CARS signal were observed in contrast to control samples, which may be a result of carotenoid accumulation induced by QDs.

[1] R. M. Goodhead and et.al, Tracing engineered nanomaterials in biological tissues using coherent anti-Stokes Raman scattering (CARS) microscopy – A critical review, Nanotoxicology,2015: 1–12, DOI: 10.3109/17435390.2014.991773

Influence of Cell Shape on Lipid Droplet and Plasma Membrane Microviscosity in Mesenchymal Stem Cells

Jekaterina Skibickaja[1,2], Džiugas Jurgutis[1,3], Airina Mazėtytė-Godienė[4], Martynas Gavutis[4], Jelena Dodonova-Vaitkūnienė[2], Ramūnas Valiokas[4], Vitalijus Karabanovas[1,5]

[1]National Cancer Institute, Biomedical Physics Laboratory, P. Baublio str. 3b, 08406 Vilnius, Lithuania
[2]Faculty of Chemistry and Geosciences, Vilnius University, Naugarduko str. 24, Vilnius, 03225, Lithuania
[3]Life Sciences Center, Vilnius University, Saulėtekio Ave. 7, 10257 Vilnius, Lithuania
[4]Center for Physical Sciences and Technology, Department of Nanoengineering, Savanorių 231, 02300 Vilnius, Lithuania
[5]Vilnius Gediminas Technical University, Department of Chemistry and Bioengineering, Saulėtekio Ave. 11, 10223 Vilnius, Lithuania
jekaterina.skibickaja@chgf.stud.vu.lt

Changes in the shape of mesenchymal stem cells (MSCs) significantly influence the spatial organization and distribution of subcellular components, which in turn affects the cellular mechanical properties. These properties are critical for processes such as proliferation, migration, and differentiation [1-2]. Structural changes and variations in cell shape can impact the physical properties of a cell, including microviscosity, which is a key factor in governing the structural and functional balance of the subcellular structures and regulating intracellular transport. However, the precise relationship between the cell shape and microviscosity remains unclear.

In this work, we have applied BDP-H (Fig. 1A) and BODIPY-PM (Fig. 1B) molecular rotors in combination with fluorescence lifetime imaging microscopy (FLIM) to assess the microviscosity of MSCs. BDP-H has been shown to accumulate in lipid droplets [3], while BODIPY-PM localizes within plasma membranes [4]. Both molecular rotors exhibit changes in the fluorescence lifetime in response to alterations in the surrounding microviscosity, making them valuable tools for microviscosity measurements using FLIM [3-4].

The aim of our research was to measure the microviscosity of lipid droplets and plasma membranes in human skin-derived MSCs cultured on adhesive micropatterns of varying shapes and sizes.

MSCs were cultured on polyethylenglycol hydrogel with covalently immobilized adhesion promoting fibronectin micropatterns [5] shaped like circles, drops and triangles. Each shape was present in three different sizes: 710 μm^2, 1260 μm^2, 2000 μm^2. Live-cell imaging was conducted using a laser-scanning confocal microscope, and the fluorescence lifetimes of BODIPY-PM and BDP-H were measured using time-correlated single photon-counting based FLIM.

Results show that the fluorescence lifetime of BDP-H in MSCs cultured on different adhesive micropatterns remains unchanged compared to MSCs grown in monolayers, suggesting that the microviscosity of lipid droplets is not affected by the cell shape or size. In contrast, the fluorescence lifetime of BODIPY-PM varies significantly depending on the cell geometry and size, indicating that plasma membrane microviscosity is highly dynamic and sensitive to changes in cell morphology. Taken together, our results suggest that organelles respond differently to morphological changes. Manipulation of the cell geometry through adhesive micropatterns specifically alters the plasma membrane microviscosity but not lipid droplet microviscosity.

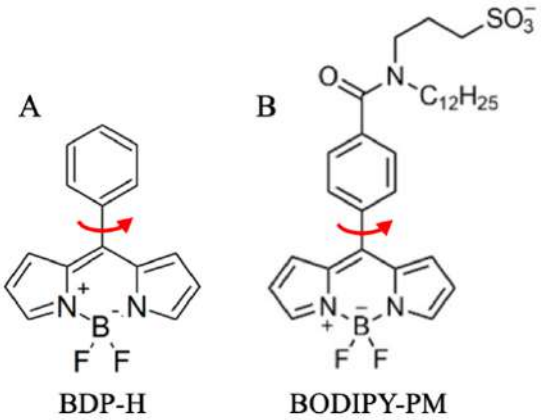

Fig. 1. The structures of BDP-H (A) and BODIPY-PM (B) molecular rotors used in this work. [3-4]

[1] J Manuel Théry,. *J. Cell Sci.*, 123 (24): 4201–4213 (2010).
[2] I. Poudel et al., *Biomed. Eng. Lett,.* 2, 38–45 (2012).
[3] D. Jurgutis et al., *Int. J. Mol. Sci.,* 23, 5687 (2022).
[4] A. Polita et al., *RSC Adv*., 13(28): 19257-19264 (2023).
[5] V. Cėpla et al. *ACS Appl. Mater. Interfaces* 12(29) 32233-32246 (2020).

Enhanced Gene Delivery by Combining Nanosecond Electric Pulses with Low-Amplitude Continuous Waves

Paulius Ruzgys[1], Neringa Barauskaitė-Šarkinienė[1], Neringa Barauskaitė-Šarkinienė[1] Simona Gelažunaitė[1], Diana Šiurnaitė[1], Vitalij Novickij[2], Saulius Šatkauskas[1]

[1] Research Institute of Natural and Technological Sciences, Vytautas Magnus university, Universiteto st. 9, Kaunas district, Akademija, Lithuania.
[2] Faculty of Electronics, Vilnius Gediminas Technical University, Plytinės st. 25, Vilnius, Lithuania.
paulius.ruzgys@email.for.contacts

This study investigated a novel method to improve the efficiency of gene delivery into cells using a technique called electroporation. Electroporation uses electrical pulses to create temporary pores in the cell membrane, allowing molecules like DNA to enter. While effective, traditional electroporation methods using microsecond pulses can be more efficient and less toxic on cells.

This research focused on using nanosecond pulses combined with a novel approach: applying low-voltage continuous waves after the initial pulses. The goal was to enhance DNA uptake when compromising cell viability as less as possible.

Experiments were conducted on CHO cells, a common cell line used in research. A concentration of 2 million cells per milliliter was prepared in a laboratory-made electroporation medium with a conductivity of 0.1 S/m, pH of 7.1, and an osmolarity of 270 mOsm. Cell electroporation was performed using a 1 mm electroporation cuvette. Each treated sample contained 50 µl of cell suspension. GFP-coding plasmid DNA was used at various concentrations ranging from 50 to 300 µg/ml. Nanosecond electroporation was conducted using a nanosecond pulse generator developed at VilniusTech University (Lithuania). By adding the low-voltage sinus waves after the nanosecond pulses, they observed a significant improvement in transfection efficiency, increasing it from 20% to 60-70%. Importantly, this method maintained high cell viability (around 80%), indicating minimal cell damage.

Fig. 1 A) A nanosecond pulse triggered electrotransfection and viability dependence on amplitude. B) Sinus continues wave triggered electrotransfection and viability dependence on amplitude. C) A nanosecond pulse and sinus continues wave triggered electrotransfection and viability dependence on amplitude.

This research offers a promising new strategy for efficient gene delivery. This may give new insights for advancements in gene therapy and other biomedical applications.

[1] P. Ruzgys, V. Novickij, J. Novickij, S Šatkauskas., *Scientific Reports*. **8,** 15502 (2018).
[2] S. Sungailaitė, P. Ruzgys, I. Šatkauskienė, K. Čepurnienė, S Šatkauskas, *The Journal of gene medicine*. **17**, 85-86 (2015).
[3] M. Pavlin, M. Kanduser. *Scientific Reports*. **5**, 9132 (2015).

Double Stokes polarimetry: a novel method for investigating fibrillar structures with SHG microscopy

Viktoras Mažeika[1,2], Kamdin Mirsanaye[3,4,5], Leonardo Uribe Castaño[3,4], Serguei Krouglov[3,4], Mehdi Alizadeh[2,3,4], Mykolas Mačiulis[2], Lukas Kontenis[2,6], Vitalijus Karabanovas[2,7], Virginijus Barzda[2,3,4]

[1]Institute of Biosciences, Life Sciences Center, Vilnius University, 7 Saulėtekio Ave., LT- 10257, Vilnius, Lithuania
[2]Laser Research Centre, Faculty of Physics, Vilnius University, 9 Saulėtekio Ave., III Bld., 10222, Vilnius, Lithuania
[3]Department of Chemical and Physical Sciences, University of Toronto Mississauga, 3359 Mississauga Rd., Mississauga, ON, Canada
[4]Department of Physics, University of Toronto, 60 St. George St., Toronto, ON, Canada
[5]Wellman Center for Photomedicine and Center for Systems Biology, Massachusetts General Hospital and Harvard 11 Medical School, 50 Blossom St., Boston, MA, USA
[6]Light Conversion, 2B Keramikų St., LT-10233 Vilnius, Lithuania
[7]Biomedical Physics Laboratory, National Cancer Institute, 3B P. Baublio St., LT-08406, Vilnius, Lithuania
viktoras.mazeika@gmc.stud.vu.lt

Second harmonic generation (SHG) microscopy is a powerful tool for investigating noncentrosymmetric fibrillar structures, such as collagen and myosin. It can be used together with various polarimetric techniques in order to get more information on the sample. Most of these techniques require fitting of the polarimetric data, which is time consuming and not suitable for analysis of large images [1, 2, 3]. Here, we present double Stokes polarimetry (DSP), a reduced polarimetric method derived from double Stokes-Mueller polarimetry (DSMP) [4]. DSP allows to calculate ultrastructural parameters with simple matrix calculations without data fitting, which significantly speeds up the analysis. We test the technique with rat tail tendon samples sectioned at different orientations with respect to collagen fiber axis. Nonlinear susceptibility tensor component ratios, collagen fiber in-plane orientation and the phase difference between chiral and achiral susceptibility components are calculated and compared between the samples. Owing to its capability of rapid analysis, DSP has great potential for clinical histopathology with applications in cancer diagnostics, prognostics and treatment planning.

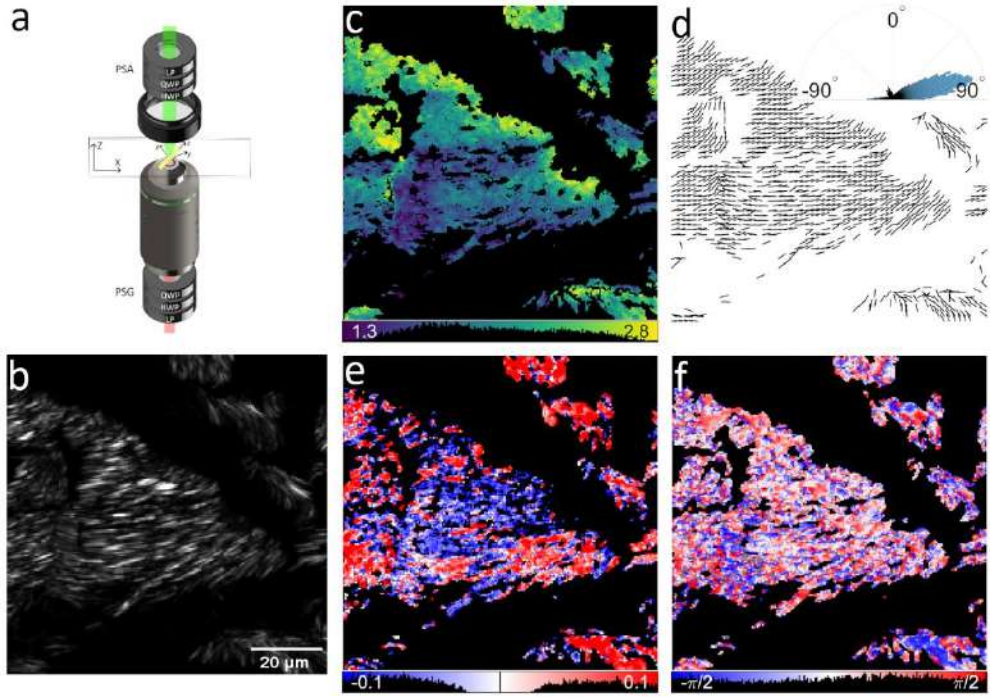

Fig. 1. Measurement scheme (a) with laboratory (XZ) and molecular (xyz) coordinate frames (PSG – polarization state generator, PSA – polarization state analyzer, LP – linear polarizer, HWP – half wave plate, QWP – quarter wave plate), SHG intensity image (b) and ultrastructural parameter maps of obliquely cut rat tail tendon: R-ratio (c), in-plane fiber orientation (d), C-ratio (e), and phase difference between chiral and achiral nonlinear susceptibility tensor components (f).

[1] A. E. Tuer, M. K. Akens, S. Krouglov et al., *Biophys J.* **103**, 2093-2105 (2012).
[2] A. Golaraei, L. Kontenis, K. Mirsanaye et al., *Sci. Rep.* **9**, 12488, (2019).
[3] I. Gusachenko, G. Latour and M.-C. Schanne-Klein, *Opt. Express* **18**, 19339-19352 (2010).
[4] V. Mazeika, K. Mirsanaye, L. U. Castaño et. al., preprint, 10.21203/rs.3.rs-4739645/v1 (2024).

Effects of Metformin on Spontaneous Ca^{2+} Signals in Cultured Microglia Cells under Normoxicand Hypoxic Conditions

Natasa Svirskiene[1], Silvija Jankeviciute[1], Gytis Svirskis[1], Vilmante Borutaite[1]

[1]Neuroscience Institute, Lithuanian University of Health Sciences, LT-50161 Kaunas, Lithuania
natasa.svirskiene@lsmu.lt

Microglia are the main resident immune cells that are among the first responders to hypoxic/ischemic brain damages. Because of their sensitivity to blood flow fluctuations, microglia become activated and undergo morphological changes under hypoxic/ischemic conditions. However, intracellular mechanisms mediating microglial activation under hypoxic conditions are not well understood. When activated, microglia can cause a cascade of inflammatory processes and initiate cytokine release, activate reactive oxygen species production. It is known that intracellular Ca^{2+} signaling is linked with pathophysiological functions of microglia and its signaling changes, arising in response to brain damage. Previous studies found that calcium signaling is important for microglial immune function—cytokine release, P2X receptor trafficking and diffusion. Imaging of calcium-dependent fluorescence in vivo has demonstrated that microglial cells have spontaneous Ca^{2+} signaling which is important for microglial function. Spontaneous signals and their rate were changed by lipopolysaccharide and by local neuronal tissue injury. Also, changes in neuronal activity triggered increased microglial process Ca^{2+} signaling, which was related to process extension. However, there is still little knowledge on how Ca^{2+} spontaneous signals change in response to hypoxia.

Metformin is widely used as anti-hyperglycemic agent for non-insulin-dependent (type 2) diabetes therapy. It has been suggested that metformin decreases hepatic glucose production mostly via inhibition of complex I of the mitochondrial respiratory chain and activation of AMP-kinase signaling pathway. Recent studies suggest that metformin can also act as a neuroprotective agent during hypoxia/ischemia by suppressing mitochondrial complex I activity in neuronal cultures, by reducing ischemic stroke-induced oxidative stress, inhibiting neuronal apoptosis and suppressing neuroinflammation. Metformin has also been suggested to inhibit mitochondrial permeability transition pore (mPTP) opening and to exert neuroprotective effects by this mechanism. However, the link between mitochondrial dysfunction and inflammatory responses mediated by the activated microglia are not clear yet, and the role of metformin in these processes remains largely unknown. It has been demonstrated that metformin and phenformin at pharmacologically relevant concentrations differently improve Ca^{2+} homeostasis in hypoxia-affected primary cortical neuronal cell cultures, but little is known about their role in microglial cultures.

In this study, we investigated the effect of metformin on spontaneous calcium signals in cultured microglia cells grown under normoxic and mild hypoxic conditions in order to elucidate the mechanism by which ischemic-hypoxic injury induce spontaneous calcium signaling changes in microglia. By using Ca^{2+} sensitive fluorescence dye, we studied how inhibition of mitochondrial respiration changed spontaneous Ca^{2+} signals in soma of microglial cells from 5–7-day-old rats grown under normoxic and mild-hypoxic conditions. In microglia under normoxic conditions, metformin or rotenone elevated the rate and the amplitude of Ca^{2+} signals 10–15 min after drug application. Addition of cyclosporin A, a blocker of mPTP, antioxidant trolox, or inositol 1,4,5-trisphosphate receptor (IP3R) blocker caffeine in the presence of rotenone reduced the elevated rate and the amplitude of the signals implying sensitivity to reactive oxygen species, and involvement of mitochondrial mPTP together with IP3R. Microglial cells exposed to mild hypoxic conditions for 24 h showed elevated rate and increased amplitude of Ca^{2+} signals. Application of metformin or rotenone but not phenformin before mild hypoxia reduced this elevated rate. Thus, metformin and rotenone had the opposing fast action in normoxia after 10–15 min and the slow action during 24 h mild-hypoxia implying activation of different signaling pathways. The slow action of metformin through inhibition of complex I could stabilize Ca^{2+} homeostasis after mild hypoxia and could be important for reduction of ischemia-induced microglial activation.

Targeted Therapy of Cancer by Multifunctional Nanoplatforms and Mesenchymal Stem Cells

Simona Steponkiene[1], Aleja Marija Daugelaite[1,2], Greta Butkiene[1], Evelina Kazlauske[1,3], Ilona Uzieliene[4], Vilius Poderys[1], Riccardo Marin[5], Artiom Skripka[6], Fiorenzo Vetrone[6], Ričardas Rotomskis[1,7], Vitalijus Karabanovas[1,3]

[1] Biomedical Physics Laboratory of National Cancer Institute, Vilnius, Lithuania
[2] Institute of Chemistry, Faculty of Chemistry and Geosciences, Vilnius University, Naugarduko St. 24, Vilnius, Lithuania
[3]Department of Chemistry and Bioengineering, Vilnius Gediminas Technical University, Vilnius, Lithuania
[4]Department of Regenerative Medicine, State Research Institute Centre for Innovative Medicine, Santariskiu g. 5, Vilnius LT-08406, Lithuania.
[5]Nano for Bioimaging Group (nanoBIG), Departamento de Física de Materiales, Facultad de Ciencias, Universidad Autónoma de Madrid, Madrid 28049, Spain.
[6]Centre Énergie, Matériaux et Télécommunications, Institut National de la Recherche Scientifique, Université du Québec, Varennes, QC, Canada
[7]Biophotonics group of Laser Research Centre, Vilnius University, Vilnius, Lithuania

Cancer remains a global health challenge, and the main treatment methods lack effectiveness and specificity, causing adverse effects. In the past decade, mesenchymal stem cells (MSCs) have been derived to track down and destroy malignant cells taking advantage of their tumor-tropic property. MSCs are multipotent cells found in all adult tissues and have the ability to self-renew and differentiate into various tissues. MSCs are able to escape the immune system and migrate to sites of pathology including tumors by using specific receptors or ligands to facilitate trafficking. Due to their migratory properties, MSCs can be used as delivery systems to transport nanoparticles (NPs) directly to cancer cells [1]. However, the cargo for such transportation is not that easy to construct. Traditional cytotoxic drugs might not be suitable, therefore the development of smart materials with a controlled release of cytotoxicity effect would solve the biocompatibility problem of MSCs.

One of the trigger-activated materials are photosensitizers (PSs). PSs has no toxicity in the dark, while upon light exposure they generate reactive oxygen species and kill cancer cells [2]. However, PSs has limited application due to low penetration of light into deeper tissues. Photoluminescent NPs exhibit better optical features than conventional organic dyes. They are more photostable, brighter, capable of excitation and emission at the infrared region, which is a region of so called “tissue transparency window”. NPs can be combined with photosensitizers, thus creating innovative multifunctional nanoplatforms capable of diagnostics and therapeutics in a single agent with a possibility to “turn on” the killing effect on the demand. However, NPs themselves lack selectivity to tumors and tend to accumulate non-specifically in certain organs, for example, liver, lymph nodes, spleen. A recent study showed that only 0.7% of systemically administered NPs are delivered to tumors in animal models and as tumors are made of different cell types including non-cancerous ones, only 2 out of 100 cancer cells are exposed to NPs [3].

In this study, we created a multifunctional nanoplatform by combining rare-earth-doped upconversion NPs (RENPs) and PSs chlorin e6 (RENPs-Ce6). We have shown that RENPs-Ce6 accumulates in MSCs. Furthermore, The RENPs-Ce6 cargo did not alter the viability of MSCs, and surprisingly, increased the migration efficiency of MSCs when loaded with the complex in comparison to non-loaded MSCs. Also, we have demonstrated that MSCs can transport the nanoplatform to cancer cells without losing optical signal. Finally, our results showed that 980 nm laser exposure can trigger phototoxic effect on cancer cells in 2D and 3D cell models.

In our study, we proved the concept of MSCs employment in the targeted delivery of multifuntional nanotherapeutics to cancer cells to be valid for RENP-Ce6s cargo. Further studies are needed to understand the behavior and therapeutic efficacy of RENP-Ce6-loaded MSCs in more complex biological models.

Acknowledgment

This work was partially supported by the funds of Lithuania (Grant No. S-MIP-22-31).

[1] Xia, Jiazhi Duan, Hengxing Zhou et al., A Living Material Constructed from Stem Cells for Tumor-Tropic Oncotherapy with Real-Time Imaging Advanced Funcional Materials, 2022; 32(24): 2201013.
[2] Xueze Zhao, Jiangping Liu et al. Recent progress in photosensitizers for overcoming the challenges of photodynamic therapy: from molecular design to application. Chem Soc Rev. 2021 Mar 21;50(6):4185-4219.
[3] Dai, Q.; Wilhelm, S et al. Quantifying the Ligand-Coated Nanoparticle Delivery to Cancer Cells in Solid Tumors. ACS Nano 2018, 12 (8), 8423–8435.

Mechanical Resistance of Spray-Coated Antiviral Coatings Based on fs-Laser Ablated Copper Nanoparticles

Shahd Elkhider[1], Tomas Klinavičius[1], Mohamed A. Baba[1], Rasa Mardosaitė[1], Simas Račkauskas[1], Asta Tamulevičienė[1,2], Dainius Zienius[3], Raimundas Lelešius[3], Algirdas Šalomskas[3], Tomas Tamulevičius[1,2]

[1]Institute of Materials Science, Kaunas University of Technology, Kaunas, Lithuania
[2]Department of Physics, Kaunas University of Technology, Kaunas, Lithuania
[3]Faculty of Veterinary Medicine, Lithuanian University of Health Sciences, Kaunas, Lithuania
shahd.fateh@ktu.edu

Nanoparticles (NPs) with significant antimicrobial and antiviral properties have been extensively studied in the last two decades [1, 2], especially Copper (Cu NPs) which indicated destructive oxidative stress mechanisms [3, 4].

In this work femtosecond laser ablation of Cu target in water was utilized to generate colloidal Cu NPs which were applied as an active material for the antiviral coatings. The coatings on glass substrates were applied by spraying polyvinyl butyral (PVB) and Cu NPs (see Fig. 1 a). Coatings appeared effective against model Coronavirus and Herpesvirus. The sclerometer made scratches on the coating appeared (Fig. 1 b) when the applied force reached 2 ± 1 N and were visible better under an optical microscope with the increased applied force.

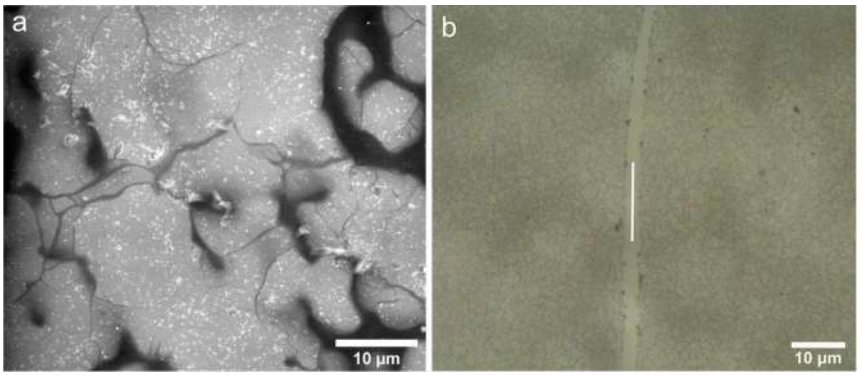

Fig. 1. PVB-Cu NPs coating. (a) Typical scanning electron microscope micrograph. (b) Optical microscope micrograph of the coating after mechanical resistance testing with 5 N load.

This work was supported by the European Regional Development Fund, Project No.: 13.1.1-LMT-K-718-05-0018.
Keywords: Copper nanoparticles, laser ablation, viruses, Sclerometer.

References:
[1] K.M. Rajesh, et al., Optik, 154 (2018) 593-600.
[2] M. Salavati-Niasari, et al., Polyhedron, 27 (2008) 3514-3518.
[3] A. Tavakoli, et al., Journal of virological methods, 275 (2020) 113688.
[4] S. Bakhet, et al., Applied Surface Science, 670 (2024) 160642.

Intercellular electrical communication in macroalgae: investigation of glutamate-induced modulations of action potential propagation and transmission

Indrė Lapeikaitė, Svetlana.Blashchuk, Radvilė Janušauskaitė, Vilmantas Pupkis, Vilma Kisnierienė

[1]Vilnius University, Life Sciences Center, Department of Neurobiology and Biophysics, University st. 3, LT-01513 Vilnius, Lithuania

In plants electrical signals participate in cell-to-cell signaling, conveying information about different stimuli, e.g. abiotic stress, pathogen infection or mechanical injury. Action potentials (APs) belong to the basic long-distance electrical signals recorded in plant cells whose generation is dependent on an influx of calcium ions into the cytoplasm, followed by an efflux of chloride, then potassium. APs can initiate both non-specific e.g. suppression photosynthetic activity and highly specific adaptational responses. Yet the modus of conveying information through spatiotemporal properties of these signals is not evident in *plantae*. Although APs are discrete signals, their shape can be modulated by various environmental factors, including nutritional supply in soil or water. The occurrence of amino acid glutamate (Glu) in the proximity of a tissue is regarded as a signal of wounding or as an indication of a source of nutrients. Previously we described how externally applied glutamate modulates the parameters of action potentials. Under glutamate, the action potentials of prolonged repolarization and lower excitation threshold are observed. Mathematical modelling of electrical excitation propagation in plants suggests that hyperpolarized excitation threshold should increase the velocity of APs along the cell. Whether the Glu-induced modulations of APs encompass the properties of AP propagation or transmission is yet unknown.

To test this hypothesis we investigated whether the propagation velocity and transmission probability of electrical excitation to the neighbouring cell is altered in any way by externally applied glutamate (1 mM) in the aquatic macroalgae *Nitellopsis obtusa* (Characeae). The thallus of Characeae consists of elongated internodal cells connected by nodes. The node is a complex structure of small cells which connect the internodal cells by a single layer at the nearest point of approach. The electrical coupling *via* plasmodesmata between some internodal cells is sufficient for an action potential in one cell to initiate an action potential in the neighbouring cell.

For this aim two sets of intracellular microelectrodes were used – an electrode is impaled in each of two neighbouring internodal cells or in the opposite ends of a cell. Thus the electrically induced action potentials in one cell can be recorded in the adjacent cell, or in the opposite end of single internodal cell. We compared the transmission probabilities and propagation velocities of electrical signals in opposite directions of the cell/thallus.

The results indicate an intrinsic direction-wise disparity of AP propagation velocity along a single cell and an uneven probability of transmitting this excitation to a neighbouring cell. Although glutamate increases the excitability of a single cell and enhances the propagation velocity along the internodal cell, extensive thallus exposure to this amino acid leads to a restricted transmission of electrical excitation through the node (Fig. 1). These results expand the scope of amino acids' regulated physiological functions in photosynthetic organisms and highlights the fine-tuning of electrical signalling.

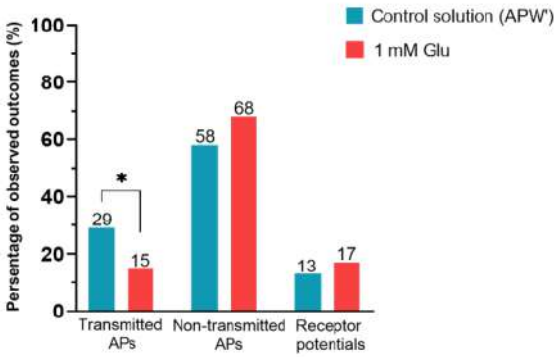

Fig. 1. Action potential transmission analysis between two internodal cells of *Nitellopsis obtusa* encompassing both apical and basal directions in control conditions (APW') and under exposure to 1 mM Glu where three possible outcomes are depicted: transmitted APs, non-transmitted and receptor potentials, n=15 (investigated cells), k=90 (analysed action potentials)

Detergent-Like Membrane Solubilization Induced by the Pro-Inflammatory S100A8 Protein

Rimgailė Tamulytė[1], Darius Šulskis[2], Marija Jankunec[1]

[1]Institute of Biochemistry, Life Sciences Center, Vilnius University, Saulėtekio av. 7, Vilnius, Lithuania
[2]Institute of Biotechnology, Life Sciences Center, Vilnius University, Saulėtekio av. 7, Vilnius, Lithuania
rimgaile.tamulyte@bchi.stud.vu.lt

Inflammation is a critical factor in the development of neurodegenerative disorders [1], yet it remains unclear whether it is a consequence or a cause of these conditions. Beyond neuroinflammation, the disruption of cell membranes may also play a significant role in neuronal loss [2]. In this study, we explored the effects of the pro-inflammatory protein S100A8 on model lipid membranes with various biophysical properties, including anionic, zwitterionic, and those derived from natural brain lipid extract. To monitor S100A8-lipid interactions, we employed several biophysical techniques, including electrochemical impedance spectroscopy, fluorescence spectroscopy, and high-speed atomic force microscopy. Our findings underscore the critical role of membrane charge and the presence of divalent cations in the disruption process initiated by S100A8. Specifically, we observed that apo-S100A8 selectively interacts with anionic lipid membranes composed of phosphatidylserine (PS), leading to membrane disruption via a detergent-like mechanism, primarily affecting regions where phospholipids are less tightly packed (Fig. 1). Interestingly, the introduction of Ca^{2+} ions was observed to inhibit S100A8-induced membrane disruption, suggesting that S100A8 might be most effective at disrupting plasma membranes within intracellular compartments, where calcium levels are low and PS concentrations in the inner leaflet of the membrane are high. Overall, our results provide a mechanistic framework for understanding the molecular interactions between S100A8 and plasma membrane, which is crucial for gaining deeper insights into the pathogenesis of neurodegenerative disorders.

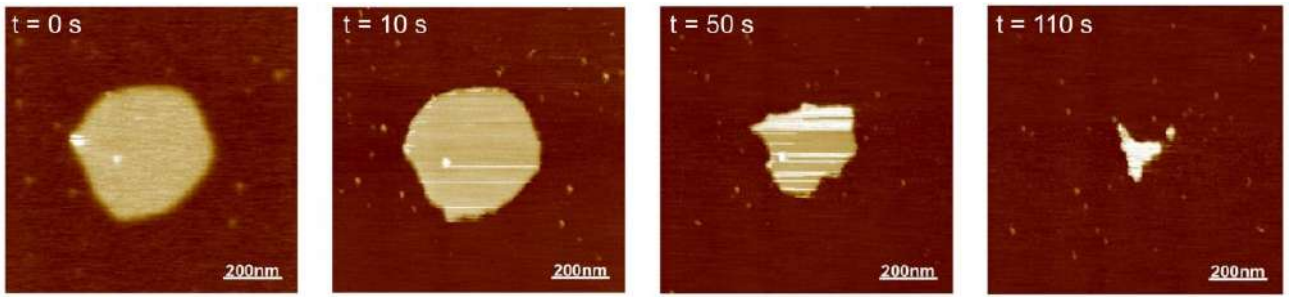

Fig. 1. High-speed atomic force microscopy images of S100A8-induced membrane dissolution. At the initial time point (t = 0 s), the protein was injected into the fluid cell. The interaction between S100A8 and the negatively charged membrane leads to a detergent-like effect.

[1] Zhang, W., Xiao, D., Mao, Q. *et al. Sig Transduct Target Ther* **8**, 267 (2023).
[2] Fernandez-Perez, E.J., Peters, C., Aguayo, L.G. *Curr Pharm Des*. **22**, 1295-1304 (2016).

Investigation of Novel Upconverting Nanoparticle – Bovine Serum Albumin Stabilised Gold Nanoclusters – Chlorin e6 Photo Drug Platform for PDT

Vilius Poderys[1], Marius Saulenas[1], Greta Butkiene[1], Gabriele Suziedelyte[1], Egle Ezerskyte[2], Arturas Katelnikovas[2], Vaidas Klimkevicius[2], Vitalijus Karabanovas[1]

[1]Biomedical Physics Laboratory of National Cancer Institute, Baublio 3b, LT-08406, Vilnius, Lithuania.
[2] Institute of Chemistry, Vilnius University, Naugarduko 24, LT-03225 Vilnius, Lithuania.
vilius.poderys@nvi.lt

Photodynamic therapy (PDT) is an established cancer treatment method that employs light-activated compounds, known as photosensitizers (PS), which produce reactive oxygen species (ROS) upon exposure to light. The generated ROS cause cellular damage, leading to the death of cancer cell. However, the efficiency of PDT using conventional photosensitizers is limited to superficial tissue layers due to the poor penetration of visible (VIS) light into tissues. In contrast, near-infrared (NIR) light can penetrate deeper into biological tissues but lacks the energy for direct excitation of photosensitizers via single-photon absorption. Photosensitizers can be excited using NIR light via the two-photon absorption process; however, this requires expensive ultrafast lasers and raster scanning systems. Additionally, it is often difficult to avoid thermal effects due to the extremely high laser power densities required for non-linear excitation. To address these issues, upconverting nanoparticles (UCNPs) offer a promising solution. UCNPs absorb NIR light and convert it into higher-energy UV-VIS light. Excited UCNPs can serve as energy donors for the excitation of photosensitizers, which in turn generate ROS and initiate PDT. This mechanism would allow deeper tissue penetration while maintaining the ability to activate photosensitizers. A significant advantage of such a nanoplatform is that excitation of UCNPs could be achieved via steady-state NIR lasers with relatively low power densities (compared to two-photon excitation).

It is known that exposing nanoparticles to protein-rich media leads to the formation of a protein corona around the nanoparticles, which can alter their properties. To address this, a protein corona can be formed in solution under controlled conditions using suitable proteins before applying such complexes *in vitro* or *in vivo*. This protein layer can also be decorated with PS molecules to form a UCNP-protein-PS complex. In our previous research, we demonstrated that bovine serum albumin-stabilized gold nanoclusters (BSA-Au NCs) can generate ROS when excited with VIS light [1]. In this work, we used these BSA-Au NCs to form a protein corona around UCNPs. Thus, we create a system that combines the deep tissue penetration of NIR light with the ROS-generating capability of the nanoclusters. To further enhance ROS generation, a complex of BSA-Au NCs together with the photosensitizer chlorin e6 (Ce6) was formed prior to the formation of the protein corona.

BSA-Au NCs were obtained through the in-situ reduction of chloroauric acid in protein-rich media under alkaline conditions, whereas core-shell UCNPs ($NaGdF_4$:18%Yb^{3+}, 2% Er^{3+}@$NaGdF_4$:5% Yb^{3+},40% Nd^{3+}) were synthesized via the thermal co-precipitation method. The ROS generation efficiency of the UCNP-BSA-Au NCs-Ce6 complex under NIR (808nm and 980nm) irradiation was evaluated using SOSG, a fluorescent singlet oxygen sensor.

Our results showed that adding Ce6 to a BSA-Au NCs solution led to complex formation, as indicated by a red shift of the Ce6 fluorescence band. The molar ratio of BSA-Au NCs to Ce6 in the complex was determined to be 1:1, which is in good agreement with results presented in the literature for BSA-Ce6 complex [2]. The BSA-Au NCs-Ce6 complex was used in further experiments to study the formation of a protein corona on UCNPs. Various molar ratios (from 1:1 to 1:100) were used to study the interaction between UCNPs and the BSA-Au NCs-Ce6 complex. This was assessed by measuring changes in the UCNPs emission decay upon adding different amounts of the BSA-Au NCs-Ce6 complex and estimating the energy transfer efficiency. Adding the BSA-Au NCs-Ce6 complex to the UCNPs solution caused a decrease in the UCNPs' red (656 nm) emission band decay time. Results showed that the energy transfer efficiency from UCNPs to the BSA-Au NCs-Ce6 complex increases up to a 1:10 molar ratio (approximately 32% at the 1:10 ratio). Further increasing the BSA-Au NCs-Ce6 complex concentration does not affect the energy transfer efficiency. This indicates that adding the BSA-Au NCs-Ce6 complex to the UCNPs solution led to the formation of a corona on the surface of the UCNPs. We can also estimate that 10 BSA-Au NCs are required to form a corona on one UCNP. It is worth mentioning that there is no change in UCNPs emission decay spectra if the protein corona is formed using BSA-Au NCs without Ce6. This indicates that excited UCNPs act as energy donors to Ce6 molecules attached to the protein corona, and this energy transfer could lead to singlet oxygen generation.

Further, we investigated the ability of this system to generate singlet oxygen upon irradiation with NIR (808 nm/980 nm) light using the singlet oxygen sensor SOSG. Irradiation of samples with NIR light led to an increase in SOSG fluorescence, whereas in samples kept in the dark (control), SOSG fluorescence intensity remained constant. This indicates that upon light exposure, singlet oxygen was generated and that the UCNP-BSA-Au NCs-Ce6 complex is a promising candidate for further investigation as a photodrug platform in NIR-initiated PDT.

Acknowledgment: This work was supported by the Research Council of Lithuania (Grant No.S-MIP-23-5).

[1] V. Poderys, G. Jarockytė, S. Bagdonas et al. *Journal of Photochemistry & Photobiology, B: Biology*, 2020, Vol. 204, 111802.
[2] Y. Zhang, H. Görner. *Dyes and Pigments, 2009, 83(2), 174–179.*

Theoretical modelling of self-assembling $TPPS_4$ and $TPPS_3$ supramolecular aggregates of core-tail J-type

Vilius Poderys[1], Alytis Gruodis[2], Ričardas Rotomskis[1,3]

[1]Biomedical Physics Laboratory of National Cancer Institute, Baublio 3B, LT-08406, Vilnius, Lithuania
[2]Institute of Chemical Physics, Vilnius University, Sauletekio 9, c.3, LT-10222, Vilnius, Lithuania
[3]Biophotonics Group of Laser Research Centre, Vilnius University, Sauletekio 9, c.3, LT-10222, Vilnius, Lithuania
vilius.poderys@nvi.lt

Porphyrin derivatives, such as 5, 10, 15, 20-tetrakis(4-sulfonatophenyl)porphyrin ($TPPS_4$) and its analog 5-phenyl-10, 15, 20-tris(4-sulfonatophenyl) porphyrin ($TPPS_3$), have attracted considerable attention in the field of supramolecular chemistry due to their remarkable ability to self-assemble into highly ordered structures. These molecules can form J-type aggregates, characterized by a distinctive red-shift in their absorption spectra, which is attributed to strong excitonic coupling between adjacent chromophores. The self-assembly process of $TPPS_4$ and $TPPS_3$ is driven by a combination of non-covalent interactions, including π-π stacking and electrostatic attractions, leading to the formation of complex supramolecular architectures. These supramolecular aggregates can be applied in photonics, optoelectronics, and biomedical imaging. Understanding the mechanisms underlying the self-assembly of these porphyrin aggregates is crucial for controlling their structural and optical properties. Theoretical modeling plays a pivotal role in elucidating these mechanisms at the molecular level. Computational methods can predict the preferred aggregation pathways, binding energies, and the influence of various environmental factors on the stability and functionality of the aggregates.

In this study, we used quantum chemistry simulations to calculate the arrangement of $TPPS_4$ and $TPPS_3$ molecules in core-tail J-type aggregate (as hexamer structure) and used this data for prediction of spatial structure of large supramolecular aggregates composed from these molecules.

Gaussian16 package was used for quantmechanical simulations of hexamer structures of $TPPS_4$ and $TPPS_3$ bonded in core-tail style (J-aggregates). Intermolecular structure optimization (in the ground state) was done by means of density functional B3LYP method using 6-31G(d) basis set including polarization functions. Environmental effects were included using PCM(water) method. Electronic excitations were estimated using semiempirical TD (singlets) method. Literature [1] and our previous modelling experiments showed that TPPS molecules tend to assemble to a bending chain of molecules. Such an arrangement was chosen as an initial aggregate structure. Due to asymmetric structure of $TPPS_3$ molecule, two types of arrangements were used as initial aggregate structures – one where phenyl group that is lacking [$–SO_3^-$] group is in the inner side of bending chain and other where it is in the outer side of bending chain.

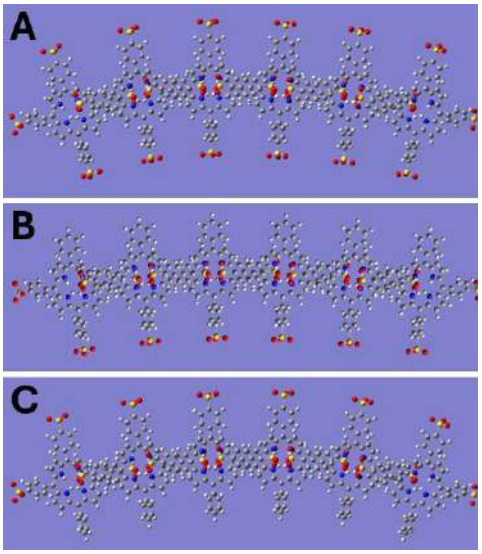

Fig. 1 Optimized structures of hexamers formed by $TPPS_4$ (A) and $TPPS_3$ (B and C)

We conducted theoretical modeling studies on the self-assembly of $TPPS_4$ and $TPPS_3$ molecules into supramolecular aggregates. Optimized structures of hexamers are presented in fig.1. Our simulations reveal that the average slip between molecules is highly consistent at approximately 10.5 Å in all modeled hexamers formed from both $TPPS_4$ and $TPPS_3$ molecules. $TPPS_3$ molecules assemble into ring or spiral aggregates with the non-sulfonated benzene rings oriented toward the interior, the diameters of the resulting aggregates are nearly identical as in case of TPPS4 aggregate - approximately 21 nm. However, for $TPPS_3$ aggregates where the side [$–SO_3^-$] groups are positioned inside the spiral (and the non-sulfonated benzene rings are on the exterior), the ring diameter significantly increases to about 32 nm. This increase is likely due to electrostatic repulsion between the negatively charged sulfo groups located at the center of the spiral.

Our findings suggest that the symmetry of $TPPS_4$ molecules leads to a highly ordered arrangement within the aggregates they form. In contrast, $TPPS_3$ aggregates with side [$–SO_3^-$] groups inside the ring/spiral exhibit less orderly molecular orientations, although their spatial parameters (such as ring/spiral diameter) remain almost identical to those of $TPPS_4$ aggregates. Additionally, in $TPPS_3$ aggregates where the side [$–SO_3^-$] groups are on the exterior (and the non-sulfonated benzene rings are inside), the ability of the molecular chain to bend is hindered, resulting in an increased spiral diameter.

These results align nicely with our previous results obtained by atomic force microscopy [2], which show that $TPPS_3$ aggregates have a larger diameter than $TPPS_4$ aggregates. Spectroscopic studies also indicate that $TPPS_3$ aggregates possess less orderly molecular arrangements, evidenced by a broader J-absorption band in solutions of $TPPS_3$ aggregates compared to those of $TPPS_4$. We hypothesize that $TPPS_3$ aggregates could be formed according to a third model, where side [$–SO_3^-$] groups and non-sulfonated benzene rings alternate between the interior and exterior of the ring.

[1] R. Rotomskis, R. Augulis, V. Snitka, et al. J. Phys. Chem. B, 108, 9, p. 2833–2838. 2004,
[2] V. Poderys, A.Selskis, R.Rotomskis. *Solid State Phenomena* V. 97-98, p. 221-224, 2004.

Morphology-Dependent Effects of $GdPO_4:Eu^{3+}$ nanoparticles on *Daphnia magna*

Augustas Morkvėnas[1,2], Jonas Venius[1], Marius Burkanas[1], Vitalijus Karabanovas[1,2]

[1]Biomedical Physics Laboratory, National Cancer Institute, P. Baublio str. 3b, Vilnius, LT-08406, Lithuania
[2]Department of Chemistry and Bioengineering, Vilnius Gediminas Technical University, Sauletekio Ave. 11, LT-10223 Vilnius, Lithuania
augustas.morkvenas@vilniustech.lt

Nanoparticles (NPs) are widely utilized across various industries because their physical and chemical properties differ significantly from those of bulk materials with the same chemical composition [1]. Nanoparticles incorporating rare-earth (RE) metals are advancing rapidly, demonstrating potential in numerous applications. In the medical field, these NPs are transforming biomedical imaging by improving diagnostic precision and therapeutic effectiveness, thanks to their distinctive optical and magnetic characteristics [2]. Despite significant progress in synthesizing RE-based orthophosphate particles with various shapes, there is still a significant gap in understanding their toxicological impact. Urgent and extensive research is needed in this area to comprehend the potential risks and benefits of these NPs fully [3]. Therefore, it is crucial to determine which NPs morphology offers the best balance between imaging performance and biocompatibility. This understanding is key to advancing the use of NPs in biomedical applications, where their unique properties can significantly improve diagnostic accuracy and therapeutic outcomes.

In this study, we synthesized $GdPO_4$ NPs with varying morphologies and evaluated their effects on MRI contrast enhancement, optical properties, and biological interactions. Our data show a strong correlation between NPs surface area and MRI capabilities, with nanorods having the largest surface area exhibiting the most pronounced improvement in MRI signal. The optical properties of $GdPO_4$ NPs with different shapes were studied through their excitation and emission spectra. The excitation spectra highlighted typical optical transitions of Eu^{3+} with the highest intensity peak at 393 nm. The emission spectra revealed a prominent peak around 695 nm. Sub-microspheres showed the highest emission intensity overall, followed by nanoprisms and nanorods. Despite variations in shape, the photoluminescence lifetimes were consistent across all particle types.

Using Daphnia magna as a model organism for toxicity testing, we observed that while nanoparticle shape did not significantly influence toxicity, smaller particles like nanorods were more likely to accumulate in the gut of D. magna than the larger ones. Additionally, nanorods and nanoprisms significantly increased heart rate (HR) at higher concentrations (≥12.5 μg/mL), while sub-microspheres showed inconsistent effects on HR. Behavioral impacts were also observed, with nanorods and nanoprisms causing a reduction in movement and velocity at concentrations of 25 and 50 μg/mL.

This research contributes to understanding how NP morphology affects imaging performance and biological interactions. It also highlights the potential risks associated with the bioaccumulation of nanoparticles in living organisms, offering insights into the safer and more effective use of RE-based materials in biomedical imaging.

This work was supported by the Research Council of Lithuania, agreement No [S-MIP-24-92].

1] N. Joudeh and D. Linke, "Nanoparticle classification, physicochemical properties, characterization, and applications: a comprehensive review for biologists," J Nanobiotechnol, vol. 20, no. 1, Art. no. 1, Jun. 2022, doi: 10.1186/s12951-022-01477-8.
[2] M. Janulevicius, V. Klimkevicius, A. Vanetsev, V. Plausinaitiene, S. Sakirzanovas, and A. Katelnikovas, "Controlled hydrothermal synthesis, morphological design and colloidal stability of GdPO4·nH2O particles," Materials Today Communications, vol. 23, p. 100934, Jun. 2020, doi: 10.1016/j.mtcomm.2020.100934.
[3] E. Demir, "A review on nanotoxicity and nanogenotoxicity of different shapes of nanomaterials," Journal of Applied Toxicology, vol. 41, no. 1, pp. 118–147, 2021, doi: 10.1002/jat.4061.

Monitoring Lipid Droplet Microviscosity After Mesenchymal Stem Cell Differentiation

Džiugas Jurgutis[1,2], Greta Butkienė[1], Vilius Poderys[1], Jelena Dodonova-Vaitkūnienė[3], Ričardas Rotomskis[1], Vitalijus Karabanovas[1,4]

[1]Biomedical Physics Laboratory, National Cancer Institute, P. Baublio St. 3b, 08406 Vilnius, Lithuania
[2]Life Sciences Center, Vilnius University, Saulėtekio Ave. 7, 10257 Vilnius, Lithuania
[3]Faculty of Chemistry and Geosciences, Vilnius University, Naugarduko str. 24, 03225 Vilnius, Lithuania
[4]Department of Chemistry and Bioengineering, Vilnius Gediminas Technical University, Saulėtekio Ave. 11, 10223 Vilnius, Lithuania
dziugas.jurgutis@nvi.lt

Lipid droplets are cytoplasmic organelles involved in energy storage and lipid metabolism. Alterations in lipid droplet size, number, or composition are observed during differentiation of mesenchymal stem cells (MSCs), and are linked to various diseases, including obesity and metabolic osteoarthritis [1]. These alterations may affect the biophysical properties of lipid droplets, such as microviscosity. However, there is still limited knowledge on the impact of cell differentiation on lipid droplet microviscosity. Monitoring lipid droplet microviscosity in differentiated MSCs, such as adipocytes, osteoblasts, and chondrocytes, can enhance our understanding of differentiation-specific organelle behavior and cellular mechanisms underlying diseases associated with these cell types.

Intracellular microviscosity can be determined using fluorescence lifetime imaging microscopy (FLIM) with viscosity-sensitive molecular rotors [2]. In this study, we applied the BDP-H molecular rotor, previously validated for its sensitivity to viscosity and compatibility with live-cell imaging [3-4]. BDP-H undergoes intramolecular rotation upon excitation, which leads to enhanced non-radiative decay and shorter fluorescence lifetimes in low-viscosity environments, while higher viscosity hinders this rotation, resulting in longer fluorescence lifetimes.

The objective of this work was to evaluate microviscosity of lipid droplets after differentiation of human MSCs.

MSCs were differentiated using StemPro differentiation kits (Gibco). Live-cell imaging was conducted using a laser-scanning confocal microscope. Fluorescence lifetimes of BDP-H were measured using time-correlated single photon-counting based FLIM system. A calibration curve, obtained at 40 °C in toluene-castor oil mixtures of varying viscosities, was applied to convert fluorescence lifetime values to microviscosity.

Our findings indicate that BDP-H accumulates in lipid droplets of MSCs: colocalization with lipid droplet probe Nile red yielded $tM_1 = 0.85 \pm 0.15$ and $tM_2 = 0.81 \pm 0.15$. After MSC differentiation, a significant decrease in BDP-H fluorescence lifetime was observed in lipid droplets of adipocytes and chondrocytes, while no notable change occurred in osteoblasts compared to undifferentiated MSCs. Additionally, BDP-H fluorescence lifetimes in lipid droplets of differentiated cells were unaffected by the tissue source of MSCs.

In conclusion, our findings demonstrate that MSC differentiation results in distinct changes of lipid droplet microviscosities, highlighting the functional significance of these organelles after each specific differentiation.

[1] A. Zadoorian, X. Du & H. Yang, *Nat Rev Endocrinol*, **19**, 443–459 (2023).
[2] M.K. Kuimova et al., *Phys. Chem. Chem. Phys.,* **14**, 12671-12686 (2012).
[3] S. Toliautas et al., *Chem. – Eur. J.,* **25**, 10342-10349 (2019).
[4] D. Jurgutis et al., *Int. J. Mol. Sci.,* **23**, 5687 (2022).

A SPECTROSCOPIC STUDY OF PHOTOSENSITIZERS: RIBOFLAVIN AND MAGNESIUM CHLOROPHYLLIN

Goda Mažeikaitė[1], Irina Buchovec[1], Pranciškus Vitta[1]

[1]Institute of Photonics and Nanotechnology, Faculty of Physics, Vilnius, Lithuania
goda.mazeikaite@ff.stud.vu.lt

The rising emergence of antibiotic resistance among bacteria is a critical global health issue, affecting various sectors, including hospitals, food facilities, and even spacecraft. This challenge has accelerated the search of alternative antimicrobial technologies, such as Antimicrobial Photodynamic Inactivation (API). API combines light, photosensitizer (PS), and molecular oxygen to generate reactive oxygen species (ROS) that cause oxidative damage to microbial cells. PS can act on cell surfaces or penetrate cells depending on their properties and conditions. This study focuses on the photostability of two natural PS, riboflavin (RF) and magnesium chlorophyllin (Mg-Chl), analyzing their performance under different concentrations, solvents (distilled water and PBS buffer), and pH conditions.

The research involves spectrophotometric measurements using a PerkinElmer Lambda 950 spectrophotometer, selecting light wavelengths that align with the absorption peaks of RF and Mg-Chl within the 300-700 nm range (Fig 1). Experiments measured absorption and temperature changes during illumination to evaluate photostability and identify degradation products. Results showed that both PS had higher stability in distilled water than PBS buffer. This study offers insights into the degradation pathways and conditions influencing the efficacy of these PS.

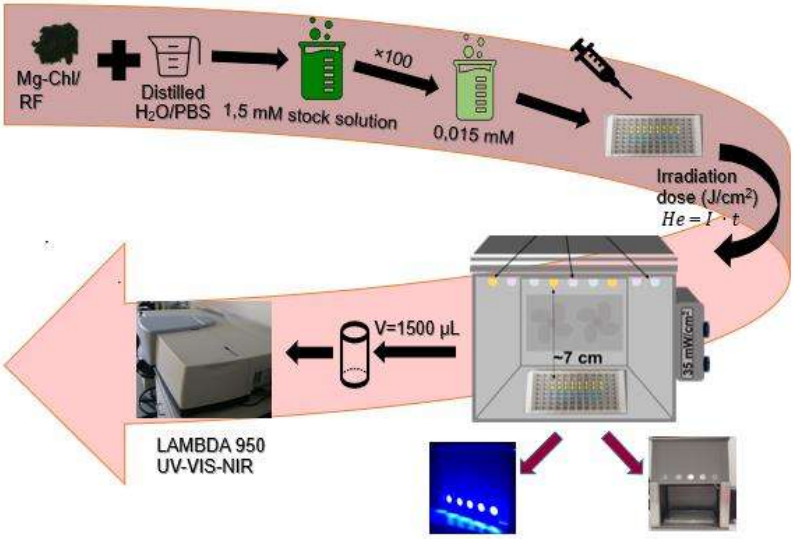

Fig. 1. Schematic iliustration of photostability experiments

In conclusion, while the study shows the potential of riboflavin and magnesium chlorophyllin as natural photosensitizers for antimicrobial photodynamic therapy, it also highlights the need for further research. Investigating their stability and photochemical characteristics under diverse environmental conditions is essential to fully realizing their potential in practical applications.

Revealing Lipid Order Differences Between Cancerous and Non-Cancerous Cells Using Fluorescent Viscosity Probes

Artūras Polita[1]
[1]Vilnius University, Institute of Biochemistry, Saulėtekio av. 7, Vilnius, Lithuania
arturas.polita@gmc.vu.lt

Microviscosity is a key property of biological membranes, influencing passive solute diffusion, lipid raft formation, and overall membrane fluidity. Microviscosity measurements provide a convenient way for estimation of lipid order and observation of compositional changes in lipid systems. Viscosity-sensitive dyes, known as molecular rotors, can quantify microviscosity variations that result from cholesterol differences or phase separations in lipid bilayers or amorphous lipid systems [1,2].

In the case of cancer, multiple mutations produce cell signalling and metabolic aberrations, which change the overall composition of intracellular lipids and may allow for the identification of malignancies via microviscosity measurements [3]. Moreover, cancerous cells often generate elevated levels of reactive oxygen species, which can oxidize and subsequently increase lipid order in affected systems [4]. However, while the compositional differences in plasma membranes between cancerous and non-cancerous cells have been well studied, there have been few efforts to identify cancer cells based on the viscosity and lipid order of intracellular organelles.

In this study, we investigate the potential of BODIPY viscosity-sensitive dyes as diagnostic tools for cancer detection. Using fluorescence lifetime imaging microscopy (FLIM) combined with organelle-specific BODIPY dyes—whose fluorescence lifetimes increase with rising microviscosity—we examine the lipid order in lysosomes and lipid droplets of live cancerous and non-cancerous cells. Our findings reveal significant variability in lipid order within lipid droplets across different cancerous cells in the same culture (Fig. 1A). In contrast, lipid droplets in non-malignant cells exhibit a uniform lipid order (Fig. 1B). Additionally, we show that both lysosomes and lipid droplets in malignant cells have microviscosities up to three times higher than those in non-malignant cells. Finally, we demonstrate the utility of molecular rotors in observation of compositional changes in lipid droplets and lysosomes under the chemotherapeutic drug treatment.

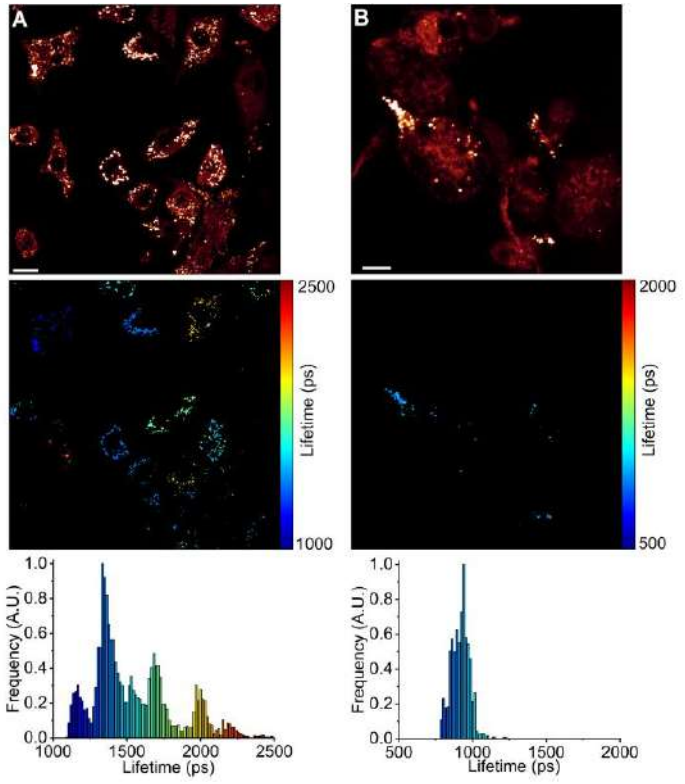

Fig. 1. FLIM of BODIPY fluorescent viscosity probe in lipid droplets of human lung cancer cells A549 (A) and human embryonic kidney cells HEK 293T (B). The top panel shows images of fluorescence intensity. FLIM images are shown in the middle panel. The corresponding fluorescence lifetime histograms are displayed in the bottom panel. Scale bars are 10 µm.

[1] A. Polita, M. Stancikaitė, R. Žvirblis et al., *RSC Adv.* **13**, 19257-19264 (2023).
[2] A. Polita, S. Toliautas, R. Žvirblis et al., *Phys. Chem. Chem. Phys.* **22**, 8296-8303 (2020).
[3] A. Polita, R. Žvirblis, J. Dodonova-Vaitkūnienė et al., *J. Mater. Chem. B.* **12**, 3022-3030 (2024).
[4] T. Kurz, J. Eaton, U. Brunk, *Antioxid. Redox. Signal.* **13**, 511-523 (2010).

Impact of Microsecond and Nanosecond Pulses on the Bystander Effect

Ugnė Borinskytė[1], Neringa Barauskaitė Šarkinienė[1], Paulius Ruzgys[1], Saulius Šatkauskas[1]

[1]Biophysical Research Group, Faculty of Natural Sciences, Vytautas Magnus University, Lithuania

ugne.borinskyte@stud.vdu.lt

Cancer remains a major cause of death within the European Union. According to 2022 cancer statistics, the European Union accounts for 50.2% of all cancer-related deaths and 54.2% of newly diagnosed cancer cases [1]. In Lithuania alone, malignant neoplasms caused 7899 deaths that year [2]. This has prompted the development of innovative treatments, such as electrochemotherapy. This approach uses electric fields to enhance the permeability of cell membranes. Through electroporation, bleomycin (an anticancer drug) can be delivered into the cells' cytoplasm, or calcium can be introduced via calcium electroporation. Both methods reduce cell viability when similar electrical parameters are applied [3].

Electrical pulses lasting between microseconds and nanoseconds are used in cell electroporation. Electroporation often occurs when 100 µs (intensity 1-16 kV/cm) or 100-300 ns (10-19 kV/cm) electrical pulses are used. It is believed that the effects of conventional and nanosecond electroporation on the cell can differ significantly [4].

Ruzgys and his team found that the bystander effect occurs during electrochemotherapy with microsecond electric fields. This effect describes how cells not directly exposed to the electric fields or therapeutic agents (like bleomycin or calcium) can still be affected by the treatment applied to neighbouring cells. Several studies suggest that the bystander effect can happen in electrochemotherapy or electroablation with microsecond pulses. However, there is limited understanding of how this effect occurs with nanosecond electrical pulses.

The impacts of the bystander effect following *in vitro* bleomycin electrotransfer and calcium electroporation are covered in the study. For the research, three cell lines were used: Chinese hamster ovary cells (CHO-K1), human adenocarcinoma alveolar basal epithelial cells (A-549), and mouse mammary cancer cells (4T1). The bystander effect was identified using the same methods following both electroporation treatments, BLM (20 nM) and CaCl2 (1 mM). A single electrical pulse with an amplitude of 1400 V/cm and a duration of 100 µs was used for microsecond electroporation. Ten pulses lasting 200 ns each were employed simultaneously for nanosecond electroporation with an electric field of 13 kV/cm. Propidium iodide, a fluorescent chemical that helps distinguish between living and dead cells, was observed as it diffused into the cells using a flow cytometer. Another method to measure cell viability was a colony assay using crystal violet dye.

Viability was significantly reduced by microsecond electroporation following both the bleomycin and calcium treatments compared to the control. Almost no reduction in cell viability occurred during either the bleomycin or calcium electroporation processes when the cells were exposed to nano pulses. A-549 cells were the only ones where bleomycin electrotransfer caused 0% cell viability (as evidenced by the clonogenic assay). Using this clonogenic investigation, an off-effect (reduced cell viability) was observed between CHO-K1 and 4T1 cell cultures following microsecond electroporation, whereas no effect was seen following nanosecond electroporation.

[1] European Commision, *Cancer estimates factsheet 2022* (2023).
[2] R. Gaidelytė, M. Garbuvienė, *Lietuvos sveikatos statistika 2022* (2023).
[3] B. Geboers, H. J. Scheffer, P. M. Graybill et al., *Radiology* **295(2)**, 254–272 (2020).
[4] P. Ruzgys, N. Barauskaitė, V. Novickij et al, *Molecules* **26(19)**, 6001 (2021).

Spectroscopic studies of $TPPS_4$ and $TPPS_3$ Aggregation

Skaiste Talanovaite[1,3], Alytis Gruodis[2], Vilius Poderys[1], Ricardas Rotomskis[1,3]

[1]Biomedical Physics Laboratory of National Cancer Institute, Baublio 3B, LT-08406, Vilnius, Lithuania
[2]Institute of Chemical Physics, Vilnius University, Sauletekio 9, c.3, LT-10222, Vilnius, Lithuania
[3]Biophotonics Group of Laser Research Centre, Vilnius University, Sauletekio 9, c.3, LT-10222, Vilnius, Lithuania
skaiste.talanovaite@gmc.stud.vu.lt

Porphyrins acquire unique electronic and photonic properties which makes them potential materials for biomedical applications [1]. One of porphyrin properties, which could play a leading role in phototherapy or other areas of application, is self-assembly. It is important to understand the interaction between porphyrin molecules and the affect of environment to control the aggregation process [2].

Here we report differences of self-assembly into supramolecular structures that is affected by number of polar sulfonic groups of 5,10,15,20-Tetrakis(4-sulfonatophenyl)porphyrin ($TPPS_4$) and 5,10,15-tris(4-sulfonatophenyl)-20-phenylporphyrin ($TPPS_3$). After in-depth spectrophotometric analysis we noticed that $TPPS_4$ and $TPPS_3$ exhibit some differences in aggregation and protonation processes.

In acidic media due to π-π stacking and electrostatic interaction between the negatively charged sulfonated phenyl groups and positively charged porphyrin core $TPPS_4$ and $TPPS_3$ can form aggregates. The first step in this process is protonation of TPPS porphyne ring (changing its symmetry from D_{2h} to D_{4h}). Second step is interaction between protonated species and negative SO_3^- group of another molecule that leads to formation of a dimer. This dimer can couple with next molecules and undergo spontaneous assembly, forming large J-aggregates. These aggregates are clearly identified by appearance of absorption bands (J-bands) at 490 nm and 709 nm. This self-aggregation process depends on pH of the solvent and concentration of TPPS.

We performed spectrophotometric titration experiments with various $TPPS_4$ and $TPPS_3$ concentrations, however isosbestic point was not detected for either of investigated molecules. Although $TPPS_4$ and $TPPS_3$ possesses similar spectral characteristics, our experiments showed that $TPPS_3$ pK_a value (pK_a=4.8) is slightly lower compared to pK_a value of $TPPS_4$ (pK_a=4.9). This is likely due to bigger negative charge of $TPPS_4$. Our experiments also showed that higher concentration of $TPPS_4$ (compared to $TPPS_3$) is necessary to form J-bands. Experiments with high concentration solutions ($c=5\cdot10^{-5}$ M) showed that the aggregation dynamics of $TPPS_4$ and $TPPS_3$ is different when pH of the solution is slowly lowered below pH=4.5 (Fig. 1). $TPPS_4$ shows a clear transformation from a free-base porphyrin to J-aggregates, while $TPPS_3$ begin to form protonated forms simultaneously with J-aggregates. In neutral media, while increasing concentration, $TPPS_4$ and $TPPS_3$ absorption spectra behave differently- $TPPS_4$ 634 nm band exhibits a slight redshift. Spectral differences between $TPPS_4$ and $TPPS_3$ were also noticed in 320-360 nm region while forming J-aggregates. $TPPS_4$ absorbance bands in ultraviolet region are more intense and clearer, while $TPPS_3$ bands are less distinguishable. Theoretical calculations using quantum chemical simulations (*Gaussian16* package, density functional B3LYP method using 6-31G(d) basis set) confirmed that there are slight differences in formation of core-tail form dimers between $TPPS_4$ and $TPPS_3$- number of polar SO_3^- groups influences interaction between molecules and structure of a dimer.

Our spectrophotometric experiments showed that number of polar SO_3^- groups has only slight effect on pK_a value, however it has big influence on aggregation dynamics at pH values lower than 4.5. Theoretical modelling and atomic force microscopy showed that different number of polar SO_3^- influences spatial characteristics of TPPS aggregates formed in acidic conditions.

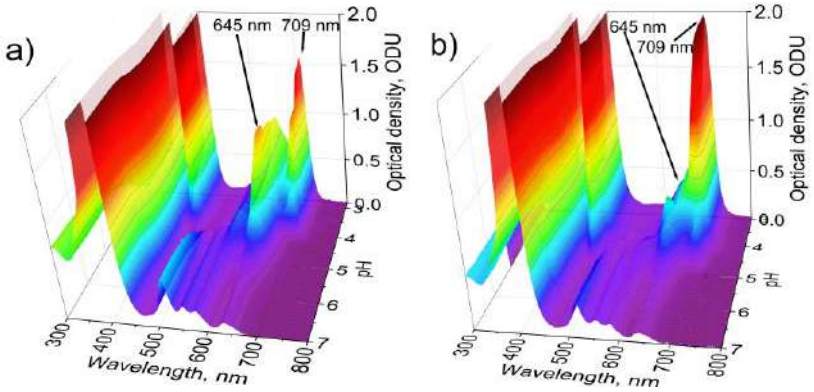

Fig. 1. a) TPPS4 and b) TPPS3 absorption spectra at various solution pH values (pH 7→2), $c=5\cdot10^{-5}$ M, l=1 cm.

[1] A. Arlegui, Z. El-Hachemi, J. Crusats, and A. Moyano, 5-Phenyl-10,15,20-Tris(4-sulfonatophenyl)porphyrin: Synthesis, Catalysis, and Structural Studies, *Molecules*, **23(12)**, 2018.
[2] P. Jayachandran, A. Angamuthu, and P. Gopalan, Quantum Chemical Study on the Structure and Energetics of Binary Ionic Porphyrin Complexes, *J. Chin. Chem. Soc.*, **65(8)**, 908-917,2 018.

Effect of Alkylphospholipids on the Biophysical Properties of Model Lipid Bilayers

Rūta Bagdonaitė[1], Artūras Polita[1], Gintaras Valinčius[1]

[1]Institute of Biochemistry, Life Sciences Center, Vilnius University, Sauletekio av. 7, LT-10257, Lithuania
ruta.bagdonaite@bchi.stud.vu.lt

High toxicity and limited efficacy of commonly used anticancer chemotherapeutics are still significant problems in cancer therapy. Thus, development of novel anticancer drugs is of great importance. Synthetic alkylphospholipids (APLs) represent a promising class of antitumor agents, derived from lysophosphatidylcholine, that unlike most of the chemotherapeutic drugs do not target DNA. APLs act on cell membranes and selectively induce apoptosis in tumour cells [1]. However, a detailed understanding of APLs interaction with lipid bilayers is still lacking.

In this work we investigated three APLs differing in hydrocarbon chain length and headgroup composition – miltefosine (hexadecylphosphocholine), edelfosine (1-O-octadecyl-2-O-methyl-sn-glycero-phosphocholine) and perifosine (Octadecyl-(1,1-dimethyl-4-piperidylio) phosphate). We employed fluorescence lifetime imaging microscopy (FLIM) using a viscosity sensitive molecular rotor BODIPY-PM [2] to image APLs induced viscosity changes in supported lipid bilayers (SLBs). We also used electrochemical impedance spectroscopy (EIS) to assess possible defect formation on tethered bilayer lipid membranes (tBLMs).

Incubation of APLs with lipid bilayers composed of dopc and cholesterol induced dielectric membrane damage corresponding to defect formation in a time and concentration-dependent manner, with miltefosine being less damaging compared to edelfosine and perifosine at the same concentrations. However, FLIM measurements showed, that introduction of APLs results in an initial increase in membrane viscosity (Fig. 1), which can be associated with incorporation of APLs in the bilayer and increased overall lipid order. Interestingly, it was later followed by a decrease in membrane viscosity, possibly arising from eventual destabilization and loss of material from the lipid membrane surface.

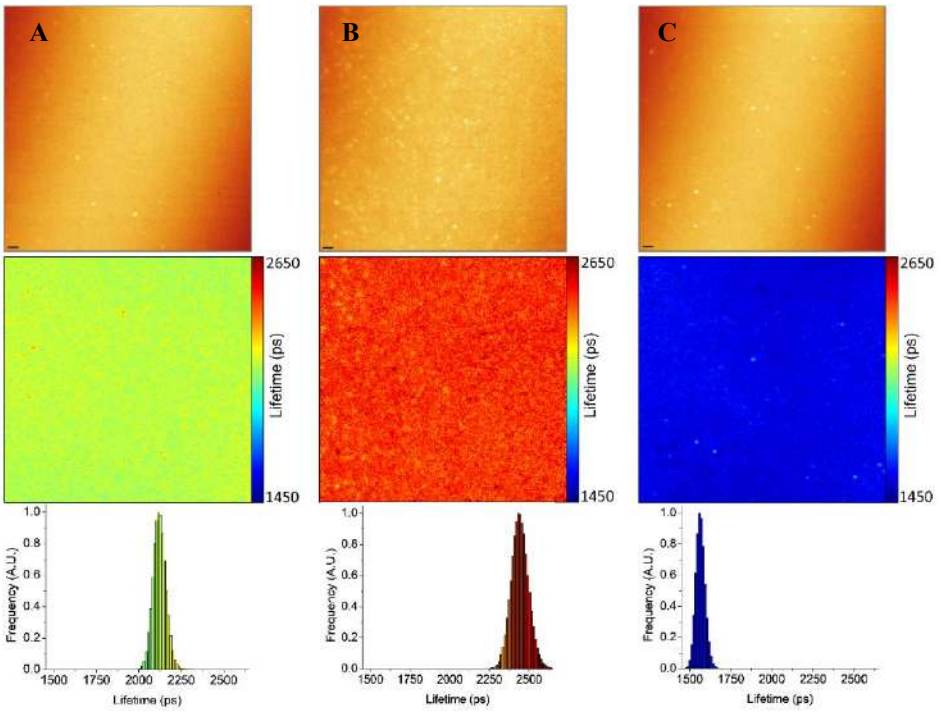

Fig. 1. FLIM of BODIPY-PM in DOPC:Chol 6:4 SLB of initial membrane (A), 30 min (B) and 90 min (C) after addition of 10 μM miltefosine. The top images show fluorescence intensity, the middle images show FLIM and corresponding lifetime histograms are displayed at the bottom. Scale bars are 1 μm.

[1] PA. Jaffrès, C. Gajate, A. M. Bouchet et al., *Pharmacol. Ther.* **165,** 114-131 (2016).
[2] A. Polita, M. Stancikaitė, R. Žvirblis et al., *RSC Adv.* **13**, 19257-19264 (2023).

Prostate Cancer Imaging with Nonlinear Optical Microscopy

Austėja Bareikytė[1], Viktoras Mažeika[1,2], Mykolas Mačiulis[1], Margarita Žvirblė[2,3], Darius Dasevičius[4], and Virginijus Barzda[1,5]

[1]Laser Research Centre, Faculty of Physics, Vilnius University, Saulėtekio al. 9, Vilnius, Lithuania
[2]Institute of Biosciences, Life Sciences Center, Vilnius University, Saulėtekio al. 7, Vilnius, Lithuania
[3]Laboratory of Immunology, National Cancer Institute, Santariškių g. 1, Vilnius, Lithuania
[4]Center of Pathology, Vilnius University Hospital Santaros Clinics, P. Baublio g. 5, Vilnius, Lithuania
[5]Department of Chemical and Physical Sciences, Department of Physics, University of Toronto, 3359 Missisauga Road, Missisauga, ON, Canada
austeja.bareikyte@ff.stud.vu.lt

Prostate cancer is the most common oncological disease in Lithuania and the second most frequently occurring cancer among men globally [1] with over 1.4 million new cases and 300 000 deaths annually [2]. Traditional diagnostics is based on the biopsy and examination by a pathologist which is not the ideal procedure for early-stage diagnosis since around 20% of cases end up in misdiagnosis [1]. Nonlinear imaging microscopy is a promising alternative for examining biological samples since collagen can generate a second harmonic image contrast. Usually, second harmonic generation is sensitive to collagen structural changes induced by tumour. The aim of this work is to use imaging techniques that involve nonlinear processes and polarization to get a deeper structural understanding of the histological prostate cancer samples.

Nonlinear imaging of four histological samples was performed with a home–built laser-scanning microscope. Brightfield hematoxylin and eosin (H&E) stained image of prostate cancer tissue is provided in Fig. 1a. The second harmonic generation (SHG), third harmonic generation (THG), and multiphoton excitation fluorescence (MPF) responses were measured and nonlinear images were generated. THG, SHG and MPF are provided in Fig. 1b, c, d, respectively.

Collagen, which is the main extracellular matrix component, has the ability to generate second harmonic. SHG was produced only from the prostate tissue stroma since there is no collagen in the glands, and it was of low intensity. Third harmonic generation occurs in regions where there is difference in refractive indices in the cell. Therefore, THG images provided information about gland and cell nuclei arrangement in prostate tissue illustrating that prostate cancer regions can be characterized by reticular pattern instead of papillary. Additionally, double Stokes – Mueller polarimetry (DSMP) and polarization-in polarization-out (PIPO) measurements were performed and R ratio (illustrates ultrastructural changes to the extracellular matrix due to the presence of tumour) and C ratio (describes polar arrangement of collagen) was calculated. R and C ratio colour maps and histograms showed a deeper understanding of collagen arrangement and fiber orientation in the tissue. The MPF highlights the proteins including collagen and elastin from the extracellular matrix.

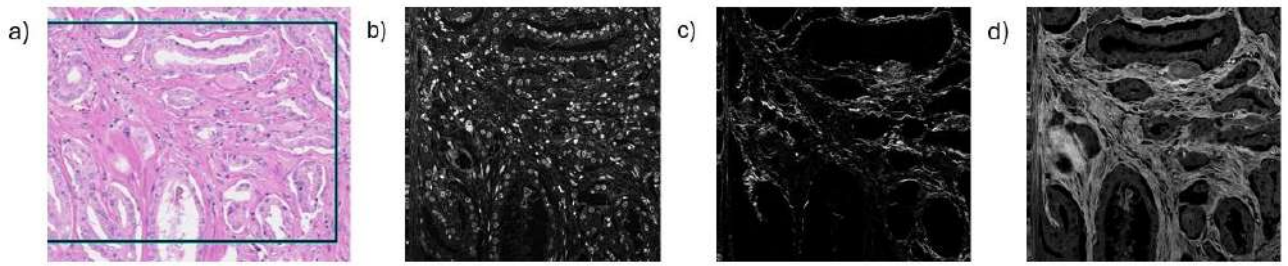

Fig. 1. Prostate tissue sample No. 1 imaging results: a) brightfield H&E reference; b) THG; c) SHG; d) MPF.

This study shows the potential to use nonlinear imaging microscopy to help with cancer-invaded prostatic tissue interpretation. The investigations demonstrate that THG microscopy provides with a high contrast images that can be used for artificial intelligence (AI) assisted investigation of prostate tumors. The comparison of SHG and MPF provide detailed information about cancer induced ECM modifications. The combination of THG, SHG and MPF contrast mechanisms have potential to provide the new avenues for improving tumor diagnostics and prognostics.

[1] *Apie prostatos vėžį,* Vilniaus universiteto Onkologijos institutas (2006).
[2] L. Wang, B. Lu, M. He, Y. Wang, Z. Wang, and L. Du, *Prostate Cancer Incidence and Mortality: Global Status and Temporal Trends in 89 Countries From 2000 to 2019*, Front Public Health, vol. **10**, p. 811044 (2022).

Bystander Effect Induced by Combined Calcium Electroporation, Bleomycin Electrotransfer, and Irreversible Electroporation

Neringa Barauskaitė-Šarkinienė[1], Ugnė Borinskytė[1], Paulius Ruzgys[1], Saulius Šatkauskas[1]

[1]Vytautas Magnus University, Research Institute of Natural and Technological Sciences, Kaunas, Lithuania

neringa.barauskaite-sarkiniene@vdu.lt

Electroporation, a technique utilizing electric fields to permeabilize cell membranes, holds promise for localized cancer treatment. Depending on the intensity and duration of the electric pulses, electroporation can be either reversible, facilitating drug delivery (e.g., electrochemotherapy with bleomycin[1]), or irreversible, leading to cell death (electroablation [2]). Similar to radiotherapy, electroporation-based therapies can induce the "bystander effect," where treated cells release signalling molecules that impact neighbouring, untreated cells [3]. While well-documented in radiotherapy, the bystander effect in electroporation remains poorly understood. Only few studies have been published showing the Bystander effect after electroporation-based anticancer therapies [4,5]. This study investigates the bystander effect on cell viability following combination of three electroporation-based treatments: irreversible electroporation, bleomycin electrotransfer, and calcium electroporation.

Mouse breast cancer (4T1) cells were affected one of three treatments: (1) irreversible electroporation (1 HV, 2800 V/cm, 100 µs), (2) bleomycin electrotransfer (1 HV, 1400 V/cm, 100 µs), or (3) calcium chloride ($CaCl_2$) electroporation (1 HV, 1400 V/cm, 100 µs). Treatment, cells were incubated for 48 hours. The conditioned media from these treated cells was collected and applied to untreated 4T1 cells to assess the bystander effect. Cell viability was evaluated using a colony formation assay (for ability to form colonies), flow cytometry (for real number of cells) and alamar blue assay (for metabolic activity).

All three electroporation treatments (irreversible electroporation, bleomycin electrotransfer, and calcium electroporation) induced a significant bystander effect, leading to complete or near-complete death of unaffected cells by electric fields but exposed to the conditioned media. Interestingly, combining conditioned media from cells that had different treatments resulted in varying effect intensities of bystander effect. For instance, combining media from irreversible electroporation and bleomycin electrotransfer produced a more pronounced effect than either treatment alone. Diluting the conditioned media reduced the bystander effect, suggesting a dose-dependent response.

This study demonstrates that electroporation-based therapies, including irreversible electroporation, bleomycin electrotransfer, and calcium electroporation, can induce a potent bystander effect, impacting the viability of neighbouring, untreated cells. These findings highlight the importance of considering the bystander effect when evaluating the efficacy and potential off-target effects of electroporation-based cancer treatments.

Acknowledgment: The research was funded by the Research Council of Lithuania, Grant Nr. S-MIP-23-124

[1] U. Probst, I. Fuhrmann, L. Beyer and P. Wiggermann. "Electrochemotherapy as a new modality in interventional oncology: A review". Technol. Cancer Res. Treat, vol 17 (2018).

[2] J. Zhao, X. Wen, L. Tian, T. Li, C. Xu and X. Wen. Melancon, M.P.; Gupta, S.; Shen, B.; Peng, W.; et al. "Irreversible electroporation reverses resistance to immune checkpoint blockade in pancreatic cancer". Nat. Commun. vol. 10, pp. 1–14 (2019).

[3] B N. Jalal, S. Haq, N. Anwar, S. Nazeer and U. Saeed. "Radiation induced bystander effect and DNA damage". J. Cancer Res. Ther., vol. 10, pp. 819–833 (2014).

[4] E. Pirc, C. Federici, M. Bošnjak, B. Perić, M. Reberšek, M., L. Pecchia, L, N. Glumac, M. Čemažar, M. Snoj, G. Serša. "Early Cost-effectiveness Analysis of Electrochemotherapy as a Prospect Treatment Modality for Skin Melanoma". Clin. Ther., vol. 42, pp. 1535–1548, (2020).

[5] P. Ruzgys, N. Barauskaite, V. Novickij, J. Novickij, S. Satkauskas. "The Evidence of the Bystander Effect after Bleomycin Electrotransfer and Irreversible Electroporation". Molecules. vol. 26,19 6001 (2021).

Enhancing Precision in Computational Drug Design: The Role of Intrinsic Versus Observed Binding Parameters

Ernestas Urniežius, Vytautas Petrauskas, Asta Zubrienė, Daumantas Matulis

Department of Biothermodynamics and Drug Design, Institute of Biotechnology, Life Sciences Center, Vilnius University, Saulėtekio Ave 7, LT-10257, Vilnius, Lithuania
ernestas.urniezius@gmc.vu.lt

One of the major goals of computer-aided drug design is the accurate prediction of protein-ligand binding parameters. Traditionally, binding affinity is represented by dissociation constant (K_d) and Gibbs energy change (ΔG). However, experimentally measured binding parameters can be influenced by experimental conditions such as pH, buffer composition, and temperature. Intrinsic binding parameters, which correct for those influences, provide a more accurate representation of the inherent protein-ligand interaction strength [1].

Utilizing knowledge-based biases in molecular modeling, tailored for particular biological targets and based on such prior information as protein-ligand crystal complexes, can enhance the accuracy of computational predictions. Aligning molecular modeling results with intrinsic binding data enables better optimization of lead compounds by accurately reflecting structural modifications' impact on binding parameters.

In this case study, we used binding data from the recently published Protein-Ligand Binding Database - PLBD (https://plbd.org) [2]. This database features both observed and intrinsic binding parameters, including detailed thermodynamic and kinetic parameters for various biological targets. This also includes binding data for over 500 sulfonamide-based compounds interactions with 12 catalytically active human carbonic anhydrase (CA) isozymes, alongside 127 crystal structures of various CA isoforms in complex with ligands.

We present a comparative analysis of sulfonamide ligands binding to three CA isozymes (CA1, CA2 and CA9), using both intrinsic and observed binding parameters retrieved from the PLBD database. This analysis is complemented by molecular modeling, incorporating results from docking simulations performed by several docking programs. Our analysis highlights the differences between observed and intrinsic affinities and shows that intrinsic parameters can be utilized to refine computational predictions and improve the overall efficacy of computational drug design approaches by correcting for binding-linked protonation reactions.

Intrinsic binding parameters provide a more accurate representation of 'true' binding affinities, offering a robust foundation for Q(SAR) analysis and computational modeling. In our study, docking scores aligned more precisely with intrinsic than observed parameters, indicating that it is important to correct for experimental artifacts which influence observed binding data. This allows not only to improve computational predictions, but also to further our understanding of molecular recognition processes.

[1] D. Matulis (ed.), Carbonic Anhydrase as Drug Target: Thermodynamics and Structure of Inhibitor Binding, Springer Nature, 2019.
[2] D. Lingė, M. Gedgaudas, A. Merkys, V. Petrauskas, A. Vaitkus, A. Grybauskas, V. Paketurytė, A. Zubrienė, A. Zakšauskas, A. Mickevičiūtė, J. Smirnovienė, L. Baranauskienė, E. Čapkauskaitė, V. Dudutienė, E. Urniežius, A. Konovalovas, E. Kazlauskas, K. Shubin, H. B. Schiöth, W.-Y. Chen, J. E. Ladbury, S. Gražulis, D. Matulis, PLBD: protein–ligand binding database of thermodynamic and kinetic intrinsic parameters, Database, Volume 2023, baad040, 2023. https://doi.org/10.1093/database/baad040

Comparison of the Thresholds for Electroporation and Excitation for Pulses within Nanosecond–Millisecond Duration Range

Gintautas Saulis[1], Mantas Šilkūnas[2], Rita Saulė[1]

[1]Faculty of Natural Sciences, Vytautas Magnus University, Kaunas 44248, Lithuania
[2]Frank Reidy Research Center for Bioelectrics, Old Dominion University, Norfolk, VA 23508, USA
gintautas.saulis@vdu.lt

Exposure of cells with pulses of strong electric field can electroporate the cell plasma membrane, stimulate of excitable cells, or cause both effects. In some applications, e.g. non-thermal ablation of cardiac or tumour tissue with irreversible electroporation, excitation of muscle cells is not desirable, while in other ones, it would be better to avoid electroporation.

Theoretical analysis and experimental data available show that, depending on the membrane charging time constant, pulse strength and duration, the complex interplay of excitation and electroporation can be observed. Excitation with or without damaging of the cell plasma membrane due to electroporation can be achieved.

However, while carrying theoretical analysis, some minor simplifications were used. Meanwhile, these simplifications might be important for the detailed comparison of electroporation and excitation thresholds as for some pulse durations these thresholds are close to each other. The aim of this study was to analyse theoretically the dependence of the threshold for electroporation in more details within a wide range of pulse durations (nanoseconds–milliseconds) and compare these results with experimental data on excitation of neurons obtained earlier.

Electroporation of mouse hepatoma MH-22A cells was determined from the increase of the plasma membrane permeability to potassium ions. It was assumed that the threshold of electroporation corresponds to the formation of one pore. Theoretical dependences of the threshold of electroporation of a neuron on pulse duration were calculated based on the mechanism of electroporation. Parameters required were estimated from the experimental data obtained in mouse hepatoma MH-22A and Chinese hamster ovary cells. For the comparison with experimental data, the dependence of the threshold for excitation of dissociated E18 rat hippocampal neurons, determined for single square-wave electric pulses with the durations from 100 ns to 1 ms obtained earlier was used.

The experimental excitation-duration curve can be approximated by the straight line in a log-log plot with the slope equal to -0.5, which remains the same for all range of pulse durations studied (from 100 ns to 1 ms). Meanwhile, the slope of the dependence of the electric field strength required to electroporate the cell on the pulse duration varies from -0.06 to -0.9 within the same range of pulse durations.

From this analysis, it can be concluded that the results of the exposure of neurons by a single square-wave pulse depend strongly on its duration:

1) For pulses longer than 10–20 μs the threshold for neuron excitation is much lower than that for electroporation.
2) Pulses with the durations from 200–300 ns to 10–20 μs, which cause neuron excitation, should also electroporate them.

Threshold for excitation becomes close to or even lower than the threshold for electroporation for pulses shorter than 200–300 ns.

[1] M. Casciola, T.K. Feaster, M.J. Caiola, D. Keck, K. Blinova, *Front. Physiol.* **13**, 1064168 (2022).
[2] A.G. Pakhomov, O.N. Pakhomova, *Bioelectrochemistry* **136**, 107598 (2020).
[3] C.W. Zemlin, *Bioelectrochemistry* **141**, 107882 (2021).
[4] M. Silkunas, E. Gudvangen, V. Novickij, A.G. Pakhomov, *Biochim. Biophys. Acta* **1864**, 184034 (2022).
[5] G. Saulis, R. Praneviciute, *Anal. Biochem.* **345**, 340-342 (2005).
[6] G. Saulis, *Food Eng. Rev.* **2**, 52-73 (2010).

Generation of Hypochlorous Acid by High-Voltage Pulses and its Influence on the Cell Plasma Membrane

Gintautas Saulis[1], Raminta Rodaite[1], Jurgita Sventoraitiene[2], Viktorija S. Dainauskaite[1], Danute Batiuskaite[1], Alexander Golberg[3], Rita Saulė[1]

[1]Faculty of Natural Sciences, Vytautas Magnus University, Kaunas 44248, Lithuania
[2]Institute of Anatomy, Faculty of Medicine, Lithuanian University of Health Sciences, LT-44307 Kaunas, Lithuania
[3]Porter School of Environment and Earth Sciences, Tel Aviv University, Tel Aviv, Israel
gintautas.saulis@vdu.lt

Pulses of strong electric field utilized for cell electropermeabilization, also cause electrolysis reactions at the electrode–solution interfaces. Tissues and solutions usually contain high amounts of chloride ions. As a result of electrolysis, Cl_2 gas can be formed at the anode [1]. Chloride ions react with the water molecules and form hypochlorous acid (HOCl), which is a powerful oxidant – it can react with a wide variety of biomolecules including DNA, RNA, cholesterol, and proteins [2]. For practical applications of electroporation, e.g, when using electroporation to extract DNA, RNA or proteins (e-biopsy) [3], it is important to avoid any contamination of samples.

The aim of this work was to study the formation of HOCl acid as a result of electrolysis during high-voltage pulses, as well as its influence on the viability of cells and the barrier function of the cell plasma membrane. The formation of hypochlorous acid was evaluated with fluorescent indicator of hypochlorite 3'-p-Aminophenyl fluorescein (APF) [4] along with the scavengers of various reactive oxygen species (ROS). The viability of Chinese hamster ovary (CHO) cells was determined by a colony-forming assay [5]. The size of the pores created in human erythrocytes was estimated by studying the protective action of xylitol (152 Da), mannitol (182 Da), and sucrose (342 Da) against colloid-osmotic lysis [6].

It has been obtained, that during high–voltage electric pulses, ROS are generated. In cell–free media, micro–millisecond pulsed electric field increased fluorescence of hypochlorite indicator APF proportionally to the pulse number and amplitude. APF fluorescence was reduced by both vitamin C and mannitol. Also, it has been shown that ROS formation was more intensive in the case of stainless–steel electrodes comparing to the aluminum ones. The results of this work can be useful for optimizing the electroporation technology used in biotechnology, medicine, and food industry.

The influence of hypochlorous acid on the viability of Chinese hamster ovary (CHO) cells *in vitro* was evaluated. HOCl caused the reduction of CHO viability. Less than 50 % of CHO cells survived, when the concentration of hypochlorous acid in the cell growth medium was 0.8 mM.

The influence of HOCl on the plasma membrane of human erythrocytes was also studied. HOCl increased the permeability of the cell plasma membrane to ions and small molecules, what caused haemolysis of erythrocytes. The estimated radius of permeable structures, which appeared in the plasma membrane of erythrocytes, was about 0.3–0.5 nm. This is close to the size of the pores generated by the exposure of cells with pulses of strong electric field [6].

Conclusion: hypochlorous acid can be formed due to electrolysis during high-voltage pulses. It can increase permeability of the cell plasma membrane to ions and small molecules, which can cause the reduction of the cell viability.

[1] G. Saulis, R. Rodaite-Riseviciene, V.S. Dainauskaite, R. Saule, in: Ravishankar Rai, V. (Eds.), *Advances in Food Biotechnology*, John Wiley & Sons, West Sussex, 575-591 (2016).
[2] C.M.C. Andres, J.M. Perez de la Lastra, C.A. Juan, F.J. Plou, E. Perez-Lebena, *Int. J. Mol. Sci.* **23**, 10735 (2022).
[3] A. Golberg, J. Sheviryov, O. Solomon, L. Anavy, Z. Yakhini, *Sci. Rep.* **9**, 15750,(2019).
[4] K. Setsukinai, Y. Urano, K. Kakinuma, H.J. Majima, T. Nagano, *J. Biol. Chem.* **278**, 3170-3175 (2003).
[5] I.R. Freshney, *Culture of animal cells: a manual of basic techniques*, John Wiley & Sons, Inc., New York, 2000
[6] G. Saulis, *Biomed. Sci. Instrum.* **35**, 291-296 (1999).

BEHAVIOUR AND IMPORTANCE OF ANNEXIN A4 PROTEIN FOR ACTIVE MEMBRANE REPAIR AFTER ELECTROPORATION

Baltramiejus Jakštys[1,3], Dominykas Makarovas[2], Inga Morkvėnaitė-Vilkončienė[3], Saulius Šatkauskas[1]

[1]Cell and Tissue Biotechnology Research Group, Research Institute of Natural and Technological Sciences, Vytautas Magnus University, Kaunas, Lithuania
[2]Biochemistry Cathedral, Faculty of Natural Sciences, Vytautas Magnus University, Kaunas, Lithuania
[3]Department of electrical engineering, Vilnius Gediminas Technical University, Vilnius, Lithuania
baltramiejus.jakstys@vdu.lt
dominykas.makarovas@stud.vdu.lt
saulius.satkauskas@vdu.lt
inga.morkvenaite-vilkonciene@vilniustech.lt

Keywords: electroporation, electropermeabilization, annexin A4, membrane repair, cell viability

Treatment with short, high-voltage electric pulses (electroporation) increase cell membrane permeability, which is related to the formation of hydrophilic pores or phospholipid oxidation. After the cell plasma membrane is permeabilized, its recovery plays a crucial part in sustaining cell viability. Annexins' protein family plays a major role in cell plasma membrane reparation. One of the most abundant annexin protein is the annexin A4. The activity of annexin A4 is ATP independent and Ca^{2+} is its ligand making annexin A4 protein the first defence wall after unpredicted permeabilization [1]. It is known that Ca^{2+} helps for the cell plasma membrane to recover faster after electroporation. We intended to investigate the involvement of annexin A4 protein in cell plasma membrane recovery after cell electroporation and its impact on cell viability, and pore resealing in presence and absence of Ca^{2+} [2].

MCF7 wild-type cells with intact annexin A4 gene and MCF7-AnxA4-KO cells with blocked annexin A4 gene expression were used. To visualise the annexin A4 activity in KO cells, we restored annexin A4 protein by lipofection of MCF7-AnxA4-KO cells with AnxA4-GFP plasmid. We used an MTS assay to assess cell viability and flow cytometry to determine the dynamics of electropermeabilization and plasma membrane repair. Fluorescence microscopy was used to monitor translocation of Anx-A4-GFP protein within the cells after pulsing.

Results revealed that MCF7-WT cells were less susceptible to electroporation compared with the MCF7-AnxA4-KO cells. Secondly, the number of cells with recovered cell plasma membrane 35 mins after electroporation increased in both cell lines but was more pronounced in the MCF-WT cell line, signifying active cell plasma membrane restoring processes dependent on Anx A4 protein. Fluorescence microscopy revealed that calcium had a drastic impact on Anx A4 activity because of faster translocation from the cytosol to the plasma membrane after pulsing. The Anx A4 translocation speed increased with pulse intensity and Ca^{2+} addition into the pulsing buffer. In addition, we determined that annexin A4 translocated from cytosol to nuclear envelope in Ca^{2+} medium, while electroporation of cells in Ca^{2-} medium caused Anx A4 translocation only to the plasma membrane.

[1] T. Boye, K. Maeda, W. Pazeshkian et al., *Nature Communications* 8(1): 1623 (2017). doi: 10.1038/s41467-017-01743-6
[2] D. Navickaitė, P. Ruzgys, M. Maciulevičius et al., *Bioelectrochemistry* 107927. doi: 10.1016/j.bioelechem.2021.107927

The Influence of Circular Arcs on Length Perception

Vilius Marma[1,2,3], Aleksandr Bulatov[1,2], Natalija Bulatova[2], Laimutis Kučinskas[2], Edgaras Diržius[2]

[1]Lithuanian University of Health Sciences, Institute of Biological Systems and Genetics Research, Laboratory of Visual Neurophysiology, Eivenių st. 4, Kaunas, Lithuania
[2]Lithuanian University of Health Sciences, Institute of Biological Systems and Genetics Research, Eivenių st. 4, Kaunas, Lithuania
[3]Lithuanian University of Health Sciences, Department of Physics, Mathematics and Biophysics, Eivenių st. 4, Kaunas, Lithuania
Vilius.Marma@lsmu.lt

Aim:

The aim of the study was to further develop a quantitative model of the filled-space illusion and test it to account for the effects caused by stimuli containing an unconventional form of contextual distractor.

Methods:

Illusion was measured as a function of the radius of the circular arcs oriented orthogonally and parallel to the main stimulus axis, and the endpoints of imaginary arcs positioned symmetrically with respect to lateral terminator of the three-dot stimulus. The stimuli used in the experiments consisted of three horizontally arranged dots (diameter, 3 min of arc; luminance, 20 cd/m^2), which were considered as terminators (t_R, t_C, and t_T, Fig. 1) specifying the ends of the reference and test stimulus intervals; the length of the reference interval, R was fixed at 90 min of arc. The two distracting circular arcs (line-width, 2 arcmin; luminance, 20 cd/m^2; circular radius, 25 arcmin) were arranged symmetrically with respect to the lateral stimulus terminator (t_R) and the central angle (ϕ) of the arcs was used as an independent variable, which randomly changed in a range from 0º to 180º. Subjects adjusted the length of the empty test interval to that of the reference, and the matching errors were considered as the illusion magnitude. It was demonstrated that the model calculations properly predict all the illusion magnitude changes for stimulus (Fig. 1a) with vertical circular arcs (i.e., oriented orthogonally to the main stimulus axis) were presented as well as for stimulus (Fig. 1b) with horizontally oriented arcs were used, also for stimulus (Fig. 1c) with only the endpoints (dot-size, 2 arcmin; luminance, 20 cd/m^2) of imaginary arcs were presented.

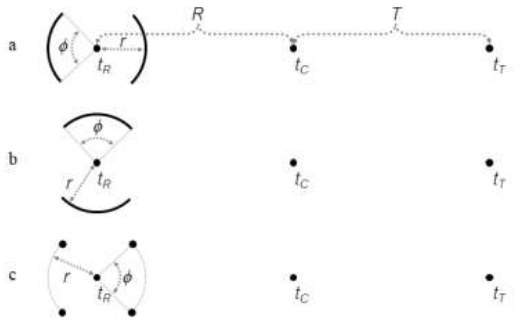

Fig. 1. Examples of stimuli used in experiments. The three-dot (t_R, t_C, and t_T) stimuli with distractors arranged symmetrically with respect to the lateral terminator (t_R): the circular arcs oriented orthogonally (a) and parallel (b) to the main stimulus axis, and the endpoints of imaginary arcs (c). R and T the length of the reference and test interval, respectively; r the radius of the circle; ϕ the central angle of the arcs. In experiments, white stimuli (luminance of all the dots and lines, 20 *cd/m^2*) were presented against a dark round-shaped background (8° in diameter and 0.4 *cd/m^2* in luminance). *Dotted lines*, the dimensions were not part of the actual display.

Results:

In the model, the task of length judgments is concerned with neural calculations based on information about visual coordinates of terminators of stimulus spatial intervals. In turn, this information is encoded by the magnitude of integrated responses of relevant attentional windows (AWS) centered at the terminators. The magnitude of the illusion (i.e., overestimation of the length of the filled reference stimulus interval in comparison with that of the empty test one) as a function of the length of the central angle of the endpoints of imaginary circular arcs, ϕ can be evaluated by the formula:

$$P_{end}(r, \phi, \sigma, k) = \frac{k}{4}\pi r \cos\left(\frac{\phi}{2}\right) e^{-\frac{r^2}{4\sigma^2}} \quad (1)$$

where k is some coefficient of proportionality; r represents the radius; ϕ is the central angle of the imaginary arcs; σ is the standard deviation assumed for Gaussian profiles of neural excitation and AWS. It was shown that the model satisfactorily describes all changes in the illusion magnitude for stimulus with the vertical or horizontal oriented circular arcs and the endpoints of imaginary circular arcs. The dependencies established were used for further development of our quantitative model.

Conclusions:

A good correspondence between the experimental and theoretical results supports the suggestion that the context-evoked augmentation of neural excitation can determine the occurrence of the filled-space illusion.

Lateral Diffusion in Biocompatible Stainless Steels During Patterned Plasma Nitriding

Paulius Andriūnas

Kaunas University of Technology, Physics Department, Studentų g. 50, Kaunas, Lithuania
paulius.andriunas@ktu.edu

Plasma nitriding of austenitic stainless steel through the mask at temperature of 400 °C is considered in the presented work. This presentation aims to show induced changes in surface geometric dimensions resulting from the distribution of nitrogen in the alloy after nitriding and the effect of undermask adsorption on anisotropy of nitrogen distribution in the nitrided zone. Therefore, 2D simulations of stainless steel nitriding through a mask were performed with two configurations: a) with lateral adsorption under the mask when mask is not adhered to a surface of the sample and b) without lateral adsorption under the mask when mask is firmly adhered to a surface of the sample. The main mechanisms of nitrogen mass transport in proposed model are the stress-induced diffusion and trapping–detrapping process, equations 1 and 2 respectively [1]:

$$\frac{\partial C_{dif}}{\partial t} = \frac{\partial C_{adsorb}}{\partial t} + \nabla\left(D\nabla C_{dif} - \frac{V_m D C_{dif}}{RT}\nabla\sigma\right) - \frac{\partial C_{trap}}{\partial t} \quad (1)$$

$$\frac{\partial C_{trap}}{\partial t} = K\left[C_{dif}\left(H_t - C_{trap}\right) - N_0 C_{trap} exp\left(\frac{-E_B}{k_B T}\right)\right] \quad (2)$$

where C_{dif} and C_{trap} re the nitrogen concentrations in diffusion and trap sites, respectively, D is the diffusion coefficient, σ is the internal lattice stress.

Changes in surface topography were described by the inclusion of nitrogen-induced dimensional expansion of the material. The surface concentration profiles and topographical profiles along the surface are calculated and compared with experimentally registered ones taken from the literature, and they show a good agreement. The anisotropic aspect of nitriding are analyzed, because nitriding processes takes place in vertical and horizontal directions. The results show that during the gradient nitriding, the expansion of material is more significantly expressed perpendicularly to the surface; however, in the parallel direction, the expansion takes place as well and can be an important aspect in the case of small pattern dimensions. The process of lateral undermask adsorption is a quite important process and can not be neglected in the case of masks which are not well adhered. The mask's adherence has a significant influence on the formation of the geometrical shape of the surface topographical profile during pattern nitriding. The adherence of the mask influences the anisotropy of nitriding: if the mask is well adhered, the lateral adsorption under the mask can be neglected and the nitriding become almost isotropic, and only at short times during nitriding is some anisotropy observed. In the case of not well adhered masks because of lateral adsorption process under the mask the anisotropy of nitriding is significant, dependent on time and diffusivity. Quite often observed step in the lateral nitrogen concentration profile at the edge of the mask, which is also dependent on diffusivity, and is formed because of nitrogen atoms being trapped in trap sites. It can be considered as direct evidence of the trapping detrapping process.

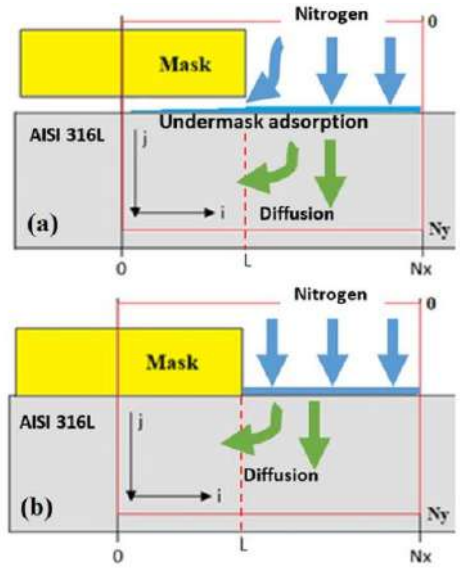

Fig. 1. The schematic presentation of nitriding through a mask in two simulated cases: with (a) and without (b) undermask adsorption.

[1] P. Andriūnas, R. Čerapaitė-Trušinskienė, A. Galdikas, *Coatings*, 14, 1014 (2024).

Index

A

Abakevičienė, B 54
Abouhagger, A 62
Abramavičius, D 49, 88
Adamonė, D 91, 92
Åden, J 27
Adomavičiūtė-Grabusovė, S 42
Akhtar, P 26, 31, 59
Alaburda, A 4
Alizadeh, M 106
Almanaitytė, M 92
Ambrazevičiūtė, S 66
Ammar-Merah, S 58
Andriukonis, E 62
Andriūnas, P 128
Anužienė, G 85
Arbačiauskaitė, J 93
Artyushenko, V 42
Ayscough, S 27

B

Baba, MA 109
Bagdonaitė, R 120
Bagdonas, S 31, 69, 82, 103
Baliulyte, L 49
Ballerini, L 22
Balodis, M 42
Bandzevičiūtė, R 71, 72
Banys, J 79
Barakauskas, E 92
Baranauskas, G 19, 77
Barauskaitė-Šarkinienė, N 5, 66, 105, 118, 122
Bareikytė, A 121
Baronaitė, I 76, 79
Baronas, D 101
Barzda, V 31, 58, 64, 106, 121
Batiuskaite, D 125
Beleckas, P 44
Belosludtsev, A 67
Bertulis, A 45
Bielevicius, A 45
Bikulčienė, I 72
Bitinaitis, I 67
Blashchuk, S 110
Bordel Velasco, S 86
Borinskytė, U 118, 122
Borusevičiūtė, F 73
Borutaite, V 107
Buchovec, I 60, 116
Budvytyte, R 30, 48
Bulatov, A 127
Bulatova, N 127
Burkanas, M 58, 114
Butkienė, G 4, 5, 58, 84, 97, 108, 112, 115
Byčius, EG 72

C, Č

Čalnerytė, D 102
Castaño, LU 106
Celiešiūtė-Germanienė, R 55
Čeponkus, J 71, 72, 85

Chang, KS 15
Chmeliov, J 36
Čiurlienė, R 64
Čiužas, IA 85
Clifton, L 27

D

Dapkūnas, J 34
Dapšys, K 28
Dainauskaite, VS 125
Dasevičius, D 121
Daugėlaitė, AM 84, 97, 108
Daugelavičius, R 95, 96
Dementjev, A 103
Diržius, E 127
Dodonova-Vaitkūnienė, J 104, 115
Dudutienė, V 101

E

Elkhider, S 109
Ežerskytė, E 83, 97, 112

F

Frey, W 25

G

Gavutis, M 29, 61, 104
Gečaitė, J 40
Gedminaitė, D 80
Gelažunaitė, S 105
Gelzinis, A 36
Germanavičius, A 28
Golberg, A 125
Golovinas, E 23
Grigalevičiūtė, R 53
Grigaliunas, A 50
Grinciene, G 58
Gröbner, G 27
Grybauskas, A 23
Gruodis, A 113, 119
Gudaitis, L 38, 52, 94
Gulla, A 30
Guobienė, A 54
Gusbeth, C 25
Guzulaitis, R 32, 93

H

Hafed, ZM 18
Henzie, J 74

I

Ilickas, M 54

J

Jagminas, A 58
Jakštys, B 65, 78, 126
Jančiukė, G 89
Jankeviciute, S 107
Jankunec, M 111
Janušauskaitė, R 110
Janužis, G 44
Jelinskas, T 61
Jonynaitė, K 55
Jurevičius, J 33, 73, 91, 92
Jurgelaitis, E 23
Jurgutis, D 104, 115

K

Kalnaitytė, M 69
Kalnaitytė-Vengelienė, A 4, 31, 69, 80, 82, 103
Karabanovas, V 58, 83, 97, 104, 106, 108, 112, 114, 115

Karalkevičiūtė, V 76
Karčiauskaitė, D 72
Kasabji, FA 74
Kašėta, V 40, 56
Kasperavičiūtė, K 62
Katelnikovas, A 112
Kavalevskaja, A 84
Kavaliauskas, P 53
Kavaliauskas, Ž 55
Kazlauske, E 108
Keršulis, S 55
Keršys, L 102
Khalid, MU 63
Khinevich, N 100
Kirsnytė-Šniokė, M 63
Kirvelis, D 43
Kisnierienė, V 35, 81, 82, 110
Klepka, BP 37
Klimkevičius, V 83, 97, 112
Klinavičius, T 100, 109
Kontenis, L 106
Kozal, J 77
Kraujalienė, L 5, 38, 52, 70, 94
Kraujalis, T 5, 38, 52, 70, 94, 102
Kreišmontaitė, T 99
Krisciukaitis, A 50
Kriščiūnas, A 102
Krouglov, S 106
Kučinskas, L 127
Kudrevceva, A 34
Kulbacka, J 40
Kurg, R 16

L

Lambrev, PH 26, 31, 59
Lankutytė, I 91, 92
Lapeikaitė, I 35, 81, 82, 110
Lastauskienė, E 85
Lekešytė, B 40, 47, 51
Lelešius, R 109
Li, Y-K 15
Lukinavičius, G 4, 14

M

Mačianskienė, R 4, 33, 91, 92
Mačiulis, M 64, 106, 121
Maciūnas, K 33
Makarovas, D 126
Makniusevičius, O 38, 52
Malakauskaitė, P 40, 51, 56
Maleckaitė, I 35
Malyško-Ptašinskė, V 40, 51
Manakova, E 23
Marcinauskas, L 55
Mardosaitė, R 109
Marin, R 108
Marma, V 127
Marozas, V 33
Martišienė, I 73
Matulis, D 4, 101, 123
Mažeika, V 64, 106, 121
Mažeikaitė, G 116
Mažerimas, M 48

Mazėtytė-Godienė, A 61, 104
Melo, W 62, 63
Meyer-Almes, F-J 24
Michaś, A 37
Mickevičiūtė, E 40, 46, 51
Mickus, R 5, 39, 87, 89
Mikalayeva, V 87
Mikalčiūtė, A 88
Miknaitė, J 98
Miliukaitė, R 80, 103
Mirsanaye, K 106
Mlynska, A 97
Morkvėnaitė-Vilkončienė, I 126
Morkvėnas, A 114
Mougin, K 74
Moussavi, M 74
Müller, A 25

N

Navakauskienė, R 28
Navalinskas, A 91, 92
Navickaitė, A 82
Nemeikaitė-Čėnienė, A 51
Nenartavičius, T 96
Niedźwiecka, A 37
Nikić-Spiegel, I 21
Novickij, V 40, 46, 47, 51, 53, 56, 105

O

Osteikaitė, E 64

P

Palmer, LM 32
Pankevičiūtė-Bukauskienė, M 86
Paukstaitiene, R 50
Pečiukaitytė, E 83
Pečiulis, A 61
Peckus, D 74
Peštenytė, K 79
Petrauskas, V 123
Petrolis, R 50
Plečkaitis, M 58, 84
Poderys, V 58, 99, 108, 112, 113, 115, 119
Pocevičiūtė, R 23
Polita, A 117, 120
Pupkis, V 4, 5, 35, 81, 82, 110

R

Račkauskas, S 109
Radzevičiūtė-Valčiukė, E 40, 51
Rafanavičius, A 68
Rakickas, T 61, 67
Rankelytė, G 36
Raškevičius, V 39, 87, 90
Razumiene, J 30
Reshetnyak, V 67
Riauka, M 64
Rodaite, R 125
Rossowska, J 40
Rotomskis, R 31, 58, 83, 84, 97, 99, 108, 113, 115, 119
Ruzgys, P 4, 5, 65, 66, 78, 105, 118, 122

S, Š

Šablinskas, V 42, 71
Saleem, A 17

Šalomskas, A 109
Sarapinienė, I 5, 87, 89
Šarpilo, M 57
Sasnauskas, G 23
Šatkauskas, S 4, 65, 66, 68, 78, 92, 105, 118, 122, 126
Šatkauskienė, I 68
Saudargienė, A 4
Saulenas, M 112
Saulė, R 124, 125
Saulis, G 124, 125
Schulz, A 17
Sheu, J-T 15
Shmeleva, L 67
Sibirny, A 96
Silanskas, A 23
Šilkūnas, M 124
Šimėnas, M 79
Singhal, S 26
Šiurnaitė, D 105
Skeberdis, AV 4, 39, 87, 89, 90
Skibickaja, J 104
Skripka, A 108
Skurdelytė, L 75
Smirnovas, V 75, 76, 79
Šnipas, M 38, 52, 70, 94
Solomon, S 17
Spangenberg, A 74
Sparrman, T 27
Stanevičius, T 96
Stankevič, V 55
Steiner, G 71
Steponkienė, S 83, 97, 108
Stirkė, A 4, 55, 62, 63
Šulskis, D 75, 76, 79, 111
Sunnerhagen, M 13
Suprun, A 67
Surkys, T 45
Suziedelyte, G 112
Sventoraitiene, J 125
Svirskienė, N 107
Svirskis, G 107

T

Talanovaite, S 119
Tamoliūnaitė, G 99
Tamulevičienė, A 74, 100, 109
Tamulevičius, S 74, 100
Tamulevičius, T 4, 74, 100, 109
Tamulytė, R 111
Tan, H-S 26, 59
Taraškevičius, T 72, 85
Teske, C 71
Treinys, R 4, 5, 33
Tsou, P-H 15
Toleikis, A 57

U

Ul Mushtaq, A 27
Urbanskas, E 65, 78, 92
Urniežius, E 123
Uscila, R 55
Usevičius, G 79
Uzieliene, I 97, 108

V,W

Wacklin-Knecht, H 27
Valinčius, G 120
Valiokas, R 104
Valiulienė, G 28
Valiulis, V 28
Valkunas, L 36
Vansevičiūtė, E 95
Vasiliauskaitė, G 60
Vaškevičius, A 101
Vencius, M 44
Venckus, J 65, 78
Venclovas, Č 23
Vengelis, J 44
Venius, J 58, 114
Verselis, VK 38, 70
Vetrone, F 108
Vidal, L 74, 100
Williams, SE 33
Williamson, A 20
Visockis, M 92
Vitta, P 116
Vykertas, S 65, 78
Wojciechowski, T 37
Voitechovic, E 67

Z, Ž

Zagorskaitė, E 23
Zaremba, M 23
Žėkas, V 72
Želvys, A 40, 53
Zentelytė, A 28
Žiaunys, M 76, 98
Zienius, D 109
Zigmantaitė, V 73, 91, 92
Zinkevičienė, A 40
Zubrienė, A 101, 123
Zucca, S 17
Zuokaitė, G 39, 90
Žurauskas, E 64
Žvirblė, M 121

Platinum sponsor

RCL

Research Council of Lithuania

Gold sponsors

EBSA

Biophysics in Europe

NOVA

VILDoma

BIOTECHA

Silver sponsors

ANIMA LAB

LITHUANIAN UNIVERSITY OF HEALTH SCIENCES

Bronze sponsors

OPTOGAMA

KAUNAS

Linea libera

SPARNAI ATRADIMAMS

MONO SPEKTRA

AMBER CHARGE

ISBN 978-609-96492-0-7